



Muhammad Suleman Tahir

Application of Corona Discharge in Off-gas and Wastewater Treatment

Effect of Electrode Geometry on Performance

DISSERTATION

To Obtain the Academic Degree of Doctor of Technical Sciences

at

University of Technology Graz, Austria

Supervisor:

Univ.-Prof. Dipl.-Ing. Dr.techn. Matthäus Siebenhofer

Institut für Chemische Verfahrenstechnik und Umwelttechnik

Technische Universität Graz

External Examiner:

Draxler, Josef, Ao.Univ.-Prof. Dipl.-Ing. Dr.techn.

March 2011

Acknowledgement

This work was written during my activity as a project assistant/ PhD student at the Institute of Chemical Engineering and Environmental Technology at the Graz University of Technology. On my way to the successful completion of this work I have a lot of support and motivations of many professionals. I want to thank all of them at this point.

Also special thanks to Higher Education Commission Pakistan for financial support and OEAD Austria for organizing this program.

My special thanks to:

The head of the Institute of Chemical Engineering and Environmental Technology at the Graz University of Technology, **Mr. Univ.-Prof. Dipl.-Ing. Dr. techn. Matthäus Siebenhofer**, for the possibility of implementation and technical support of this scientific work, the provision of necessary financial resources, many fruitful discussions as well as his professional involvement to provide me a chance to attend conferences and lectures, which contributed significantly to the success of this work and for the initial assessment of this work.

- The staff of this project, Mr. Rane and Gruber for their dedication and diligence in the construction of equipment and Mis. Herta for analytical services.
- All my colleagues at the Institute of Chemical Engineering and Environmental Technology for the good working atmosphere and their continuous support with their advice and their willingness to help. I appreciate the cooperation of Mr. Peter Letonja and Hanes Noll.

For my parents and teachers

Abstract

Processes of wastewater treatment and off-gas purification will gain significance in a near future. In this thesis advanced oxidation processes were investigated for applicability in off-gas treatment, wastewater treatment and simultaneous separation of particulate matter from off-gas. The process principle is based on corona discharge.

Oxidation processes were investigated to eliminate different organic pollutants from several effluents. The process is conducted without using any chemicals. The technology is called Advanced Oxidation Processes (AOPs) through corona discharge. A decision tree was developed to evaluate a proper technology for specific applications in off-gas purification as well as in wastewater treatment. For this purpose comparison and documentation of approved photochemical and electrochemical processes for different substance classes have been conducted. Criteria for comparison were the potential of degradation of different constituents in different processes.

Governing topic was the investigation of the impact of geometry of discharge electrodes on the corona field intensity, UV-irradiation and ozone generation under specific conditions with and without air and water circulation. Enhanced corona intensity of brush type discharge electrode also increases the collection efficiency of submicronic particles. Brush discharge electrodes produce significant amount of ozone. Ozone generation is function of optimum corona current. Concentration of ozone was higher without water circulation because of absorption in water. Ozone immediately reacts very effectively with organic contaminants either present in waste water or in the gaseous phase. Due to these specific process characteristics, corona discharge in wet electrostatic precipitators provides advanced oxidation of several constituents.

Degradation of several test substances like acetone, iso-propanol, EDTA and phenol was investigated under various operation conditions. At specific current/voltage-characteristics depletion of total organic carbon (TOC) was significant. Complete degradation of acetone and Iso-propanol and dissociation of phenol was observed during operation. Simultaneous removal of particulate matter from off-gas as well as hazardous organic pollutants from wastewater and off-gas is possible through direct corona discharge in WESP.

Contribution in Conferences

Oral Presentation:

1. Tahir, M. S.: Electrostatic precipitation (ESP) in off gas purification. (4th Minisymposium, Verfahrenstechnik, Leoben Austria, 3- 4. July 2008).
2. Tahir, M. S.: Impact of the design of discharge electrode on the Current/Voltage characteristics and the rate of migration in Electrostatic precipitation. (ICAPE 13-14 October 2008, Islamabad, Pakistan).
3. Tahir, M. Suleman: Acetone degradation through corona discharge (WASET 27-29 June 2010, Paris, France).
4. Tahir, M. Suleman: Advanced wastewater treatment by corona discharge (AIChE, 7-12 November 2010, Salt lake city USA).
5. Tahir, M. Suleman: Comparison of advanced oxidation process with wet tube type electrostatic precipitators (AIChE, 7-12 November 2010, Salt lake city USA).
6. Tahir, M. Suleman: Advanced oxidation technologies (AIChE, 7-12 November 2010, Salt lake city USA)
7. Tahir M. Suleman: Removal of hazardous ozone from dry ESPs (ICEAPE, 28-29 December 2010, Pakistan).
8. Tahir, M. Suleman: Phenol degradation through tubular corona reactor (4th Symposium on engineering sciences 2011 Pakistan).

Poster Presentation:

1. Tahir, M. Suleman: Effect of gas velocity on the Current-Voltage characteristics of Electro-filters, (5th Minisymposium, Verfahrenstechnik, Wien Austria, 24-25 June 2009).
2. Tahir, M. Suleman: Electrode geometry effect on corona current and onset field intensity (3rd Symposium on engineering sciences 2010 Pakistan).
3. Tahir, M. Suleman: Effect of various electrodes on C/V curves, 6th. Minisymposium, Verfahrenstechnik, Austria 2010.
4. Tahir, M. Suleman: Enhanced corona onset field intensity with brush discharge electrode (Germany Aachen 2010).

5. Tahir, M. Suleman: An Innovative and advanced oxidation process for degradation of Organic and Non biodegradable pollutants from waste water by using corona discharge reactor (Accepted in 3rd EPIC, Manchester, UK).

1	Introduction	1
1.1	Technologies available for particle precipitation, water and wastewater purification	2
1.1.1	Particle precipitation technologies.....	2
1.1.2	History of electrostatic precipitators (ESPs)	2
1.1.3	Particle separation techniques	3
1.1.4	Off-gas purification by oxidation and reduction.....	4
1.2	Wastewater treatment technologies	5
1.2.1	Chemical processes	5
1.3	Pollutants in air, water and wastewater.....	7
1.3.1	Pollutants in air.....	7
1.3.2	Pollutants in water and wastewater	8
1.3.3	Organic and inorganic pollutants in water pollutants	8
1.4	Wet-tube electrostatic precipitator	8
1.4.1	Electrostatic precipitation fundamentals.....	9
1.4.2	Electrostatic precipitation.....	9
1.4.3	Corona discharge	11
1.4.4	Types of corona discharges.....	11
1.5	Literature review	12
2	Design and development of experimental set up	21
2.1	Basic design empirical correlation for ESPs.....	21
2.1.1	Corona onset field intensity.....	21
2.1.2	Corona onset voltage.....	22
2.1.3	Specific corona current	22
2.1.4	Maximum operation voltage.....	23
2.1.5	Collection efficiency/Grade precipitation efficiency	23
2.1.6	Migration rate of particles	23
2.1.7	Precipitation field intensity.....	24
2.1.8	Components of wet tube electrostatic precipitators	24
2.1.9	High voltage power supply	25
2.1.10	Discharge electrode geometry.....	28
2.1.11	Collecting/ Counter electrode	30
2.1.12	Insulators.....	33
2.1.13	Water circulation and flow rate calculation	34
2.1.14	Film formation in the tube	34
2.1.15	Air purging system.....	35
2.2	Summary.....	36

3	Chemicals and analytical techniques	37
3.1	Ethylenediaminetetraacetic acid (EDTA)	37
3.1.1	Preparation of EDTA solution	37
3.2	Phenol	38
3.2.1	Preparation of phenol solution	39
3.3	Acetone	39
3.3.1	Acetone solution preparation	39
3.4	Iso-propanol.....	40
3.4.1	Iso-propanol solution.....	40
3.5	Potassium iodide.....	40
3.5.1	Potassium iodate	41
3.5.2	Solution preparation for actinometrical measurement	41
3.5.3	Ozone measuring in water	44
4	Characterization of partial and complete brush discharge electrodes	45
4.1	Corona generation with brush type discharge electrodes	45
4.1.1	Characterization of brush type discharge electrodes	46
4.1.2	Current/Voltage characteristic	47
4.1.3	Partial brush type discharge electrodes (active length 700 mm)	48
4.1.4	Discussion of the results of partial brush discharge electrodes (5 mm diameter and brushing wire 0.15 mm)	49
4.1.5	Batch.....	50
4.1.6	Various air purging condition	50
4.1.7	Low air purging.....	50
4.1.8	Increased air purging	51
4.1.9	Ozone generation with partial brush type discharge electrodes	53
4.1.10	Effect of air flow on the ozone generation	53
4.1.11	Validation of ozone degradation at high corona currents	53
4.1.12	Current/Voltage characteristics with complete brush discharge electrode	54
4.1.13	Current/Voltage behavior at batch and 0.5 m ³ /h air purging (CBDE)	56
4.1.14	Comparison of batch and air purge (1.2 m ³ /h, 2 m ³ /h and 3 m ³ /h)	56
4.1.15	Ozone generation with complete brush type discharge electrodes under constant corona current over duration of 60min	58
4.1.16	Ozone generation with complete brush type discharge electrodes under batch and various air purge conditions	59
4.1.17	Comparison of current/voltage characteristics of partial and complete brush discharge electrode with various applied conditions	60
4.1.18	Batch mode.....	61

4.1.19	Effect of 3 m ³ /h on current/voltage curves	62
5	Experimental investigation of various brush type discharge electrodes with active length of 500 mm; installed at the bottom.....	69
5.1	Current/Voltage behavior with brush type discharge electrodes (4 mm, 0.1 mm), active length of 500 mm at bottom.....	70
5.2	Ozone generation with brush type discharge electrodes (4 mm, 0.1 mm wire diameter)	71
5.3	Current/Voltage curves for brush type discharge electrodes with 500 mm active length at bottom.	73
5.3.1	Ozone generation with brush type discharge electrodes (5 mm, 0.15 mm wire diameter) with 500 mm active length at bottom.	73
5.4	Current/Voltage curves with brush e discharge electrodes (6 mm, 0.1 mm)	74
5.4.1	Ozone generation with brush type discharge electrodes (6 mm, 0.1 mm)	74
5.5	Current/Voltage curves with brush discharge electrodes (6 mm, 0.15 mm)	76
5.5.1	Ozone generation with brush type discharge electrodes (6 mm, 0.15 mm) with 500 mm active length at bottom	76
5.6	Current/Voltage curves for brush type discharge electrodes (8 mm, 0.1 mm wire diameter) with 500 mm active length at bottom	77
5.6.1	Ozone generation with brush type discharge electrodes (8 mm, 0.1 mm wire diameter) with 500 mm active length at bottom	79
5.7	Current/Voltage curves with brush discharge electrodes (8 mm, 0.15 mm)	79
5.7.1	Ozone generation with brush type discharge electrodes (8 mm, 0.15 mm) with 0.5m active length at bottom.....	81
5.8	Comparison of ozone formation with batch mode	81
5.9	Comparison of ozone generation under air purge conditions.....	82
5.10	Comparison of corona current at 20 kV under various operation conditions	83
5.11	Summary	84
6	Modelling of current/voltage relations and ozone generation with brush type discharge electrodes	86
6.1	Comparison of current/voltage data for tungsten wire and brush type discharge electrodes	86
6.1.1	Fit data determination	89
6.2	Ozone generation and determination of kinetic equation through table curve 2D program.....	95
6.2.1	Modelling of ozone generation with 8 mm (0.15 mm) at batch mode.....	95
6.2.2	Ozone generation with 8 mm (0.15 mm) at air purge mode	97
6.2.3	Ozone generation with 8 mm (0.15 mm) at air plus water mode	99
6.3	Ozone generation with 6 mm (0.15 mm) at batch mode	100
6.3.1	Ozone generation with 6 mm (0.15 mm) at air purge mode	101

6.3.2	Ozone generation with 6 mm (0.15 mm) at air plus water mode	102
6.3.3	Ozone generation with 5 mm (0.15 mm) at batch mode	104
6.4	Summary.....	107
7	Modelling of experimental current/voltage data with proposed equation.....	108
7.1	Basic information and assumptions	108
7.1.1	Discussion.....	111
7.1.2	Summary.....	113
8	Modelling of ozone formation.....	114
8.1	Summary.....	116
9	Applications of wet tube-type electrostatic precipitator.....	117
9.1	Off- gas purification	117
9.2	Waste water treatment.....	117
9.3	Acetone degradation	117
9.4	Mineralization of EDTA	119
9.5	Solution preparation, sampling and results	121
9.6	Phenol degradation and mineralization	125
9.6.1	Colour observation	127
9.6.2	Phenolic industrial waste water treatment through corona discharge.....	127
9.7	Actinometric measurements	128
9.7.1	Photon flux.....	129
9.7.2	Preparation of solution and experimental method.....	130
9.8	Experimental method	130
9.9	Summary.....	134
10	Summary.....	136
11	List of figures and table.....	141
11.1	List of figures	141
11.2	List of tables	146
12	Literature	148
13	Appendix	155

Nomenclature and Abbreviations

Symbol	Name	Units
A	Area	[m ²]
A ₃₅₂	Extinction	[mol/g.cm]
A _c	Surface area of collector	[m ²]
c ₀	Speed of light	[m/s]
c	Concentration	[mol/l]
c	Particle concentration	[kg/Nm ³]
D	Frictional resistance	[kg. m/s ²]
D _i	Internal diameter	[m]
D	Diffusions coefficient	[m ² /s]
d _p	Particle diameter	[m]
E ₀	Onset field intensity	[kV/m]
E	Radiation intensity	[1/mol]
E	Energy	[V]
E _a	Charging field intensity	[kV/m]
E _p	Precipitation field intensity	[kV/m]
E _u	Euler-Number	[-]
F	Faraday constant	[C/mol]
g	Acceleration due to gravity	[m/s ²]
h	Height	[m]
h	Planck's constant	[J.s]
I	Current density	[mA/m]
I	Current	[A]

K	Ion mobility	[m ³ /kg]
k ₁	Rate constant	[m/mA]
k ₂	Rate constant	[m/mA]
l	Length	[m]
M	Molecular weight	[g/mol]
m	mass	[kg]
n	Number of moles	[mol]
N	Particle number	[-]
N _A	Avogadro-constant	[1/mol]
P	Power	[W]
p	Pressure	[Pa]
ν	Kinematic viscosity	[m ² /s]
ρ	Density	[kg/m ³]
η	Dynamic viscosity	[kg/(m·s)]
R	Radius of tube	[m]
r _b	Radius of brush	[m]
r _w	Radius of wire	[m]
t	Time	[s]
T	Temperature	[K]
U ₀	Startup voltage	[kV]
U	Operation voltage	[kV]
U _{max}	Maximum voltage	[kV]
v	Velocity	[m/s]
V	Volume	[m ³]

\dot{V}	Flow rate	[m ³ /s]
W	Power	[J]
w	Particle migration	[m/s]
w_m	Average velocity	[m/s]
x	Particle diameter	[m]
δ	Relative gas density	[-]
δ	Film thickness	[m]
ϵ_{352}	Extinction coefficient	[mol/g.cm]
Φ_λ	Quantum yield	[-]
ϕ_P	Photon flux	[1/mol. s]
ν	Kinematic viscosity	[m ² /s]
ρ	Density	[kg/m ³]
η	Dynamic viscosity	[kg/(m· s)]
λ	Wave length	[nm]
ρ_p	Particle density	[kg/m ³]
HVPS	High voltage power supply	
HVCP	High voltage control panel	
WESP	Wet electrostatic precipitator	
ppm	Parts per million	
AOP	Advanced oxidation process	

1 Introduction

The increased interest and awareness in recent years for the improvement of technologies for wastewater and off-gas treatment processes is of high priority. Development of new technologies for efficient removal of hazardous pollutants from effluents as well as off-gas is a major task. Commercially available methods for effluent treatment may need costly chemicals and infrastructure which increases operational and process cost as well as the chemical impact on the environment.

Water is abundantly used in the chemical industry, in agriculture and private consumption. Wastewater from agricultural sources may be contaminated with pesticides, herbicides and fungicides while wastewater from the chemical industry may contain multiple hazardous persistent organic pollutants. Water contaminations especially with persistent organic pollutants from several sources are still subject of suspected or recorded impact. Specific processes may emit hazardous gases as well as particulate matter. Particulate matter such as dust, unburned carbon, metals, powders, etc, hazardous chemicals, and many hazardous gases such as NO_x, SO_x, HCl, CO_x, VOC, etc. may form mixtures of hazardous pollutants causing formation of acid rain, photochemical smog, deforestation, global warming. These hazardous pollutants also badly affect the human health, terrestrial and aquatic life.

In order to remove pollutants from wastewater and off-gas, different approaches and technologies are available on the market. Various state of art technologies, applied to separate particulates from off-gas are dry electrostatic precipitation, cyclone separation, bag house filtration and scrubbing. Commonly applied wastewater treatment processes to destroy and degrade various organic pollutants are advanced oxidation processes. To achieve the Kyoto protocol emission targets and to face the strict environmental legislation for hazardous pollutants along with ultrafine particles, we have need for efficient and affordable processes to mitigate pollutants from off-gas/wastewater which can not be separated by simple state of the art technologies.

Electrostatic precipitation has been invented about hundreds years ago. Different types of electrostatic precipitators are available in the market. Normally electrostatic precipitators are used to separate particulate matter from off-gas. Different investigations to improve collection efficiency, performance and design parameters of electrostatic precipitator are available in literature [1], [2] and [3]. Wet electrostatic precipitation is a very effective method to separate micronic/submicronic particles,

metallic or conductive particles and also hazardous gases from off-gas. Wet electrostatic precipitators have the ability to separate submicronic, sticky particles and hazardous gases from off-gas [1].

Corona discharge in the wet type operation mode is capable of eliminating particulate matter, hazardous gaseous compounds by absorption from off-gas and it is also capable of mineralizing/degrading persistent organic pollutants in wastewater by rinsing the collecting electrodes.

1.1 Technologies available for particle precipitation, water and wastewater purification

Various state of the art processes are available individually for air purification and wastewater treatment. Technologies for off-gas purification are not in principle applicable for wastewater purification and there is still no process available which can be used simultaneously for off gas and wastewater treatment.

1.1.1 Particle precipitation technologies

Precipitation of particles [especially submicronic size], removal of organic and inorganic pollutants is still a major challenge in off-gas purification. It is also a great challenge for the scientific community to provide affordable technologies. Several boundaries, whether it is the technological progress in general, necessity of increased attention for safety and health affairs or the demand of a balanced environment, need to be considered. We nowadays need the highest possible standards with regard to prevention of particle emission and emission control. Therefore particle precipitation is a highest priority task along with the degradation of hazardous pollutants [organic, inorganic].

1.1.2 History of electrostatic precipitators (ESPs)

Many people believe that atmospheric pollution control is a modern concept. Air pollution is as old as first fire. Actually impact of air pollution was realized 400 years ago when the first recorded measure was taken in UK. Later on the Parliament of UK approved the legislation as clean air act in 1956 and prohibited the use of bituminous sea coal causing air pollution [2].

An electrostatic static precipitator is a particulate matter collection device which is highly efficient in separation of particles from off-gas. Electrostatic precipitators are being used in the market for a hundred years. The first use of corona discharge to

remove particles from an aerosol was recorded by Hohlfeld in 1824. However, it was not commercialized until almost a century later. In 1907 Dr. Frederick G. Cottrell applied for a patent on a device for charging particles and then collecting them through electrostatic attraction. Cottrell [3] first applied the device for the collection of sulfuric acid mist and lead oxide fume emitted from various acid-producing and smelting activities.

Particle precipitation has been an important role in off-gas purification since industrial activities have raised and has become a significant factor in environmental issues. A significant and rapid progress in industrial off-gas purification was made with the invention of dry electrostatic precipitation [ESP]. Different types of electrostatic precipitators [plate type, tube type] were developed in the last century and various authors investigated enhancement of the performance of ESPs which is measured in terms of collection efficiency. ESPs are capable of treating huge quantities of off-gas, highly loaded with dust and aerosols.

Precipitation efficiency of ESPs depends upon various design parameters, e.g. geometry of electrodes. Deviation from design may affect its performance negatively, gas temperature, moisture of the gas and the specific electrical resistance. The construction must not deviate strongly from design specification. Rapid loss in collection efficiency has to be accepted in case of out-of-specification operation parameters. The particles to be precipitated must nearly have ideal adhesion properties, since they must be collected on the precipitation electrodes on one hand and removed by rapping without redistributing (remixing) in the off-gas on the other hand. Good performance of the precipitator does not permit deviating electrode/counter electrode distance from central positioning and without assurance of specific tension in discharge electrodes. Electrical insulation has to consider application of high voltage under increased thermal, mechanical and electrical stresses.

1.1.3 Particle separation techniques

In the last two decades, there was no significant development in the field of electrostatic precipitation. As electrostatic precipitation technology was used only for particulate matter separation, with limiting application for state of the art design. Various types of electrostatic precipitators like plate type, tube type under dry

operation conditions are commonly used in the market. Cost of investment is still an alarming issue.

Separation of particulates from off gas is accomplished with following devices

- Electrostatic precipitators
- Bag house filters
- Venture scrubbers
- Cyclone separator

These devices are applicable and their efficiency depends upon the size of particles. Except application of fabric filters and venture scrubbers, removal efficiency for fine particles is better in electrostatic precipitators compared with other devices and based on specific energy consumption.

1.1.4 Off-gas purification by oxidation and reduction

Several manufacturing processes and facilities may lead to the formation of gaseous by-products with oxidizing or reducing properties.

Oxides of sulfur and nitrogen in the atmosphere are source of acid rain and cause serious problems for the environment. Removal of SO_2 is accomplished with various processes. Nitrogen oxides are also preferably removed from off-gas by reduction processes by forming nitrogen and water.

Several manufacturing operations may cause emission of gaseous solvents. The atmospheric interaction of solvents also needs increased attention. Emission of solvents is limited by law. Emission control is possible by several techniques, including recycling processes and oxidation processes. Latter techniques are predominately carried out by combustion.

Oxidizing and reduction processes in solvent emission control cover the field of combustion, catalytic combustion, reduction and catalytic reduction of pollutants according to their individual properties

Sometimes both techniques can be combined in one operational step. Ordinarily pollutants of either oxidizing or reducing properties are emission determining. Technology and process design have to be adjusted to the needs of individual emission conditions [1] and [4].

1.2 Wastewater treatment technologies

Demand for high quality water has increased rapidly in recent decades, and also environmental pollution control is of highest priority. Increased consumption of water from industry as well as municipal consumers is directly or indirectly increasing pollutants in ground water. Untreated or inefficient process water may still contain a variety of pollutants. The hazardousness of these pollutants badly affects human health, aquatic life and agriculture land as well.

Various processes for wastewater treatment are under operation and they are designed to mitigate specific constituents in wastewater. The efficiency of such processes is limited to a specific range of pollutants. It is important to realize the significance of wastewater treatment processes and the impact of pollutants and physical–chemical interaction of pollutants. We may have wastewater streams from various origins and each stream of wastewater should be treated separately for efficient control.

For the design, development and execution of off-gas/water purification processes, literature of various authors and specifically literature [1] and [4] was consulted.

Efficient wastewater treatment processes are describing various ingredients in wastewater, qualitatively and quantitatively. Knowledge of chemical and physical properties of ingredients is helpful to get them under control.

Wastewater treatment is classified in various categories on basis of technology and use. These are mechanical, biological, physical, thermal processes and chemical processes, as discussed in *Table1*.

1.2.1 Chemical processes

Advanced oxidation processes are classified on the basis of the medium used for oxidation of the pollutants in wastewater and air.

The use of UV radiation/light and technology, UV radiation/light and environment, and environment and technology is interrelated and extraordinarily versatile with respect to their future development potential. Therefore the use of UV radiation in diverse applications especially in waste treatment represents the basic advanced technologies of 21 century. Advanced oxidation technologies (AOTs) focus the reaction mechanisms and engineering concepts of technologies by using UV radiation as a selective reagent for the cleavage of chemical bounds and hence for the destruction of unwanted chemicals or microorganism [4].

Table 1: Methods used for water treatment and their technical specification

Process	Technical Specification
Mechanical process	A process in which the wastewater is purified by some mechanical means is called mechanical process. Mechanical means may be grits/meshed, screens, scrapers, grill, flotation, sedimentation, settling, coagulation, adsorption, desorption, filtration etc
Biological processes	A process in which bacteria is a worked as process activator. Commonly used processes are-Anaerobic and Aerobic activated process
Physical processes	A process in which physically separates the pollutants. Most commonly used processes are filtration, microfiltration etc
Thermal processes	Processes are temperature and heat based. Processes are Crystallization, Disinfection, absorption, Evaporation and Distillation.
Chemical processes	A process in which water is treated by the use of chemicals and a chemical change is observed. Chemical processes are further classified on the bases of process activity, Incineration, combustion, disinfection, neutralization, Ion exchange, chemical oxidation, and advanced oxidation [photochemical oxidation] as well. Advanced oxidation processes are further classified on the basis of medium used for oxidation of the pollutants in wastewater and air.

Advanced oxidation processes with UV-radiation and combination of UV-radiation with oxidizing reagents like ozone or hydrogen peroxide are listed in **Table 2**. Possible combination of processes is illustrated.

Table 2: Photochemical advanced oxidation processes used and available in the market

Combination/ Source of process	Process name
UV	photolysis
UV/H ₂ O ₂	UV-peroxide process
UV/O ₃	Ozonolysis
UV/O ₃ / H ₂ O ₂	PEROXON-process/ technology
Fe ²⁺ / H ₂ O ₂	FENTON-Reaction/Process
UV/Fe ²⁺ / H ₂ O ₂	Photo-Fenton process
UV/TiO ₂	photo catalysis

In the last two decades hydroxyl radicals were also used for oxidation of pollutants to decontaminate water and air. Hydroxyl radical is an economical and ecologically important industrial chemical, vastly used in water purification industry.

1.3 Pollutants in air, water and wastewater

Air, water and wastewater contain several different pollutants. Perhaps the concentration and specific type of ingredients in water depend upon the source of pollutants.

Some pollutants are very common in air and water. Air pollutants are different from water pollutants, quantitatively and in hazardousness, therefore it is discussed separately to classify the major pollutants in both phases.

1.3.1 Pollutants in air

Human made sources of air pollutants cover a wide variety of chemicals and physical activities. They are the major contributors to urban air pollution.

The main classes of pollutants are particulates, carbon monoxide, hydrocarbons, nitrogen oxides, sulfur oxides and hydrogen halides. Classification may also consider the origin [primary or secondary].

Specification of gaseous substances has to distinguish between inorganic and organic pollutants shown in *Table 3*.

Particulates include solid and liquid matter whose diameter is larger than a molecule but smaller than about 100 μm . Particulates dispersed in gaseous carrier are termed

an „aerosol“. Aerosols are difficult to classify on a scientific basis in terms of their fundamental properties such as settling rate, optical activity, reaction activity or physiological action [1].

Table 3: Organic and inorganic pollutants in air

Inorganic pollutants	Organic pollutants
Sulfur oxides	Hydrocarbons[paraffins/
Hydrogen sulfide	olefins/aromatics]
Nitrogen oxides	Oxygenated aliphatic HC
Halogenes	[alcohols/aldehydes/ketones
Halides	/ acids/ peroxides]
Ozone and oxidants	Organic halides
Cyanides	Organic sulfides
Ammonium compounds	Amines

1.3.2 Pollutants in water and wastewater

Water and wastewater contains a variety of pollutants. Mainly these pollutants are classified into two categories on basis of nature, physical and chemical impurities. Our task in wastewater treatment is to decontaminate chemical impurities.

1.3.3 Organic and inorganic pollutants in water

Major organic substances are hydrocarbon, Fats, Proteins, Carbohydrates, ingredients of detergents, cleaning chemicals and many other industrial chemicals prepared from petroleum origin. Effect of organic substances in water/ wastewater is measured in terms of biological oxygen demand [BOD], the chemical oxygen demand [COD], and total organic carbon [TOC].

Commonly observed inorganic impurities in wastewater are ammonium, nitrate, nitrite, phosphate and heavy metal ions etc.

1.4 Wet-tube electrostatic precipitator

Our application focuses on wet electrostatic precipitation. The wet tub-type electrostatic precipitator is an excellent device for dust collection from off-gas. Wet ESP does not have to consider the specific electrical resistance of particles to be precipitated. The adhesive properties of dust do not limit precipitation as the collecting electrodes are formed by an aqueous film which is renewed continuously.

Entrainment of collected particulate matter is also impossible, as it is continuously removed from the counter electrode. Moreover hazardous ozone, formed during electrical discharge in air, is also absorbed in the circulating water and can be used to oxidize organic pollutants in off-gas. The wet tube-type electrostatic precipitator is capable of separating particulate matter and disintegrating hazardous organic pollutants from off-gas and wastewater simultaneously. Uniform corona discharge, a specific attribute of tube-type ESPs, has an enhancing effect on the collection efficiency of ESPs.

In this project the effect of the geometry of discharge electrodes on current/voltage characteristics under various operation conditions was investigated and modeled based on the empirical correlations available in literature [4]. Effect of brush discharge electrodes on corona onset field intensity and corona current was investigated.

1.4.1 Electrostatic precipitation fundamentals

Basic mechanism of charge generation, electrostatic precipitation and types of corona discharge are discussed in this section.

1.4.2 Electrostatic precipitation

Electrostatic precipitators [ESPs] are normally used for separation of particulates from gases. The particles are basically separated by using electrical discharge forces for ionizing the particles and air molecules which are finally drifted towards the counter electrodes. Process of electrostatic precipitation is accomplished in many basic sub processes or steps. These sub processes are categories in five sub steps for better understanding of electrostatic precipitation phenomenon shown in **Figure 1**.

- A. Producing the Charge carrier
- B. Ionization or charging of particles
- C. Migration of the charged particle to the counter electrodes
- D. Collection of the particle on the collection electrodes
- E. Removal of the collected particle from the surface of collecting electrodes

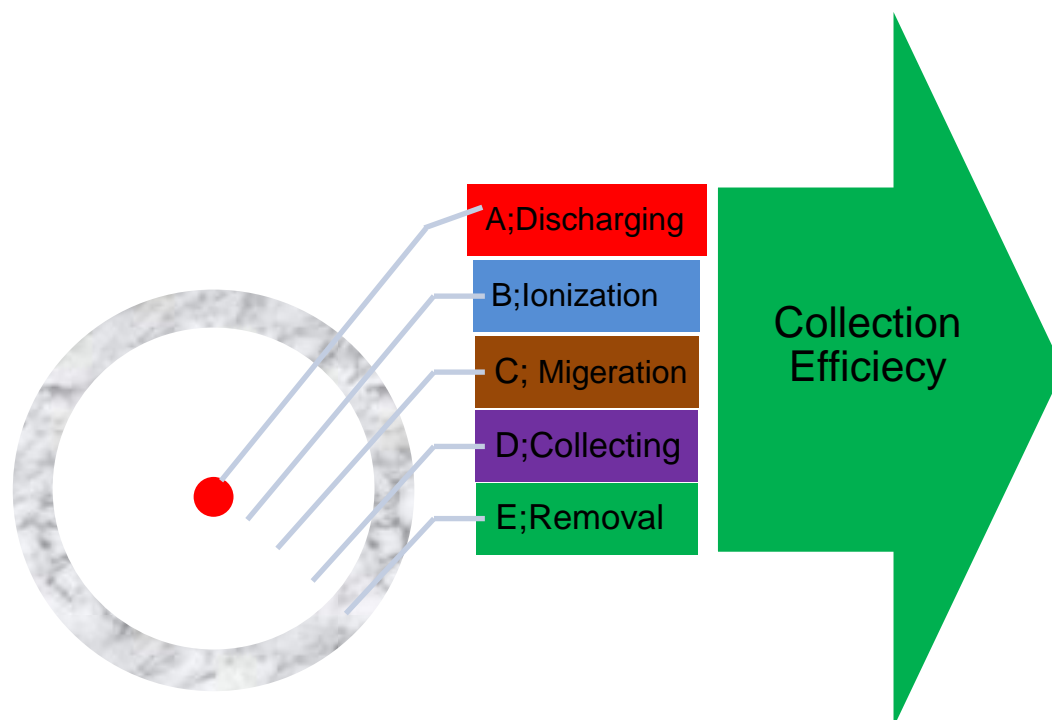


Figure 1: Discharging, ionizing, migration of particle, finally precipitation and removal from discharge electrode.

Normally gases are not conductors but under specific circumstances current can flow and gases act like a conductor. In ESPs, above the critical field strength and due to intensive ionization of air molecules, current flows from the discharge electrodes to the collecting electrodes. Depending upon the corona current intensity, we can visualize the behavior of various discharge mechanisms which are classified on basis of shape, typical behavior and color. For electrical discharge in gaseous gaps, we have to distinguish between sparking, arc formation, glow discharge and corona discharge. Each type of discharge has its own characteristics.

Uniform corona discharge is a self-supporting type of electrical discharge in gas. The regions between two electrodes are active and passive. The active region is only few percent of passive region. Corona discharge at ambient pressure is limited to a geometric ratio of the electrodes distance b and radius of the discharge electrodes r of at least the value of [the Euler number e] $b/r = 2.71$.

Particle motion is promoted by Coulomb-force which is proportional to the product of the charged particle times the electrical field. These results in 3000 times the gravitational acceleration for 10 μm -sized particles and still 300 times the gravitational acceleration for 1 μm -sized particles. Coulomb-force is counteracted by inertia and friction force. While inertia force may be neglected, friction force,

described by Stokes Law, determines counter action. The resulting particle migration is therefore, controlled by Coulomb-force and by Stokes-force. It is called the rate of migration and it is about 3 to 20 cm/s in the mean. Process performance is based on the ratio of electrodes distance to the rate of migration. The ratio must be less than the ratio of the length of the precipitator and the gas velocity [1].

1.4.3 Corona discharge

Sufficient electrical discharge from the surface of electrodes which is capable of ionizing the fluid surrounding the discharge electrodes and potential gradient must exceed a certain value of electrical field strength before electrical breakdown. Sparking/arcing will cause a break down due to local short circuiting.

The particular characteristics of corona discharge are a function of geometry, the shape of the electrodes, the polarity, the size of the gap, and also the ionizing medium (gas, mixture of gases). Besides geometry, the gas composition, the temperature, the pressure, the type of discharge electrodes, the type of discharge current and the polarity of the current/voltage characteristic determine the performance of corona discharge.

Investigations explain the importance of corona discharge and its application in off-gas and wastewater purification. The electrical conductivity in gases must be induced by ionization and corona discharge is induced by ionization impact. Free electrons in the gas phase are produced and accelerated in an electrical field. Interaction of charged particles with dust particles results in emission of further electrons. Emission of electron refers to ion mobility which has an important role in the collection efficiency of ESPs.

Classification of corona discharge process and investigations on the behavior of different discharge mechanisms is well explained in literature [8], [9] and [12].

1.4.4 Types of corona discharges

Two types of corona discharges are commonly discussed as positive corona and negative corona discharges. Jen-Shih Chang et al. [10] discussed different technologies available and their ability to remove pollutants from off-gas and waste liquids. Author reviewed and pointed out the efficiency of technology, energy required per unit removal, reuse of the product and how the technology is effectively applied for pollution control. Literature [11] and M. Abdel-Salam et al. [12]

investigated the space charge density, effect of potential and corona current characteristics in electrostatic precipitators. Positive corona discharge can generate electrons, positive ions, photons and photoelectrons while the negative corona discharge generates negative ions, electrons and photons from negative corona, and literature [2] and [13] also explain the corona behavior in electrostatic precipitation.

Corona discharge is further classified on the basis of behavior of emission and physical shape/color formation during streaming. Positive polarity corona is classified in burst pulse corona, streamer, glow corona, spark and negative polarity corona is trickle pulse corona, pulse less corona and spark as discussed in literature [14].

Type of discharge also characterizes the electron emission process and its effect on the corona process. Different discharging mechanisms contribute to develop a corona field in the active and passive zone. Highly intense corona ionizes air molecules and particulates which are finally migrated to the counter electrodes. Migration velocity of particulates has a direct effect on the collection efficiency of electrostatic precipitators.

1.5 Literature review

In this section the literature relevant to development of ESPs and especially the effect of geometry of discharge electrodes on current/voltage characteristics reviewed or revisited. Section 1.5.1 through 1.5.6 discusses investigations reflecting the effect of design of discharge electrodes on corona generation characteristics, collection efficiency of ESPs, ozone generation or oxidizing reagent formation as well as degradation of environmental pollutants.

1.5.1 Effect of geometry of discharge electrodes on corona discharge and collection efficiency of electrostatic precipitator

Design and geometry of the discharge electrodes is relatively more important for corona generation and ionization of particles to be separated from off-gas. The screw type discharge electrodes generate ozone more efficiently and quantitatively than pyramid type electrodes [15]. Literature [16] and [17] discussed the electrical field strength. It is decreased with the increase of plate-to-plate spacing while the operation conditions are same. The electrical field intensity and current/voltage characteristics also depend upon the surface roughness of discharge electrodes and it may vary even of same diameter of wire electrodes. The collection efficiency and performance of electrostatic precipitators is increased with the decrease in diameter

of ionizing wire. The discharge current is also increased with decrease in diameter of the discharge electrodes at same applied voltage. The electrical field strength is decreased with the increase of plate-to-plate spacing under the same operation conditions. Literature [18] and I. Suarasana et al. [19] experimentally investigated the effect of multi-point discharge electrodes for ionization and ozone generation compared to conventionally used discharge electrodes. Authors [20] investigated the application of brush discharge electrodes to ignite volatile fuels and hazards in the earthed electrodes due to charge accumulation. Z. Tamus et al. [21] described the measuring method for current density distribution on small segments of a PVC plate in front of brush discharge electrodes which is nearly constant. Laurentiu Marius Dumitran et al. [22] concluded from their computational studies that electric field strength and space charge density is a function of inter-electrode gap and geometry of discharge electrodes. Sheng-Hsiu Huang and Chih-Chieh Chen [23] experimentally investigated the effect of increase of dust cake thickness on the collecting/ electrodes, the ionic current, collection efficiency and ozone generation decreased. Yousuke Kurode et al. [24] described from their experimental studies that a punched discharge electrodes has higher collection efficiency than plain electrodes for similar applied voltage. D. Brocilo et al. [25] explained and discussed the mechanism of improved space charge and collection efficiency for collection of ultra fine particles by using spike type discharge electrodes. M. R. Thalaie et al. [26] presented a model and they proved that with the increase of applied voltage the current density on the plate is increased and formation of streamer corona from coaxial geometry of discharge electrodes not only depends upon the electric field but also on the curvature of surface. G. Mischkulnig and Porfirio Bento [27] investigated innovative design of discharge electrodes [G-spike type] and observed enhanced corona and collection efficiency of ESPs. They also compared the performance of other design with G-spike type discharge electrodes to determine the effect of number of spike on discharge electrodes.

1.5.2 Ozone generation through corona discharge

Various authors investigated the effect of corona current on ozone generation under various applied conditions. Material and composition of the ionizing wire has a major effect on ozone generation in electrostatic precipitation. Ozone generation from stainless steel discharge wire is 24 times more than from silver wire ionizing

electrodes under same conditions for positive corona in electrostatic precipitators. Ozone generated by negative corona is higher than that of positive corona under same operation conditions and geometry of ionizing electrodes. Ozone generation is also directly related to the input power to electrostatic precipitators [28]. Comparatively higher ozone concentration is generated in case of pulsed corona than of DC and AC corona with similar operation parameters. The direction of air flow affects ozone generation and the concentration of ozone is higher for parallel flow than for normal flow in the corona reactor as authors discussed in literature [30] and [31]. For the production of ozone, electronic and ionic collisions are important to dissociate oxygen molecules. The efficiency of ozone generation from pure oxygen is better than from air [32] and power consumption is also less. The effect of gas composition may enhance side reactions to form toxic gases [32]-[33]. Literature [33] has explained the effect of gas temperature on rate of reaction of ozone generation from free radicals. With increase in gas temperature, ozone formation is remarkably decreased and also reverse reaction occurred from ozone to oxygen molecules along with different oxides of nitrogen. Studies of Serji Kanazawa et al. [34] and literature [35] show that contaminated surface of discharge electrodes can produce much higher ozone than clean wire discharge electrodes in electrostatic precipitation. Andrew s. Viner et al. [36] explained net rate of ozone formation which depends on oxygen content, relative humidity of air, quantity of current, ozone destruction rate, radius and polarity of discharge electrodes. Y. Nomoto et al. [37] compared the effect of silent-surface hybrid discharge with surface discharge and silent discharge. The author described that ozone generation efficiency and the ozone concentration rate is much higher with silent-surface hybrid system than with surface discharge electrodes and silent discharge for same applied voltage. Ozone generation is also increased with increase of applied voltage and decreases with increase of residence time. T. Ohkubol et al. [38] investigated the effect of increased temperature of discharge electrodes on ozone generation and described that ozone generation is decreased due to external heating of discharge wire. Ionic wind also affects the convective heat transfer from discharge wire to the collecting electrodes which ultimately influences the ozone reaction mechanism. Zhi Fang et al. [39] described in their experimental studies and determined the effect of various electrode (wire–cylinder and cylinder–cylinder electrodes) designs on ozone generation. They demonstrated that the wire-cylinder electrodes is more effective in

generating ozone at lower applied voltage while cylinder–cylinder electrodes are more effective in producing ozone at higher applied voltage. Jae-Duk Moon et al. [40] and literature [41] studied the effect of ferroelectric-pellet barrier on ozone generation in point-plate type ESP and stated that concentration of ozone produced is many times higher than without ferroelectric-pellet barrier. They also described that the negative charge DC power produces more ion mobility than the positive polarity. Jae-Duk Moon [43] has found micro discharge on the AC corona-charge surfaces of ferroelectric pellet barrier. They can produce corona discharge twice per half cycle at same applied high voltage as with out pellets. Due to dense discharge from wire and ferroelectric pellets, the plasma reactor has potential to generate increased amounts of ozone but due to high temperature dissociation of ozone also take place. Discharge wires emit the charges and ferroelectric pellets can store charge depending upon relative permittivity. I. Jenei et al. [44] discussed the effect of electrical field and potential distribution on the ozone generation characteristics. S. Parker et al [45] described the mechanism of meshed and plate electrodes with DBD respectively and found experimentally an increasing effect on ozone generation. They also discussed the effect of increasing gap spacing on the discharge corona and increasing effect on ozone generation. Jody et al. [46] described from their experimental analysis that contaminated electrodes produce more ozone in ESP due to back corona in the inter-electrodes region. S. Pekarek et al. [45] also used TiO₂ as photo catalysis and investigated the quantity and its location in the discharge chamber and found that it will increase ozone production and yield.

1.5.3 Reduction of nitrogen oxide and hydrogen supplied with DC-corona

Oxides of nitrogen are constituents of the family of hazardous chemicals. Oxides of nitrogen contribute to acid rain and nitrogen eutrphication, therefore their removal from off-gas is important. J.S Chang et al. [10] investigated the removal of oxides of nitrogen along with other pollutants from off-gas. L K. HENSELM [47] reported that NO_x reduction under negative discharge is several times higher than under positive polarity because of higher generation of ozone. Keeping in view the discharge stability, the negative corona discharge is more stable than positive corona discharge.

Z. Xei et al. [48] discussed a corona process to decompose carbon dioxide from combustion gases with a streamer corona. Decomposition of carbon dioxide generates oxygen molecules which can be utilized for ozone generation simultaneously. Y. I. Chengwu et al. [49] and Yan Wu et al. [50] studied the effect of different process parameter on the removal of sulphur dioxide from off-gas and concluded that removal efficiency increased at higher applied voltage and also calcium to sulphur ratio. Literature [51] focused on pollution control technologies and various reaction mechanisms. Moo Been Change et al. [52] concluded from their investigations that generation of OH radicals increases with increase of oxygen and water vapor in corona atmosphere. Increased OH radical also enhance the removal of sulphur dioxide from flue gas. T. Ohkubo et al. [53] use pipe nozzle discharge electrodes and investigated the effect of gas composition and flow rate on the corona characteristics. Both parameters are significant in reduction of the oxides of nitrogen from off-gas. Their investigations are also helpful to optimize NO_x reduction at low corona power by adjusting the gas composition and gas flow rate. Yukiharu Nomoto et al. [54] recorded the effect of silent-surface hybrid discharge with surface discharge on ozone generation in their investigations. Authors reported that ozone generation efficiency was much higher in silent-surface in hybrid system than of simple surface discharge electrodes at same applied voltage. Hyun Ha Kim et al. [55] concluded from his studies that removal of NO (in lower range) in non thermal plasma reactors is an effective technique. Jae-Woo Chung et al. [56] discussed the removal of NO_x by using some chemicals which are effective to enhance the conversion process and reduce the energy consumption per NO_x molecule. Authors of literature [57] and [58] proposed a model to generate radicals by pulsed corona and their utilization for the removal of off-gas pollutants. Authors also discussed the effect of channel width and discharge wire diameter on NO_x and SO_x removal efficiency. S. Masuda and Nakao [59] experimentally found that positive pulsed corona is effective for SO_x removal while positive pulsed corona is more effective than negative pulsed corona to scrub NO_x from flue gases and use of ammonia enhanced the removal of NO_x. Moo Been Chang et al. [52] demonstrated that removal of SO_x is a function of OH-radicals generation and injection of oxygen and water increase the formation of OH radical's. Yuo et al. [60] investigated the potential difference in DBD (Dielectric barrier discharge) and pulse corona discharge to eliminate hazardous components from air. Their experimental studies focus on the

chemical reactivity of different energy electrons produced during both processes and their effect on generation of radicals. Y. Kawada et al. [61] investigated the effect of gas velocity on the removal of oxides of nitrogen and collection efficiency of electrostatic precipitators along with barrier discharge. Collection efficiency decreases with increase in gas velocity and removal of nitrogen monoxide remains high at all velocities while the removal of nitrogen dioxide is high at low velocity. Literature [78] described mechanism to remove different pollutants from off-gas simultaneously.

1.5.4 Collection efficiency of electrostatic precipitator

The overall collection efficiency of electrostatic precipitators and power consumption is a very important parameter regarding its industrial application. There are many parameters which influence the collection efficiency and performance of electrostatic precipitators. Size and shape of particles is also an important factor, affecting the migration velocity through passive zone to collecting electrodes. Continuous removal of particulates from the collecting electrodes increases the performance of electrostatic precipitators. Inefficient removal of dust particles from collecting electrodes causes scaling and if the resistivity of scaled material is higher than the limit, the charge accumulation causes back-corona which negatively affects the efficiency of electrostatic precipitators [62]. The ion mobility of negative corona is higher than positive corona. The current density at the plate or cylinder for negative corona is also higher than the positive corona at same applied voltage and operation conditions. The collection efficiency and the current/voltage characteristics of electrostatic precipitators also depend upon the magnitude of air flow rate [63]. Proper distribution of the gas and particles in the active and passive zone is required for optimum operation of precipitators. Positive corona from discharge electrodes is uniform and negative corona is in the form of tufts, causing turbulence and turbulence influence on the field intensity and efficiency of precipitators as described in literature [1]-[2]. Gas velocity directly affects the turbulence, gas distribution, migration velocity, residence time of particle, and re-entrainment from the collecting plate [64]. To optimally operate the electrostatic precipitator, it was taken into account that all operation parameters of ESPs are depending on gas velocity. The migration velocity of the particles closely correlates with the collection efficiency. With the increase in gas velocity the migration velocity trend is also increasing but

collection efficiency decreases [65], [1] and [2]. Shape, size and concentration of the particle have a strong influence on the level of charging when applied voltage and ion density is same. Density of particles and increased dust loading has a negative influence on the collection efficiency when electrostatic precipitators are operated under DC-mode [65]. Simultaneous removal of gaseous and particulate emission from flue gas is explained by J. H. Parker [67] and literature [78]. Charging of particles and decomposition of gas is done in a first section of ESP and collection mechanism in a second section of the reactor. The collection efficiency was satisfactory and unwanted gases were also negligible. Y. Kuroda et al. [68] postulated that the collection efficiency is dependent on the discharge electrodes design and the diameter of the holes in plate type discharge electrodes. The collection efficiency of discharge electrodes containing holes was higher than that of plane electrodes under same operating conditions. Collection efficiency also depends on the migration velocity. Migration velocity can be increased by increasing the temperature, voltage field and decreasing the velocity/viscosity of gas [51]. D. Brocilo et al. [69] demonstrated that collection efficiency of spiked discharge electrodes is higher than conventional discharge electrodes. They compared the electric field and ionizing mechanism of submicronic particles in three dimensions by using spiked and rounded wire discharge electrodes under same operation conditions. K. Yamada [70] reported that current/voltage characteristics of negative corona discharge obey the Townsend relation. The on-set voltage is proportional to the reciprocal of product temperature and power of electrodes gap. Literature [71] investigated the effect of geometric parameters on the collection efficiency of electrostatic precipitator and with the change in geometry of discharge electrodes, corona current behavior changed which also lead to affect the collection efficiency.

1.5.5 UV-radiation and hydroxyl radical formation by corona discharge

Mayank Sahni and Bruce R. Locke [72] determined from their experimental investigations that with the increase in applied voltage quantity of hydroxyl radical linearly increased and this also varies with the conductivity of solution used. Multi point discharge electrodes produce active UV-radiation in the discharge region which is the source for generate ozone and hydrogen peroxide in water and gas phase, well explained in literature [73].

1.5.6 Effect of electrical discharge and dielectric barrier discharge (DBD) on photo catalysis

Effect of micro discharge from surface of discharge electrodes is discussed in this section. From different studies and investigations it is extracted that micro discharges are from the sharp surfaces and there are other types of discharges, glow discharge, streamer discharge, filamentary discharge etc. depending upon the surface and shape of wire electrodes. Cheng ron. et al. [74] used modified silicone DBD to change the filamentary discharge and glow discharge into uniform discharge. Y. Nomoto et al. [75] conducted experiments by using different discharge electrodes to improve ozone generation. Hybrid surface and silent discharge increase the ozone yield and concentration. Feasibility study by Yinghui Han [76] for De-SO_x and De-NO_x discussed photo catalysis reaction with plasma. Jerome Taranto et al [77] studied the effect of cold plasma and photo-catalysis on the gaseous effluent treatment.

1.5.7 Summary of literature review

Prediction of use of electrostatic precipitators or corona technology to date is based on semi-empirical correlations and experience. Semi-empirical correlations evolved various parameters and are applicable for limited geometry of discharge electrodes. Experimental investigations and theoretical studies are reported in literature to provide the understanding of corona discharge mechanism, effect of geometry of discharge electrodes on current/voltage characteristics, collection efficiency of ESPs and reduction of hazardous pollutants from off-gas. The effect of dielectric barrier discharge and corona discharge on generation of oxidizing reagents is also well explained.

Effect of geometry of discharge electrodes on ozone generation and production of oxidizing reagents is considered for investigation.

1.6 Task

In this project studies have to be conducted to investigate and model the corona onset field intensity, current/voltage characteristics and the effect of the geometry of discharge electrodes on the operation characteristics of electrostatic precipitators. The current/voltage characteristics of brush type discharge electrodes with different brush diameter as well as wire diameter has to be investigated and modeled.

Modeling is based on state of the art correlations for wire type discharge electrodes following the Peck equation. Ozone generation has to be quantified and modeled for various discharge electrodes and specific operation conditions.

The WESP process has to be applied for investigation of degradation and mineralization of test substances like acetone, iso-propanol, phenol and ethylenediaminetetraacetic acid [EDTA], representing compounds of different classes of substances. The results have to be compared with studies done by Gangl [2006] and Hoislbauer [2009]. The aim is to provide a new integrated process for wastewater treatment and comparison with established advanced oxidation technologies.

2 Design and development of experimental setup

A wet tube-type electrostatic precipitator was designed, constructed and commissioned after review of experimental set ups proposed by various authors [1-80]. Theoretical and experimental boundary conditions regarding operation parameters, design and geometry of the discharge electrode were extensively reviewed. Experimental setup of WESP is equipped with all necessary instruments, control devices and safety installations.

Main focus was to design a new geometry of discharge electrode which can produce an enhanced uniform corona. A brush discharge electrode was designed and manufactured with different design specifications and active length locally in the TVTUT workshop.

Theoretical and experimental techniques are applied to design and develop a model for wet tube-type ESPs with brush discharge electrode. Practical experience and technical expertise was available in-house (my supervisor) and consulted to construct the WESP.

2.1 Basic design empirical correlation for ESPs

Literature [1-3] reports empirical correlations and they were used for the design of the tube type electrostatic precipitators.

2.1.1 Corona onset field intensity

Corona discharge is initiated by exceeding the critical corona field intensity E_0 . For given radius r of the discharge electrode and the relative density δ of the gas the corona starting field intensity E_0 can be estimated empirically, as shown by equation (2-1).

$$E_0 = 3000 \cdot \delta + 90 \cdot \sqrt{\frac{\delta}{r}} \left[\frac{kV}{m} \right] \quad (2-1)$$

With the relative gas density δ

$$\delta = \frac{T_o \cdot P}{T \cdot P_o}$$

Calculated from $T_o = 293$ [K], $P_o = 1013$ [hPa], T : operation temperature [K], P : operation pressure [hPa] and r : radius of the discharge electrode [m]

The corona starting field intensity E_0 does neither consider the gas composition nor the gas velocity v . Experience led to an empirically obtained correction of $[E_{0, \text{corr}}]$ according to equation (2-2) and literature [1]

$$E_{0,corr} = E_{0,calc} * \left(3 + 3 \cdot \ln V - \frac{0.23}{\ln V} \right) \left[\frac{kV}{m} \right] \quad (2-2)$$

Equation (2-2) considers the change of E_0 in the range of gas purging between $0.8 \text{ m/s} < v < 2.5 \text{ m/s}$.

Based on electrostatic SI-units we may apply the following conversion factors:

$$1kV = 1.05 \cdot 10^{-2} \left[\frac{\sqrt{kg \cdot m}}{s} \right]$$

$$1A = 9 \cdot 49 \cdot 10^4 \left[\frac{kg^{0.5} \cdot m^{1.5}}{s^2} \right]$$

The conversion factors are based on the conventional system:

$$1ESL = 1\sqrt{dyn} \cdot cm$$

$$1C = 3 \cdot 10^9 ESL$$

2.1.2 Corona onset voltage

With the corona starting field intensity E_0 the corona onset voltage U_0 can be calculated with equation (2-3) which is specifically applicable for tube-type electrostatic precipitators.

$$U_0 = E_0 \cdot r \cdot \ln \left(\frac{R}{r} \right) \left[\frac{\sqrt{kg \cdot m}}{s} \right] \quad (2-3)$$

R radius of the collector tube [m]

r radius of the discharge electrode [m]

2.1.3 Specific corona current

For low current density the specific corona current I [in terms of A/m] is calculated with equation (2-4) and enhanced corona current at higher applied voltage follows the equation (2-4.1).

$$I = \frac{U_{op} * 2 * K * (U_{op} - U_0)}{R^2 * \ln \left(\frac{R}{r} \right)} \quad (2-4)$$

$$I = \frac{2 * K}{R^2} \left[(U - U_0)^2 + \frac{U_0(U - U_0)}{\ln \left[\frac{R}{r_0} \right]} \right] \quad (2-4.1)$$

Corona current units are [mA/m] and can also be expressed [kg^{0.5}·m^{0.5}·s⁻²]

With the ion mobility K, K = 17 to 21 [m^{1.5} kg^{-0.5} s⁵]. This value of ion mobility is

valid for negative corona polarity. And given operation voltage U_{op} , $U_{Op} =$ operation voltage [$kg^{0.5} m^{0.5} s^{-1}$]

2.1.4 Maximum operation voltage

Maximum operation voltage can be estimated on the basis of distance between two electrodes. Maximum voltage is about 6 to 8 kV/cm of distance between two electrodes and can be expressed as U_{max} and discussed in literature [1]

$$U_{max} = [6 \text{ kV/cm to } 8 \text{ kV/cm} \cdot (R-r)]$$

2.1.5 Collection efficiency/Grade precipitation efficiency

Evald Anderson's pioneering work in 1919 and Walther Deutsch's in 1922, presented an empirical equation for collection efficiency of electrostatic precipitators and known as the Deutsch-Anderson equation. Various authors predicted corrections for given equation but Deutsch equation is still widely applicable and acceptable.

The grade precipitation efficiency $T[x]$ is derived from the Deutsch equation, as represented by equation (2-5).

$$T(x) = 1 - \frac{C(x)_L}{C(x)_E} = 1 - \exp\left(\frac{-2 \cdot W(x) \cdot L}{R \cdot V}\right) \quad (2-5)$$

$T(x)$ grade precipitation efficiency

$C(x)_L$ grade particle content of the off-gas at the exit of the precipitator

$C(x)_E$ grade particle content of the off-gas at the feed of the precipitator

$W(x)$ particle migration velocity [m/s]

V gas velocity [m/s]

L length of the precipitator [m]

x particle size [m]

R radius [m]

V Volumetric flow rate [m^3/s]

2.1.6 Migration rate of particles

The migration rate $W[x]$ is calculated with equation (2-6).

$$W(x) = \frac{E_a \cdot E_p \cdot x}{4 \cdot \pi \cdot \eta} \left[\frac{m}{sec} \right] \quad (2-6)$$

with

E_a discharge field intensity [$\text{kg}^{0.5} \text{m}^{0.5} \text{s}^{-1}$]

E_p precipitation field strength intensity [$\text{kg}^{0.5} \text{m}^{0.5} \text{s}^{-1}$]

x particle diameter [m]

η Dynamic viscosity of the gas [Pas]

For plain discharge electrodes with small diameter [< 1 mm], the discharge field intensity is proportional to the corona starting field intensity E_0 (2-1).

2.1.7 Precipitation field intensity

The precipitation field intensity E_p is derived from the empirically evaluated Equation (2-7).

$$E_p = \sqrt{\frac{2 \cdot I}{K}} \quad (2-7)$$

And discharge field strength (E_a) is

$$E_a = \frac{U_{op}}{b} \quad (2-8)$$

Where b is the distance between discharge and collecting electrode ($R-r_b$)

Basics of electrostatic precipitation and various empirical correlations are extracted from the literature [1, 2].

2.1.8 Components of wet tube electrostatic precipitators

Electrostatic precipitators consist of various components and each component is designed and fabricated by consulting the technical literature [1].

Basically wet tube-type electrostatic precipitators consists of following components

- High voltage power supply
- Discharge electrode (brush type)
- Collecting/counter electrode (tube type)
- Insulators (high grade polymer)
- Water circulation system
- Water distribution system for proper film formation
- Air purging system

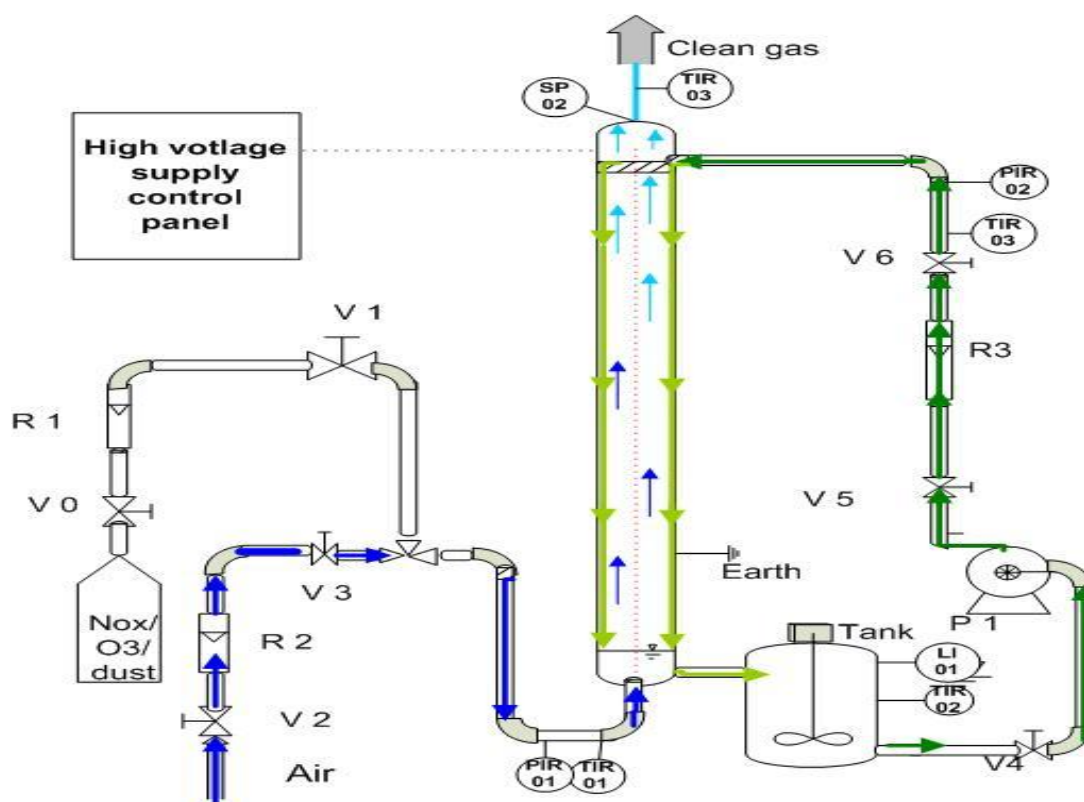


Figure 2: Experimental set up. Collecting electrode (E): Stainless steel; Tube diameter: 66 mm; Tube length: 1500 mm; Discharge electrode (DE): stainless steel, Brush type, with various diameters like 4 mm, 5 mm, 6 mm and 8 mm with 0.1 mm and 0.15 mm diameters of brush wires. Figure 2 shows the direction of phase flow and the water rinsing system.

2.1.9 High voltage power supply

High voltage power supply (HVPS) is a very important, sensitive and highly safety relevant component of WESP. It consists of two compartments; one is the high voltage control panel (HVCP) and the DC-supply to the WESP. Overall system can be described as high voltage power supply (HVPS).

High voltage control panel (HVCP) is equipped with all necessary electrical control devices and detection meters. Digital and analog meters are installed in HVCP to record the current (mA) and voltage (kV). Application range of HVPS is up to 25kV. High voltage supply system can control sparking and sparking is limited by counting the number of sparks over specific time. If sparking too intensive and beyond the sparking limits (set point) then the DC supply will trip and restart automatically.



Figure 3: High voltage electrical control panel and DC power supply 3a and 3b respectively used for energizing the wet electrostatic precipitator

The set point for the sparking limits can be adjusted; it can be increased or decreased. Excessive sparking is disliked, as sparking may damage the components of equipment and also affect the precipitation efficiency. The high voltage power supply is shown in **Figure 3**, 3a is control panel and 3b is the DC-supply unit. The high voltage power supply panel was manufactured by E.C.E Wurmitzer company. Specification of the high voltage power supply panel meets all requirements of WESP and it is capable of tolerating the stress of sparking and continuous operation.

Figure 3 shows an actual high voltage control panel with analog, digital current and voltage meters. A sketch of the front view of the high voltage power supply is shown in **Figure 4** and operation indicators are explained in **Table 4**.

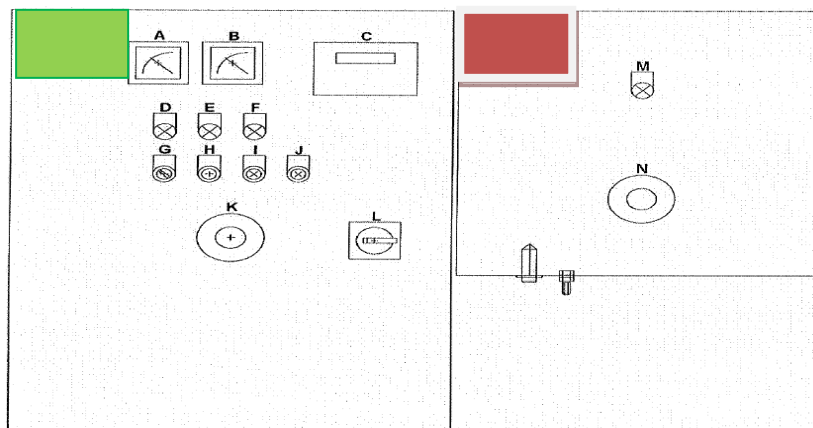


Figure 4: Sketch of the high voltage control panel and DC supply on left and right side respectively.

Table 4: Various functions of the high voltage power supply and control panel

Symbol	Function
A	Applied voltage display [kV]
B	Current [mA] (shows the output current)
C	MPCS panel
D	Indicator with control light ready to start (which shows that voltage regulator is turned on)
E	Indication; system is active (shows that HVPS turned to the operation mode)
F	MPCS error display indicator (shows failure mode or status)
G	Local or remote control switch (We can operate the HVSP from panel (local) or from long distance (remote, DCS (Distribution control system))
H	Reset switch (ready to start again)
I	start power button and indicator (HVPS is on and status "on")
J	Off button and indicator (HVPS is off and status "off")
K	Emergency stop switch
L	Main switch
MA	High voltage indicator (Indication for danger, high voltage is in operation)
N	Emergency stop 2

MPCS is used to control the set points for applied voltage and sparking limits. If the system is shut down due to sparking, the system will automatically restart.

2.1.10 Discharge electrode geometry

The discharge electrode is the heart of an electrostatic precipitator. Emission discharges from discharge electrodes are known as corona discharges. Corona discharge and its intensity totally depend upon the design, size, structure and shape of discharge electrodes. Investigations of various authors [2, 27] on rigid discharge electrodes and several designs of discharge electrodes were critically reviewed before designing the new brush discharge electrodes.

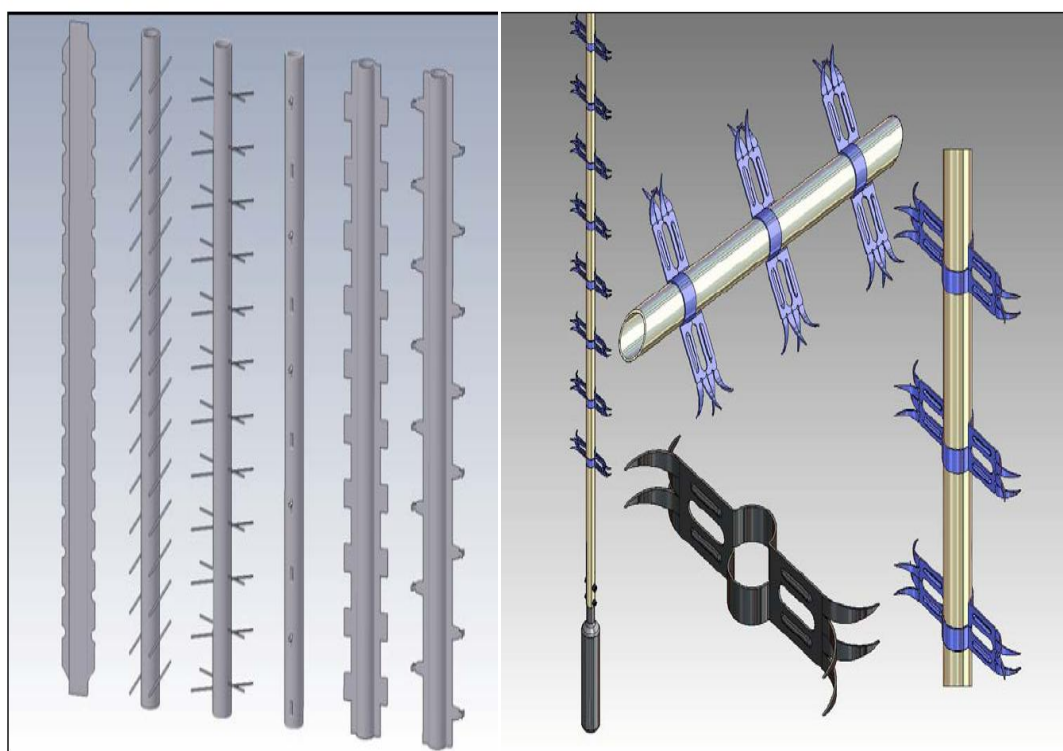


Figure 5: Various geometries of rigid discharge electrodes mentioned in literature [27]

Keeping in view the state of the art design and geometries, a brush type discharge electrode was designed and its current/voltage characteristic was compared with others.

Types of discharge electrodes investigated, shown in **Figures 6** through **13** were:

- Wire type
- Screw type
- Rod type (larger diameter than wire)
- Brush with 500 mm active length at bottom
- Partial brush type and partial rod type with different arrangements (700 mm)
- Complete brush type discharge electrodes (1500 mm)



Figure 6: Tungsten wire discharge electrode of 0.15 mm diameter



Figure 7: Screw type discharge electrode (3 mm)



Figure 8: Rod type discharge electrode (Copper coated)



Figure 9: Rod type discharge electrode (stainless steel).



Figure 10: Brush type discharge electrode (stainless steel 4 mm diameter)



Figure 11: Brush type discharge electrode (stainless steel 5 mm diameter)



Figure 12: Brush type discharge electrode (stainless steel 6 mm diameter)



Figure 13: Brush type discharge electrode (stainless steel 8 mm diameter)

No doubt, impact of geometry of discharge electrode on current/voltage characteristic is significant. Therefore impact of design of discharge electrode was investigated under various operation conditions like voltage, batch operation (still air) and flow conditions. Flow condition was further investigated under different air and water flow rate to get the optimum operation conditions for specific discharge electrodes.

The geometric specification of various investigated discharge electrodes are summarized in **Table 5**. Discharge electrodes are classified in terms of active length, diameter of electrodes and type of discharge electrodes.

Table 5: Type of discharge electrodes under investigation and their specification

Electrode type	Dia.[mm]	Surface	Active length[mm]
Tungsten wire	0.15	plain	1500
Screw type	3	threaded	1500
Rod type(S.S)	3	plain	1500
Rod (copper)	3	coated	1500
Brush type	4	Wire(0.1mm, 0.15 mm)	500, 700, and 1500 mm
Brush type	5	Wire(0.1 mm, 0.15 mm)	500, 700, and 1500 mm
Brush type	6	Wire(0.1 mm, 0.15 mm)	500, 700, and 1500 mm
Brush type		Wire(0.1 mm, 0.15 mm)	500, 700, and 1500 mm

2.1.11 Collecting/Counter electrode

A stainless steel tube of 66 mm internal diameter was used as collector or counter electrode. Each and every part of the whole equipment was earthed. The collecting stainless steel tube holds the insulator for the discharge electrode to keep it apart from the collecting electrode. The stainless steel tube was fabricated as per technical design requirement of equipment already mentioned in literature and it was completed in the institute workshop. The sketch of the counter electrode is shown in **Figure 14** and dimensions (length, radius and wall thickness of collector) are well explained.

Table 6 explained the calculation of total volume and total surface area of the collector available with specific length of the collector. Total volume of the collector is described in m^3 and surface area in m^2 .

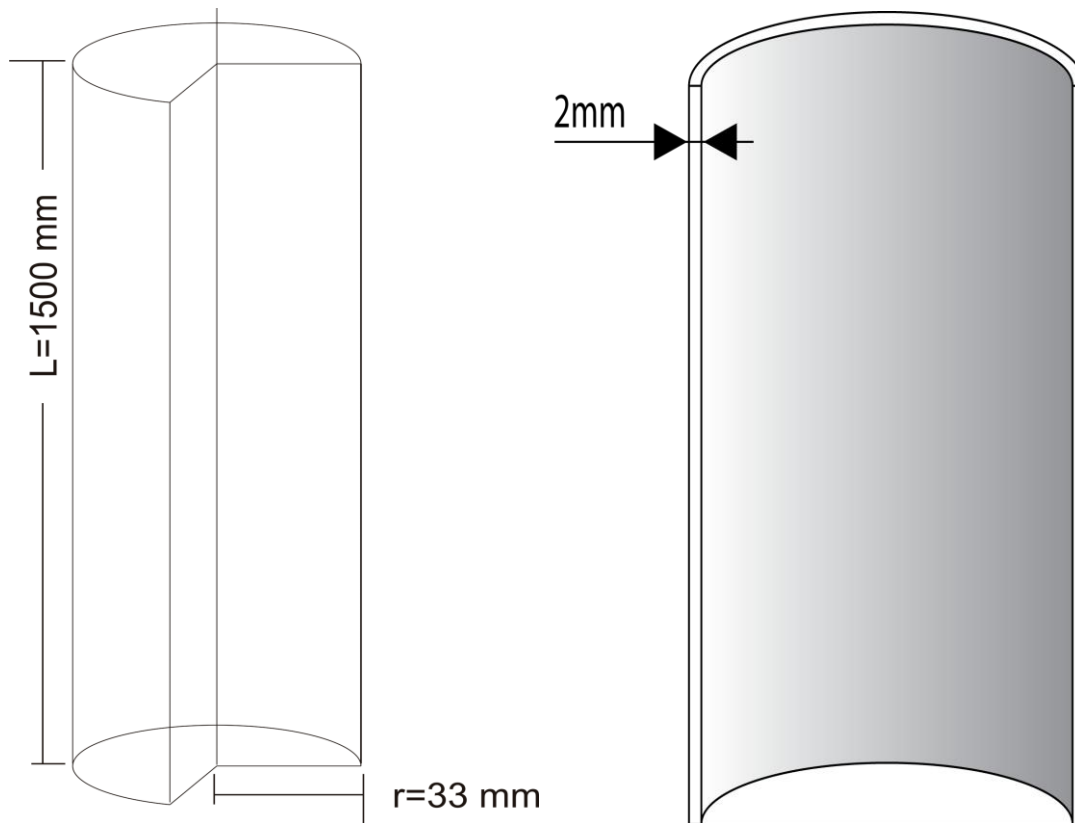


Figure 14: Tube type counter charged electrode (stainless steel 66 mm internal diameter, length 1500 mm and wall thickness 2 mm) used for investigations

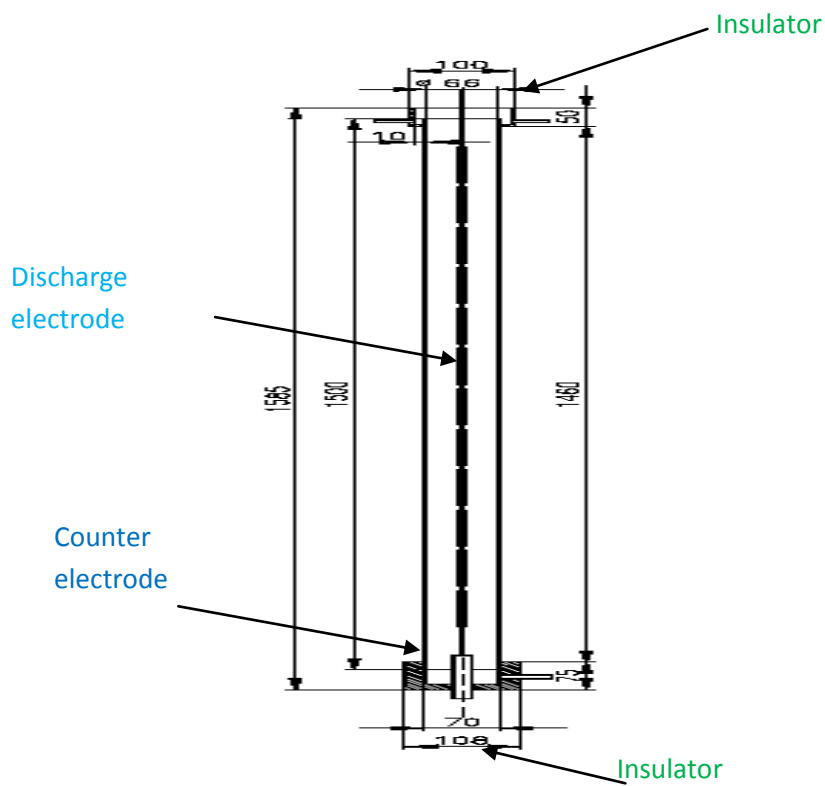


Figure 15: Sketch of the ESPs with brush discharge electrode and collecting electrode made of stainless steel.

Table 6: Total volume and surface area of collector

Total volume of collector (V_t)	surface area of collector (A_c)
$\pi * R^2 * L$	$2 * \pi * R_i * L$
0.005134 m ³	0.00707 m ²

Where

V_t = Total volume of collector [m³]

$R=R_i$ = Radius of collector[m]

L = length of collector[m]

A_c = Internal surface Area of collector [m²]

D_i = Internal diameter of collector[m]

To extend investigations and the application range regarding material selection, a glass tube collector was designed, constructed and fitted with similar discharge electrodes as used in the stainless steel collector [91]. For the glass tube collector a continuous water rinsing film is necessary to develop the current/voltage characteristics. The specification of the glass tube collector with various fitting arrangement is shown in **Figure 16**.

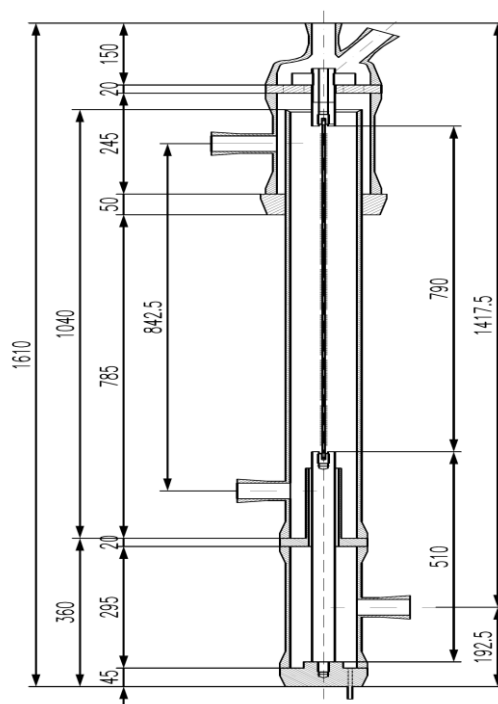


Figure 16: Sketch of the WESP with brush-type discharge electrode with glass- tube collector.

2.1.12 Insulators

Performance and smooth functioning of electrostatic precipitators also depends upon complete electrical insulation of the discharge electrode from collector, therefore the insulator must be able to separate the collector for the applied potential difference, even to avoid tracking and short circuiting as well.

Two insulators were used to hold the discharge electrode, one at the bottom and the second on top of the WESP as shown in **Figure 17**. Insulators were designed and fabricated locally in the TVTUT workshops. Insulators are capable to withstand the stress of high voltage, temperature and corrosive liquids. Material of insulators is high grade polymers (Teflon or HD polyethylene).

Insulators are designed in such a way that they can work as water distributor at top to devolve a water film and a receiver at bottom of ESP.

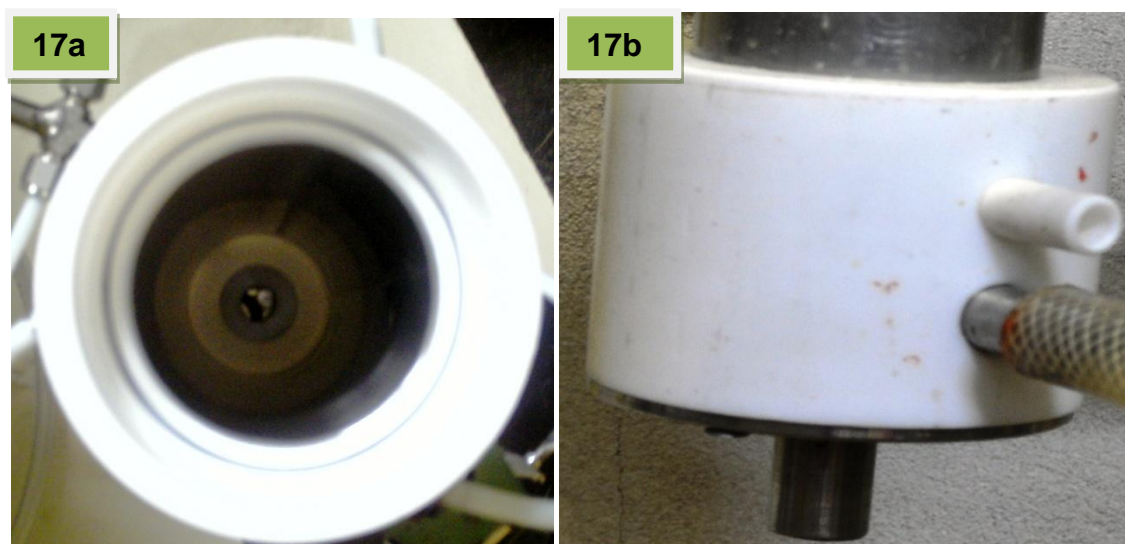


Figure 17: Water distributor to form a proper water film (17a) and water collector (17b) collect the falling water and flush to the circulation tank. Water distributor and collector are manufactured with high grade polymer (Teflon). This high-grade polymer is also used as insulator.



Figure 18: Complete film developed during the operation of WESP (water is circulated from top)

2.1.13 Water circulation and flow rate calculation

Target was to investigate the degradation of pollutants in waste water; therefore water circulation is designed to meet the technical requirement of process water manipulation to flush the collected particles from the surface of the collector. A circulation loop of water was established with adjustable flow rate as per process requirements to develop a thin film on the surface of the collecting electrode. The water circulation system consists of circulation tank, centrifugal pump, flow meter, control valves and recycle flow arrangement, temperature measuring points, pH and sampling points from circulation tank. An overflow weir was maintained on top of WESP and a collector at the bottom. The system was operated with designed and calculated water injection; neither splashing nor hold up of water was observed during investigations.

The rule of thumb for flow rate and to develop a complete film in the collector tube was calculated as. Water flow rate for complete film formation = $1-1.4 \text{ m}^3/\text{h}$ per meter circumference = $1 \text{ m}^3/\text{h}$ per meter circumference = $1 * 2 * \pi * r = 0.200 \text{ m}^3/\text{h}$

2.1.14 Film formation in the tube

A continuous and uniform water film was maintained to displace the collected particles on the inner surface of collector. Flow rate was adjusted to renew the film continuously. The water was collected in the circulation tank and continuously fed to the water distributor as shown (17a) and complete film formation is demonstrated in **Figure 18**.

During the process the film was maintained which is usually possible with luminary flow. Forces are acceleration due to gravity which is used to calculate the pressure drop and the form of equation is (2-9) as

$$\rho \cdot g = -\eta \frac{d^2 w}{dx^2} \quad (2-9)$$

After integration (2-9) and applying the boundary conditions on film thickness

$$x = 0 \Rightarrow \frac{dw}{dx} = 0$$

$$x = \delta \Rightarrow w = 0$$

On integration

$$-\eta \frac{dw}{dx} = \rho \cdot g \cdot x, \quad -w = \frac{\rho \cdot g}{\eta} \cdot \frac{x^2}{2} + C_2, \quad C_2 = 0 - \frac{\rho \cdot g \cdot \delta^2}{2 \cdot \eta}$$

Eliminating C_2 we got equation ((2-10)

$$w = \frac{\rho \cdot g}{2 \cdot \eta} \delta^2 - x^2 \quad (2-10)$$

To calculate the throughput of water according to equation (2-11), the velocity integrated over x and y multiplied by the width of the film

$$\dot{V} = y \frac{\rho \cdot g}{2 \cdot \eta} \left(\delta^2 \int_0^\delta dx - \int_0^\delta x^2 dx \right) = y \frac{\rho \cdot g}{2 \cdot \eta} \left(\delta^3 - \frac{\delta^3}{3} \right) = y \frac{\rho \cdot g}{3 \cdot \eta} \delta^3 \quad (2-11)$$

The average flow rate is given in equation (2-12)

$$w_m = \frac{\dot{V}}{y \cdot \delta} = \frac{\rho \cdot g}{3 \cdot \eta} \delta^2 \quad (2-12)$$

The characterization the shape of film through water flow rate and Reynolds number is expressed in Equation (2-13).

$$Re = \frac{w_m \cdot 4 \cdot \delta \cdot \rho}{\eta} \quad (2-13)$$

Water flow in the tube can be classified on the basis of Reynolds number. With specific Reynolds number (for laminar flow), we can determine the film thickness. In WESP water film flow is usually from top to bottom and gas stream is moving up. This gas flow affects the film surface, which is not covered by the Reynolds number of the liquid. By friction the gas flow speed is reduced to $x = 0$ to a certain extent. At high gas velocity, the water film surface is open or film de-structured.

Table 7: Change of type of water flow with Reynolds number

Reynolds number	Type of flow
$Re < 20$	Smooth surface
$20 < Re < 1000$	Laminar flow
$1000 < Re < 1500$	Transitional flow
$Re > 1500$	Turbulent flow

2.1.15 Air purging system

The wet ESP is designed for air purification and water treatment simultaneously. Air is purged from the bottom of the WESP without creating any turbulence. Gas was fed through flow measuring and pressure regulating devices in order to control the

whole process.

Air purging/distributor was designed and fabricated very carefully. The air distributor was capable of providing a homogenized and uniform purging of air in WESP. Laminar air flow is preferred over turbulent. Turbulent air purging may decrease efficiency of ESP. A suitable purging pressure and air velocity is required for investigations and smooth operations of WESP.

Ionization of air molecules and dust particles is shown in **Figure 19**. Active and passive zones are also described and classified.

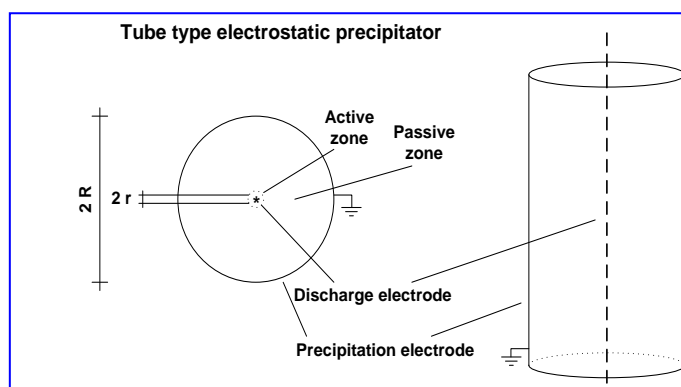


Figure 19: Shape of tube type electrostatic precipitator. The discharge electrode is located in the centre and the tube forms the counter electrode.

2.1.16 Summary

A wet tube type electrostatic precipitator with brush discharge electrode was designed and developed. It is efficient in removing sub micron and sticky particles from off-gas.

Brush discharge electrodes (with different geometry of wire) were designed and constructed. Brush discharge electrodes with various diameters like 4 mm, 5 mm, 6 mm and 8 mm were fabricated with different active lengths (500 mm, 700 mm and 1500 mm) for investigation. Wires of various diameters (0.1 mm and 0.15 mm diameters) were used for fabricating the brush discharge electrode and to validate modeling.

Keeping in view the operation voltage and design limitation, stainless steel tube ($D_i=0.066$ m, $L=1.5$ m) and glass tube ($D_i=76$ mm) was selected as collecting electrode. With suitable water rinsing, the glass tube is as effective as the stainless steel collecting electrode. Air purging, water circulation and insulator were designed with suitable high grade polymer.

3 Chemicals and analytical techniques

Various chemicals were used for investigations. The specification of different chemicals are compiled and extracted from the thesis of Hoislbauer (2009) [90]. Solutions of various chemicals were prepared as per process needs and used for investigations.

3.1 Ethylenediaminetetraacetic acid (EDTA)

Formula:	$C_{10}H_{16}N_2O_8$
Molecular weight:	292.24 g/mol
Melting point:	>150 °C
Boiling point:	Decomposition
Solubility in water:	0.5 g/l at 25°C
Appearance:	Colourless crystals
Use:	Chelating agent for metals, food industry etc
Analysis:	HPLC (Column: Agilent Technologies RP18 type, Mobile phase: Tetra butyl ammonium hydrogen sulfate and tetra butyl ammonium-solution; flux= 1 ml / min, UV / VIS absorption at 260 nm)TOC, GC (Agilent 19091X-116, HP-Wax Bonded Polyethylene Glycol; FID Detector)

3.1.1 Preparation of EDTA solution

The EDTA solution was prepared by dissolving 0.5 g/l of EDTA and 7.01 g/l of Na_2SO_4 (0.05 molar) in de-ionized water. 5 g of EDTA and 71.1 g sodium sulphate was dissolved in 10 litre of water to prepare the required volume of EDTA solution. The pH of EDTA solution was measured with pH meter (WTW pH 522) and pH recorded was 5.4 to 5.5.

Degradation of EDTA in solution was investigated at various pH values. From photochemical EDTA degradation a strong effect of the pH value on the rate of degradation is known [Gangl-thesis [92], Zelenka-thesis [93]]. **Figure 20** shows the predominant species of EDTA for several pH values.

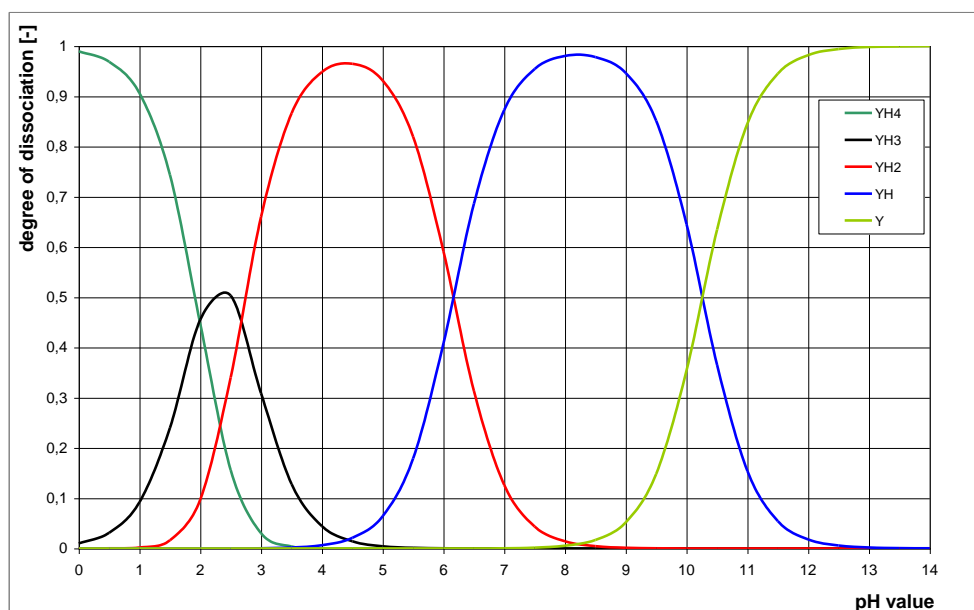


Figure 20: Domain of EDTA dissociation species vs. pH-value; $T = 293\text{ K}$

pH 2.5 was maintained by adjusting with H_2SO_4 and pH 12 was achieved by adjusting with NaOH solution. The EDTA solution was circulated in the wet tube-type electrostatic precipitators. Circulation of EDTA solution was controlled with a flow meter installed in the test facility as shown in **Figure 2** (design and development, chapter 2) and flow of water was adjusted over range of 40 to 70 l/h as per process requirement. Samples were taken from the circulation tank and preserved in the cooling box for analysis. Samples were analyzed to determine TOC change and cleavage of EDTA.

The effect of Fe (II) and Fe (III) on degradation of EDTA was also investigated. A solution of 1 mol of EDTA and 2 mol of ferric sulphate was also prepared (sodium sulphate was not used) for that purpose.

3.2 Phenol

Formula:	$\text{C}_6\text{H}_6\text{O}$
Molecular weight:	94.11 g/mol
Melting point:	43 °C
Boiling point:	182 °C
Solubility in water:	0.5 g/l at 25°C
Description/appearance:	white crystals
Use:	For the production of phenolic resins

Analysis: GC (Agilent 19091X-116, HP-Wax Bonded Polyethylene Glycol; FID Detector) TOC

3.2.1 Preparation of phenol solution

A suitable amount (keeping in view solubility) of phenol was used to prepare the phenol solution. 4.5 g of phenol was thoroughly mixed in 10 l of de-ionized water. Phenol solution was circulated in WESP and flow was controlled with flow meter as per process needs.

Degradation of phenol was investigated at specific applied voltage and corona current. Samples were taken after regular intervals of time and change in pH was also monitored.

3.3 Acetone

Formula: C_3H_6O

Chemical structural formula:
$$\begin{array}{c} \text{O} \\ || \\ \text{CH}_3-\text{C}-\text{CH}_3 \end{array}$$

Molecular weight: 58.08 g/mol

Melting point: -95.35°C

Boiling point: 56.2°C

Solubility in water: Completely miscible

Appearance: colourless

Use: For the production of methyl methacrylate and cleaning etc.
agent and as solvent

Analysis: GC (Agilent 19091X-116, HP-Wax Bonded Polyethylene Glycol; FID Detector) TOC

3.3.1 Acetone solution preparation

The acetone (0.5 g/l) was thoroughly mixed with de-ionized water and 10 l of acetone solution was prepared. Acetone solution was circulated in wet tube-type electrostatic precipitator and circulation of acetone solution was adjusted over the range of 40-70 l/h as per requirements.

Acetone solution of same concentration was again prepared and used in photochemical degradation by low pressure mercury lamp (UV/VIS) irradiation to validate the performance of wet tube-type electrostatic precipitators.

3.4 Iso-propanol

Formula:	(CH ₃) ₂ CHOH or (C ₃ H ₈ O)
Molecular weight:	58.08 g/mol
Density	0.786 g/cm ³ (20 °C)
Melting point:	-89 °C
Boiling point:	82.5°C
Solubility :	Miscible in water, Benzene
Appearance:	Colorless Liquid
Use:	As solvent and cleaning liquids,
Analysis:	HPLC (Column: Agilent Technologies RP18 type, Mobile phase: Tetra butyl ammonium hydrogen sulphate and tetra butyl ammonium-Solution; flux= 1 ml / min, UV / VIS absorption at 260 nm)TOC

3.4.1 Iso-propanol solution

Iso-propanol was mixed with de-ionized water. An appropriate concentration of iso-propanol (2 ml/l) 20 ml was thoroughly mixed in 10 litre of water. Iso-propanol solution was also treated similarly as discussed above.

3.5 Potassium iodide

Formula:	KI
Molecular weight:	166.0028 g/mol
Density	3123 g/cm ³ (20 °C)
Melting point:	681 ° C
Boiling point:	1330 ° C
Solubility :	140 g/100 ml(20°C) water, 2 g/100 ml(ethanol) soluble in acetone
Appearance:	White crystalline solid
Use:	As source of iodide,
Analysis:	

3.5.1 Potassium iodate

Formula:	KIO ₃
Molecular weight:	214. 001 g/mol
Density	3.89 g/cm ³
Melting point:	560 ° C decomposition
Boiling point:	560 ° C decomposition
Solubility :	4.74 g/100 ml(0°) 32.3 g/100 ml (100 ° C)
Appearance:	White crystalline powder
Use:	As source of iodine,
Analysis:	

3.5.2 Solution preparation for actinometrical measurement

A solution of 0.6 molar potassium iodide (KI) and 0.1molar potassium iodate (KIO₃) in 0.01 molar borax (Na₂B₄O₇·10H₂O) can be used as a chemical actinometer with UV-radiation mainly at 254 nm irradiation. Potassium iodide, iodate solution was prepared in 5l flask very carefully and wrapped with aluminium foil. To determine the accuracy of chemical actinometric changes in the WESP and to avoid the effect of natural light intrusion, proper wrapping of equipment was also ensured as shown in **Figure 21**.

The actinometric solution was optically opaque at a wavelength of 290 nm and optically transparent at wavelength of 330 nm. Impact of UV-radiation on potassium iodide, tri-iodide was formed. The concentration of tri-iodide formed shows the quantum yield in the WESP and hence WESP also worked as a photo reactor. Potassium iodate acts as an electron collector (scavenger) and prevents the back reaction of electrons with free iodine. Borax was used as a buffer and ensures that the pH of the actinometer solution during the photochemical reaction remains constant at pH=9.25.

At time of preparation the colour of actinometric solution was colourless and during the process of radiation from discharge electrode its colour was changed via brown to dark brown (tri-iodide formation). Solution pH was increased with time and with change of colour during the process.



Figure 21: wet electrostatic precipitator in operation for actinometric measurements; the equipment was properly wrapped in aluminium foil. Prof. Dr. M. Siebenhofer is inspecting the operation of WESP.

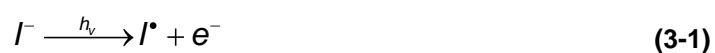


Figure 22: pH meter used for measurement of the pH changes during operation.

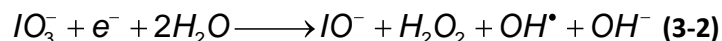


Figure 23 TOC analyzer used to measure concentration of organic carbon in terms of TOC in treated samples.

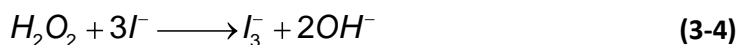
Photochemical excitation of potassium iodide results in the formation of iodine atoms and electrons dissolved.



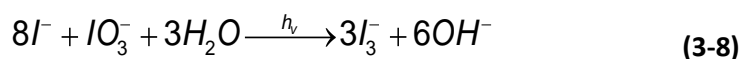
In the presence of potassium iodate, hypo-iodite, hydrogen peroxide, hydroxyl radicals and hydroxide are formed



Other basic reactions for the formation of tri iodide are



Overall reaction is summarized [89]



Specifications and working principle of Shimadzu TOC 5000A

Analyte	TC, IC, TOC (TC-IC), NPOC (non-purge able organic carbon), POC (purge able organic carbon: option)
Method	Combustion/non-dispersive infrared gas analysis method) Combustion temperature 680° C
Measuring range	4 ppb to 4000ppm (to 5000 ppm for IC) (POC: Max 400ppm)
Average analysis time	2 to 3 minutes for both TC and IC (4.5 minutes for TC and 3.5 min. for IC at the longest)
Repeatability	Standard deviation is less than 1% of full scale for the range less than 2000 to 4000 ppm (from 2500 -5000 ppm for IC)
Sample introduction	Automatic injection via micro-litre syringe
Sample injection volume	500 to 2000 μ l with a 2500 μ l syringe, 4 to 250 μ l with a 250 μ l syringe

Pre-treatment for IC	Automatic sparging function
Carrier gas	Cylinder of ultra-high purity air or oxygen; about 6 kg.f/cm ₂ (7 kg. f/cm ₂ max.) in supply pressure; 150 ml/min. in flow rate (300 ml/min. including sparging)
Data processing	<ul style="list-style-type: none">• Detector signal• Linearization, baseline correction, peak detection, and area calculation• Data• Calculation of concentration using one-point to four-point calibration curve; automatic selection of best calibration curve; store up to 18 calibration curves; automatic exclusion of anomalous value(s) and automatic re-analysis/re-calculation; calculation of standard deviation and coefficient of variation, when response goes off scale.

3.5.3 Ozone measuring in water and air

As already discussed water was circulated during operation of ESP and ozone was transported from gas phase to liquid (water) by absorption. To determine the ozone content in water a spectrophotometer was used. The specifications are given below. UV/VIS-Spectrophotometer with reference detector technology (RDT)]

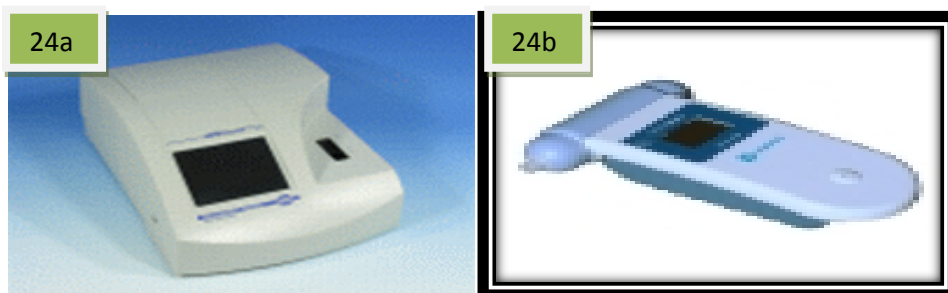


Figure 24: spectrophotometer used for measurement of ozone absorbed in water and in gas with 24a and 24b respectively.

The NANOCOLOR® UV/VIS from MACHEREY-NAGEL is a powerful UV/VIS spectrophotometer with mono-chromator (190-1100 nm) for universal use in all areas of water and waste water analysis. This includes municipal, industrial waste water, drinking water, process water, surface water, ground water as well as cooling and boiler feed water.

4 Characterization of partial and complete brush discharge electrodes

This section summarizes the characteristics of partial and complete brush type discharge electrode (5 mm, 0.15 mm) under various operation modes.

4.1 Corona generation with brush type discharge electrodes

Corona discharge is obtained by constructing an electrical field between a (thin) discharge wire (discharge electrodes) with negative/positive or alternating polarity and an earthed tube as a counter electrode. Installation was equipped with a high voltage power supply to provide sufficient operation voltage to achieve the critical field intensity. Above this critical field intensity corona current started to flow which was measured through ampere meter installed in the high voltage power supply.

For low current density the specific corona current I [in terms of A/m or electromechanical SI units] is calculated with Equation (2-4) and was discussed in chapter 2. **Table 8** illustrates the low and high current density equations.

Within the range of corona discharge, (initiated at the corona onset voltage and limited by the sparking voltage or break-through voltage) zones of high field intensity are visible by forming a regularly shaped (positive corona) or irregularly shaped (negative or alternating corona) bluish plume. The image of negative corona from brush type discharge electrodes is shown in **Figure 25**.

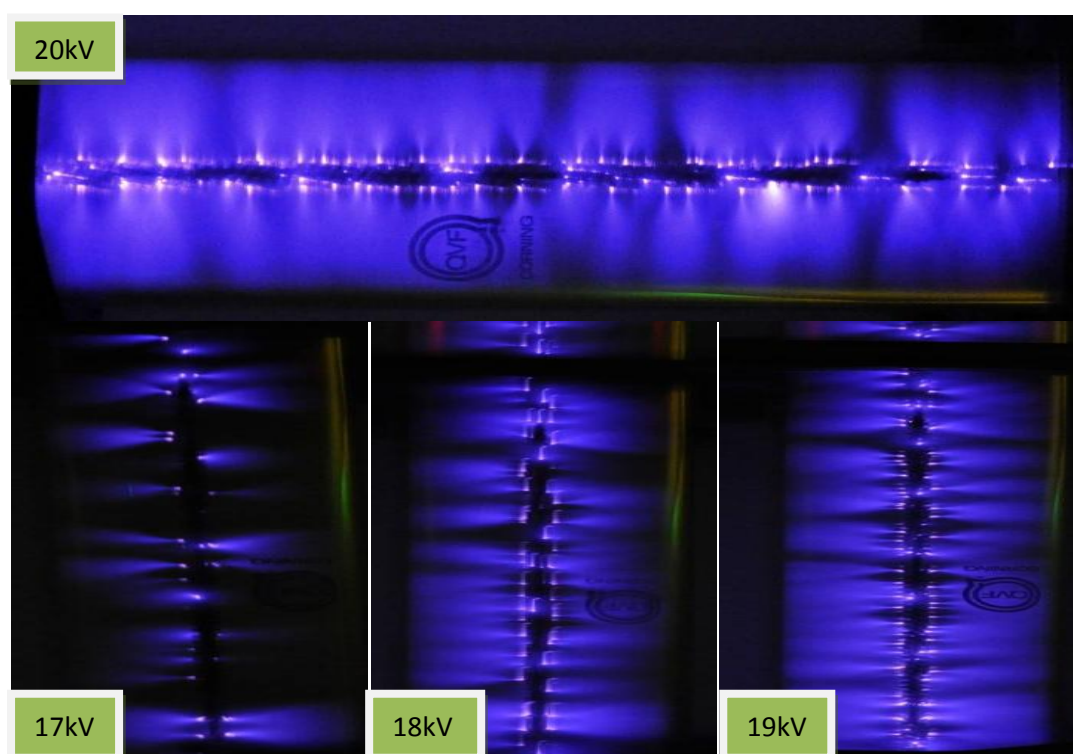


Figure 25: Image of uniform corona generation with brush type discharge electrodes at ambient conditions and at 17- 20 kV applied voltage

Table 8: Basic empirical correlation for calculation of low and high corona current

Low current	$I = \frac{2 * K * U * \left[\frac{U - U_0}{R^2} \right]}{\ln \left[\frac{R}{r_0} \right]}$
High current	$I = \frac{2 * K}{R^2} \left[(U - U_0)^2 + \frac{U_0 * (U - U_0)}{\ln \left(\frac{R}{r_0} \right)} \right]$

During the discharge process, an elevated number of positively and negatively charged particles are formed and migrate to the counter-charged electrode. Motion of particles from passive region to the counter electrode mainly depends upon the field intensity and size of particles. Any particle passing this field will be discharged within very short duration (milliseconds) by intensive ion impact. The electrical field of an electrostatic precipitator is carrier of approximately 10^8 negatively charged particles per cubic centimeter. For comparison, a dense aerosol is carrier of some 10^5 particles per cm^3 ($100 \mu\text{g}/\text{m}^3$; $x_T = 1 \mu\text{m}$).

Moreover particle motion is promoted by Coulomb-force which is proportional to the product of the charged particle times the electrical field. Coulomb-force is counteracted by inertia and friction force. While inertia force may be neglected, friction force, described by Stokes Law, determines counter action. The resulting particle migration is, therefore, controlled by Coulomb-force and by Stokes-force. It is called the rate of migration and it is about 3 to 20 cm/s in the mean. Process performance is based on the ratio of electrode distance to the rate of migration versus residence time. The ratio must be less than the ratio of the length of the precipitator and the gas velocity.

4.1.1 Characterization of brush type discharge electrodes

A partial brush type discharge electrodes was investigated to characterize the specific design of discharge electrodes under various applied conditions. Investigations were conducted with various diameters of brush type discharge electrodes (partial, complete and with other various design schemes of brush type discharge electrodes) with various diameters of brushing wires.

4.1.2 Current/Voltage characteristic

The performance of electrostatic precipitators is expressed in terms of collection efficiency of particles for specific energy consumption. Collection efficiency of ESPs is based on various factors and the main commanding parameter is the field intensity and corona current. Basic intention is to design and develop a discharge electrode with enhanced discharging properties and capable of generating a uniform corona. Mechanically strong and long life design which can also provide the ease in operation is also taken into account. Various authors [1-6, 27] investigated different discharge electrodes and experimental investigations show that geometry and configuration has direct relation with corona discharge. Their Investigations showed that geometry of discharge electrode has an enhancing effect on collection efficiency of electrostatic precipitators.

Current/voltage characteristics of any discharge electrode basically give the information for its geometry, configuration and distance from counter electrode. Application range of ESPs can be explained from applied voltage and corona current behavior. Investigations of this project are helpful to characterize brush type discharge electrodes. Various brush type discharge electrodes (with various discharging wires) were fabricated and developed in the TVTUT workshop. All other components of tube-type electrostatic precipitator were also designed, fabricated and commissioned in the premises of TVTUT TU Graz.

Brush type discharge electrodes with various specifications were designed to elaborate and broaden the aspect of investigation in the field of electrostatic precipitation. Brush discharge electrode of 5 mm diameter with 0.15 mm diameter of brush wires were investigated under three different design schemes to generate the current/voltage data under batch and flow modes. These schemes are named as

- Active length at bottom (500 mm)
- Partial brush type discharge electrodes (700mm)
- Complete brush type discharge electrodes (1500mm)

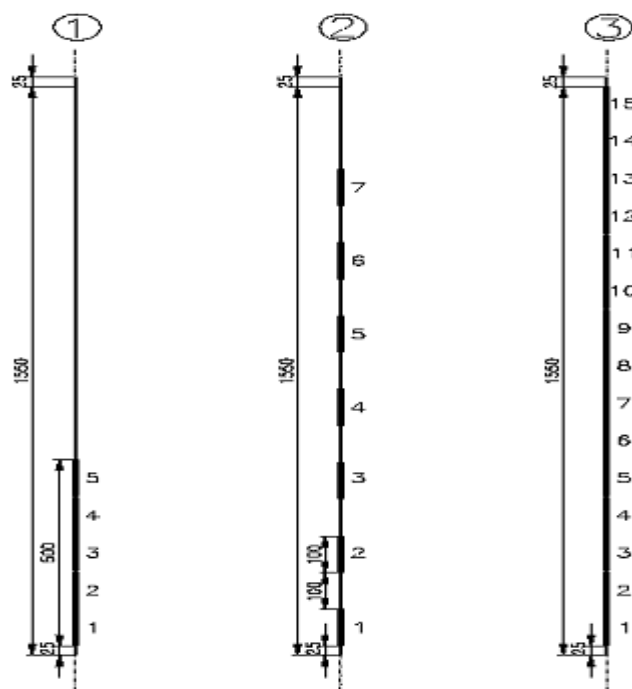


Figure 26: Different design of brush discharge electrodes. Electrode at position 1 is of 500 mm length, installed at bottom, electrode at position 2 is partial brush (700 mm) and electrode at position 3 is complete brush (1500 mm).

4.1.3 Partial brush type discharge electrodes (active length 700 mm)

Partial brush type discharge electrode was designed to decrease the active length of discharge electrode without decreasing the length of electrostatic precipitator. Partial brush type discharge electrodes was designed and fabricated as shown in **Figure 26** at position 2. Total length of discharge electrodes was 1500 mm and active length was 700 mm as mentioned and shown in the experimental setup **Figure 2**. [Mechanical sketch of partial brush type discharge electrodes is so far described as; 100 mm active brush length then 100 mm plain twisting wire length and finally 700 mm brush length and 800 mm twisting plain wire length lead to 1500 mm total length]. Active length of partial brush discharge electrodes effectively generates corona discharge from brushing wires to ionize gas molecules and particulates. Corona discharge from plain twisting wire length was very small or negligible and was not comparable with discharging intensity of brush type discharge. Therefore twisting wires did not contribute to corona generation.

Experiments were conducted under batch and various air flow conditions to characterize the partial brush type discharge electrodes. Experimental Investigations for current/voltage behavior was monitored and explained below in **Figure 27**. **Figure**

27 also explains the behavior of partial brush type discharge electrodes in terms of corona current against applied voltage at 10 to 20 kV.

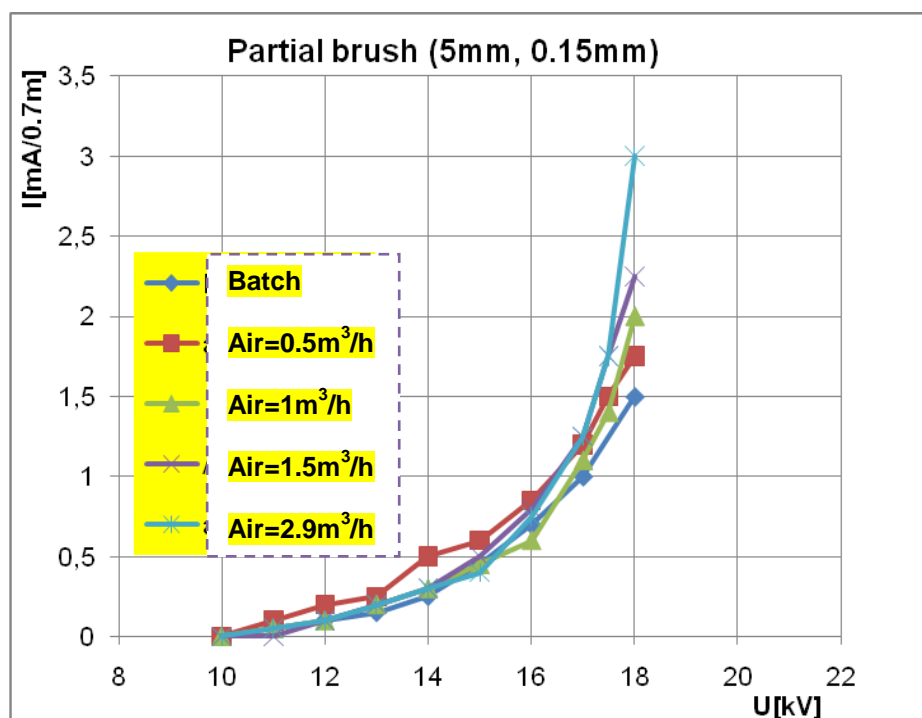


Figure 27: Comparison of current/voltage characteristics with partial brush type discharge electrodes with active length of 700 mm with 5 mm diameter and 0.15 mm wire diameter. Discharge electrodes and counter electrodes are of stainless steel. Investigations were conducted at ambient conditions with and without air purge mode.

4.1.4 Discussion of the results of partial brush discharge electrodes (5 mm diameter and brushing wire 0.15 mm)

The partial brush type discharge electrodes with active length of 700 mm (5 mm diameter and 0.15 mm diameter of brush wires) were investigated to develop the current/voltage relationship under batch and various air purge modes at ambient conditions. Investigations were conducted over the range of applied voltage of 10 to 18 kV with test facility as shown in **Figure 2** (chapter 2) and an increase in corona current was observed with increase in applied voltage. During stable operation corona current was observed to develop a true relation with applied voltage for a specific partial brush type discharge electrodes.

Experimentally observed data with partial brush type discharge electrodes was used to construct current/voltage curves as illustrated in **Figure 27**. Effect of batch and air flow modes on current/voltage curves is explained in section below (4.1.5 to 4.1.7).

4.1.5 Batch

Proportional increase in corona current was observed with increase in applied voltage over the range of 10-18 kV under batch mode (without water and air injection). It was observed that increase in corona current was very slow over the applied voltage of 10 to 15 kV. Corona current observed at 15 kV applied voltage was 0.5 mA with partial brush type discharge electrodes under batch mode. Relatively higher increase in corona current was observed from 16-18 kV as compared with 10-15 kV applied voltage. Experimentally observed corona current at 18kV was 1.5 mA. At higher applied voltage (16 to 18 kV) an increase of corona current per increase in 1 kV was 0.5mA which was approximately five times higher than increase of corona current at 10-15 kV applied voltage.

4.1.6 Various air purging condition

Effect of air flow was determined with partial brush type discharge electrodes with various air purging conditions. Current/voltage relationship curves were constructed with the experimentally observed data with partial brush type discharge electrodes and air purging of 0.5 m³/h, 1 m³/h, 1.5 m³/h, and 2.9 m³/h. Trend of corona current with increasing applied voltage was closely observed to classify the change in current/voltage behavior and to characterize the partial brush discharge electrodes with specific geometric parameters.

4.1.7 Low air purging

A very low flow (0.5 m³/h) of air purging was established from the bottom of partial brush tube-type electrostatic precipitator. Change in corona current was monitored with the increase in applied voltage at various air purging modes at ambient conditions. Increase of corona current at 10 to 16 kV applied voltage with 0.5 m³/h air purging was higher than corona current generated with batch mode. Corona current at 15 kV with 0.5 m³/h air injection was 0.75 mA while corona current under batch mode was 0.5mA under similar applied conditions. Increase of corona current with 0.5 m³/h was observed due to enhanced ionization mechanism of air molecules constructing the path to the counter electrode. Air with minimum purging forces helps to construct better corona current as compared to batch mode because of less local space charge. Corona current at higher applied voltage 16-18 kV was also higher compared with corona current with batch mode as shown in *Figure 28* and it was 1.75 mA. Current/Voltage curves under air purging conditions were not so smooth.

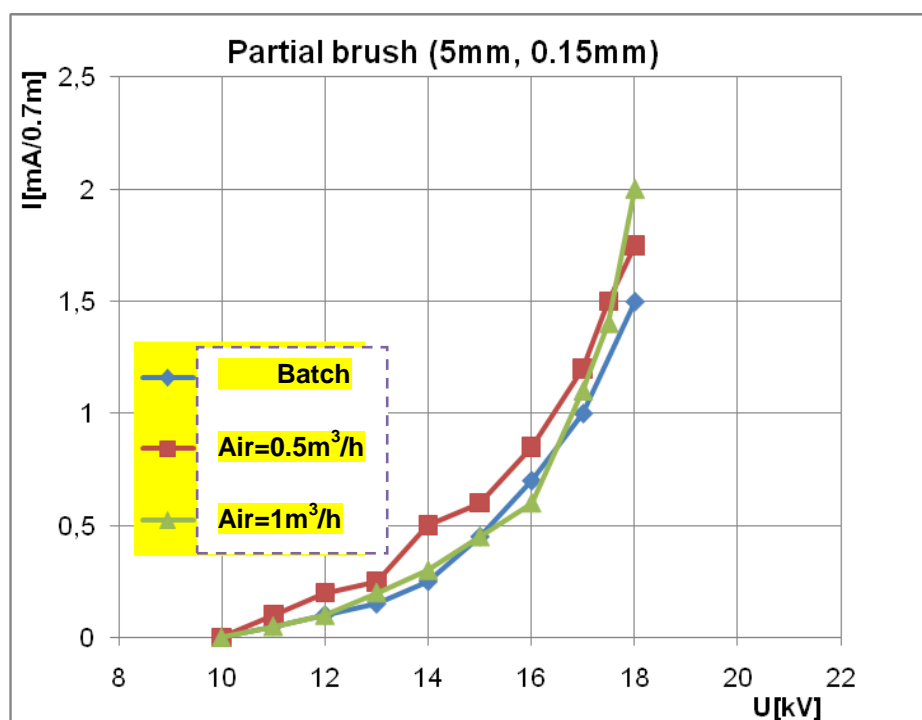


Figure 28: Comparison of current/voltage characteristics with partial brush type discharge electrodes with active length of 700 mm with 5 mm diameter and 0.15 mm wire diameter under batch and low air purge modes. Discharge electrodes and counter electrodes are of stainless steel. Investigations were conducted at ambient conditions

4.1.8 Increased air purging

Investigations were conducted at air purging mode (1 m³/h, 1.5 m³/h and 2.9 m³/h) and an increased corona current was observed under similar condition as used with batch mode. Behavior of corona current was recorded for 10-18 kV applied voltage with air purge mode and compared with corona current with batch mode. Corona current behavior under higher air purging (2 m³/h and 3 m³/h) condition was different than that of batch and even 0.5 m³/h air purging condition. Corona current generated with increased air purging was remarkably less at 10-15 kV applied voltage than that of corona current produced with 0.5 m³/h air purging and batch modes as well.

Current/Voltage behavior with partial brush type discharge electrodes was different at 16-18 kV applied voltage compared with lower applied voltage (10-15 kV). Contrary to lower applied voltage corona current was drastically increased with air purging mode at 16-18 kV applied voltage and it was much higher than for batch mode conditions. It was also observed that increase in air purging from 1 m³/h to 2.9 m³/h also caused an increase of corona current at operation voltage of 16 to 18 kV as shown in **Figure 29**. Corona current generated with 2.9 m³/h air purging at 18 kV

was 3 mA and it was higher than all other current values with batch and less air purging as shown in **Figure 29**.

Enhanced corona current was observed at 2.9 m³/h air purge and it is shown in **Figure 29**. Corona current with enhanced air purging was two times higher than corona current generated with batch mode.

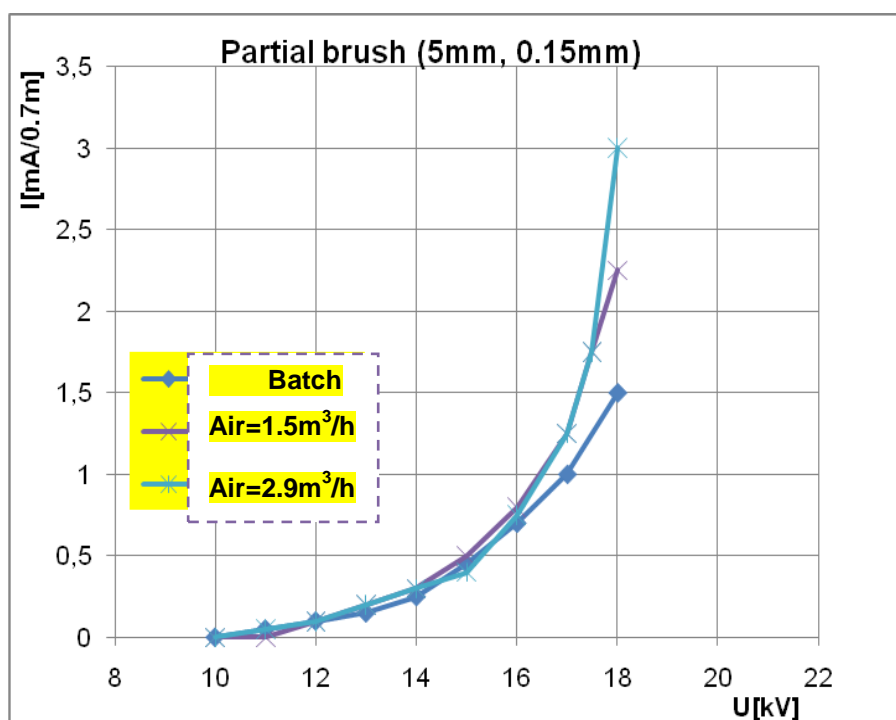


Figure 29: Comparison of current/voltage characteristics with partial brush type discharge electrodes with active length of 700 mm with 5 mm diameter and 0.15 mm wire diameter under batch and enhanced air purge mode. Investigations were conducted at ambient conditions

Experimental data clearly differentiate the current/voltage behavior under batch and air purging (low flow and higher flow) conditions with similar design specification of partial brush discharge electrodes. Corona current observed at different flow modes and batch condition at 18 kV is given below in **Table 9** to differentiate and compare the effect of operation mode. Corona current values were observed with specific active length of partial brush type discharge electrodes (700 mm active length).

Table 9: Corona current values at applied voltage of 18 kV with partial brush type discharge electrodes under various operation conditions.

Process condition	Batch	Air=0.5 m ³ /h	Air=1 m ³ /h	Air=1.5 m ³ /h	Air=3 m ³ /h
I(mA/0.7 m)	1.5 mA	1.75 mA	2 mA	2.25 mA	3 mA

4.1.9 Ozone generation with partial brush type discharge electrodes

During the investigations of partial brush type discharge electrodes, formation of ozone was also observed and quantified as well. Ozone generation at different corona current was monitored to determine optimum process parameters. Effect of air flow on the ozone generation was recorded at corona current of 0.1-3mA as shown in **Figure 30**. **Figure 30** shows ozone generation and degradation for corona discharge with and with out air flow conditions

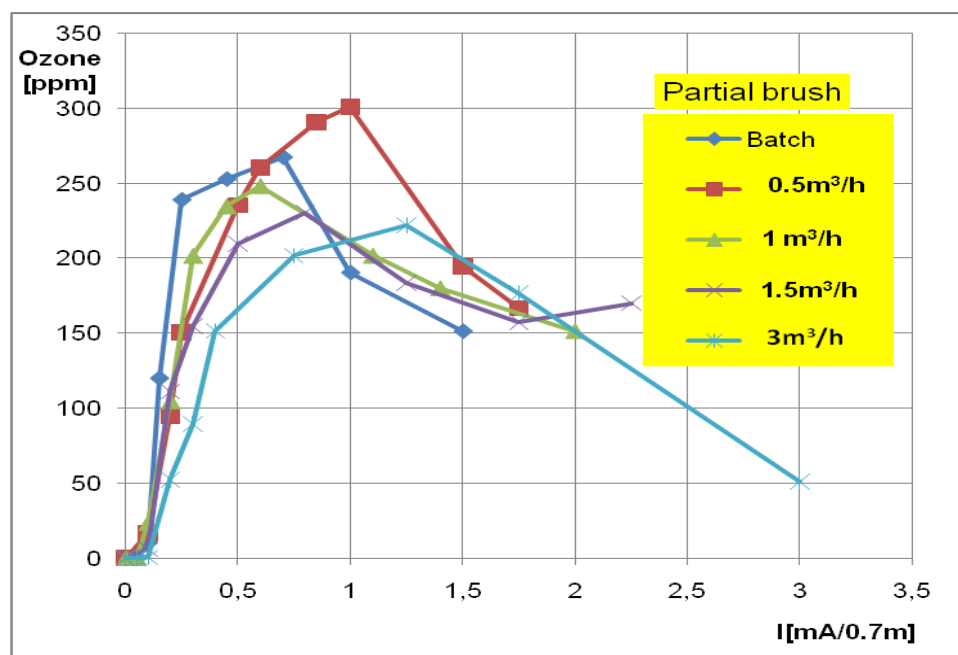


Figure 30: Comparison of ozone generation. Mean duration per experiment was 30minutes; partial brush type discharge electrode, of 5 mm diameter with 0.075 mm wire radius; investigation were conducted at ambient conditions without and with various air purge conditions.

4.1.10 Effect of air flow on the ozone generation

Ozone generation with partial brush type discharge electrodes was investigated over the range of corona current of 0.1-3 mA for batch mode and various air flow modes. At lower corona current from 0.1 mA to 0.6 mA, an increasing ozone generation trend was observed under all operation conditions like batch and various air purging conditions (0.5 m³/h, 1 m³/h, 1.5 m³/h, and 3 m³/h). At 0.75 mA to 3 mA corona current, degradation trend of ozone was observed as shown in **Figure 30**.

4.1.11 Validation of ozone degradation at high corona currents

Degradation reaction was dominating at 1mA to 3 mA corona current as shown in **Figure 30**. Degradation of ozone was also validated in **Figure 31**. Emission discharge was high enough at 3 mA corona current which has degradation effect on generated

ozone. A continuous operation of WESP at 3 mA caused degradation of ozone and on switching off the power supply, immediately increase ozone was observed shown in *Figure 31*.

Similar trend of ozone formation was observed under batch mode and various air purging modes as shown in *Figure 31*. When power supply was switched to off mode, just after peak value of corona current 3 mA, actually ozone degradation reaction was slowed down and formation reaction was dominated to enhance ozone yield. Increase in ozone was quantified at on and off mode for all operation conditions. Ozone observed at off mode was even higher than ozone obtained during generation. *Figure 31* shows ozone generation and degradation for various corona current values and also for off mode with partial brush discharge electrodes with and without air flow conditions.

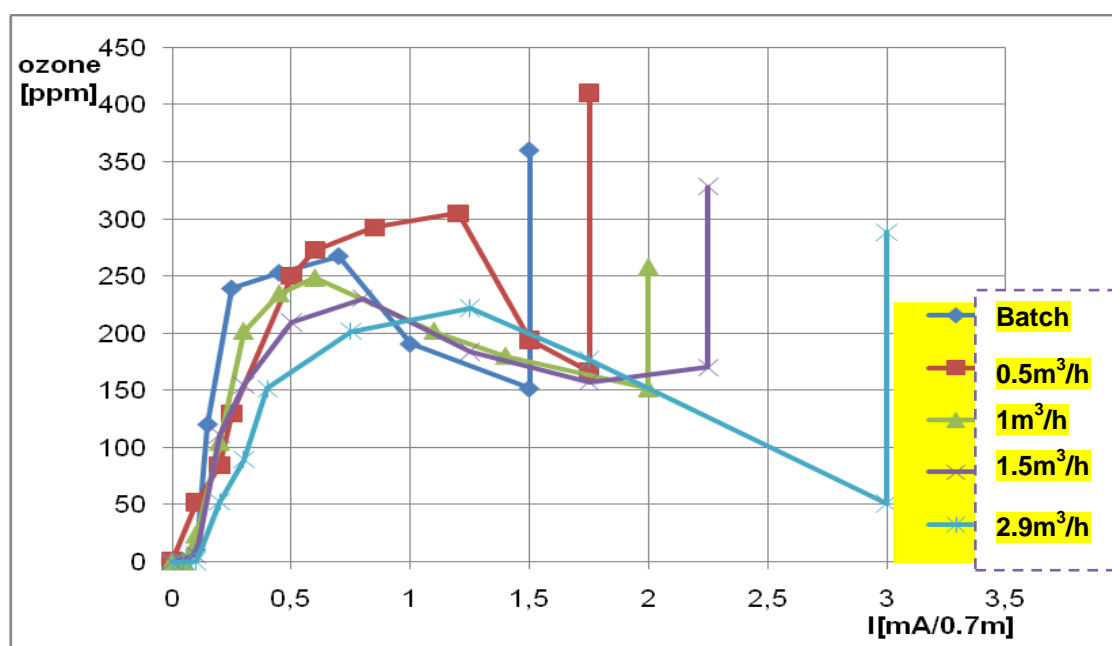


Figure 31: Comparison of ozone generation and degradation for various corona current values with partial brush discharge electrodes (PBDE) with 5 mm diameter and 0.15 mm wire diameter, with and without air flow conditions. Active length of PBDE was 700 mm.

4.1.12 Current/Voltage characteristics with complete brush discharge electrode

Complete brush type discharge electrodes (5 mm, 0.15 mm) were of an active length of 1500 mm and the whole length contributes to the corona discharge process. Complete brush discharge electrode was about twice the active length than partial brush discharge electrodes.

To characterize complete brush type discharge electrodes, investigations were conducted under similar operation conditions as applied for partial brush type discharge electrodes. Comparatively higher corona current with complete brush type discharge electrode was observed than for partial brush type discharge electrodes with similar geometry and same operation conditions. Current/voltage curves under batch and air purging conditions were developed and effect of air purging demonstrated in *Figure 32*.

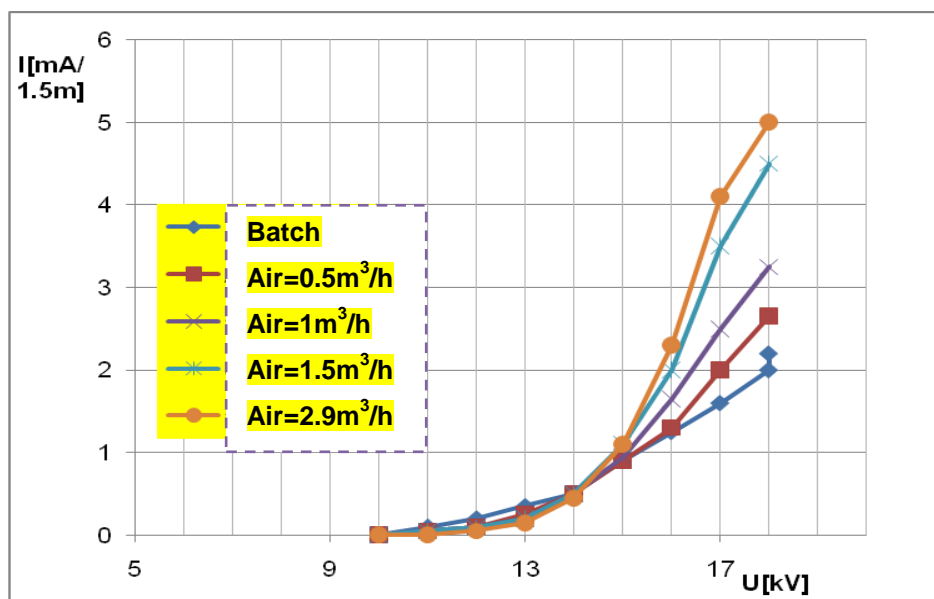


Figure 32: Comparison of current/voltage behavior with complete brush type discharge electrodes (5 mm diameter, 0.15 mm wire diameters) under batch and various air purge at ambient conditions.

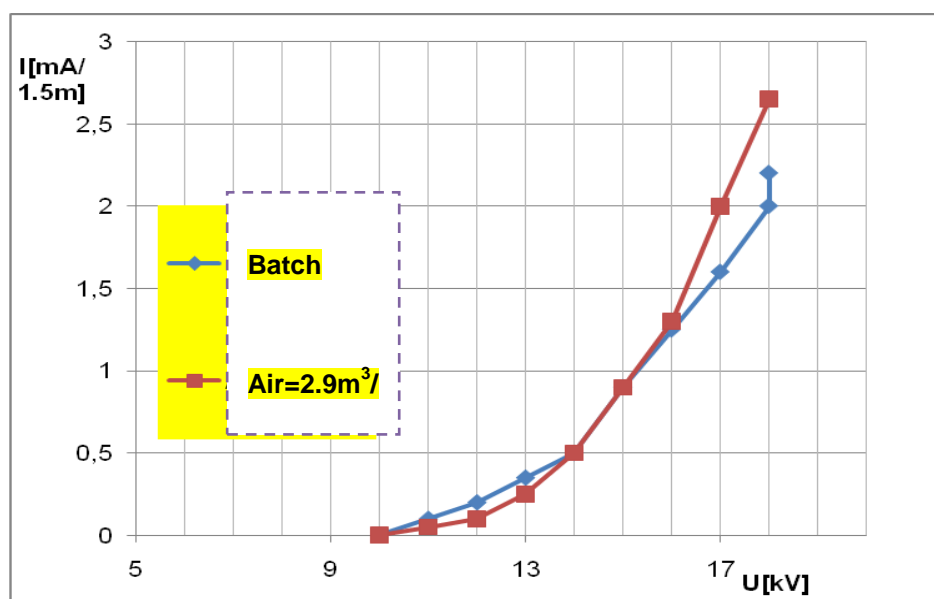


Figure 33: Comparison of current/voltage behavior with complete brush type discharge electrodes of 5 mm diameter, 0.15 mm wire diameters under batch, 0.5 m³/h air purge mode at ambient condition

4.1.13 Current/Voltage behavior at batch and 0.5 m³/h air purging with CBDE

Investigations with complete brush type discharge electrodes (CBDE) were conducted under batch and 0.5 m³/h air purge mode to determine the effect of gas flow on current/voltage characteristics. Corona current was classified into two regions of applied voltage, below 15 kV and above 15 kV for better explanation of experimental results.

Comparison of corona current under batch and air purge conditions with complete brush type discharge electrodes was demonstrated in *Figure 32*. Comparatively higher corona current was observed with 0.5 m³/h air purge conditions than batch condition with similar operation conditions. Corona current at 10 to 14 kV with air purging conditions was slightly lower compared to corona current produced with batch mode. Corona current at 15 kV was 0.9 mA under batch and air purge mode as shown in *Figure 33* and 15 kV was transition point after which current/voltage trend was drastically changed.

Corona current of complete brush type discharge electrodes with air (0.5 m³/h) purging above 16 kV applied voltage was much higher than corona current with batch conditions. Corona current with air purging and batch conditions was 2.65 mA and 2 mA respectively as shown in *Figure 33*.

4.1.14 Comparison of batch and air purge (1.2 m³/h, 2 m³/h and 3 m³/h)

Investigation were continued to characterize complete brush discharge under enhanced air purge conditions like 1.2 m³/h and 2 m³/h to investigate the effect on current/voltage characteristics.

Comparatively a decreased corona current with air purging (1.2 m³/h and 2 m³/h) at 10-14 kV was observed than corona current obtained with batch conditions with specific complete brush type discharge electrodes. Comparatively an enhanced corona current with air purge conditions at 15-18 kV was noted than corona current observed with batch conditions. Corona current at 18 kV with active length of 1500 mm discharge electrodes under batch, 1.2 m³/h and 2 m³/h conditions was 2 mA, 3.25 mA and 4.5 mA respectively as shown in *Figure 34*.

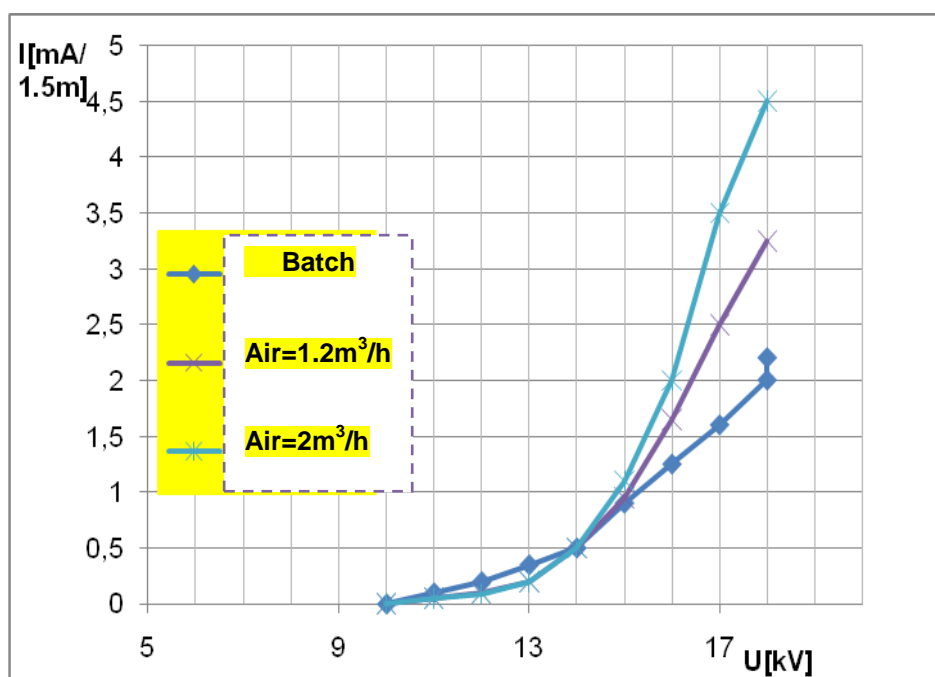


Figure 34: Comparison of current/voltage behavior with complete brush type discharge electrodes (5 mm diameters, 0.15 mm wire diameters) under batch, 1.2 m³/h and 2 m³/h at ambient conditions

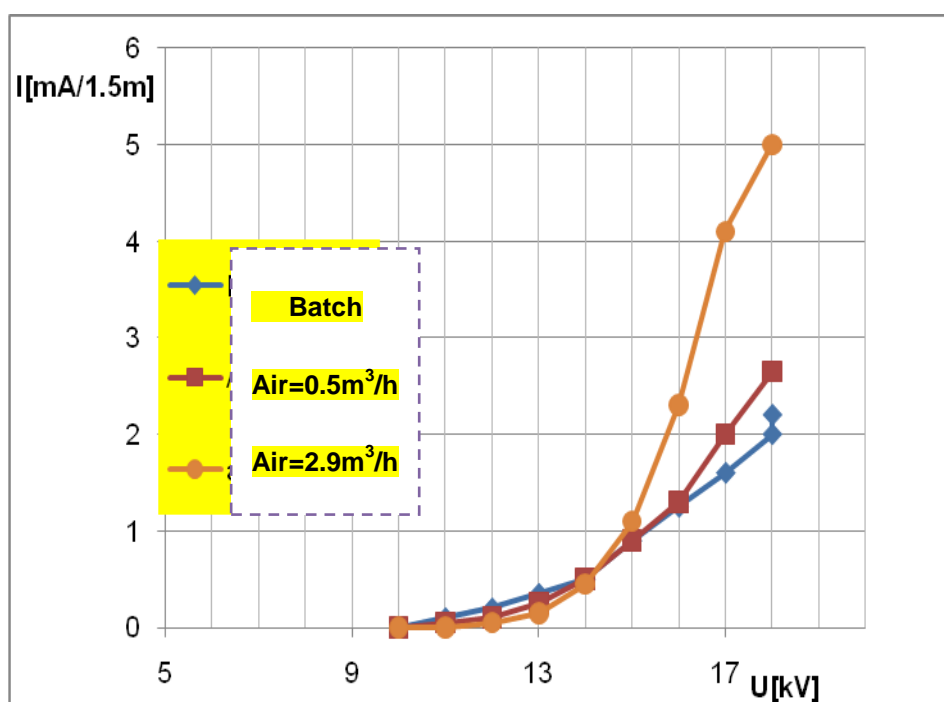


Figure 35: Comparison of current/voltage behavior with complete brush type discharge electrode (5 mm, 0.15 mm) under batch and 0.5 m³/h and 3 m³/h at ambient conditions

Current/Voltage behavior of complete brush discharge electrode was also investigated at enhanced air purge of 3 m³/h and an increased corona current of 5 mA at 18 kV was observed which was comparatively higher than all other applied conditions as shown in **Figure 35**. Enhanced air purging (3 m³/h) showed a decreased

corona current at applied voltage of 10-13 kV and it was slightly lower than corona current produced with batch mode. A sharp increase in corona current at 14-18 kV was observed under 3m³/h air purging mode as shown in **Figure 35**.

Corona current observed at 18 kV was 2 mA for batch and 5mA for 3 m³/h respectively as shown in **Figure 35**. A remarkable difference between batch, 0.5 m³/h and 3 m³/h was recorded.

4.1.15 Ozone generation with complete brush type discharge electrodes under constant corona current over duration of 60min

Effect of complete brush type discharge electrodes was investigated for constant corona current and long term measurement of ozone formation to optimize ozone generation with specific design of brush type discharge electrodes (500 mm).

Investigations were conducted to determine the effect of various constant corona currents on ozone generation for specific duration with complete brush discharge electrodes. Experiments were performed at various corona currents like 0.05 mA, 0.1 mA and 0.35 mA for 60minutes duration with complete brush type discharge electrodes under similar applied conditions. Corona current values were 0.05 mA, 0.1 mA and 0.35 mA corresponding to 12 kV, 13 kV and 14 kV applied voltage respectively, shown in **Figure 36**. Maximum ozone concentrations were observed over time span 10-20 minutes. After 20minutes a slight decrease in ozone concentrations was observed at all corona current values. Decrease in ozone concentration after 20min was the effect of simultaneous degradation reaction (decay reaction) on generated ozone. After 20 minutes accumulated corona (dense corona) may cause the degradation and dissociation of ozone as shown **Figure 36** and **Figure 37**.

Ozone concentration at 0.1 mA corona current was nearly similar to the ozone generated at 0.35 mA corona current. Although ozone produced at 0.35 mA was higher than ozone generated at 0.1mA, but energy consumed per unit of ozone was less with 0.1 mA applied corona current. Under given conditions as mentioned in **Figure 36** and 0.1 mA was optimum corona current to generate ozone with active length of 1.5 m of discharge electrodes.

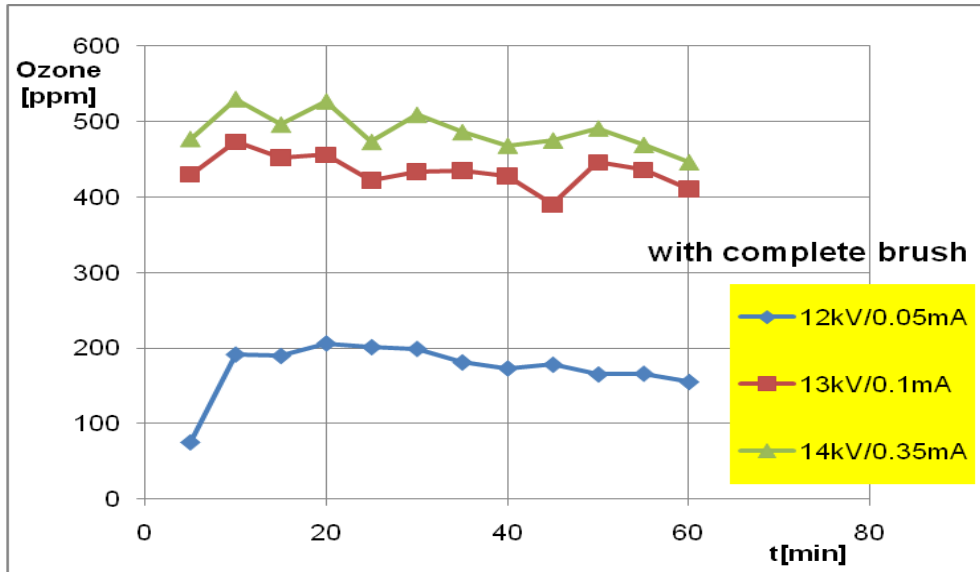


Figure 36: Comparison of ozone formation with complete brush type discharge electrode of 5 mm diameter and brush wire diameter 0.15 mm. Investigations were conducted at constant applied voltage of 12 kV, 13 kV and 14 kV which corresponds to a corona current of 0.05 mA, 0.1 mA and 0.35 mA respectively.

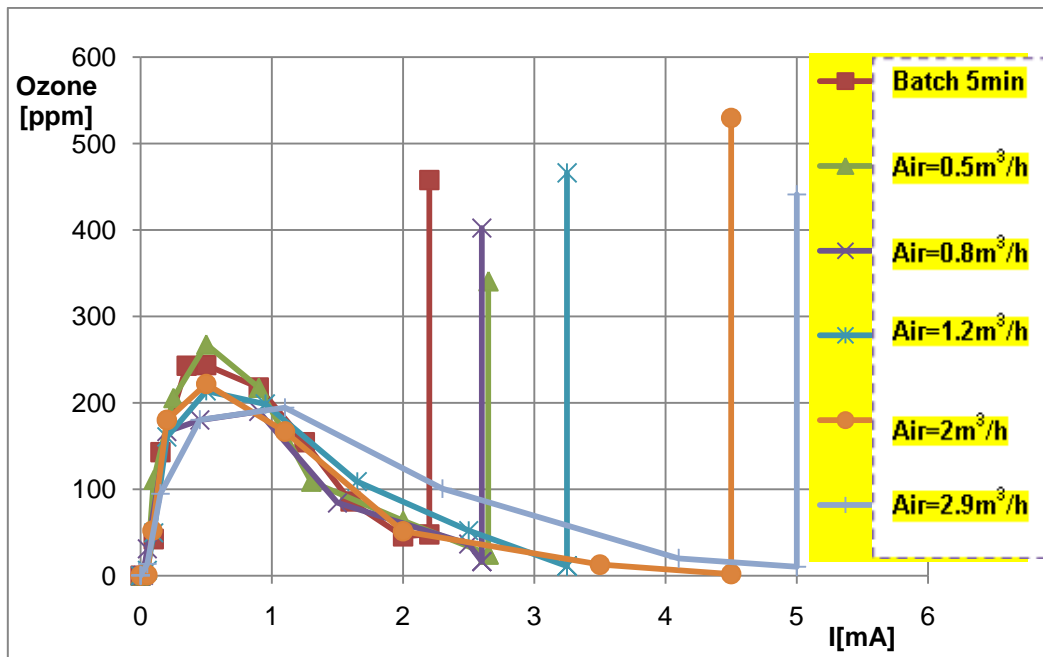


Figure 37: Comparison of ozone generation with complete brush type discharge electrodes of 5 mm diameter, and brushing wire diameter 0.15 mm. Investigations were conducted at various corona current values at batch mode and various air purge modes under ambient conditions.

4.1.16 Ozone generation with complete brush type discharge electrodes under batch and various air purge conditions

Ozone generation mechanism was investigated with complete brush type discharge electrodes (5 mm diameter and 0.15 mm wire diameter) under batch and various air

purge modes at increased corona current (0-4 mA). Increased ozone was observed with the increase of corona current from 0.05-0.5mA under batch and air purge conditions with specific design of complete brush discharge electrodes. Above 0.5 mA corona current a decreasing trend of ozone was experimentally observed at all applied conditions (batch, air purge). At enhanced corona current, a decreasing trend of ozone concentration was continued to a very low concentration of ozone at batch and all air purge conditions as **Figure 37**.

Ozone generation trends with complete brush discharge electrodes were approximately similar to trends obtained with partial brush type discharge electrodes under similar operation conditions.

Slightly enhanced and increased ozone concentration with air purging of 0.5 m³/h was observed than for batch and air purging(1.2 m³/h and 2 m³/h) conditions. Difference in ozone generation with 0.5 m³/h was not remarkably higher and above 0.5 mA corona current a very similar decreasing trends of ozone was observed under all applied conditions like batch mode and various air flow modes as **Figure 37**.

Comparatively a decreasing trend of ozone formation with enhanced air purging conditions (2 m³/h, 3 m³/h) was observed even at optimized corona current of 0.5 mA than batch and less air purging conditions with complete brush type discharge electrode (5 mm diameter, 0,15 mm wire diameter). It was also experimentally observed that ozone degradation trend with enhanced air purging condition was comparatively slower at 1 mA, 2 mA, 3 mA and 4 mA than for batch and lower air flow conditions.

Enhanced degradation of generated ozone at enhanced corona current was observed under various applied conditions as demonstrated in **Figure 37**. When high voltage power supply was switched off an immediate effect on ozone generation was monitored and a hike of ozone concentration was observed. Again a decrease in ozone was also observed after this hiked ozone quantity and within a 5 minutes duration ozone concentration reduced to very low level (4-10 ppm).

4.1.17 Comparison of current/voltage characteristics of partial and complete brush discharge electrode with various applied conditions

Partial brush discharge electrodes has an active length of 700 mm and complete brush discharge electrodes has active length of 1500 mm with similar geometric

specification. Investigations were conducted under similar applied condition of applied voltage to evaluate the corona current characteristics.

4.1.18 Batch mode

Investigations were conducted with partial and complete brush type discharge electrodes to determine the current/voltage characteristics under batch mode under identical operation conditions.

An increase in corona current was observed with the increase in applied voltage with partial and complete brush type discharge electrodes. Increasing trends of corona current with complete brush discharge electrodes were comparatively higher than data obtained with partial brush discharge electrodes under same geometric and operation conditions. Corona current values at various applied voltage for partial and complete brush discharge electrodes were demonstrated in *Table 10* and also shown in *Figure 38*. The difference in corona current was due to change in active length of brush discharge electrodes. A mixed increasing trend of corona current was observed with increase in 53% of active length with complete brush electrodes.

Table 10: Experimentally observed corona current values with partial and complete brush discharge electrodes under batch mod and percent increase in current

kV	I[mA] 700mm	I[mA] 1500mm	Diff. mA
14	0.25	0.5	50
15	0.45	0.9	50
16	0.75	1.3	42.3
17	1	1.6	37.5
18	1.5	2	25

Two discharge electrodes of 700 mm and 1500 mm active lengths were investigated with similar applied conditions to describe the effect of active length. With an increase in active length of 53% with complete brush discharge electrodes (5 mm diameter, 0.15 mm wire diameter), increased corona current was observed and trend was different at lower and higher applied voltage. At 14-15 kV applied voltage an increase of corona current with complete brush discharge electrodes (1500 mm) was 50% higher than corona current with partial brush discharge electrodes (700 mm). Comparatively a higher corona current was observed with complete brush discharge electrodes than of corona current of partial brush discharge electrodes even at 16

kV, 17 kV and 18 kV applied voltage. Increase in corona current at higher applied voltage (18 kV) was relatively lower (25%) than 10-15 kV shown **Table 10**.

4.1.19 Effect of 3 m³/h on current/voltage curves

Experiments were conducted to evaluate the current/voltage behavior under high air purge condition with partial and complete brush discharge electrodes with similar geometric and operation conditions. Investigation have shown a higher increase in corona current with complete brush discharge electrodes with the increase in applied voltage compared with partial brush discharge electrodes. Maximum corona current was observed with complete and partial brush discharge electrodes under air purging (3 m³/h) was 5 mA and 3 mA respectively. Corona currents at 16 kV applied voltage with partial and complete brush type discharge electrodes were 2.4mA and 0.75mA respectively at same operation conditions also shown in **Figure 38** (38a and 38b) respectively. Experimental data show a higher corona current with 1500 mm active length discharge electrodes than of 700 mm active length discharge electrodes which was obvious but difference in corona current was not proportional increase as increase in active length. More over relative increase in corona current with complete brush discharge electrodes as compared to partial brush discharge electrodes below 15 kV and above 16 kV was not symmetric.

Effect of active length was also investigated under various air purge conditions to determine the trend of corona current. A remarkable increase in corona current was observed with increased active length of brush discharge electrodes under similar operation conditions. Corona increasing trend under air purging mode was much higher than batch modes as shown in **Table 10**, **Table 11** and **Figure 38**.

Table 11: Experimentally observed corona current values with partial and complete brush discharge electrodes at 3 m³/h mode and percent increase in current.

kV	I[mA] 700mm	I[mA] 1500mm	% diff
14	0.25	0.5	50
15	0.4	1.2	66.6
16	0.75	2.35	68
17	1.25	4.25	70
18	3	5	40

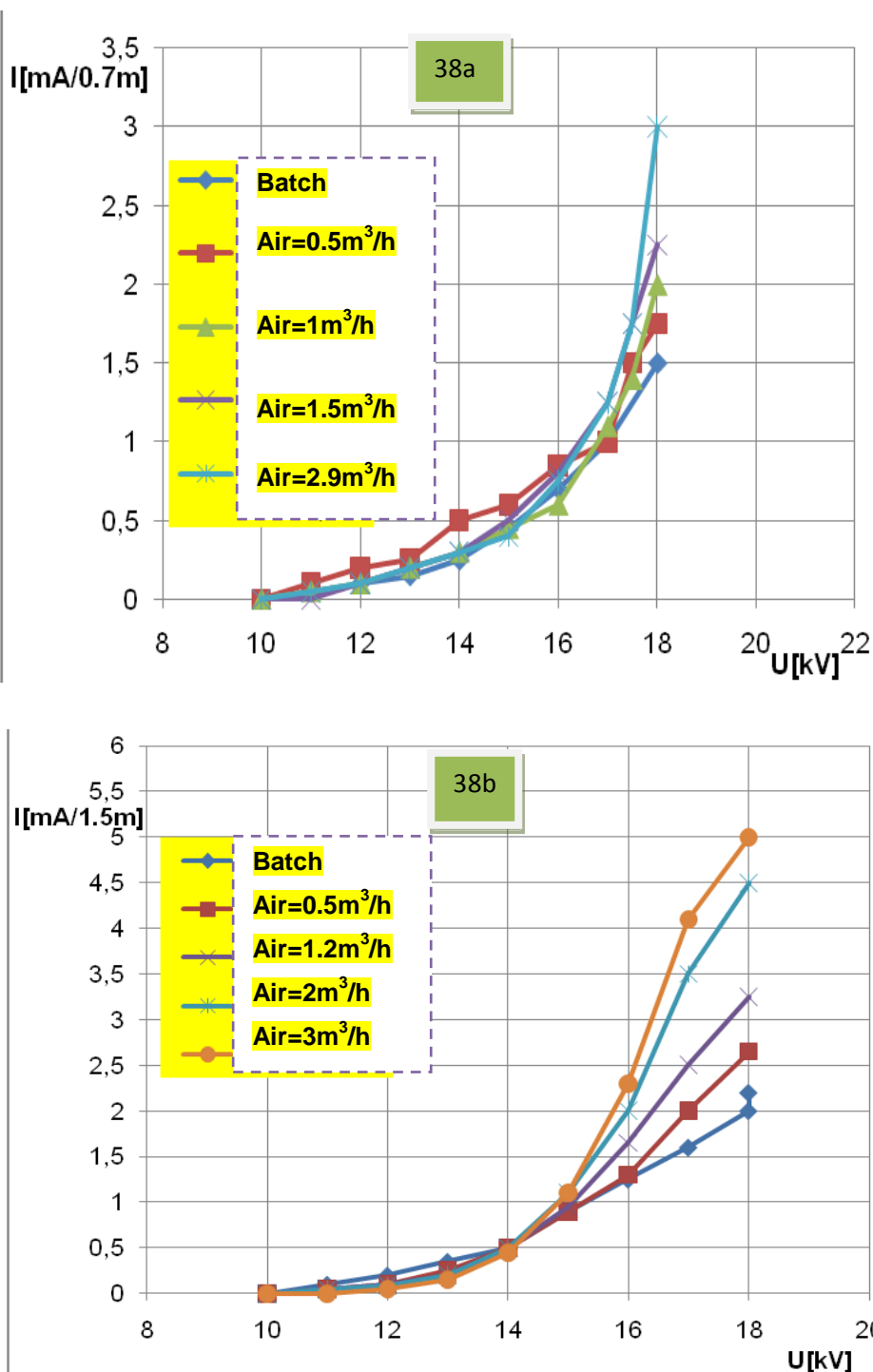


Figure 38: Comparison of current/voltage behavior of partial and complete brush type discharge electrodes (PBDE) of 5 mm diameter, with brushing wire diameter 0.15 mm. Investigations were under batch mode and various air flow modes at ambient conditions to characterize the specific brush discharge electrodes. Active length is mentioned in graphs (38a and 38b correspond to 700 mm and 1500 mm active length).

4.1.20 Comparison of ozone generation for partial and complete brush discharge electrodes with similar applied conditions

Experimental Investigations were conducted to differentiate the effect of active length of brush discharge on ozone formation under similar applied conditions. Ozone formation was monitored over corona current of 0.1-2.25 mA with partial and complete discharge electrodes under same operation conditions and same duration (3 min) for a specific corona current. Ozone formation and degradation trends were approximately similar with partial and complete brush discharge electrodes. Maximum ozone generation was observed at 0.45-0.5 mA corona current with partial and complete brush discharge electrodes even with various applied conditions (batch and air purging) as shown in *Figure 39*.

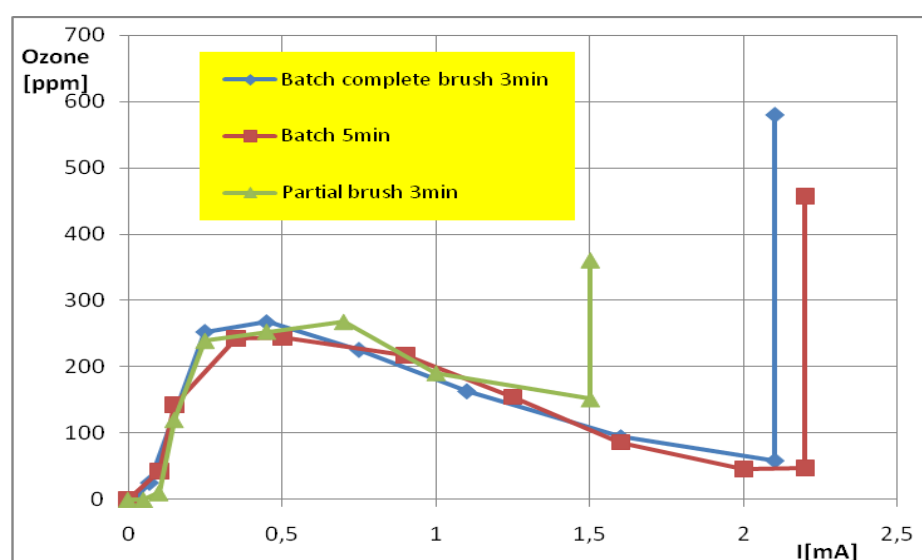


Figure 39: Comparison of Ozone generation with complete and partial brush type discharge electrode of 5 mm diameter with 0.15 mm wire diameter. Investigations were conducted at various corona current settings under batch modes for 3 and 5min duration for each set of voltage at ambient conditions to optimize ozone generation.

Ozone generation with partial brush discharge electrode was optimized at 0.45- 0.5 mA corona current and degradation of generated ozone was comparatively less than enhanced corona currents.

4.1.21 Comparison of current/voltage characteristics and ozone generation with partial brush discharge electrode under water circulation

Experimental Investigations were conducted under various water circulation; various air purging and batch modes with 5 mm diameter of partial brush discharge electrode under similar applied conditions.

It was experimentally observed that water circulation showed an effect on current/voltage curves while geometric parameters were same. Increase in water circulation and air purging caused a decrease in corona current at lower applied voltage (10-15 kV) and increased over range of 15-17 kV as compared to batch mode or without water circulation as shown in **Figure 40**. Comparatively increased corona current at 17 kV was observed with 70 l/h of water circulation and above this corona current short circuiting was observed and tripped the system. Continuous sparking was observed above 17 kV applied voltage (corona current) and hence process was limited at 17 kV applied voltage.

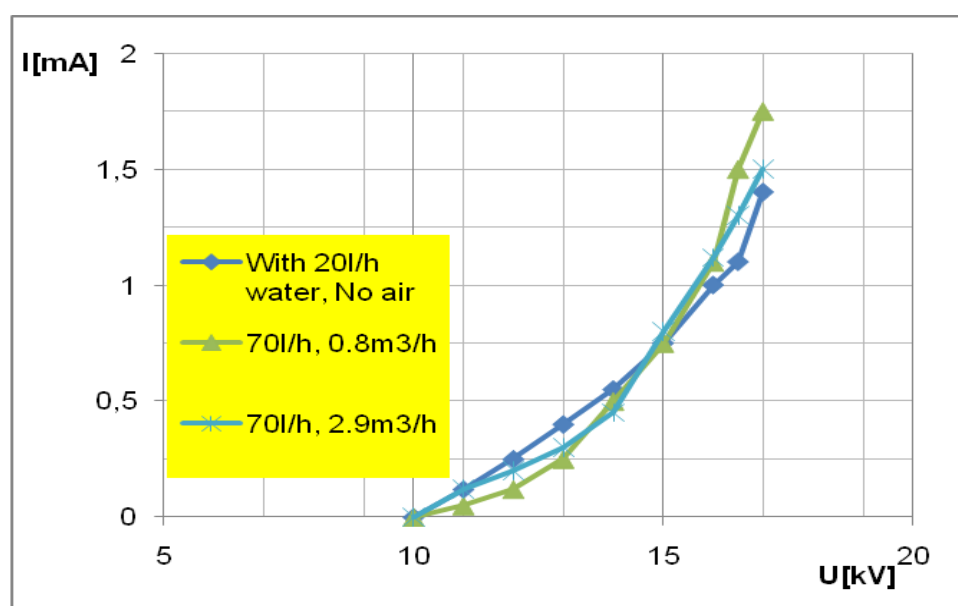


Figure 40: Comparison of current/voltage characteristics with air and water circulation with partial brush discharge electrodes (5 mm diameter, 0.15 mm wire diameter).

Ozone generation trend was also observed with various water circulation conditions and air purging modes to compare with ozone generation in batch mode under similar geometric and operation conditions. Ozone generation was decreased with increase in water circulation and with enhanced air purge conditions as compared to less water circulation and low air purge conditions. Ozone generation was optimum at 0.5 mA corona current and dissociation of ozone was also observed at elevated corona current under all applied conditions.

Ozone generated with water circulation was also compared with various water circulation conditions and from recorded data it is concluded that ozone generation with higher water circulation is seemingly lower than all other conditions as shown in **Figure 41**. With increase in water circulation absorption of ozone was also increased

and as result decreased ozone was recorded at the exit of the electrostatic precipitators. It was also experimentally observed that with increased water circulation peak of ozone was recorded at 1mA corona current instead of 0.45 mA. Moreover ozone was transported from gas phase to circulation water. Desorption of ozone from water circulation tank was also recorded by measuring ozone at top of circulation tank. **Figure 41** shows an ozone generation trend under various water circulation conditions with partial brush discharge electrode.

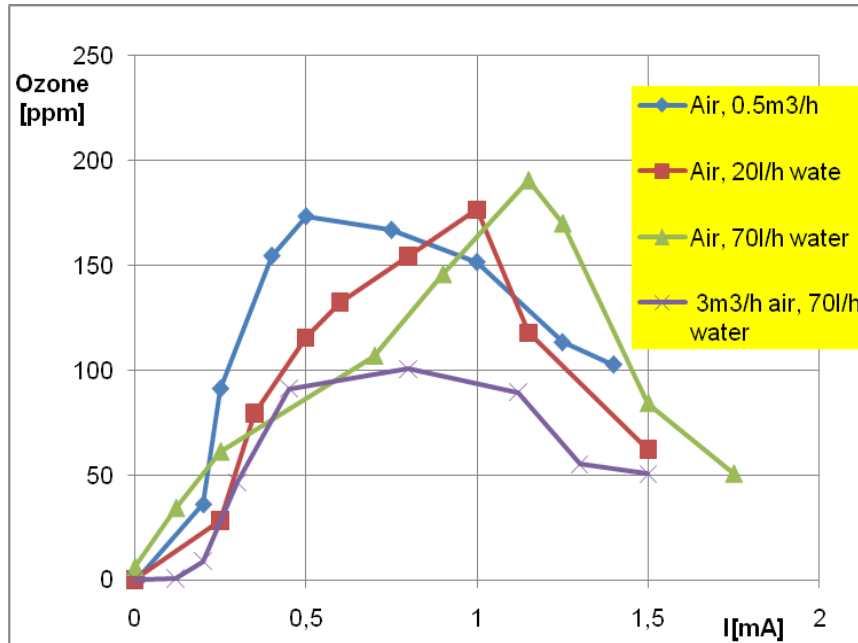


Figure 41: Comparison of ozone generation with air purge mode, with and without water circulation

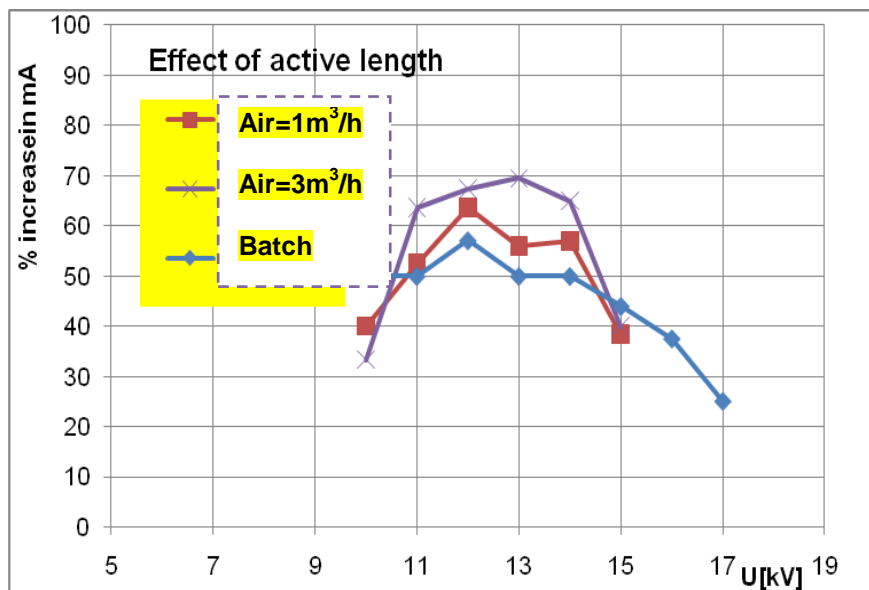


Figure 42: Trend of the percent increase in corona current with increase in active length of 53% at various air purge and batch condition. Increasing trend was different below and above 12-13 kV.

4.1.22 Effect of increased active length of discharge electrodes on current/voltage behavior at various applied voltage

Investigations were conducted to determine the effective of active length of brush type discharge electrodes on behavior of corona current at applied voltage of 10-18 kV under batch and air purge conditions.

Two types of discharge electrodes were fabricated; partial and complete brush discharge electrodes to investigate the effect of active length on current/voltage characteristics. Active length of partial and complete brush discharge electrodes were 700 mm and 1500 mm respectively. Active length of complete brush discharge electrode was 53.3% more than the length of partial brush discharge electrodes.

Experimental investigations showed that an increase in corona current with the increase in active length of complete brush discharge electrodes was observed compared to partial brush discharge electrodes under similar applied conditions. It was observed that rise of corona current was not proportional to increase of active length of discharge electrodes. Corona current increasing trend was different at different applied voltage under same applied conditions. Percent increase in corona current with increase in specific active length was maximum (50 to 70 %) at 12 kV applied voltage under all sets of experiments as shown in **Figure 42**. Increase in corona current at higher applied voltage (17 kV) was only 30 to 40 percent. Effect of increase of active length (53.3%) to increase the corona current was higher at 12 kV and above 12 kV a decreasing trend of corona current was observed with all experimental observations as shown in **Figure 42**

Effect of air purging was also monitored to evaluate enhancement of corona current with the increase in active length of discharge electrodes at similar applied conditions. It was experimentally observed that increase in corona current with specific increase in active length was also a function of air purging conditions as well. Percent increase in corona current was comparatively higher with air purging mod than of batch mode as shown in **Figure 42**. High air purge conditions caused a relatively higher increase in corona current than batch and lower air purge conditions.

4.1.23 Summary:

Various brush discharge electrodes were experimentally investigated to determine the effect of active length of discharge electrodes on current/voltage characteristics and ozone generation mechanisms. The effect of the gas flow rate was also studied to characterize partial and complete brush type discharge electrodes under similar operation conditions.

Active length:

Current/Voltage behavior depends upon the active length of brush type discharge electrodes. Corona current increases with the increase of active length of discharge electrodes. Experimental results show that increase in corona current is not proportional to the increase in active length under all operation conditions.

Gas flow rate:

Enhanced air purging shows a mixed trend of corona current behavior. With the increase of air purging, an increase of corona current was observed above applied voltage (15 kV) and decreases below 15 kV.

Ozone:

Experimental investigations show the effect of corona current on ozone generation under various operation conditions like batch, air purges, and various active lengths etc. Ozone generation was optimized at 0.4-0.5 mA under various operation conditions. A decreasing trend of ozone concentration was observed above 0.5 mA

Corona current:

Ozone generation was also observed under air and water flow conditions. An increase of water circulation causes a reduction of ozone concentration and also shifts the ozone peak region towards higher corona currents 1mA instead of 0.5mA as shown in *Figure 41*.

5 Experimental investigation of various brush type discharge electrodes with active length of 500 mm; installed at the bottom

Investigations were conducted to study the behavior of various diameters of brush type discharge electrodes like 4 mm, 5 mm, 6 mm and 8 mm with various wire diameters (0.1 mm and 0.15 mm) for similar operation conditions.

The electrostatic precipitator was operated under the operation conditions batch, air purge and air plus water circulation at ambient conditions. Investigations were conducted with different brush diameters and also with various brushing wire diameters at 10-20 kV applied voltage. The corona current recorded was compared to classify the geometric effect. Results of investigations were represented graphically with respect to specific diameters of discharge electrodes. Impact of diameter of discharge electrodes on current/voltage characteristics, ozone generation and process stability were studied and discussed. The current/voltage curves were established with various electrodes at the same operation conditions.

Different schemes of brush type discharge electrodes were constructed as shown in **Figure 26** and used for investigations under various operation modes. Multiple design schemes were constructed on the basis of active length of brush type discharge electrodes. **Figure 43** shows scheme of brush type discharge electrodes with active length 500 mm at bottom.

Brush type discharge electrode with active length of 500 mm at bottom was specifically investigated to determine the impact of design and active length of brush type discharge electrodes on current/voltage behavior and ozone formation. Multiple brushes under this scheme were studied to generate data for ozone production and simulated data was produced for determining kinetics.

Current/voltage behavior with brush type discharge electrodes (4 mm, 0.1 mm), active length of 500 mm at bottom

Brush type discharge electrodes with active length of 500 mm (4 mm, 0.1 mm wire diameter) was investigated under batch, air purge and air purge plus water circulation mode to develop the current/voltage characteristics with test facility shown **Figure 2**. Experimentally investigated data with brush type discharge electrodes (4 mm, 0.1 mm) was needed to construct current/voltage relationships. Current/Voltage curves are shown in **Figure 44**.

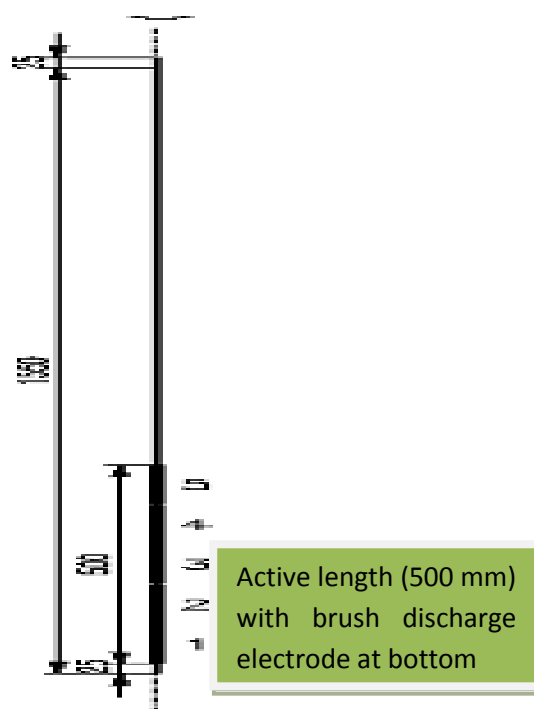


Figure 43: Various schemes of brush discharge electrodes with different active length. Discharge electrodes 1 (five brush were welded together at bottom) has 500 mm active length.

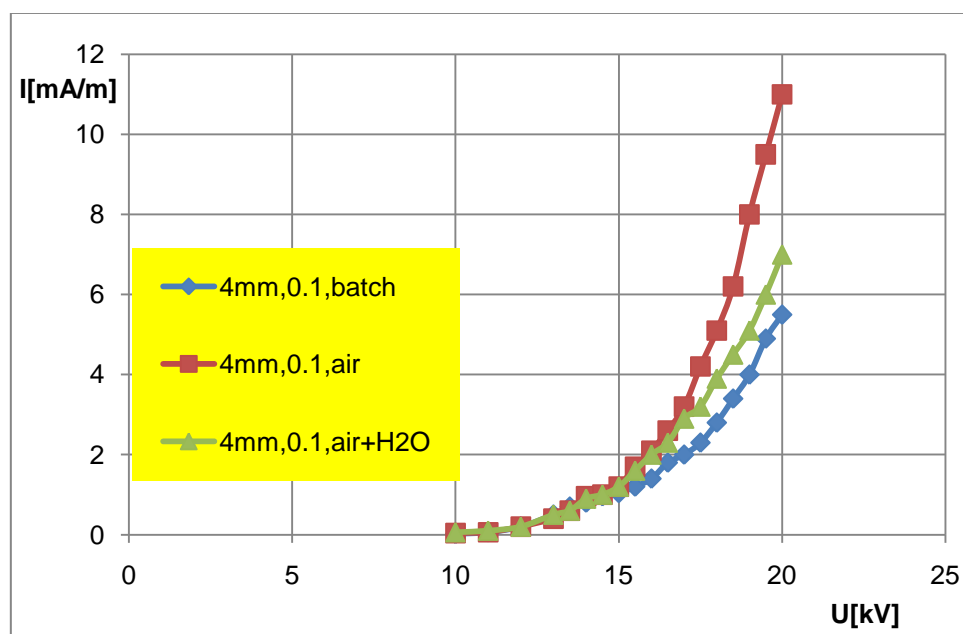


Figure 44: Comparison of current/voltage characteristics of brush type discharge electrodes with active length of 500 mm (4 mm, 0.1 mm wire diameter) under batch, air purge and water circulation conditions. Corona current generated with active length of 0.5m was converted into mA/m.

Current/Voltage behavior was different under batch, air and water circulation operation conditions. At air flow conditions a sharp increase of corona current was observed at 19-20 kV and this behavior lead to sparking and finally destabilized the

process. Sudden rise in corona current was recorded at 18-20 kV with air injection. To avoid process instability the system was operated at lower applied voltage. At 10-18 kV applied voltage with air purge mode a smooth process was observed without any deviation and process fluctuation.

Effect of air and water circulation was also investigated with brush type discharge electrodes (4 mm, 0.1 mm) under same operation conditions. Comparatively higher corona current was observed with air purge conditions than for batch and water circulation mode. Corona current with batch, water and air purge mode at 20 kV were 5.5 mA, 7mA and 11 mA respectively, also demonstrated in *Figure 44*.

5.1 Ozone generation with brush type discharge electrodes (4 mm, 0.1 mm wire diameter)

Investigations were conducted to determine the effect of geometry of discharge electrodes on ozone formation and decomposition of generated ozone under specific operation conditions. Effect of various parameters like batch, air, and air plus water circulation on ozone formation was investigated to determine the optimum operation conditions as well.

Experimental investigations show that ozone generation was a function of applied voltage, geometry of discharge electrodes and specific corona current. Ozone generation recorded was maximum at 0.4-0.5 mA corona current and above 0.5 mA corona current degradation of ozone was recorded. The data are shown in *Figure 45*.

Brush type discharge electrodes under air purge conditions produced an enhanced ozone concentration and degradation of ozone was also slow comparative to the batch and water circulation mode. Reason of slow rate of decomposition of ozone was the dilution of ozone with air. Experimental data for ozone formation and decomposition was used in table curve 2D program to determine the real kinetic equation. Rate equations for intermediate formation were applied. Details of these equations are given in chapter 7(modeling).

Generation of ozone under batch and air flow conditions was nearly similar and decomposition of ozone under batch conditions was relatively fast compared to air flow conditions shown in *Figure 45*.

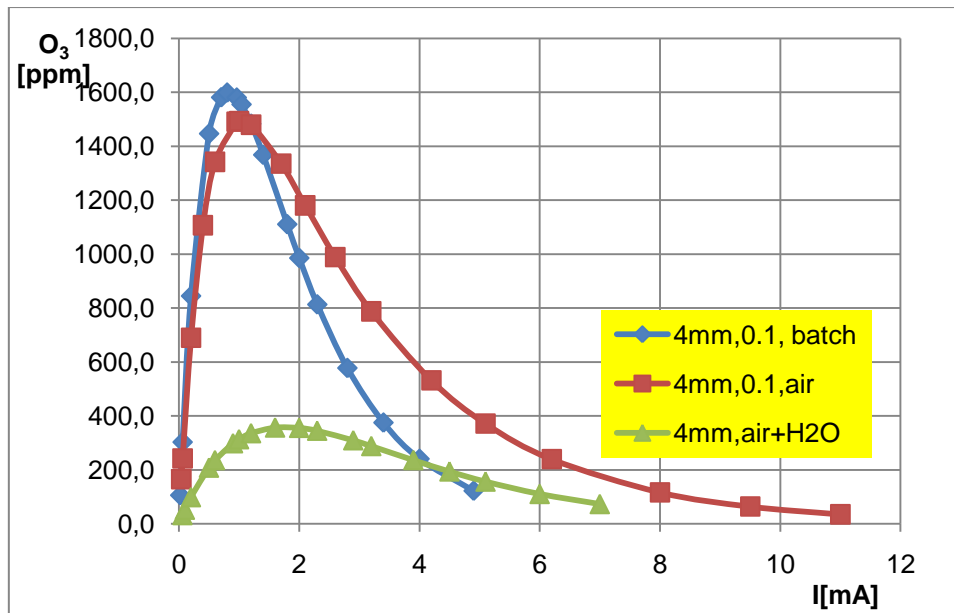


Figure 45: Comparison of ozone generation with 4 mm brush type discharge electrodes (0.1 mm wire) under batch, air and air plus water conditions with given test facility.

With circulation of water plus air, ozone formation was much less than ozone formed with batch and air flow conditions. Actually ozone generation was not less but generated ozone was absorbed in water simultaneously. Circulation water was also analyzed to determine absorbed ozone and ozone transport was confirmed. Fit curve data for all operation modes represent the same typical kinetics over the applied range of corona current shown in **Figure 45**.

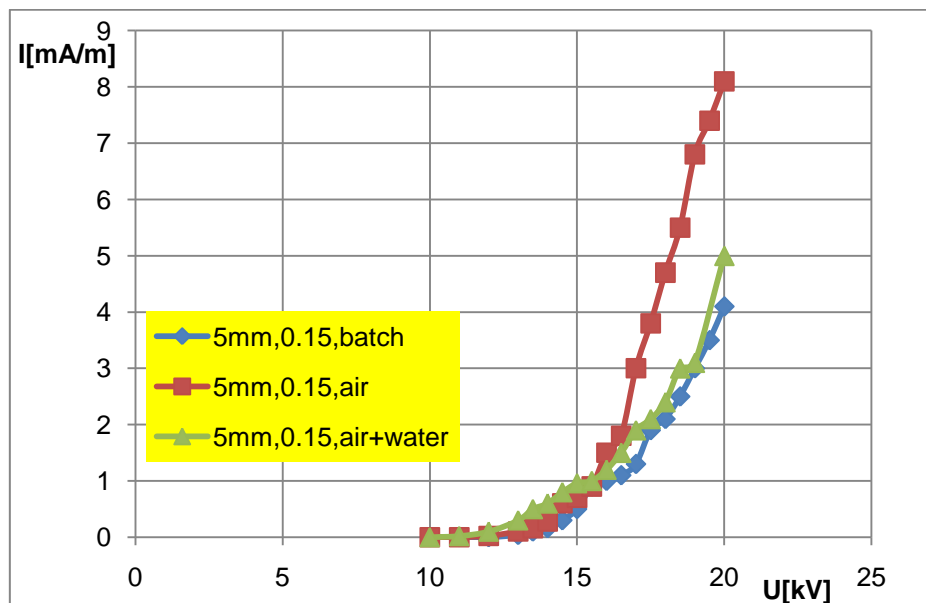


Figure 46: Comparison of current/voltage characteristics for brush type discharge electrodes (5 mm, 0.15 mm wire) with 500 mm active length at bottom under batch, air and air plus water circulation conditions.

5.2 Current/Voltage curves for brush type discharge electrodes with 500 mm active length at bottom.

Brush discharge electrodes (5 mm, 0.15 mm) were used for investigation of batch, air purge and water circulation conditions to develop current/voltage characteristics. Current/voltage curves were established as demonstrated in *Figure 46*. Application range of WESP was more flexible (over a wide span of applied voltage) with aqueous/batch mode than with air purge conditions. Under air flow conditions corona current above 16kV caused sparking. Sparking behavior badly disturbed and affected operation of ESP and this behavior may damage the components of ESP like insulators, discharge wire and electrical power supply.

Corona current with water circulation mode was initially higher at 10-15 kV than batch and air purge mode shown in *Figure 46*. Corona current with water circulation condition was higher than batch and lower than air flow condition at 15-20 kV.

5.2.1 Ozone generation with brush type discharge electrodes (5 mm, 0.15 mm wire diameter) with 500 mm active length at bottom.

Ozone generation trends with brush type discharge electrodes (5 mm, 0.15 mm) were similar to the brush of 4 mm diameter at similar operation modes. Maximum ozone generation was observed at lower corona current and corona current range was optimized at 0.5-0.6 mA. At higher applied voltage and corona currents decomposition of ozone was recorded under all applied conditions (batch, air, and air plus water circulation).

In case of air purge mode, ozone concentration at specific corona current was higher than batch and water circulation mode, as shown in *Figure 47*. For air purge conditions, a slow decomposition of ozone was observed compared with batch and water circulation conditions.

Experimental investigations with water circulation along with air injection show ozone absorbing affect and less ozone was recorded than for batch and air flow conditions as shown in *Figure 47*. Absorption of ozone at specific optimized corona current was noted and a clear effect of water rinsing on free ozone was observed. Ozone formation and decomposition was a function of corona current, air purges and water circulation. All trends of ozone formation follow kinetics for intermediate formation.

Although ozone peaks were different under various operation conditions basic mechanism for reaction kinetics remains same.

5.3 Current/Voltage curves with brush discharge electrodes (6 mm, 0.1 mm)

A brush type discharge electrode (6 mm, 0.1 mm) was experimentally investigated and current/voltage data was recorded. Current/voltage characteristics were recorded for various operation modes. Experimental data was compared and also graphically presented in *Figure 48*. A wide application range with air plus water flow conditions were recorded which was completely different from former/earlier experimental data. A stable process was observed with water circulation conditions. Corona current with air purge mode was much higher at 17-18 kV compared to water circulation condition. Under batch and air purge conditions rapid increase of corona current was recorded over range of 15-17 kV applied voltage and short circuiting /sparking was also recorded. The process was limited to 17-18 kV applied voltage. Under air flow and batch conditions the system was applicable from 10 -18 kV but with air plus water flow conditions process was supported up to 20 kV applied voltage (with enhanced application range) shown in *Figure 48*.

5.3.1 Ozone generation with brush type discharge electrodes (6 mm, 0.1 mm)

Brush discharge electrodes (6 mm, 0.1 mm) have slightly different behavior (I/V , O_3) from previously investigated electrodes (4 mm and 5 mm diameters of brush type discharge electrodes under similar operation conditions) results. With 6 mm brush type discharge electrodes ozone formation and decomposition curves for air flow and batch conditions were quite similar as shown in *Figure 49*.

Maximum ozone was observed over specific corona current of 1 mA and even at 1.5 mA and decomposition of ozone was similar at all applied conditions/modes. At air plus water circulation conditions, ozone recorded was decreased comparative to batch and air purge mode. Actually ozone generation mechanism was not affected by water circulation as ozone was absorbed in water. Ozone recorded with water circulation mode was less than batch and air flow conditions, shown in *Figure 49*.

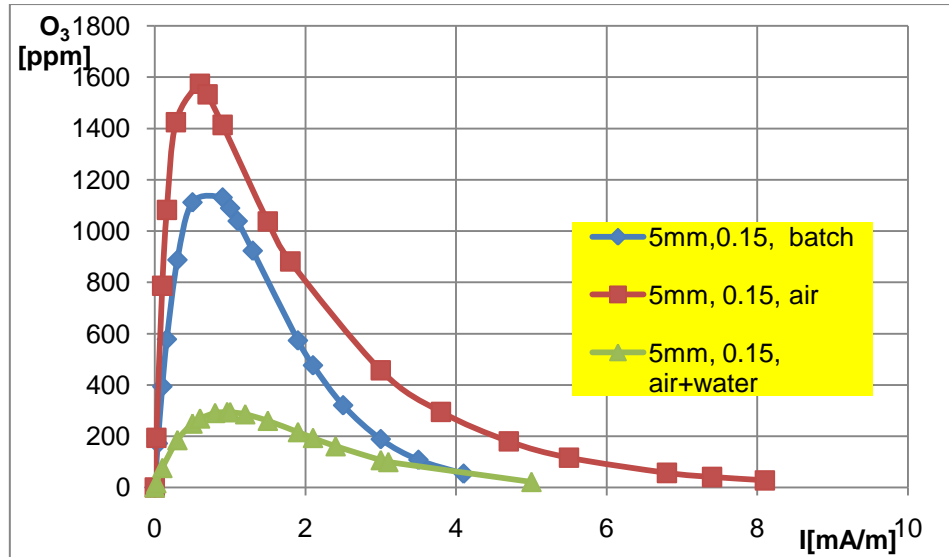


Figure 47: Comparison of ozone generation with 500mm discharge electrodes (5 mm, 0.1 mm).

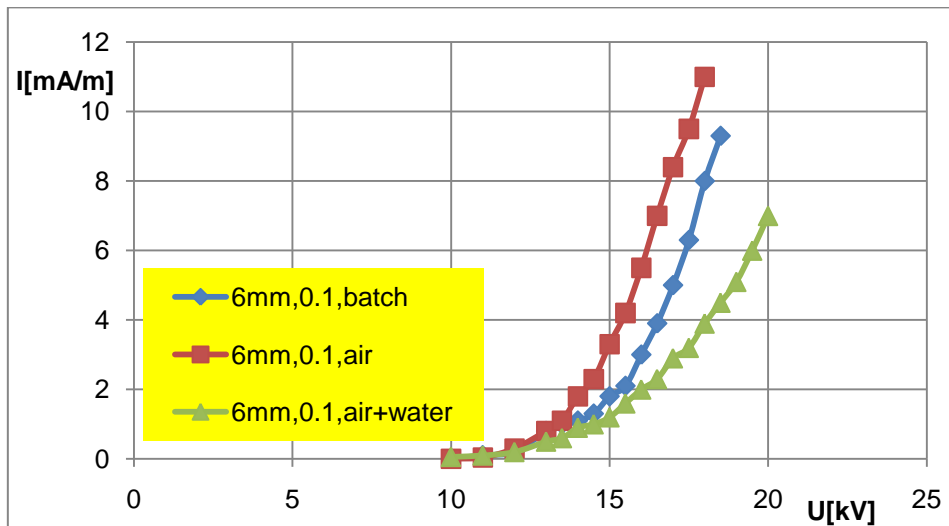


Figure 48: Comparison of current/voltage characteristics of 500 mm brush type discharge electrodes

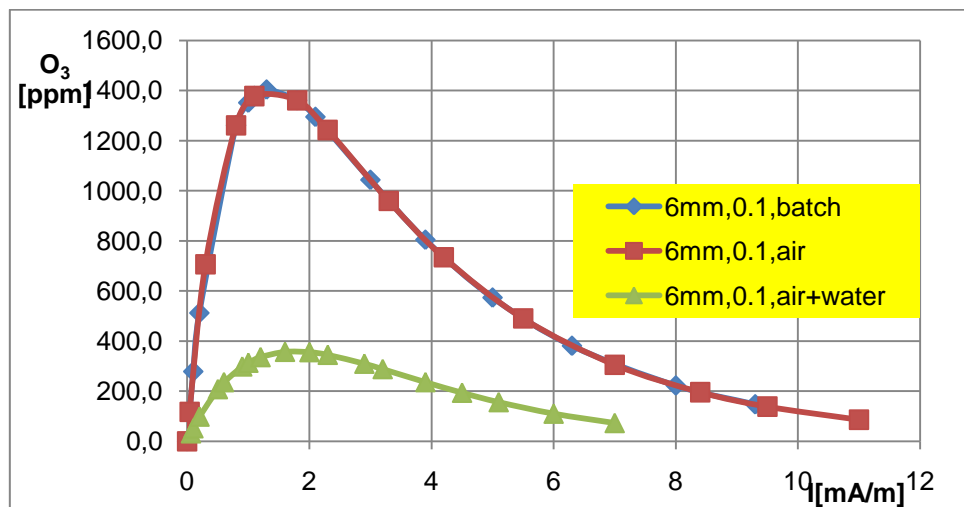


Figure 49: Comparison of ozone generation with brush type discharge electrodes (6 mm, 0.1 mm wire) with active length of 500 mm at bottom under batch, air and air plus water circulation conditions.

5.4 Current /Voltage curves with brush discharge electrodes (6 mm, 0.15 mm)

Current/Voltage behavior with brush type discharge electrodes (6 mm, 0.15 mm wire diameter) was nearly same at 15-16 kV operation voltage for batch, air and air plus water circulation mode. Above 16 kV, current/voltage behavior changed with change in operation mode (batch mode, air flow and air plus water circulation conditions). Corona current recorded for batch mode, air and water at 20 kV was 3.5 mA, 7 mA and 5 mA respectively, shown in *Figure 50*. For air flow conditions current/voltage behavior was unstable and non symmetric compared with water circulation or batch mode. Corona current recorded with air flow conditions was twice of batch modes. Corona current recorded with air purge mode was higher than batch and water rinsing mode. *Figure 50* shows that corona current with water circulation mode was higher than batch mode and less than air purge mode at similar applied voltage. Under air purge mode at 19 kV, knocking was observed and sparking was also seen. A smooth process was observed with batch and water circulation conditions with specific diameter of brush discharge electrodes (6 mm, 0.15 mm).

Corona current with brush electrodes (6 mm, 0.15 mm) was remarkably less than brush electrodes (6 mm, 0.1 mm) under same operation conditions. It was recorded that decrease of brush wire diameters has an increasing affect on corona current. This relation of discharge diameter with corona current is explained in literature [2].

5.4.1 Ozone generation with brush type discharge electrodes (6 mm, 0.15 mm) with 500 mm active length at bottom

Ozone generation and decomposition trends were very typical as earlier discussed. Ozone generation at lower corona current (0.5 mA) was higher than 2 mA corona current under all operation conditions. Experimentally investigated and recorded data for ozone generation and formation is demonstrated in *Figure 51*.

Ozone recorded with 0.15 mm wire was less compared with 0.1 mm wire diameter with same operation conditions. Ozone generation passes a maximum at lower corona current and dissociation of ozone was observed at higher applied voltage under batch, air and water circulation mode.

Ozone recorded at the exit of WESP was very low under water circulation conditions and decomposition trend was similar to air flow and batch conditions. Overall trends of ozone formation and decomposition at 0-7 mA corona current follow the same kinetics. From *Figure 51* it is very much clear that peak ozone formation was recorded

at specific corona current which was also applicable for all operation conditions. With the increase of corona current, degradation of generated ozone was confirmed from data generated with each discharge electrode.

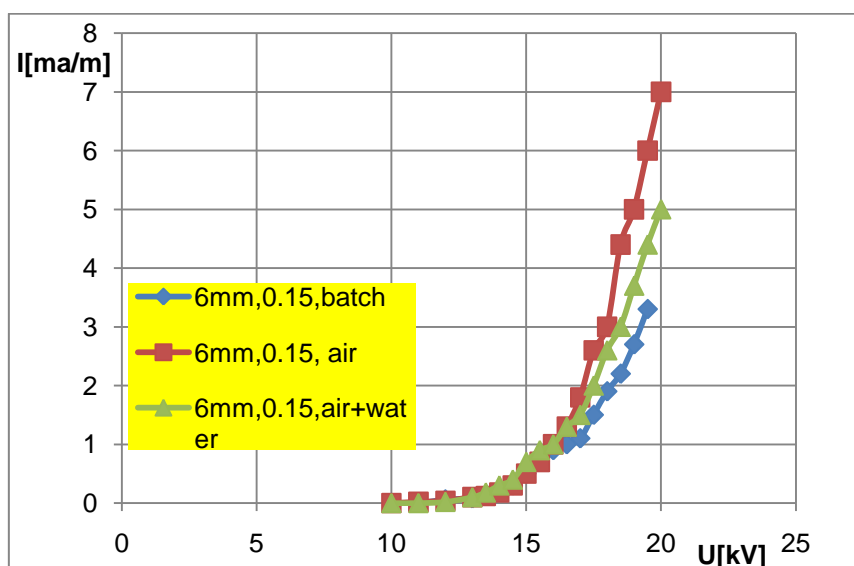


Figure 50: Comparison of current/voltage characteristics of brush type discharge electrodes (6 mm, 0.15 mm) with 500 mm at bottom under batch, air and air plus water circulation conditions.

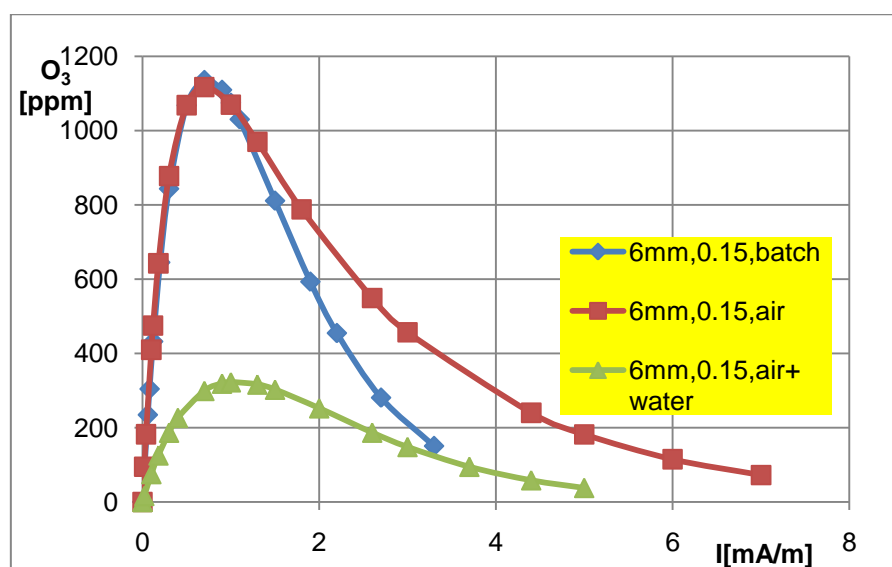


Figure 51: Comparison of ozone generation with discharge electrodes (6 mm, 0.15 mm)

5.5 Current/Voltage curves for brush type discharge electrodes (8 mm, 0.1 mm wire diameter) with 500 mm active length at bottom

Brush type discharge electrodes (8 mm, 0.1 mm) were investigated to develop current /voltage behavior for batch, air flow and water circulation conditions. Corona current with air purge conditions was higher than for water circulation and batch conditions shown in **Figure 52**. Air purge effect on the corona current was remarkably

dominant at 16-20 kV applied voltage. Corona current at 20 kV under air flow was 9mA/m and about twice of batch operation mode.

Current/voltage curves for batch and water mode remain same over the range of applied voltage of 10-17 kV. A small increase of corona current with water circulation was recorded at 18-20 kV and it was higher than for batch mode as **Figure 52**. Current/voltage curves with 8 mm (0.1 mm) diameter brush type discharge electrodes were realistic and stable at medium applied voltage compared with other diameters of brush and brush wire. Corona current at 20 kV applied voltage with air; batch and water circulation was 9 mA/m, 6.5 mA/m and 5.5 mA/m respectively.

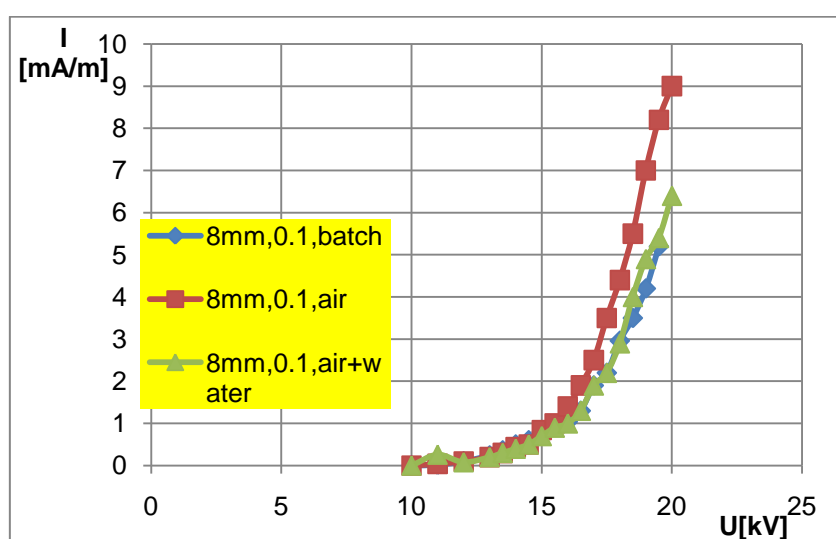


Figure 52: Comparison of current/voltage characteristics of brush type discharge electrodes (8 mm, 0.1 mm wire) under batch, air and air plus water circulation conditions.

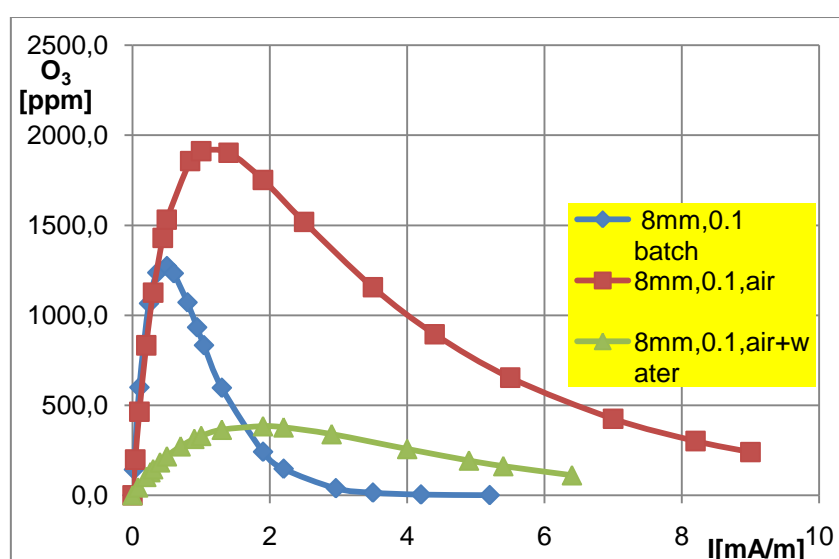


Figure 53: Comparison of ozone generation with brush type discharge electrodes (8 mm, 0.1 mm wire) with active length at bottom (500 mm) under batch, air and air plus water circulation conditions.

5.5.1 Ozone generation with brush type discharge electrodes (8 mm, 0.1 mm wire diameter) with 500 mm active length at bottom

Ozone generation with specific active length of brush discharge electrodes (8 mm, 0.1 mm) was higher than for other brush discharge electrodes (4 mm, 5 mm and 6 mm etc).

Ozone formation with air purge mode was much higher than batch and water circulation conditions shown in *Figure 53*. Ozone formation trends with 8 mm geometry of brush discharge electrodes were different from 4 mm, 5 mm and 6 mm diameters of brush discharge electrodes under same operation conditions. Decomposition of ozone with brush discharge electrodes (8 mm, 0.1 mm) was slow compared with brush of 6 mm diameter under air purge mode, shown in *Figure 53*.

Ozone generation with water circulation showed a different trend with respect to the peak ozone formation for specific corona current. Recorded data show that maximum ozone generation span was increased from 0.5 mA to 2 mA corona current, demonstrated in *Figure 53*.

5.6 Current/Voltage curves with brush discharge electrodes (8 mm, 0.15 mm)

Experimental investigations were conducted and recorded data was used to develop current/Voltage curves for various operation modes as demonstrated in *Figure 54*.

Current/voltage trends were typically similar to the trends observed with other geometries of brush discharge electrodes. Current/voltage trend with air purge mode was slightly different than previously recorded data for 4 mm, 5 mm brush type discharge electrodes under similar operation conditions. Operation range of system was decreased due to sparking and short circuiting. Corona discharge process was limited to 18.5 kV applied voltage. Reason of short circuiting may be due to the extended wire at brush surface or decreased tension in discharge electrodes.

Corona current recorded with brush type discharge electrodes (8 mm, 0.15 mm) at 20 kV was comparatively less than of brush type discharge electrodes (8 mm, 0.1 mm), shown in *Figure 54* and *Figure 52* respectively.

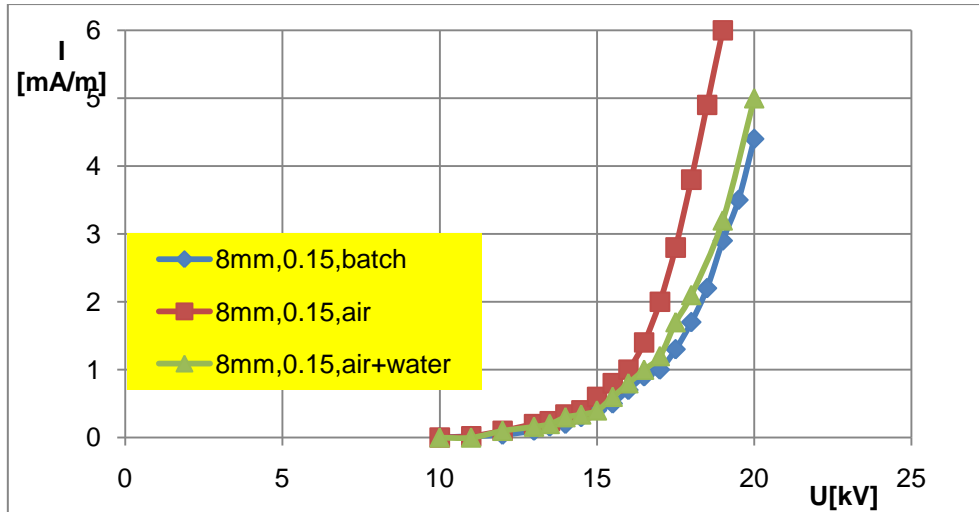


Figure 54: Comparison of current/voltage characteristics of brush (8 mm, 0.15 mm wire)

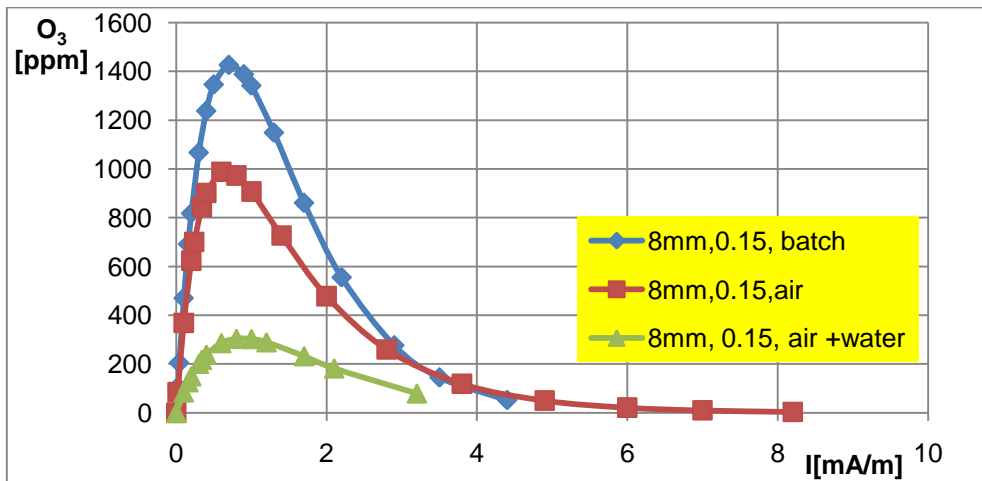


Figure 55: Comparison of ozone generation with 8 mm discharge electrodes

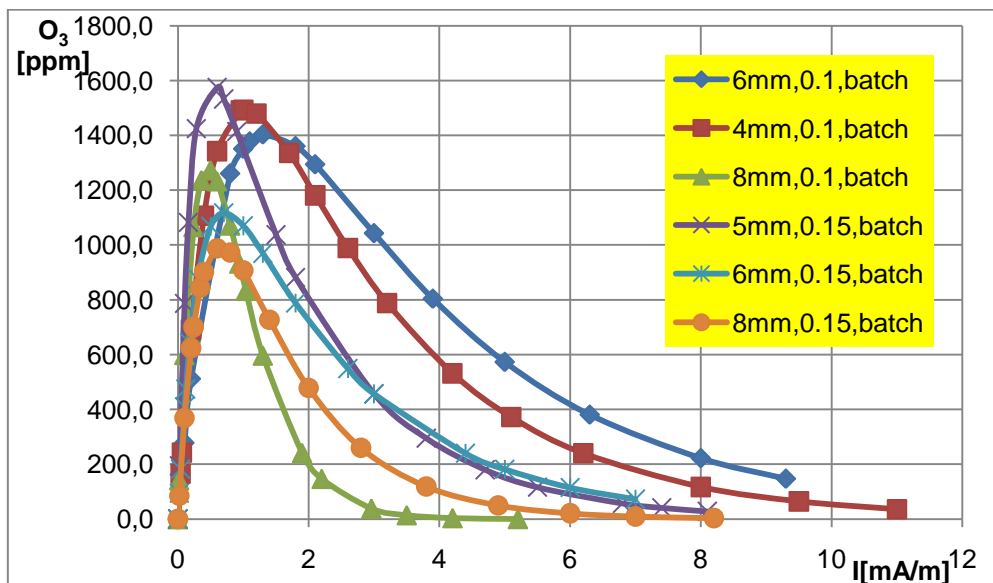


Figure 56: Comparison of ozone generation (simulated data) with various brush with active length of 500 mm at bottom under batch mode and similar applied voltage conditions.

5.6.1 Ozone generation with brush type discharge electrodes (8 mm, 0.15 mm) with 500mm active length at bottom

Experimental investigation was conducted for brush type discharge electrodes (8 mm, 0.15 mm) under various applied conditions. The recorded data for ozone generation with batch mode was higher than with air flow and water circulation conditions. This behavior of ozone generation at batch mode was contrary to the earlier investigations.

Ozone generation for batch mode was higher than for air flow and water circulation mode. Ozone generation with water circulation mode was less than air and batch mode shown in *Figure 55*.

Ozone formation and degradation trends for various operation conditions were of similar shape. Although a lot of difference in ozone concentration was observed for various operations conditions all trends represent the same kinetics (explained in chapter 6). Peak ozone was recorded at very low corona current and degradation was also observed at slightly higher corona currents shown in *Figure 55*.

5.7 Comparison of ozone formation with batch mode

For comparison of ozone generation at batch mode, simulated data was used to construct the graphical representation with various brush type discharge electrodes shown in *Figure 56*. Various brush type discharge electrodes (4 mm, 5 mm, 6 mm and 8 mm) with various wire diameters (0.1 mm, 0.15 mm) were investigated to determine ozone formation and degradation mechanism at various operations conditions (corona current, batch, air and water circulations).

Ozone generation with brush type discharge electrodes of 4 mm (0.1 mm) and 5 mm (0.1 mm, 0.15 mm) diameter was higher compared with other diameters of brush type discharge electrodes (6 mm, 8 mm) shown in *Figure 56*. Degradation rate of generated ozone with 0.1 mm wire (4 mm, 5 mm) was lower compared with other discharge electrodes (6 mm, 8 mm). Application range regarding peak ozone availability with 6 mm was high enough and stable up to 3.5 mA. Ozone generation with 4 mm and 6 mm brush discharge electrodes remains high for wide span and still higher than with 8 mm brush discharge electrodes.

Ozone generated with 8 mm brush type discharge electrodes with 0.15 mm brush wires was comparatively less than for other brush diameters at batch operation conditions. Ozone degradation rate with 8 mm brush was comparatively high and

depletion of generated ozone was accomplished over 2-3mA as shown in *Figure 56*. Ozone formation and degradation trends with various brushes follow similar specific trends under batch operations.

5.8 Comparison of ozone generation under air purge conditions

Ozone generation under air purge conditions was also investigated with various diameters of brush discharge electrodes to determine the optimum diameter with specific geometry of electrodes. Ozone generation recorded with brush discharge electrodes (8 mm, 0.1 mm) was significantly higher than for 4 mm, 5 mm and 6 mm diameters of brush type discharge electrodes under same air purge conditions.

Brush discharge electrode with wire of 0.1 mm diameter has remarkable enhancing effect on ozone generation. It was observed that ozone generation was a function brush diameter, brush wire diameter, gap between two electrodes, air flow rate and water circulation. Applied corona current has also played an important role on ozone formation in ESP.

Comparatively an increase of ozone was recorded with limited increase of air purge with various diameters of brush discharge electrodes as shown in *Figure 57*. Effect of geometry of brush type discharge electrodes regarding its diameter and wire diameters on ozone was well investigated and demonstrated in *Figure 55* and *Figure 56* under batch and air flow conditions. Comparatively higher ozone was recorded under air purge conditions than of batch mode as in *Table 12*.

Table 12: shows experimentally observed ozone peaks with various brush type discharge electrodes with active length of 500 mm at bottom (converted to 1m) at various operation modes.

Electrode specification	Maximum ozone [ppm] Batch	Maximum ozone [ppm] Air	Maximum ozone [ppm] water
4 mm, 0.1 mm	1802	1520	428
5 mm, 0.15 mm	1496	1636	352
6 mm, 0.1 mm	1544	1658	428
6 mm, 0.15 mm	1497	1211	397
8 mm, 0.1 mm	1410	1973	471
8 mm, 0.15 mm	1514	1106	410

5.9 Comparison of corona current at 20 kV under various operation modes

Experimentally investigated and recorded data for various brush type discharge electrodes under batch, air flow and water circulation was formerly explained. Recorded data is summarized in **Table 13**.

Peak corona current was recorded for active length of 500 mm, arranged at the bottom; representative data for 20 kV operation voltages are given in **Table 13**.

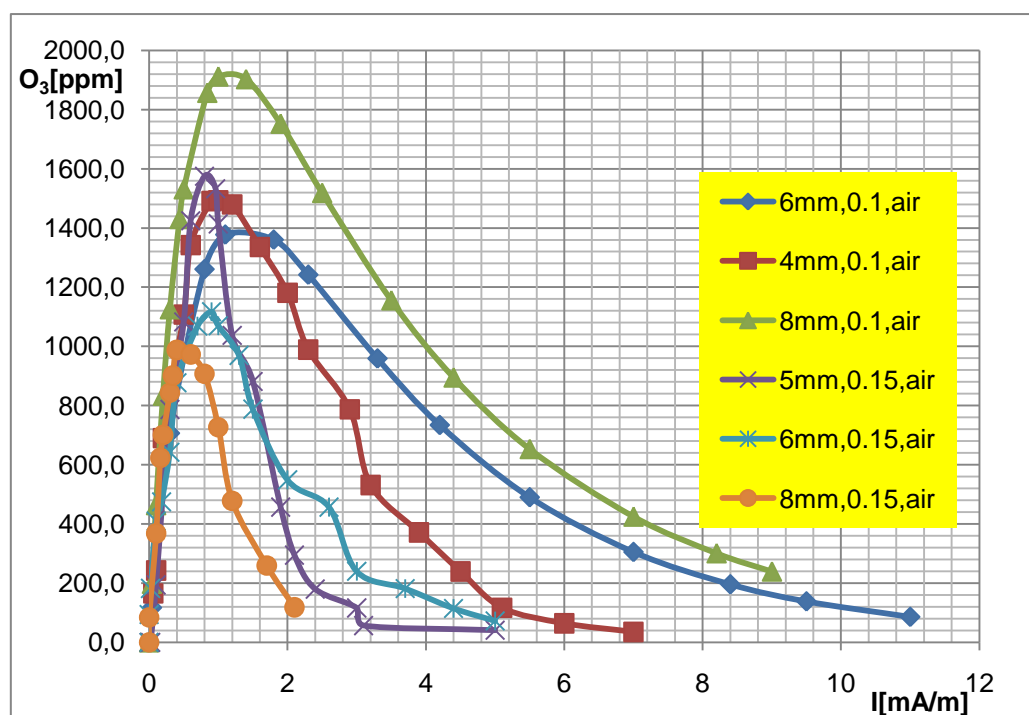


Figure 57: Comparison of ozone generation with various diameters of brush (500 mm) type discharge electrodes (0.1 mm, 0.15 mm) under air purge mode.

Table 13: shows the peak experimental corona current (mA) for various brush discharge electrodes at 20 kV at batch, air, air plus water operation conditions

Electrode specification	I [mA/m] Air purge mode	I [mA/m] Water circulation	I [mA/m] Batch mode
4 mm,0.1 mm	11	7	5
5 mm,0.15 mm)	8	5	4
6 mm,0.15 mm	7	5	3.5
8 mm,0.1 mm	9	9	5.5
8 mm,0.15 mm	8.2	8.2	4.5

5.10 Summary

Experimental investigations were conducted for various brush type discharge electrodes (4 mm, 5 mm, 6 mm and 8 mm) with various brush wire diameters to develop the current/voltage behavior and ozone generation under batch, air and air purge plus water circulation conditions.

Current/Voltage characteristic:

Current/voltage characteristics were studied with active length of 500 mm brush discharge electrodes at bottom and total length of electrode was 1500 mm as shown in *Figure 43*.

After observing a series of experimental investigations, it is concluded that brush wire diameter has a direct impact on corona current under specific operation conditions. Brush wire of 0.1 mm diameter generates higher corona current than 0.15 mm diameter of wire under same operation conditions and over similar range of applied voltage.

Also with the increase in diameter of brush discharge electrodes (5 mm, 6 mm, 8 mm) an increase in corona current was observed under batch, air flow and water circulations conditions. Brush discharge electrode of 4 mm and 0.1 mm wire diameter show a different behavior than electrodes of 5 mm, 6 mm and 8 mm diameter of the brush discharge electrode. Enhanced corona was observed with 4 mm (0.1 mm) compared with larger electrode diameters, shown in *Table 13*.

Investigation shows that higher corona current was recorded under air flow conditions than batch and water circulation mode. Corona current with water circulation mode was higher than for batch mode under similar operation conditions (in most cases).

Ozone:

Experimental studies were conducted with various brush type discharge electrodes over the range of 0-5mA corona current under similar operation conditions. Ozone generation was higher at lower corona currents (0.45-5 mA) and generated ozone was decreased at elevated corona current.

Ozone generation with air injection was higher than operation in batch and water circulation conditions. With air purge conditions ozone generation was increased for

required reaction as in Equation (5-1 to 5-2). Literature [81] also supported this reaction scheme.



At higher corona current, degradation of ozone was recorded and confirmed for all operation conditions. Further more effect of higher corona current on degradation of ozone follows the reverse reaction of equation (5-2). Ozone was converted into atomic oxygen and molecular oxygen generally. Under aqueous environment formation of hydroxyl radicals and hydrogen peroxides were also reported in literature [5].

6 Modelling of current/voltage relations and ozone generation with brush type discharge electrodes

Experimental investigations were conducted to determine the effect of geometry of brush type discharge electrodes on current/voltage characteristics and ozone formation at various operation conditions. Various geometry of brush discharge electrodes were investigated at applied voltage of 10-20 kV under batch, air purge and air plus water circulation modes.

Increase of corona current was recorded with the increase in applied voltage. Ozone generation was also investigated.

6.1 Comparison of current/voltage data for tungsten wire and brush type discharge electrodes

Investigations were conducted with tungsten wire and brush type discharge electrodes to determine the current/voltage characteristics under similar operation conditions. Investigated data with tungsten wire and brush type discharge electrode was also compared with calculated data generated from the state of the art empirical correlation as mentioned in chapter 2. Experimental and calculated data are shown in *Figure 58*.

Recorded data with tungsten wire type discharge electrodes shows a good agreement with calculated data (from semi-empirical correlation data). Corona current produced with brush type discharge electrodes shows agreement with calculated data at lower applied voltage and trend was different at higher applied voltage as shown in *Figure 58*. Comparison of experimentally recorded data with brush type discharge electrodes with calculated data shows a significant difference and hence need of correction was realized. Calculated data with proposed correction factors show good agreement with brush discharge electrodes.

Experimental data for corona current of tungsten wire was lower and similar to calculated data. Recorded data with brush type discharge electrodes (8 mm, 0.15 mm) under air purge conditions was higher than calculated data. Calculated data from state of the art empirical correlations does not truly define characteristics of brush type discharge electrodes.

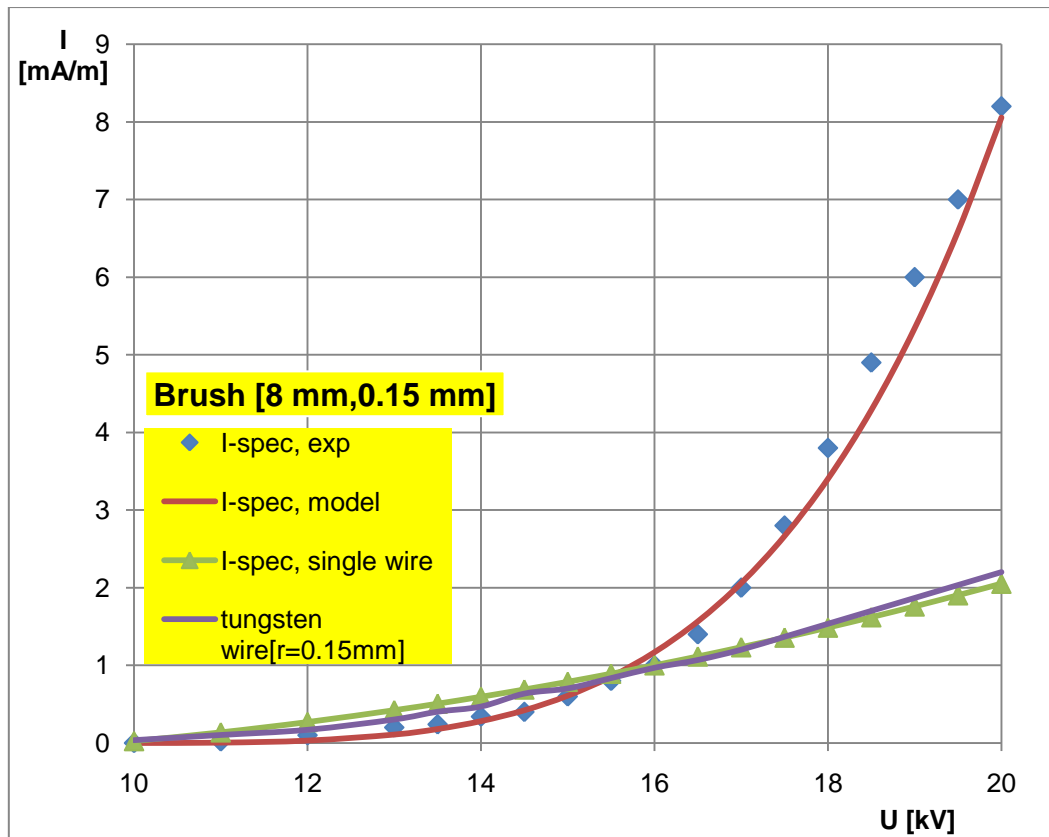


Figure 58: Current/Voltage curves with tungsten wire ($r=0.15$ mm) with active length of 1500 mm and brush type discharge electrodes (8 mm, 0.15 mm, 0.5 m³/h air purge) with active length of 500 mm. Experimental investigations were conducted at ambient operation conditions.

Basic empirical correlations used for design and development of electrostatic precipitators are corona onset field intensity and specific corona current. Corona current is directly proportional to operation/start up voltage and geometry of discharge electrodes. Start up voltage depends upon the corona onset field intensity and distance between two electrodes.

$$E_o = 3000 \cdot \delta + 90 \cdot \sqrt{\frac{\delta}{r}} \left[\frac{kV}{m} \right] \quad (6-1)$$

$$U_o = E_o \cdot r \cdot \ln\left(\frac{R}{r}\right) \left[\frac{\sqrt{kg \cdot m}}{s} \right] \quad (6-2)$$

$$I = \frac{U_{op} \cdot 2 \cdot K \cdot (U_{op} - U_o)}{R^2 \cdot \ln\left(\frac{R}{r}\right)} \left[g^{0.5} m^{0.5} S^{-2} \right] \quad (6-3)$$

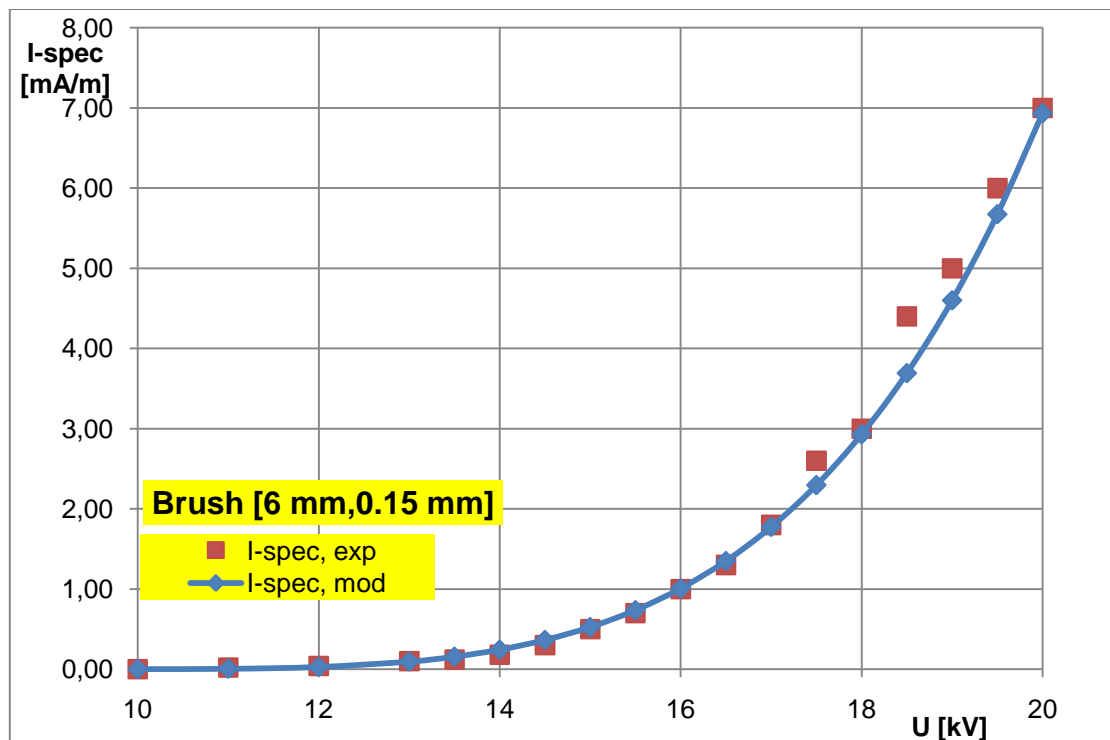


Figure 59: Current/Voltage curves with brush type discharge electrodes (6 mm, 0.15 mm) with active length of 500 mm at bottom with 0.5 m³/h air purge (data was converted into mA/m for graphical representation). Experimental investigations were conducted at ambient conditions.

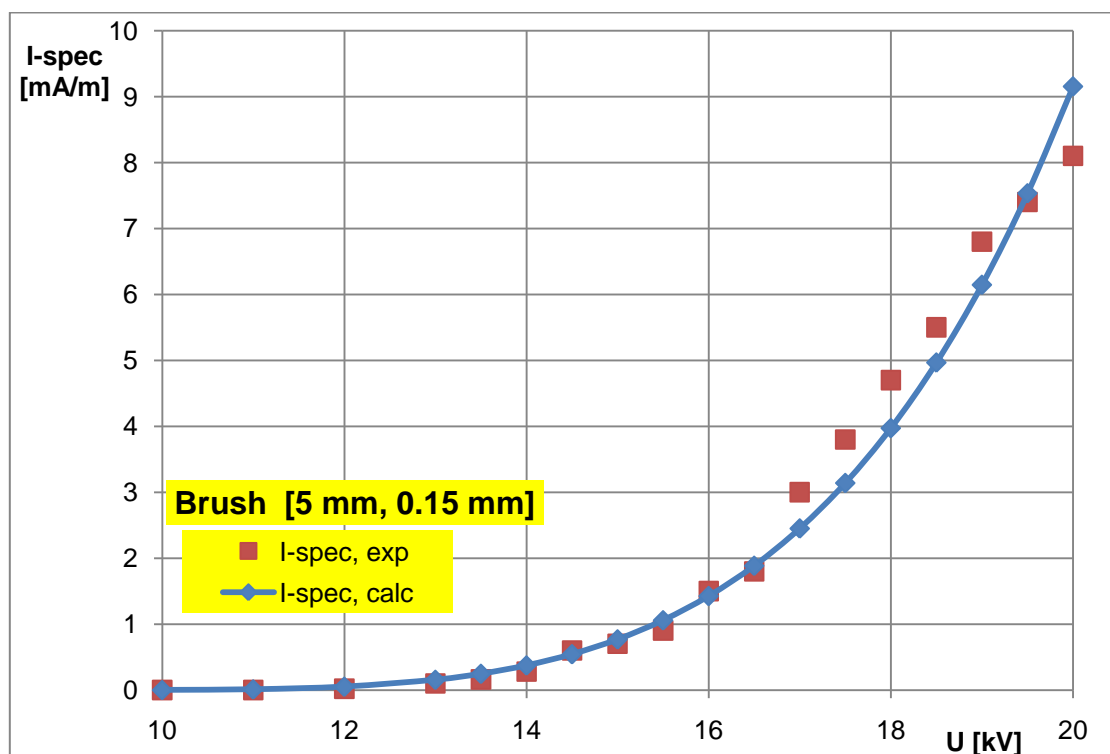


Figure 60: Current/Voltage curves with brush type discharge electrodes (5 mm, 0.15 mm) with active length of 500 mm at bottom with 0.5m³/h air purge (data was converted into mA/m for graphical representation). Experimental investigations were conducted at ambient conditions.

In case of brush type discharge electrodes, corona current behaviour was significantly different and higher than for tungsten wire type discharge electrodes. From above equations (6-1), (6-2), and (6-3), dependency of corona current on various parameters was explained. Increase in corona field intensity has increasing effect on corona current. With the increase in corona field strength rise in corona onset voltage was must not necessarily happen. Experimental data recorded with brush type discharge electrode was used for modelling of current/voltage curves and a new equation was proposed as.

$$I = \sqrt{3} * K * U^2 * \frac{\left(\frac{U - U_0}{U_0}\right)^3}{R - r_b * \ln\left(\frac{R - r_b}{r_w}\right)} \quad (6-4)$$

Generated data with modelled semi-empirical correlation was comparable and matches well with the experimental data from various (8 mm, 6 mm and 5 mm) brush type discharge electrodes shown in *Figure 58*, *Figure 59* and *Figure 60*

6.1.1 Fit data determination

Current/Voltage data generated with various brush type discharge electrodes like 4 mm, 5 mm, 6 mm and 8 mm diameters with wire of 0.1 mm and 0.15 mm diameters over the applied voltage of 10-20 kV was already explained and discussed in previous chapter 5. Experimentally obtained data at various operation modes showed similar current/voltage trends.

Experimentally investigated current/voltage behaviour was also monitored with table curve 2D program and simulated data was generated to remove the experimental errors. Each brush type discharge electrode was investigated at various operation modes like batch, air purge and air plus water circulation mode. The recorded current/voltage data at various operation modes was carefully used in table curve 2D program to get the real trend and equation of approximating functions. Nearly whole experimental current/voltage data follow similar trends and current/voltage trend was defined with power equations 8010, 8156 according to the power expression 8010 ($y = a + b * x^c$) and 8156 ($y = a * x^b$).

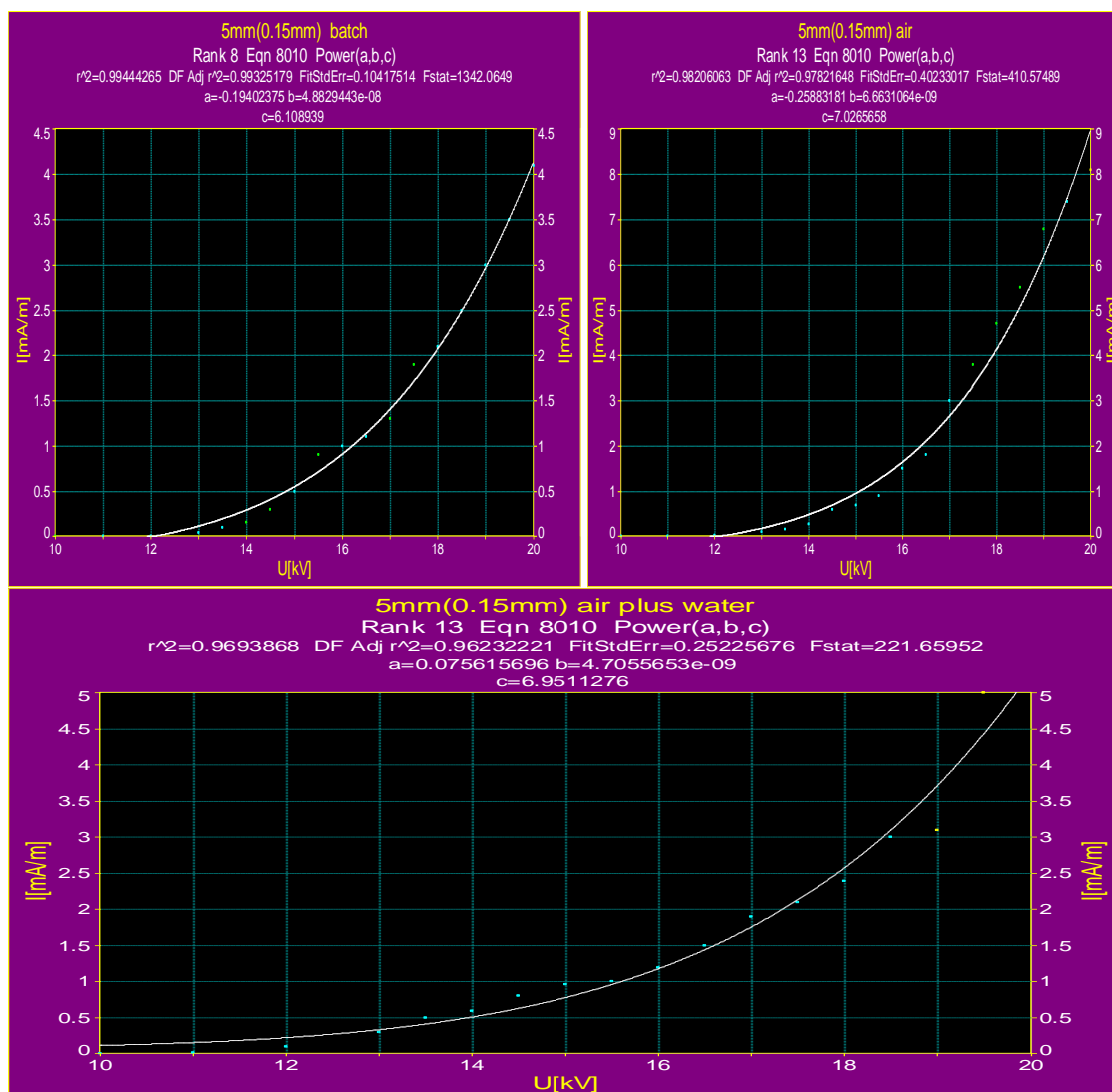


Figure 61: Current/voltage (experimental and simulated data) curves with brush type discharge electrodes (5 mm, 0.15 mm) with active length of 500 mm at bottom at batch, air purge and air plus water circulation). Current/voltage curves are representation of the typical power equation 8010.

Table 14: shows various parameters generated from approximating functions for brush type discharge electrodes 5 mm (0.15 mm) investigated under various operation modes.

Modes	Batch	Air purge	Air+water rinsing
r^2	0.99	0.98	0.97
a	0.194	0.26	0.076
b	$4.8 \cdot 10^{-08}$	$6.6 \cdot 10^{-09}$	$4.7 \cdot 10^{-09}$
c	6.11	7.02	6.95

Experimentally recorded data with 5 mm (0.15 mm) discharge electrodes and extrapolated data with table curve 2D program was determined. Extrapolated data for approximating functions (power equation 8010) and various parameters for given

equation are also illustrated in **Table 14**. Although fit data correspond to a power equation but in realy current/voltage curves do not follow this equation correctly below start up voltage.

Interpolation of X (kV) and Y (mA) coordinates with table curve 2D program rectify the experimental errors and real approximated data was produced. Simulated data was used to construct the current/voltage curves and smooth trends were obtained. Experimental and extrapolated data for current voltage curves follow two types of power equation 8010 ($y = a + b \cdot x^c$) and 8156 ($y=a \cdot x^b$).

We can select any equation having higher coefficient and lower rank number from the list of nonlinear equations. Experimental and simulated curves of 6 mm (0.15 mm) brush type discharge electrodes for batch, air purge and air plus water circulation are shown in **Figure 62**.

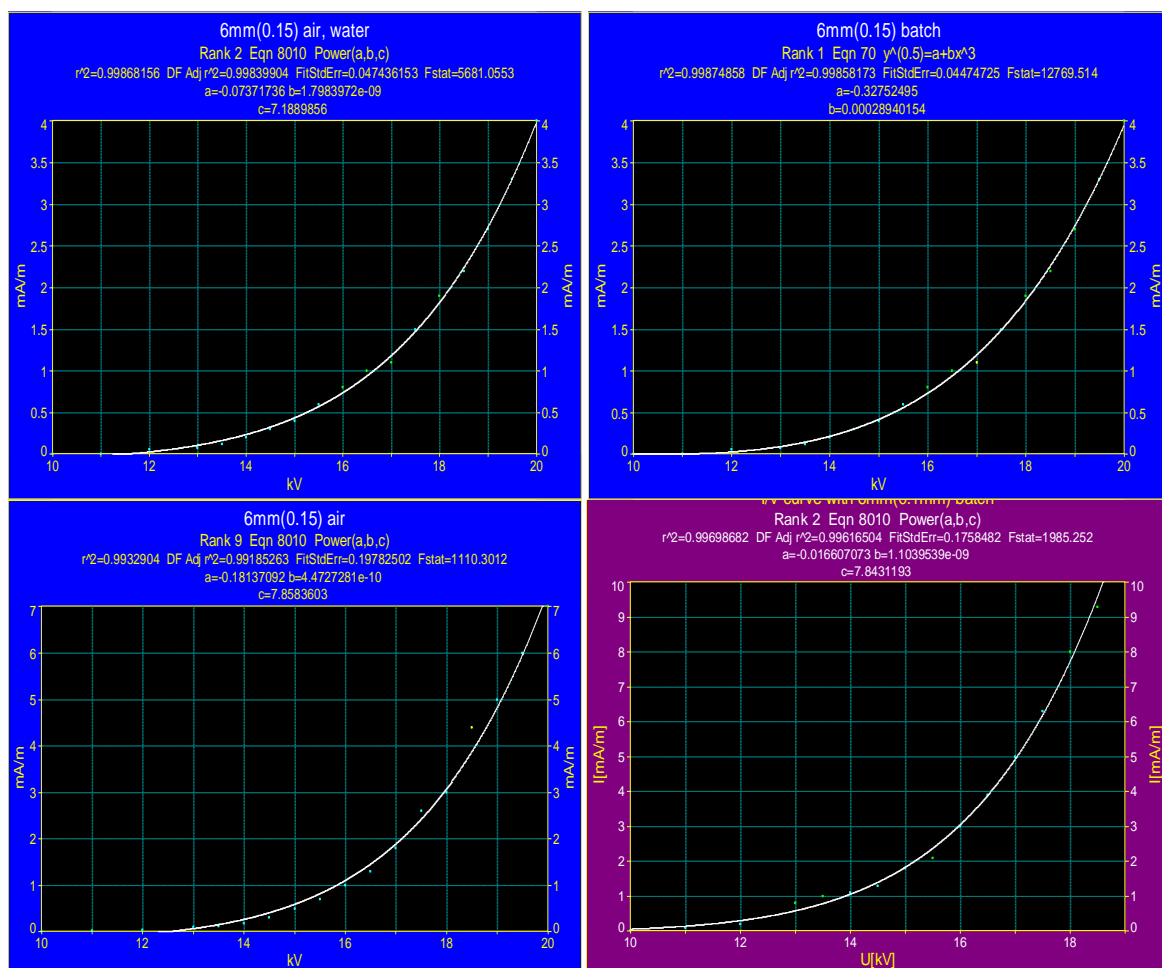


Figure 62: Current/voltage (experimental and simulated) curves with brush type discharge electrodes (500 mm, 6 mm, 0.15 mm), air purge and air plus water circulation (data was converted into mA/m for graphical representation). Current/voltage curve follow the typical power equation 8010.

Since current/voltage data for all operation modes follow the same general non-linear power equation 8010 from table curve 2D program. Power equation 8010 is explained in Equation (6-5) and extracted from table curve 2D program.

$$y = a + b.x^c$$

(6-5)

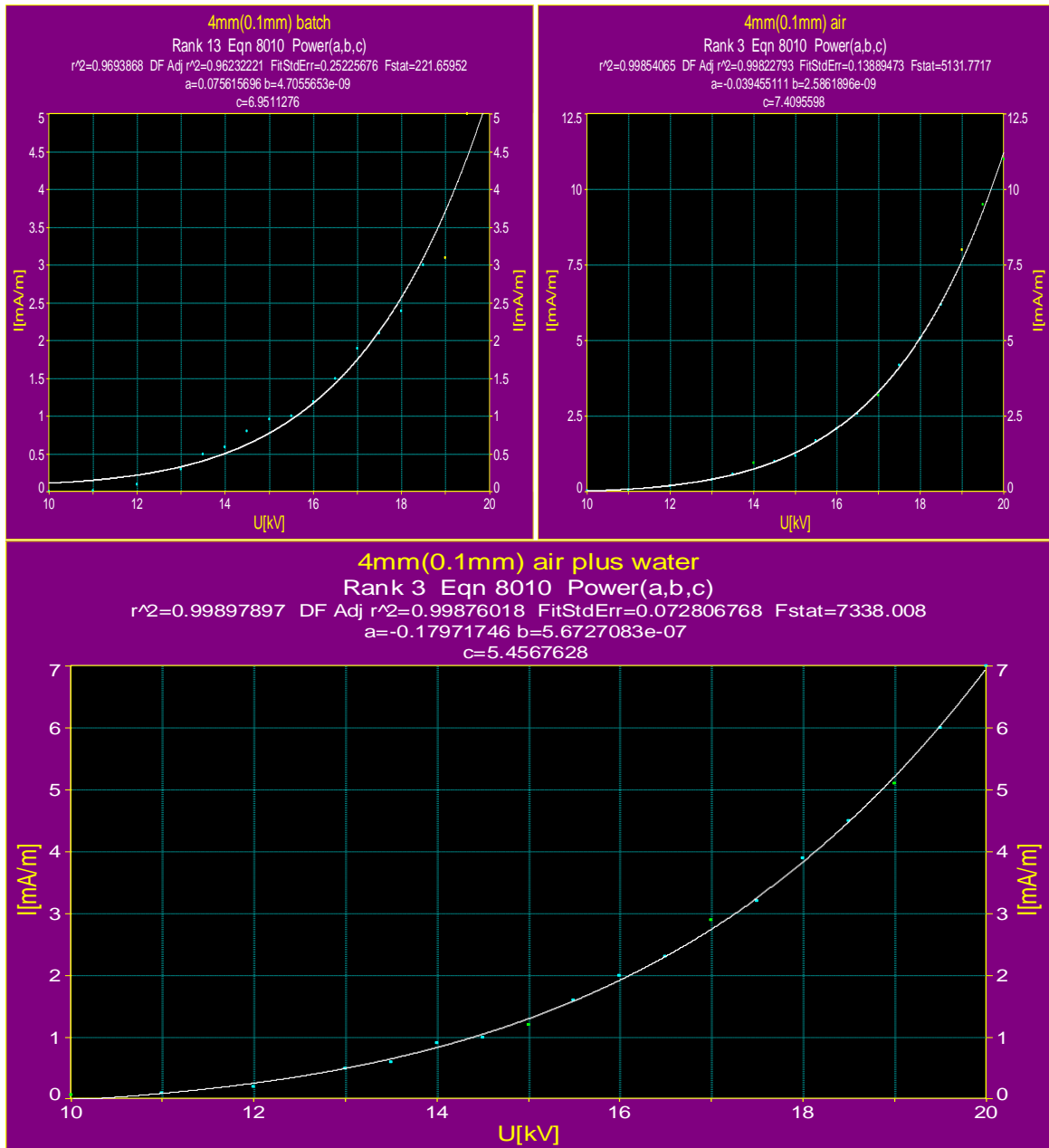


Figure 63: Current/Voltage(experimental and simulated) curves with brush type discharge electrodes (4 mm, 0.1 mm) with active length of 500 mm at bottom at batch, air purge and air plus water circulation Current/Voltage curve follow the typical power equation 8010.

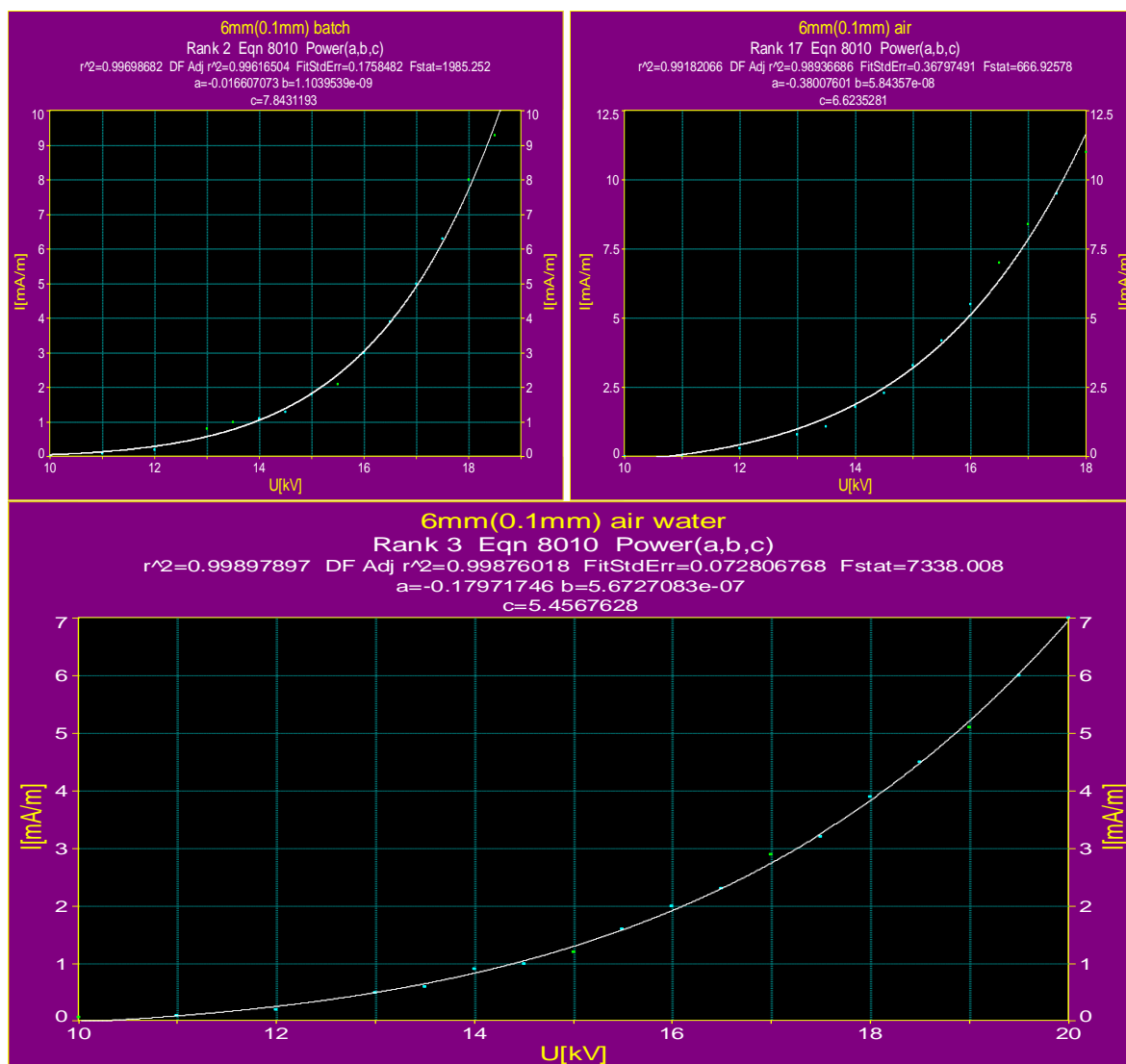


Figure 64: Current/voltage(experimental and simulated) curves with brush type discharge electrodes (6 mm, 0.1 mm) with active length of 500 mm at bottom at batch, air purge and air plus water circulation (data was converted into mA/m for graphical representation). Current/voltage curve follow the typical power equation 8010.

Table 15: shows various parameters generated from approximating functions for brush type discharge electrodes 6 mm (0.15 mm) investigated under various operation modes.

Modes	Batch	Air purge	Air + water rinsing
r^2	0.99	0.99182	0.998978
a	0.016	0.380078	0.1797174
b	$1.104 \cdot 10^{-09}$	$5.84357 \cdot 10^{-08}$	$5.672708 \cdot 10^{-07}$
c	7.8431193	6.6235281	5.4567628

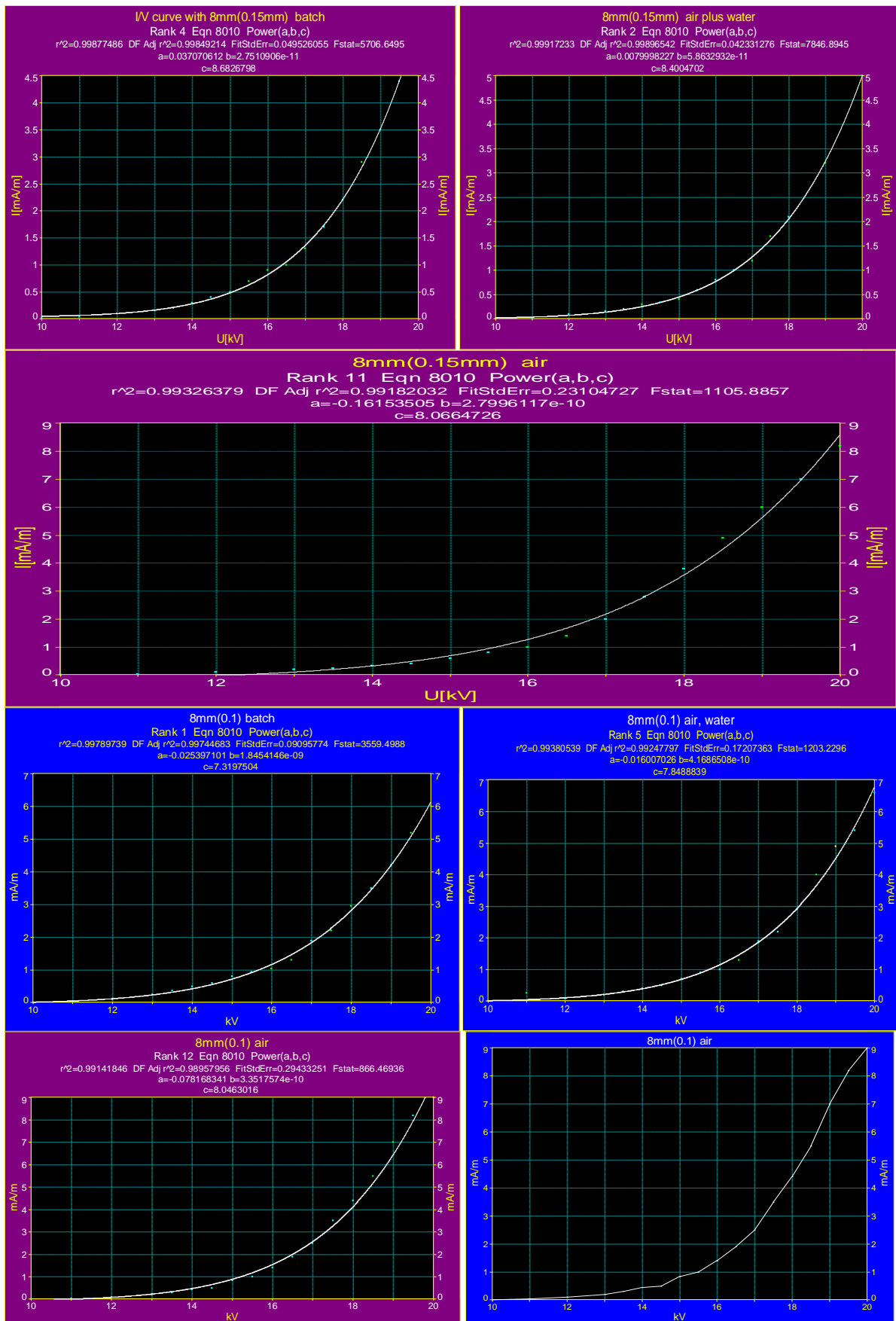


Figure 65: Experimental and simulated curves with brush type discharge electrodes (8 mm, 0.15, 0.1 mm) with active length of 500 mm at bottom at batch, air purge and air plus water circulation.

Investigations were conducted to determine the effect of geometry of brush discharge electrode on the current/voltage curves and ozone formation. Different types of brush discharge electrodes were investigated with increase in specific corona current and under similar applied conditions.

Fit data curve current/voltage data with different brush electrodes under various operation conditions follow a typical relation specified as 8010 and explained by Equation (6-5).

6.2 Ozone generation and determination of kinetic equation through table curve 2D program

Multiple design of brush type discharge electrodes were constructed and investigated to develop the current/voltage behaviour at specific applied conditions. During investigations ozone formation was recorded.

Experimental data for ozone generation was modelled by using table curve 2D program and interpolated data was determined. Data generated from table curve program was used to determine the reaction kinetics of ozone formation. Ozone generation data with 4 mm, 5 mm, 6 mm and 8 mm diameter of brush discharge electrode with wire of 0.1 mm and 0.15 mm was used to generate the fit curve equation. Experimental data with different diameters of brush discharge electrode for ozone generation was plotted against corona current and modelled-data information corresponds to intermediate formation equations 6089 and 8130. Fit curve equation for different discharge electrodes are shown in *Figure 66* to *Figure 72*. Ozone formation was maximum at specific corona current and at higher corona current dissociation of generated ozone was observed.

Ozone formation mechanism was studied to evaluate the real reaction kinetics. Experimental data was used to measure the simulated data with table curve 2D program. Simulated and fit data representing the kinetic equation was also discussed. Determination of real kinetic equation through approximation functions is an important task of the thesis.

6.2.1 Modelling of ozone generation with 8 mm (0.15 mm) at batch mode

Experimental data generated with 8 mm (0.15 mm) was used to determine the approximate function and equation representing ozone formation with corona current. Experimental data was applied for simple equation and various fit curve equations (non linear equation).

Ozone data was applied with various fit curve approximating functions and for simple linear equations data was fit to a specific equation in table curve 2D program (version applicable 97-2003 excl-MS). Analysis of curve fit equations and data represents the intermediate peak equation (8069) and equilibrium peak (8071). Rate constants are described in respective equations in reference **Table 35** .

Simulated (extrapolated) x and y data explain the Intermediate peak equation 8069



and kinetic equation is mathematical represented as:

$$y = \frac{b[\exp(-b(x-d)) - \exp(-c(x-d))]}{c-b} \quad (6-7)$$

Experimental data was also checked for curve-fit peak functions and equilibrium peak simultaneously. Equation 8071 was fit to experimental data and simulated data are shown in **Figure 66**

$$y = a[1 - \exp(-b(x-c))] - \frac{c}{c+d} \left[1 + \frac{b * \exp(-(c+d)(x-e)) - (c+d) \exp(-b(x-e))}{c+d-b} \right] \quad (6-8)$$

Equilibrium peak equation is summarized in equation 6-8 and reaction mechanism is given as:



Detail of equilibrium peak equations is summarized and given in **Table 27**.

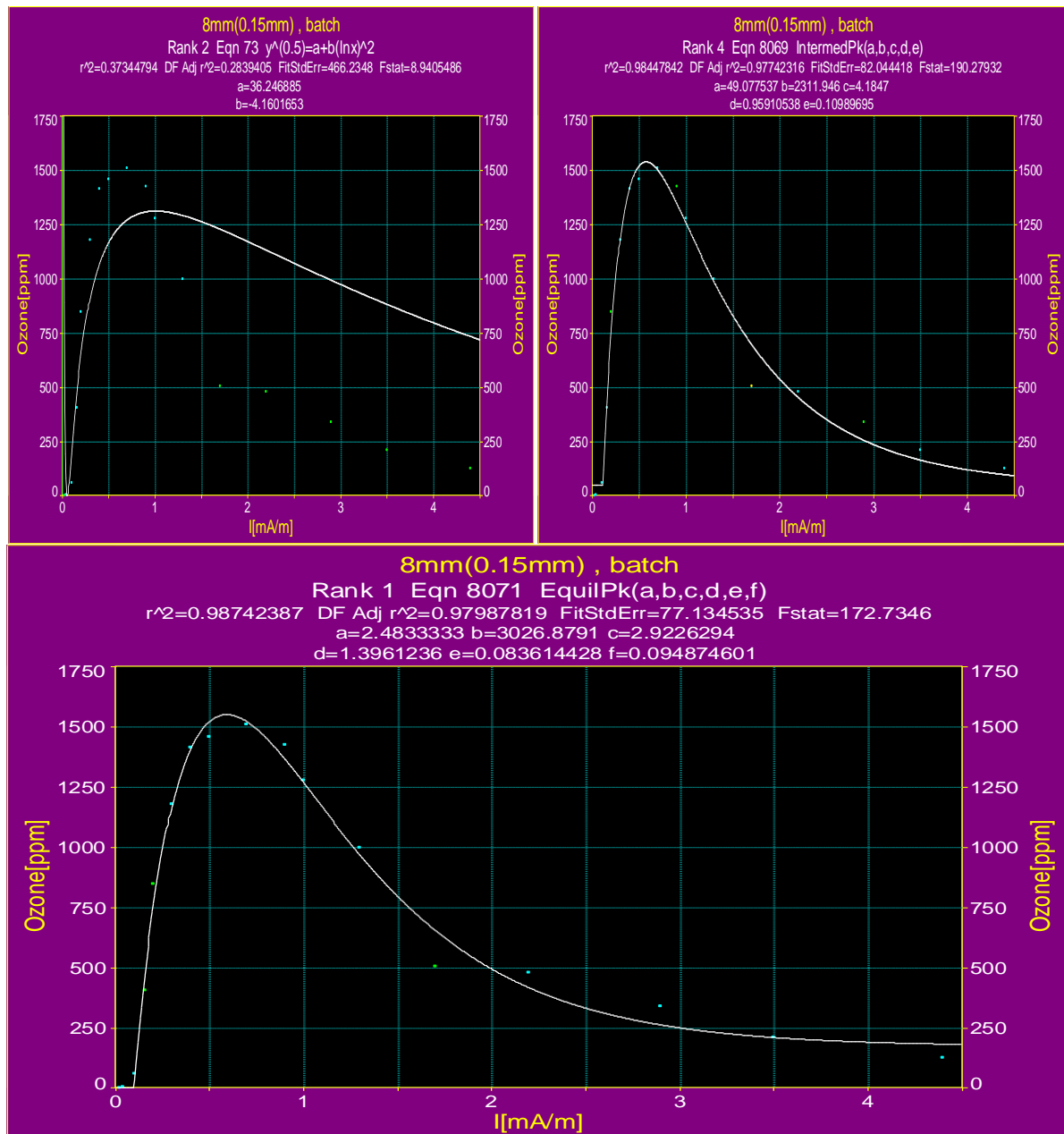


Figure 66: Ozone (experimental and simulated) curves with brush type discharge electrodes (8 mm, 0.15 mm) with active length of 500 mm at bottom at batch (data was converted into mA/m for graphical representation).

6.2.2 Ozone generation with 8 mm (0.15 mm) at air purge mode

Brush type discharge electrodes with active length of 500 mm (8 mm, 0.15 mm wire diameter) was investigated under air purge mode and ozone generation recorded as function of the corona current. Ozone formation trend was observed over range of 0-6 mA corona current. For air purge conditions, enhanced ozone formation and slow degradation was recorded compared with batch and water circulation conditions.

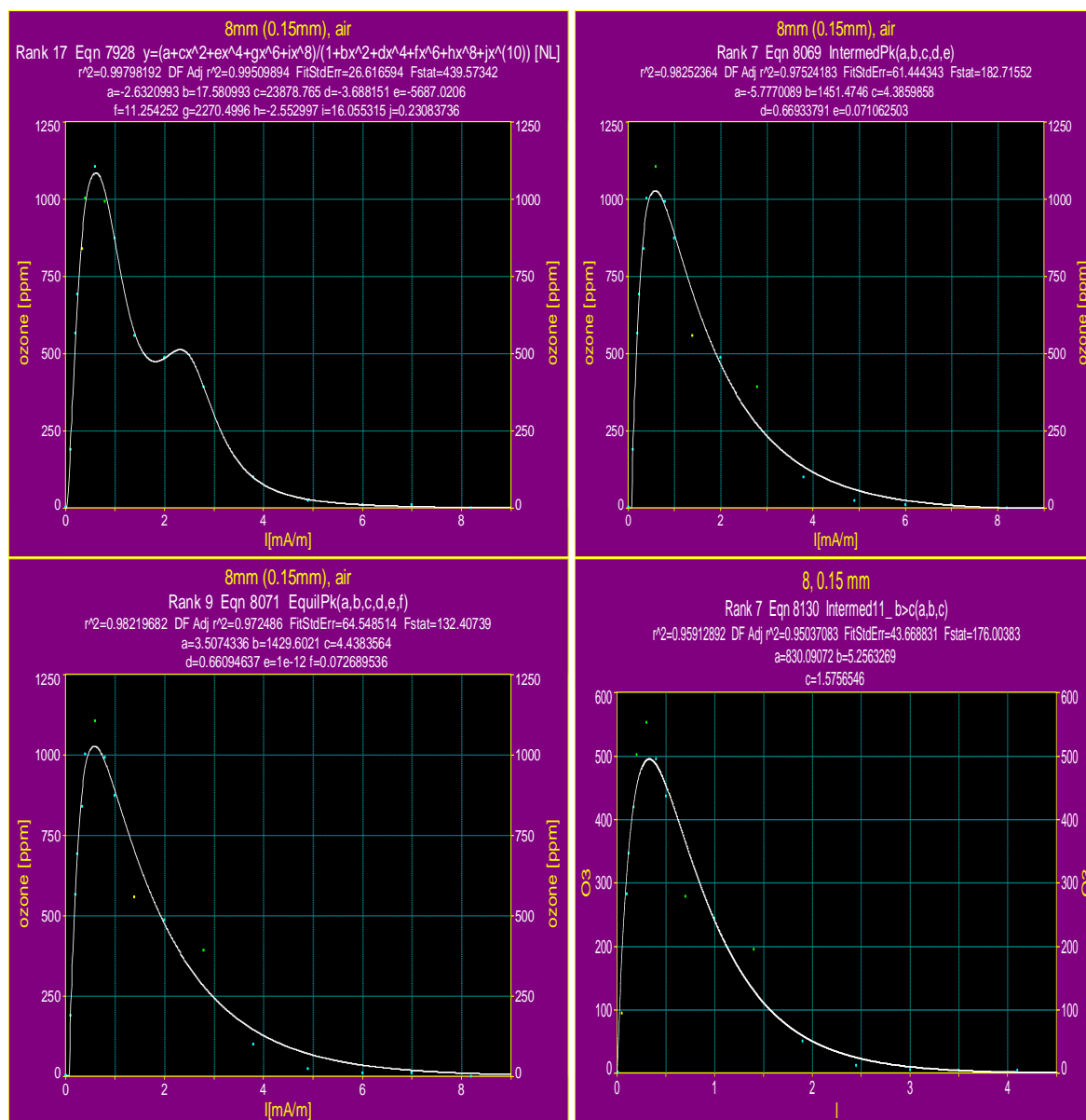


Figure 67: Ozone (experimental and simulated) curves with brush type discharge electrodes (8 mm, 0.15 mm) with active length of 500 mm at bottom at air purge conditions (data was converted into mA/m for graphical representation). Ozone data assed with table curve 2D and various curve- Fit schemes are demonstrated.

Experimentally recorded data for ozone generation against corona current was used to determine the approximated curve-fit functions (simple equations, peak function and kinetic equations) shown in **Figure 67**.

Although experimental data was approximately fit to many linear and non-linear models, kinetics of ozone reaction was best explained with 8069 intermediate peak and 8071 equilibrium peak equations. Coefficient of determination for curve-fit with rate equations (8069, 8071 and 8031) were high enough and nearly same.

First order intermediate reactions corresponds to intermediate peak functions (8069)

and reaction is $A \xrightarrow{K_1} B \xrightarrow{K_2} C$, also demonstrated in equation (6-6).

Rate equations with air purge mode were similar to batch operation mode. Reaction mechanism is already summarized in equation (6-7).

6.2.3 Ozone generation with 8 mm (0.15 mm) at air plus water mode

Ozone formation data with water circulation mode was used in table curve 2D program to determine the curve-fit kinetics and finally compare the results with batch and air purge mode.

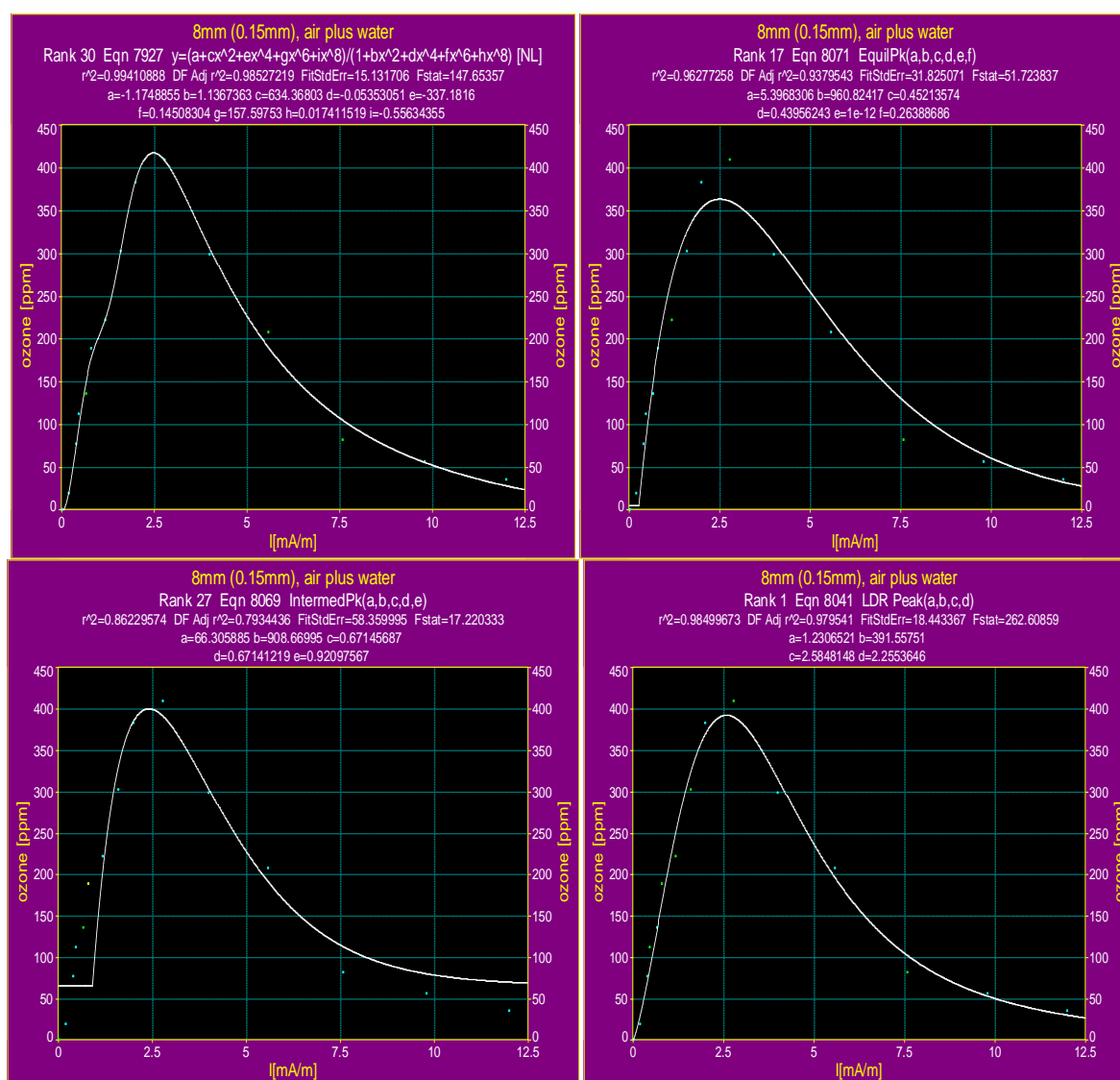


Figure 68: Ozone (experimental and simulated) curves with brush type discharge electrodes (8 mm, 0.15 mm) with active length of 500 mm at bottom at air purge plus water circulation mode (data was converted into mA/m for graphical representation). Ozone data assed with table curve 2D and various curve- Fit schemes are demonstrated.

Ozone generation with water circulation conditions was recorded and comparatively less ozone was observed than for batch and air purge modes. Experimental data was applied and concise to various linear and non linear mathematical functions shown in **Figure 68**. Although ozone formation was less with water circulation mode similar kinetic were observed as with batch and air purge mode. Equilibrium peak and intermediate peak functions (equations) are applicable to batch, air purge and water circulation.

Mechanism of reaction kinetics observed was nearly same and confirms the first order intermediate and equilibrium rate equations. Determination coefficient of kinetic equations was also in the acceptable range.

6.3 Ozone generation with 6 mm (0.15 mm) at batch mode

Experimentally investigated ozone data with brush discharge electrodes (6 mm, 0.15 mm) was used to determine the reaction kinetics of ozone formation and degradation. Curve fit of experimental data and equations with agreement of data were 7905, 8135, 8071 and 8069. All equations generally are nonlinear and approximately represent experimental data.

Kinetics of ozone formation and degradation was best explained by intermediate peak and equilibrium peak equations shown in **Figure 69**. Coefficients of determination in both peak kinetic functions were 0.988. The limitations and detail of reaction rate constants were explained in literature (table curve 2D program).

Curve-fit functions were thoroughly studied for batch, air purge and water circulations modes and data agreement with kinetics equation (non-linear peak model) were also confirmed.

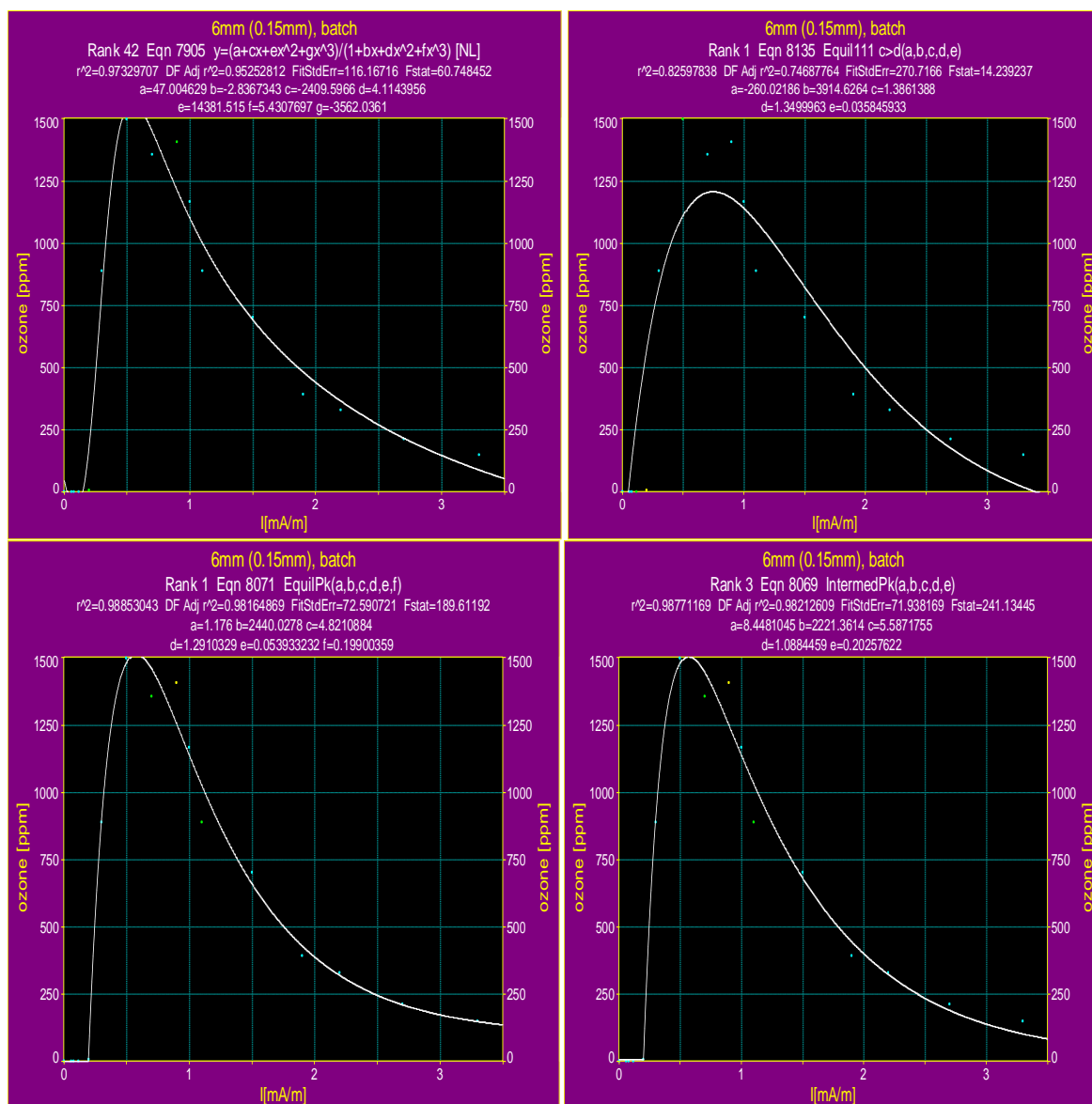


Figure 69: Ozone (experimental and simulated) curves with brush type discharge electrodes (6 mm, 0.15 mm) with active length of 500 mm at bottom and at batch mode (data was converted into mA/m for graphical representation).

6.3.1 Ozone generation with 6 mm (0.15 mm) at air purge mode

For air purge mode and 6 mm (0.15 mm) brush type discharge electrodes, curve fit equations determined were 8065 (pulse power), 7937 (simple equation, 8071 (equilibrium peak) and 8069 (intermediate peak). Although data did match simulated curves the coefficient of determination was not as high as for batch mode.

Overall experimental data follow the same kinetics of ozone formation as with 8 mm brush type discharge electrodes

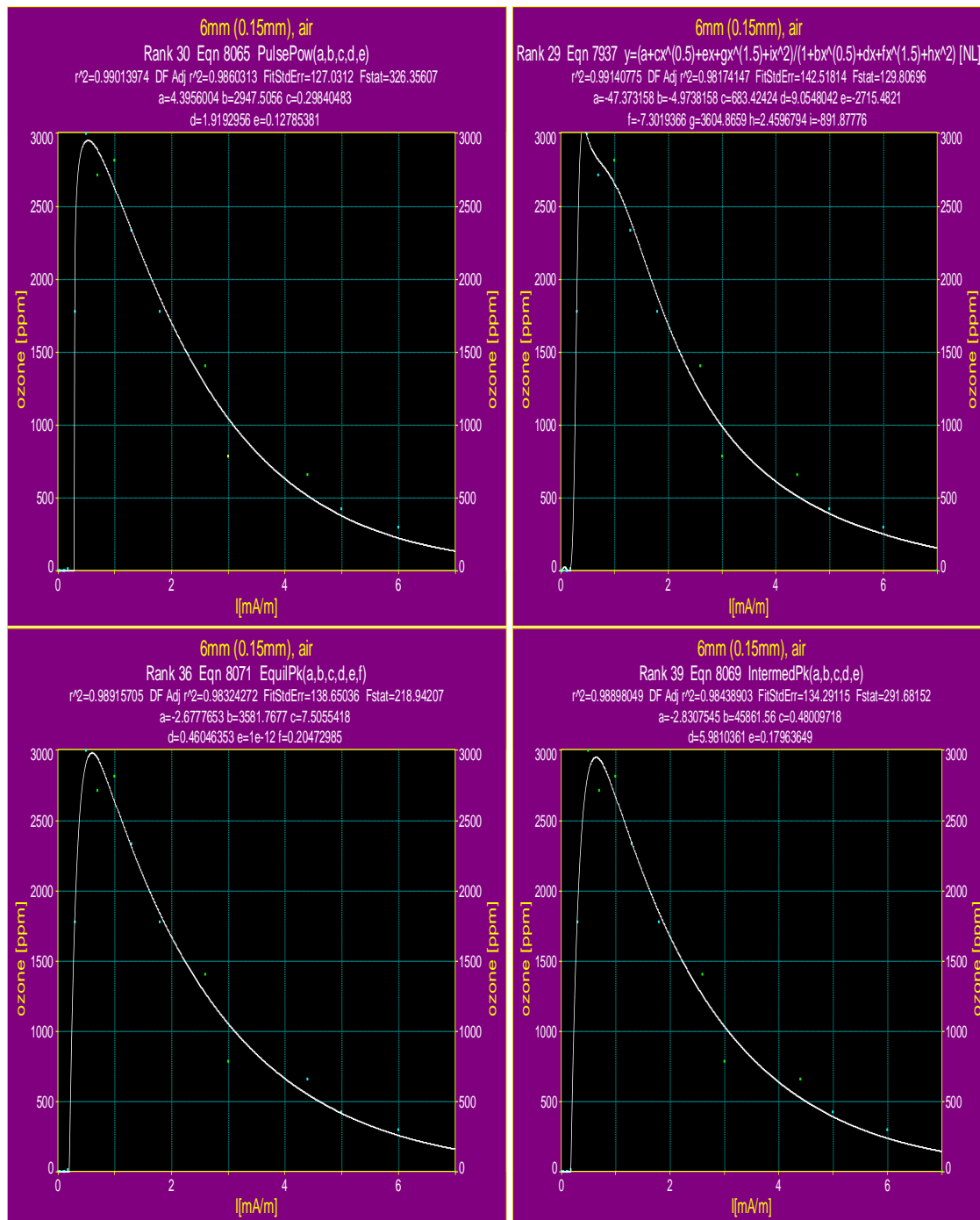


Figure 70: Ozone (experimental and simulated) curves with brush type discharge electrodes (6 mm, 0.15 mm) with active length of 500 mm at bottom and air purge mode (data was converted into mA/m for graphical representation).

6.3.2 Ozone generation with 6 mm (0.15 mm) at air plus water mode

Curve-fit 2D program was used to analyze the experimental data under air plus water circulation.

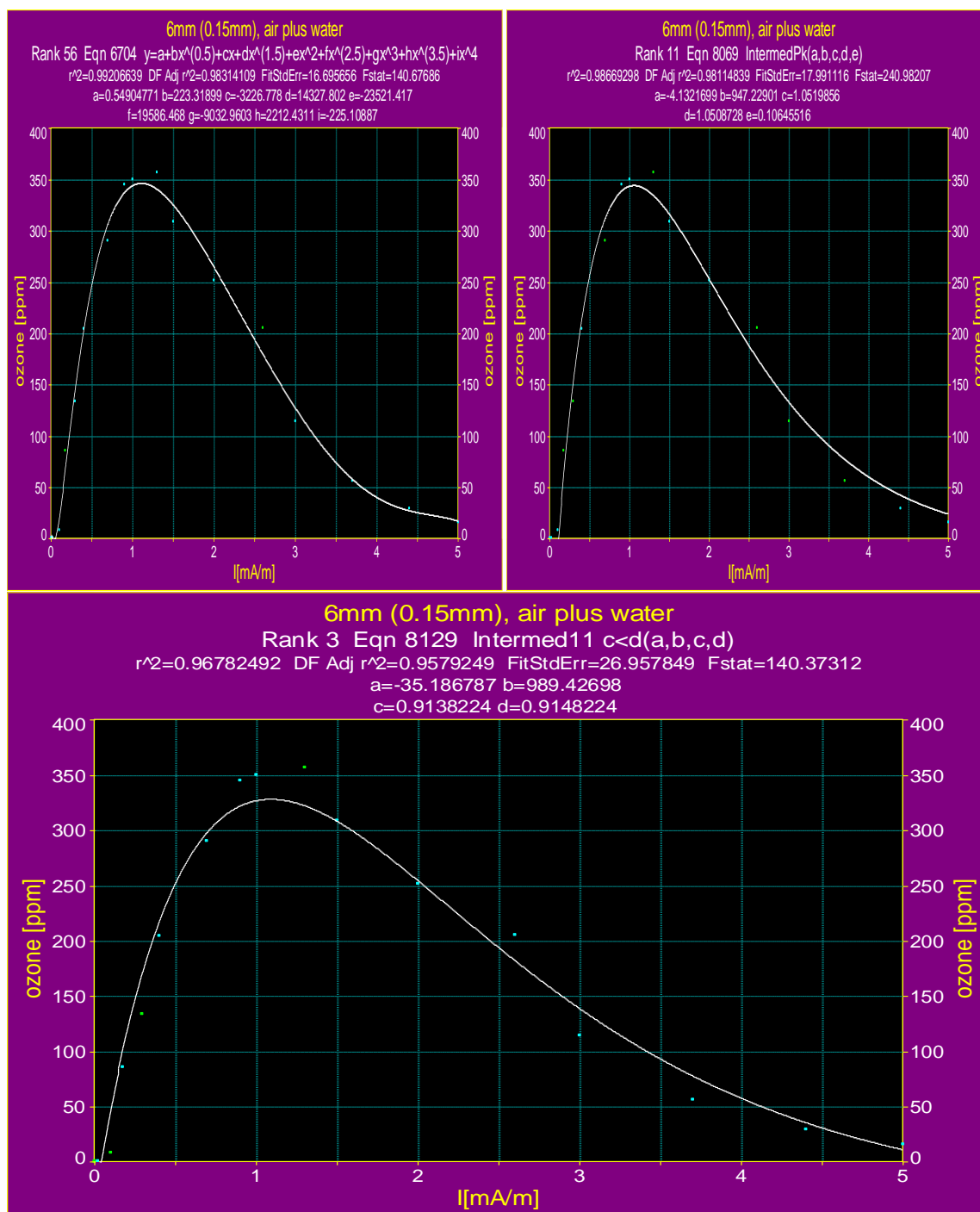


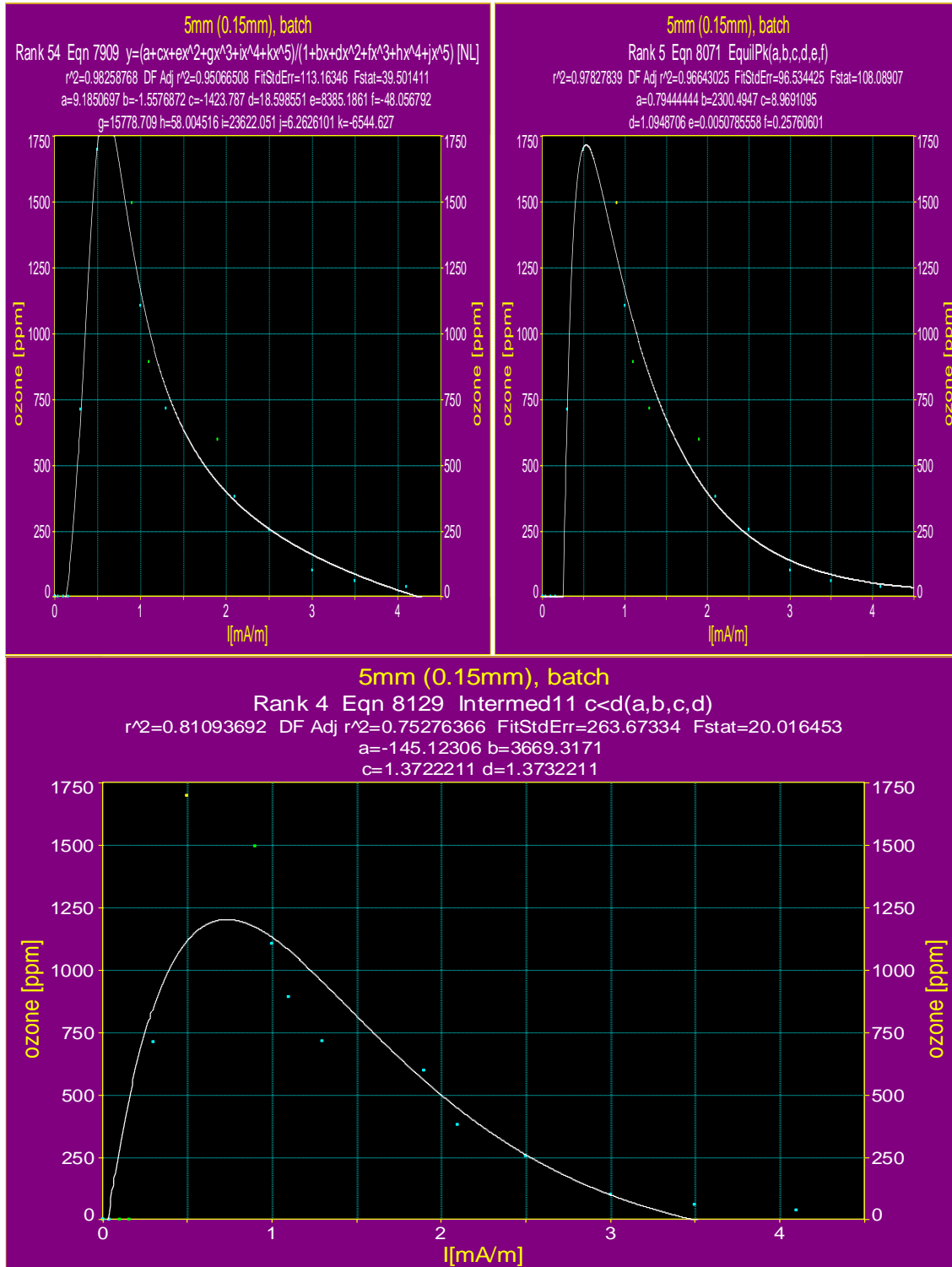
Figure 71: Ozone (experimental and simulated) curves with brush type discharge electrodes (6 mm, 0.15 mm) with active length of 500 mm at bottom and air purge plus water circulations mode (data was converted into mA/m for graphical representation).

Approximately determined functions are first order intermediate (8129), intermediate peak (8069) and 7904 (simple but non linear).

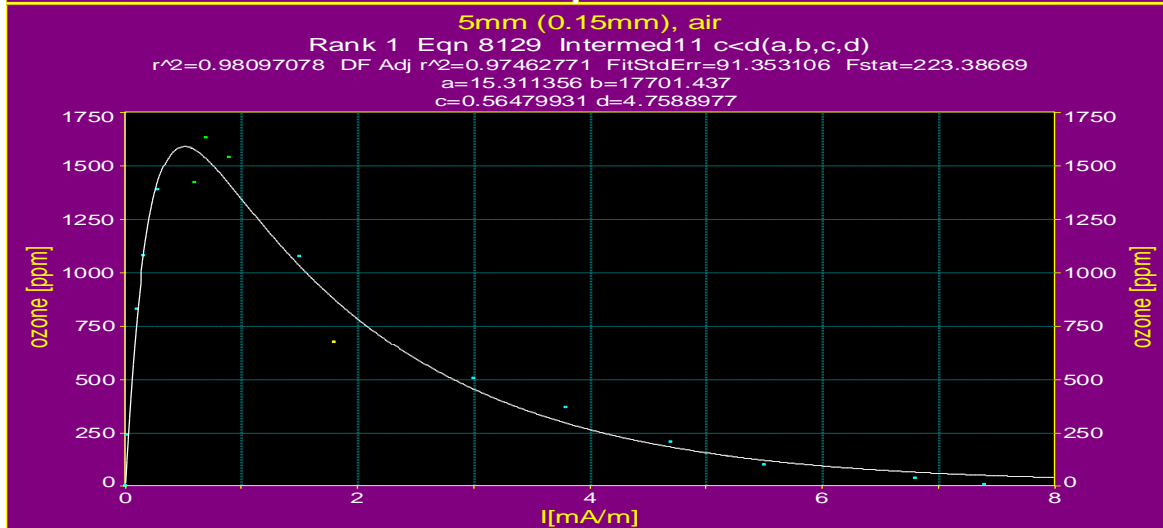
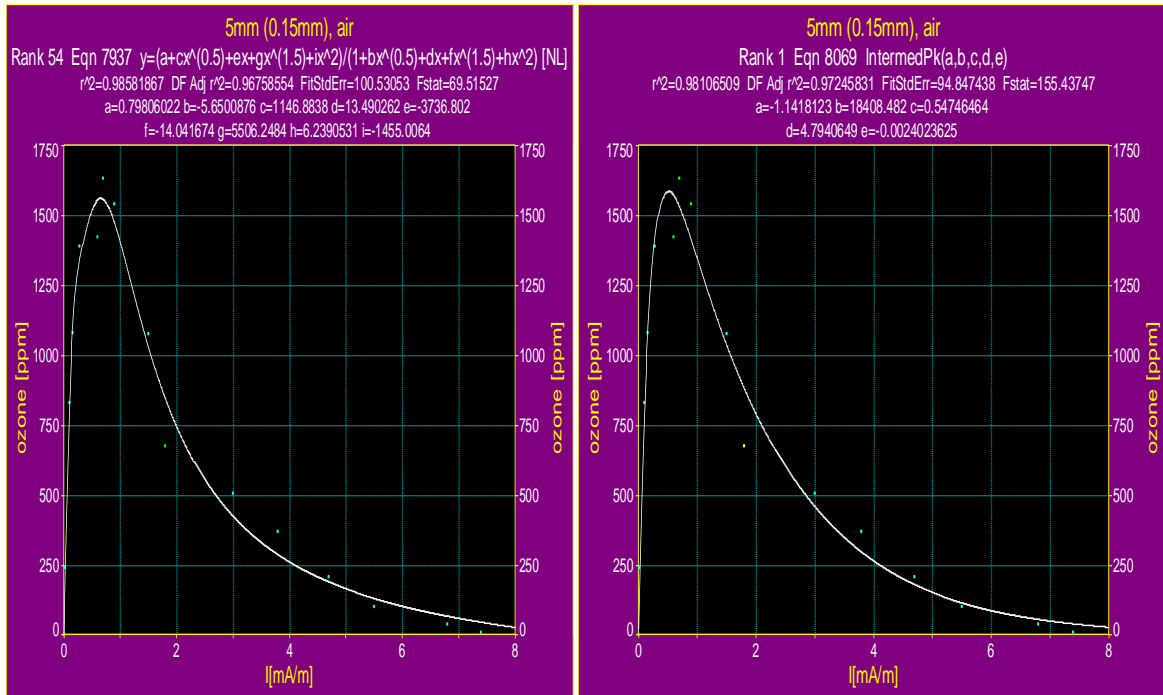
First order intermediate (8129) is of same kinetics as intermediate peak 8069 equations. Determination Coefficient of 8069 function was higher than 8129.

Therefore intermediate peak function has good interpretation of experimental data shown in *Figure 71*.

6.3.3 Ozone generation with 5 mm (0.15 mm) at batch mode



Modelling of Current/Voltage Relations and Ozone Generation



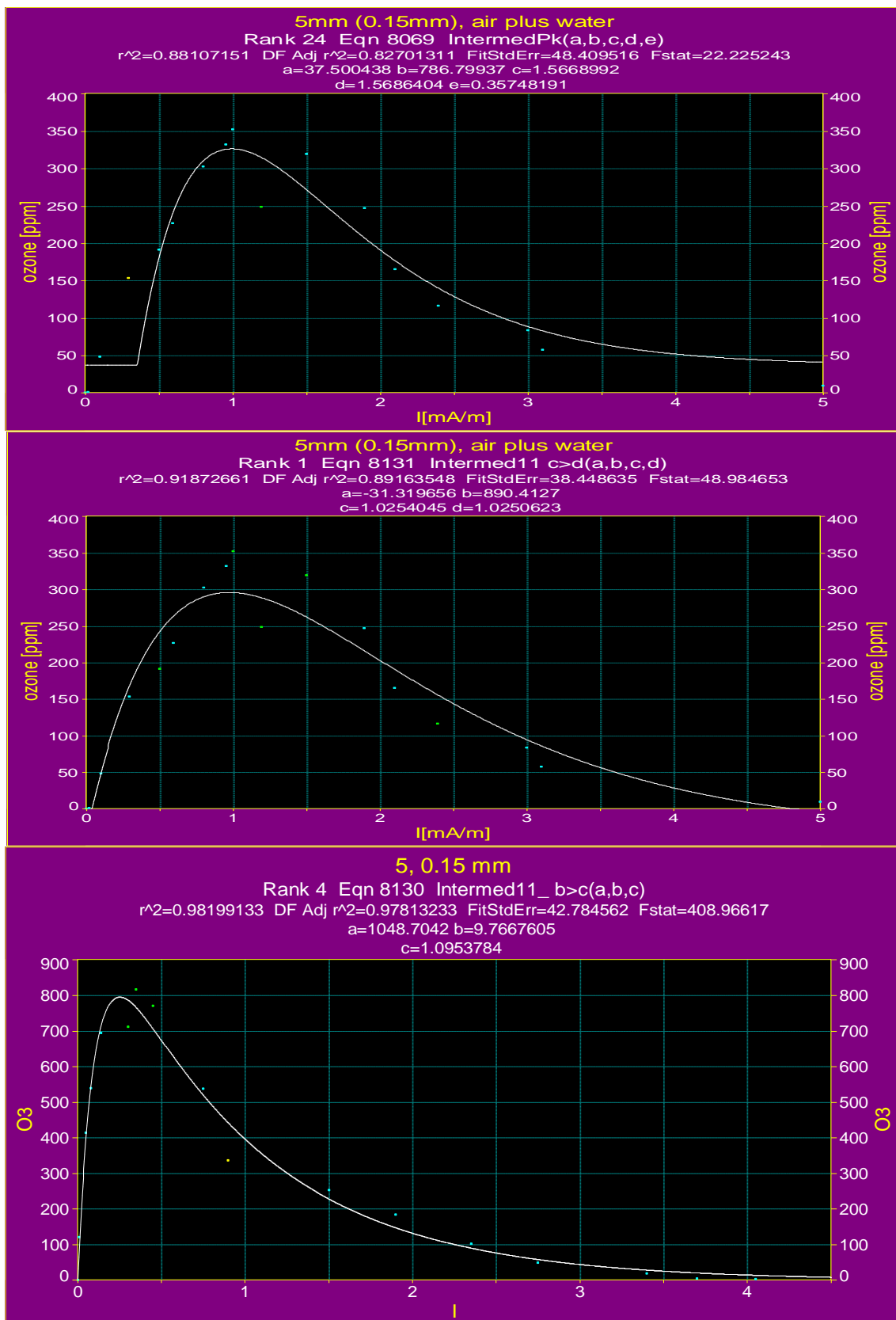


Figure 72: Ozone (experimental and simulated) curves with brush type discharge electrodes (5 mm, 0.15 mm) with active length of 500 mm at bottom under batch, air purge and air purge plus water circulations mode (data was converted into mA/m for graphical representation). Ozone data assessed with table curve 2D and various curve- Fit schemes are demonstrated.

Experimentally investigated data for ozone formation with brush type discharge electrodes 5 mm(0.15 mm) under batch, air flow and water circulation conditions was analyzed in table curve 2D program. Simulated data was studied to determine the best fit kinetic equation.

Repeatedly observed fit-functions with high determination coefficient are 8069, 8071, 8130, 8131 and 8129. All these functions are of similar nature (regarding mechanism).

6.4 Summary

Experimentally recorded formation of ozone with brush discharge electrodes 8 mm (0.1, 0.15 mm), 6 mm (0.1, 0.15 mm), 5 mm (0.15 mm) and 4 mm(0.1) under batch, air flow and air plus water circulation was used in table curve 2D program to determine kinetics of ozone formation.

Experimentally recorded current/voltage data was used and approximate fit function was determined. Power equation 8010 best defines the experimental current voltage data with various diameters of brush discharge electrodes. Power equation is applicable under various operation modes as shown in *Figure 58* to *Figure 65*.

Experimental data of ozone formation showed a good agreement with simulated data for specific kinetic equations like intermediate, intermediate peak and equilibrium peak equation shown in *Figure 66* to *Figure 72*. Although simulated data of various fit functions (like simple equations) concise to the experimental results, these simple fit functions do not explain reaction kinetics of ozone formation.

Curve fit functions with higher coefficient of determination were recognized as to represent reaction kinetics of ozone formation at lower corona current and degradation at higher corona current.

7 Modelling of experimental current/voltage data with proposed equation

Current/Voltage characteristics data were recorded with different brush type discharge electrodes under various applied conditions. Experimental data was compared with modelled data to validate the model equation.

7.1 Basic information and assumptions

Radius of tube [R] = 33 mm=0.033m

Radius of brush [r_b] = 3 mm, 4 mm,5 mm, 6 mm and 8 mm

Radius of wire [r_w] = [0.075 mm=0.000075m, 0.1 mm=0.00005m]

Start up voltage $U_0=8 - 10.5kV$

$U_{max} = 22.4kV$

With the relative gas density δ

$$\delta = \frac{T_o \cdot P}{T \cdot P_o}$$

$\delta=0.97$

Calculated from $T_o = 293$ [K]. $P_o = 980$ [h Pa]. T: operation temperature [K]. P: operating pressure [h Pa] and r: radius of the discharge electrodes [m]

Based on electrostatic SI-units we may apply the following conversion factors

$$1KV = 1.05 \cdot 10^{-2} \left[\frac{\sqrt{kg \cdot m}}{s} \right]$$

$$1A = 9.49 \cdot 10^4 \left[\frac{kg^{0.5} \cdot m^{1.5}}{s^2} \right]$$

$K=20$ [$m^{1.5} kg^{-0.5}$]

Table 16: Empirical correlations and proposed model

State of the art empirical correlation	Proposed empirical correlation
$I = \frac{U_{op} * 2 * K * (U_{OP} - U_0)}{R^2 * \ln\left(\frac{R}{r}\right)}$	$I = \sqrt{3} * K * U^2 * \frac{\left(\frac{U - U_0}{U_0}\right)^3}{(R - r_b) * \ln\left(\frac{R - r_b}{r_w}\right)}$

Modeling of Experimental I/V Data with Proposed Equation

Table 17: Comparison of experimentally obtained current/voltage data, fit data with (table curve) and calculated data with model equation. Data correspond to specific brush discharge electrodes at specific start up voltage

kV	4mm (0.1) batch [Spec. I mA/m]			4mm (0.1) plus air [Spec. I mA/m]			4mm (0.1) +air. + water [Spec. I mA/m]		
	Exp.	Fit. 2D	Model	Exp.	Fit.2D	Model	Exp.	Fit. 2D	Model
10	0	0.12	0.00	0.04	0.027	0.00	0.06	-0.02	0.00
11	0.02	0.16	0.00	0.06	0.095	0.03	0.1	0.09	0.01
12	0.1	0.23	0.03	0.2	0.217	0.10	0.2	0.26	0.04
13	0.3	0.34	0.10	0.4	0.425	0.26	0.5	0.5	0.13
13.5	0.5	0.41	0.16	0.6	0.574	0.39	0.6	0.65	0.21
14	0.6	0.51	0.25	0.96	0.764	0.57	0.9	0.84	0.31
14.5	0.8	0.63	0.37	1	1.002	0.80	1	1.05	0.46
15	0.96	0.78	0.54	1.2	1.30	1.10	1.2	1.30	0.65
15.5	1	0.96	0.75	1.7	1.67	1.48	1.6	1.59	0.89
16	1.2	1.18	1.02	2.1	2.12	1.96	2	1.93	1.20
16.5	1.5	1.44	1.36	2.6	2.67	2.55	2.3	2.32	1.59
17	1.9	1.76	1.79	3.2	3.35	3.27	2.9	2.76	2.06
17.5	2.1	2.13	2.30	4.2	4.16	4.14	3.2	3.26	2.64
18	2.4	2.58	2.93	5.1	5.13	5.18	3.9	3.83	3.34
18.5	3	3.10	3.69	6.2	6.29	6.41	4.5	4.48	4.18
19	3.5	3.72	4.59	8	7.68	7.86	5.1	5.21	5.17
19.5	5	4.44	5.65	9.5	9.32	9.56	6	6.03	6.34
20	6	5.5	6.5	11	11.2	11.53	7	6.95	7.70
Coeff.Deter.R ²			0.9841	0.9977			0.98		
Start up Voltage (U ₀)			9.65	8.8			9.1		

Modeling of Experimental I/V Data with Proposed Equation

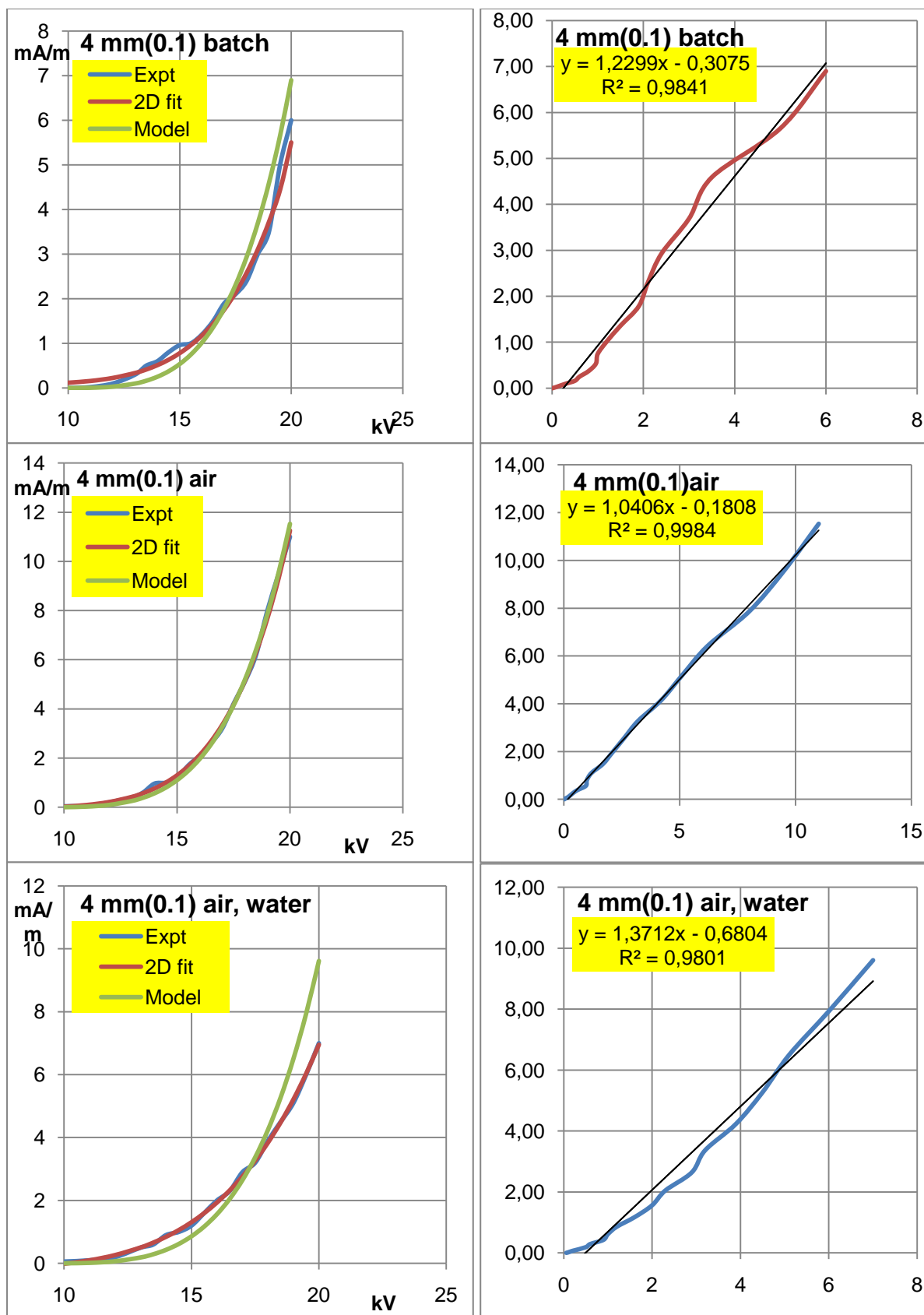


Figure 73: Comparison of experimental data with fit 2D program and model data with brush type discharge electrode 4 mm (0.1) under batch, air purge and water circulation mode. Comparison of experimental and model data was made to determine the coefficient of determination.

Modeling of Experimental I/V Data with Proposed Equation

Representative experimental, Fit and model current/voltage data with 4 mm (0.1) was demonstrated in **Figure 73** and data with 5 mm, 6 mm and 8 mm was attached in appendix as **Figure 87**. Experimental current/voltage data, fit data and calculated data with new equation with various brush discharge electrodes is summarized and data is attached as **Table 26** to **Table 31**.

Calculated data with new equation for current/voltage characteristic concise with experimental data recorded with various brush type discharge electrodes and fit data well. Further more calculated data are in agreement with experimental data under different operation mode.

7.1.1 Discussion

Experimentally investigated data was used to determine the Fit data by using Table curve 2D program. Most fit data follow the power equation 8010, explained in previous chapter 6 as well.

Data generated with brush type discharge electrode do not compare with the state of art empirical correlation for current/voltage characteristic shown in **Table 16**. Empirical correlation was adjusted according to a proposal of the supervisor [1] and model data were compared with the experimental data generated with various brush type discharge electrodes under batch, air purge and air plus water circulation conditions. The modelled data compare well with the experimental data. Start up voltage, obtained from modelled data was expectedly different for different brush diameter shown in **Table 18**.

4 mm (0.1) batch, air purge and air plus water circulations:

Experimental data with brush discharge electrode (4 mm, 0.1 mm) was plotted against model data under various applied conditions and the coefficient of determination was calculated to check accuracy of the model equation.

Start up voltage was 9.65 kV, 8.8 kV and 9.1 kV for batch, air purge and air purge plus water circulation respectively. Model data under batch, air purge mode and water circulation show good agreement with experiments.

5 mm (0.15) batch, air purge and air plus water circulations:

Model data show good agreement for batch mode and air purge mode when start up voltage of 10.1 kV and 9 kV was fixed. Poor agreement was recorded for water circulations and at 9.5 kV start up voltage. The experimental current/voltage data for

Modeling of Experimental I/V Data with Proposed Equation

water circulation may be of poor quality due to several reasons (partial arc/sparking, low tension in discharge electrode un-observed humidity level in inter-electrode region. water splashing etc)

Table 18: Shows the coefficient of determination of model and experimental data agreement. Effect of applied conditions on start up voltage is also illustrated.

Brush diam. specs.[mm]	Wire dia.[mm]	Distance b/w b.[mm]	condition	Coeff. Det. R ²	Startup voltage [U ₀]
4mm	0.1	31	batch	0.98	9.65
		31	Air purge	0.99	8.8
		31	Air + water	0.98	9.1
5mm	0.15	30.5	batch	0.97	10.4
		30.5	Air purge	0.98	9
		30.5	Air + water	0.96	9.5
6mm	0.1	30	batch	0.99	8.2
		30	Air purge	0.987	7.8
		30	Air + water	0.98	9
6mm	0.15	30	batch	0.99	10.5
		30	Air purge	0.99	9.6
		30	Air + water	0.99	10
8mm	0.1	29	batch	0.99	10
		29	Air purge	0.99	9.3
		29	Air + water	0.99	9.85
8mm	0.15	29	batch	0.99	10.3
		29	Air purge	0.99	9.5
		29	Air + water	0.95	10.1

6 mm (0.1 mm, 0.15 mm) batch, air purge and air plus water circulations:

Model data fit experiments well for 0.1 mm wire diameter when start up voltage of 8.2 kV, 7.8 kV and 9 kV is selected for batch, air purge and water circulation conditions.

For wire diameter of 0.15 mm the start up voltage had to be tuned to 10.5, 9.6 and 10kV under batch, air purge and water circulation respectively.

It was also recorded that, as expected, onset voltage was higher with 0.15 mm wire diameter than of 0.1 mm wire diameter with same brush diameter (6 mm).

8 mm (0.15 mm, 0.1 mm) batch, air purge and air plus water circulations:

Experimental data with brush discharge electrode 8 mm (0.15 mm) was again plotted against the modelled data under various applied conditions. Start up voltage under batch, air and water circulation condition was 10.3 kV, 9.5 kV and 10.1 kV respectively.

A good agreement of model data was observed for wire diameter of 0.1 mm and corresponding start up voltage under batch, air purge and water circulation was 10 kV, 9.3 kV and 9.85 kV. Start up voltage with 0.1 mm wire diameter was expectedly lower compared with 0.15 mm wire diameter.

Model data shows good agreement with experimentally investigated data under all operation conditions in general.

7.1.2 Summary

Good agreement of model data with experimental data was observed when the proposed correlation for current/voltage characteristic was applied.

This correlation satisfies the needs for getting a link between geometry of the discharge electrode (brush diameter and wire diameter) and current/voltage characteristic.

Model data agreement was strongly based on the correct choice of the start up voltage. The determined start up voltage data reflects the expected range well. The significant difference for batch and air purge operation confirms sufficient sensitivity of the data recording system.

8 Ozone formation and rate equation determination

Various brush type discharge electrodes were investigated to determine the current/voltage behavior at specific applied conditions. Effect of corona current on ozone formation was also investigated. Remarkable ozone concentration was recorded. Investigation was conducted at ambient conditions and twenty one percent of oxygen for ozone formation. For simplification of modelling it is also important that concentration of oxygen remains constant to give access to a first order reaction as proposed by Chapman. He postulated in 1930 [1] the formation and destruction of ozone in atmosphere under sun-irradiation. The reaction mechanism is summarized below.



Ozone formation mechanism was studied to evaluate the reaction kinetics. Experimental data was used to fit ozone formation with table curve 2D program. Fit data representing the various kinetic equations was discussed and illustrated in **Table 19**. Various rate constant and equation parameters were also compiled.

Irreversible first order intermediate formation reaction represented as in equation (8-5) and fits the data best.



Equation 8-6 shows the corresponding rate law based on the proposed formation mechanism of equation (8-5). The results are summarized in **Table 20**. This intermediate reaction corresponds to a typical equation containing X and Y coordinates (mA, O₃) with two rate constants having technical background and explained as

$$y = \frac{b[\exp(-b(x-d)) - \exp(-c(x-d))]}{c-b} \quad (8-6)$$

Above equation (8-6) was generated from table curve program best representing the ozone formation with applied corona current. Ozone (ppm) is plotted on x-axis and corona current (mA/m) is on y-axis, while b and c correspond to k₁ and k₂ respectively as mentioned in equation (8-5).

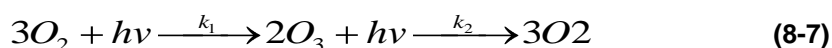
Table 19: Shows various fit rate equation determined with table curve 2D program for ozone generation. Various parameters for rate equation are also demonstrated.

Brush	Mode	Eq.	R ²	a	b	c	d	e	f
8mm (0.15)	Batch	8069	0.977	49.0	2311.9	4.184	0.91	0.11	
		8071	0.97	2.48	3026.5	2.926	1.39	0.08	0.09
	Air purge	8069	0.975	5.77	1451.4	4.36	0.66	0.07	
		8071	0.975	3.50	1429.	4.438	0.66	0.00.	0.07
	Air +water	8071	0.937	5.39	960.86	0.45	0.43	0.00.	0.26
		8069	0.79	66.3	908.66	0.67	0.67	0.97	
6mm (0.15)	Batch	8135	0.74	260.	3914.6	1.38	1.34	0.03	
		8071	0.98	1.17	2440.0	4.82	1.9	0.05	0.19
		8069	0.98	8.44	2221.3	5.58	1.08	0.20	
	Air	8071	0.983	2.67	3581.7	7.5	0.46	0.00.	0.20
		8069	0.983	2.83	45861.	0.48	5.98	0.17	
	Air, water	8069	0.98	-4.13	947.2	1.05	1.05	0.10	
	8129	0.95	-35.2	989.4	0.92	0.92			
5mm (0.15)	batch	8071	0.966	0.79	2300.4	8.96	1.09	0.00	0.26
		8129	0.752	-145.	3669.3	1.37	1.37	50	
	Air	8069	0.977	-1.14	18408.	0.55	4.79	-0.00	
		8129	0.978	15.3	17701.	0.56	4.78		
	Air, water	8069	0.82	37.5	786.79	1.56			
		8130	0.97	1048	9.76	1.09			

Table 20: Rate equations determined with table curve 2D program for ozone generation. Various parameters for rate equation are also demonstrated.

Brush	Wire	Mode	Fit Eq.	k ₁	k ₂
8mm	(0.15)	batch	8069	2311.9	4.184
		air	8069	1451.4	4.36
		Air, water	8069	908.66	0.671
6mm	(0.15)	batch	8069	2221.3	5.587
		air	8069	45861	0.48
		Air, water	8069	947.2	1.052
5mm	(0.15)	batch	8071	2300.4	8.96
		air	8069	18408.	0.547
		Air, water	8069	786.79	1.566

Corona discharge with high energy photons (5.1eV) can dissociate oxygen molecules to atomic oxygen. Atomic oxygen has affinity with molecular oxygen and immediately forms ozone. As we know ozone is not a stable compound and has short life. Kinetically speaking corona discharge initially produces the excited oxygen and ozone species at a specific rate and rate of reaction purely depends upon the intensity of corona current.



The rate equation may be transferred into terms of oxygen and ozone. The relation is expressed below in equation (8.8)

$$C_{O_3} = \frac{C_{A_0} \cdot k_1}{k_2 - k_1} \left[e^{-k_1(I-I_0)} - e^{-k_2(I-I_0)} \right] \quad (8-8)$$

k_1 and k_2 : [m/mA]

I, I_0 : [mA/m]

Equation (8-8) represents the ozone formation in the wet electrostatic precipitator under specific corona current for batch, air purge and air plus water circulation mode.

8.1 Summary

Determination of real kinetics equation through data fit is an important task of the thesis.

Experimentally recorded ozone data (formation) with different brush type discharge electrodes under various applied conditions were used to determine the fit data representing the kinetic functions. First order intermediate formation represents most of experimental data under all operation conditions.. Details of the investigated rate equations are mentioned in **Table 35**.

First order irreversible intermediate kinetic equation shows good agreement under various operation modes. Rate constants, coefficient of determination and fit equation data is shown in **Table 19** and **Table 20**.

It can be concluded that first order kinetic equation for irreversible first order intermediate formation is a representative rate equation for ozone formation at specified operation conditions.

9 Applications of wet tube-type electrostatic precipitator

The wet tube-type electrostatic precipitator equipped with brush type discharge electrodes is a multipurpose reactor which has potential applications in off-gas purifications and wastewater treatment.

9.1 Off- gas purification

State of the art application of wet tube-type electrostatic precipitators is the conditioning of off-gas, and to remove particulate matter from gases. Efficient separation of particulate matter (sticky particles, micronic and sub micronic) from off-gas was achieved with wet tube-type electrostatic precipitator. The wet electrostatic precipitator (WESP) has few advantages over dry electrostatic precipitation, as summarised.

- Efficient removal of sticky particles
- Self scrubbing water film and simultaneous cleaning of collector
- Enhanced collection efficiency

9.2 Waste water treatment

The wet tube-type electrostatic precipitator may be applied in wastewater treatment too. Investigations showed a great potential in WESP to eliminate hazardous pollutants from off-gas and wastewater simultaneously as an advanced wastewater treatment technology. Experiments were conducted to investigate the elimination of various hazardous constituents (acetone, phenol, EDTA) commonly present in wastewater. Degradation of acetone, isopropanol and mineralization of ethylene diamine tetra acetic acid (EDTA) and phenol was recorded. Degradation and mineralization of various constituents are discussed in section 9.2.1 - 9.2.3.

9.3 Acetone degradation

Water contaminated with acetone was treated in a WESP and degradation of acetone was recorded. The degradation trend was also compared with UV-radiation technology (low pressure mercury lamp). Acetone degradation with the wet tube-type electrostatic precipitator and low pressure mercury lamp irradiation was investigated. The comparison of technologies is shown in *Figure 74*. During the treatment the pH was monitored and the change of pH was recorded as indicator for chemical conversion of acetone, as shown in *Figure 75*.

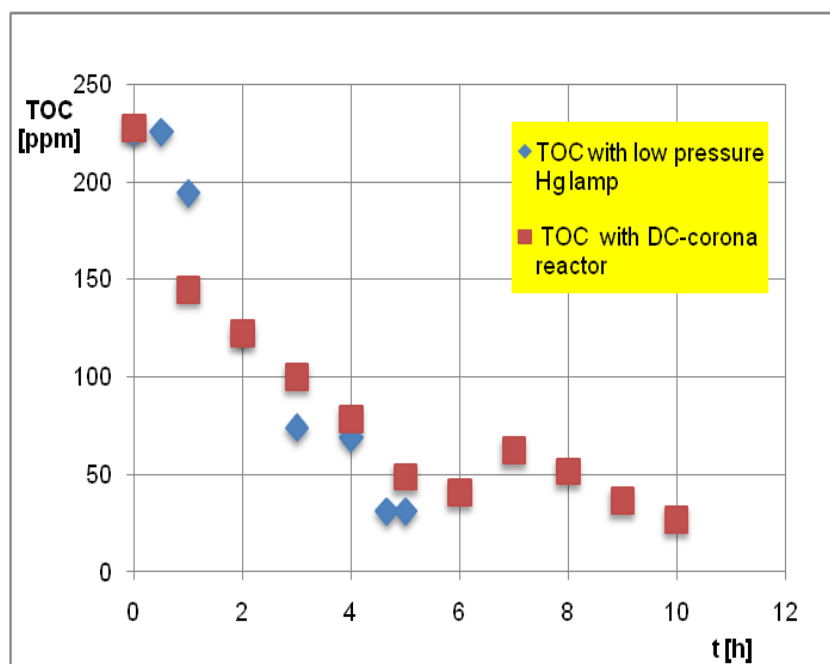


Figure 74: Decrease of TOC during the operation of a wet tube type electrostatic precipitator and under UV-radiation with low pressure Hg lamp. WESP was equipped with partial brush type discharge electrode and operated at ambient conditions.

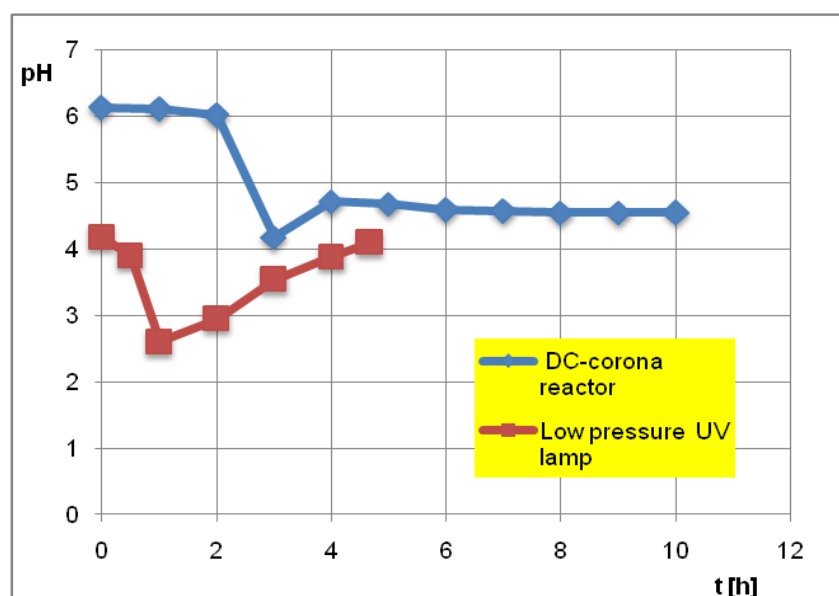
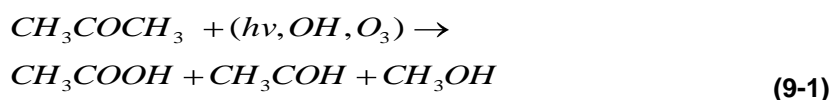


Figure 75: Shows the pH change of acetone solution during the operation of the wet electrostatic precipitator equipped with brush-type discharge electrode. Degradation is compared with low pressure Hg lamp (radiation source) irradiation.

Experiments were conducted to determine the degradation mechanism of acetone in a wet electrostatic precipitator and under irradiation with a low pressure Hg lamp with air purge at ambient conditions.

Under DC-corona discharge (WSEP) as well as UV-irradiation, depletion of total organic carbon (TOC) was observed as shown in **Figure 74**. Change in pH indicates the formation of acidic intermediates.

The trend of TOC depletion confirms the conversion of acetone into intermediate products like acetic acid, formic acid, acetaldehyde, methanol etc. Further disintegration of intermediate products into carbon dioxide and water is seemingly not affected by acidification because the rate of TOC depletion remains constant. The reaction scheme of acetone degradation is summed up through equations, (9-1) (9-2) and (9-3). Literature [88] suggests a very similar acetone degradation reaction scheme with similar primary intermediates



According to literature [82] UV-irradiation from low pressure Hg lamp is capable of ozone generation and consecutive disintegration of acetone. TOC depletion through corona discharge is comparable with TOC depletion through UV-irradiation. It can not be confirmed with these experiments whether degradation through corona discharge is supported by UV-irradiation or ozone formation only.

Change in pH value through wet electrostatic precipitation and UV-irradiation is different as shown in **Figure 75**, indicating different mechanism. Drop of the pH value indicates formation of acetic acid, formic acid, intermediates etc., from acetone. Change in pH has been observed by Taek-Soo Kim et al., [82] too.

Finally an increasing pH value during operation indicates further degradation of acidic intermediates to carbon dioxide according to a representative mechanism shown in equation (9-3).

9.4 Mineralization of EDTA

EDTA (Ethylenediaminetetraacetic acid) is a complex forming organic compound and has been widely used in many industrial applications. This chemical is not completely separated from wastewater and still going into waste streams to pollute

the environment. Scarce information is available about use of electrostatic precipitator for degradation of complex chemicals like Ethylene di-amine tetra acetic acid (EDTA) from wastewater.

The wet tube-type electrostatic precipitator was used to investigate its capability of degrading EDTA (Ethylenediaminetetraacetic acid) under ambient conditions at various applied voltage. Mineralization of EDTA was observed during operation of WESP, as shown in **Figure 76**.

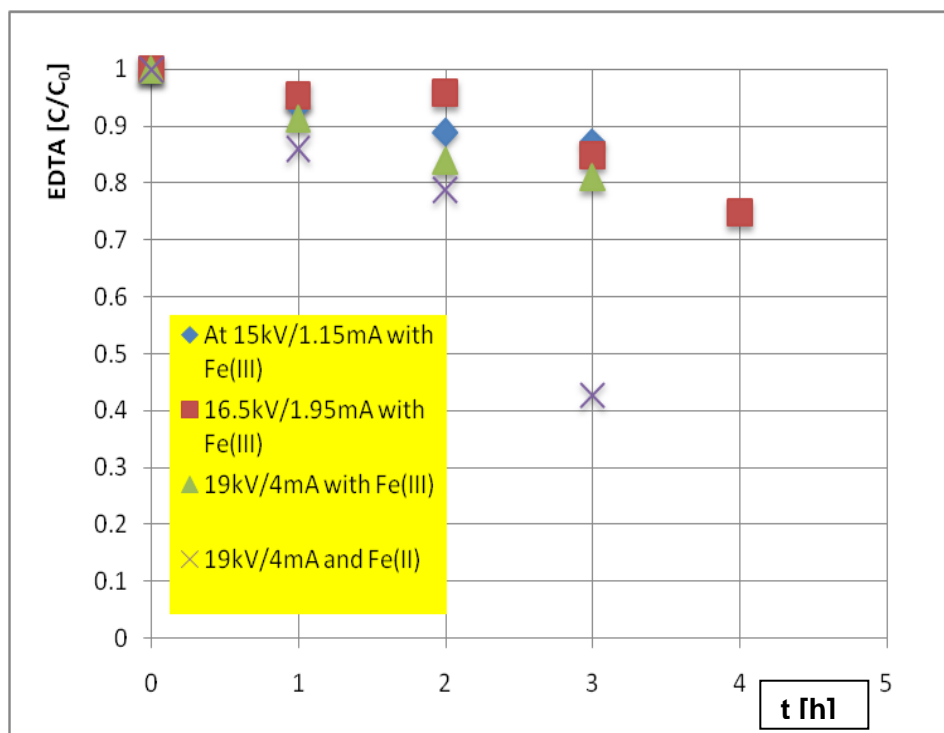


Figure 76: Trend of EDTA depletion in a WESP equipped with partial brush discharge electrode, operated at various applied voltage and ambient operation conditions. EDTA degradation was monitored with Fe (II) and Fe (III) with similar applied voltage and operation conditions.

This project also investigated the discharge characteristics of brush discharge electrodes (discussed earlier), effect of increasing current–voltage characteristics on the cleavage of EDTA and on optimisation of the operational parameters. The project also investigated the effect of Fe (II) and Fe (III) at various pH conditions on the dissociation of EDTA. Brush discharge electrodes of active length of 500 mm produce a remarkable and desired corona current at applied voltage of 15 kV under specified air and water flow conditions. Corona current increases with the increase in applied voltage as discussed in earlier chapters 4 and 5. The results show

dissociation and cleavage of the highly complex EDTA into various intermediate chemicals.

HPLC analysis confirms the formation of following intermediate chemicals like (isopropane, acetone, 3-methoxyisoquinoline-1-Carboxaldehyde, 6-methoxymethyle,xanthatin, and (1-benzol-1-methylethyl)A) at pH 5.5 and (isopropane, acetone, ethyl 9, 9 diformylnona-2, 4, 6, 8-tetrae benzene, 1-ethoxy-2-fluoro-4(1H)-pyrimidinone, 2,3-dihydro-2-thi, benzene acetic acid, .alpha., crotonitrile, butene nitrile, 2-propane, Acetone, s-Tri azolo (1, 5-a) pyridine, 8-methyle-2 benzene, azido- phenyl azide, D-Dihomoestra-1, hexacholoro-benzene, benzene ethamine, 3-choloro-5-phenyle, and 1, 2, 4 Tri-azine) at pH 2.5 - 3.

The electrostatic precipitator works similarly an advanced oxidation reactor which is capable of disintegrating EDTA. The experimentally recorded degradation is presented in **Figure 77**.

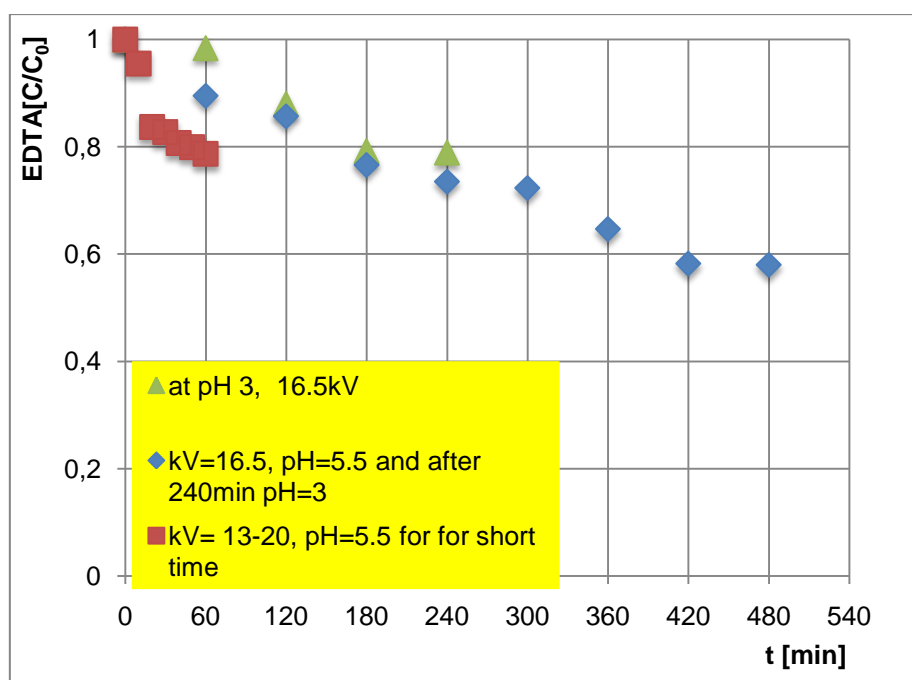


Figure 77: EDTA degradation trends at various pH and applied voltage with complete brush type discharge electrodes at ambient conditions. Wet electrostatic precipitator was operated at 16.5kV (1.95mA) and 13-20kV. pH of EDTA solution (pH=3) was maintained by using sulphuric acid.

9.5 Solution preparation, sampling and results

0.5 g per litre of EDTA and 0.05 molar Na₂SO₄ was dissolved in de-ionized water. Chemicals dissolved perfectly. EDTA solution was circulated in tube-type

electrostatic precipitator and effect of corona discharge on the degradation of EDTA was studied at various operation conditions.

At pH 5.5

A suitable water falling film was developed and required water flow rate was adjusted through flow meter and water circulation was adjusted at 40-70 l/h from top, and air ($0.5 \text{ m}^3/\text{h}$) was purged from bottom of WESP.

The system was operated at various applied voltage and samples were collected on hourly basis from circulation tank (discussed in design and development) and preserved in a refrigerator. Samples were analyzed with TOC analyzer.

TOC: There was no remarkable change in TOC during the operation of wet tube type electrostatic precipitator. Slow degradation was observed at pH=5.5. A remarkable color change was recorded. Results were also reproduced but no major degradation recorded.

HPLC: Samples were analyzed to determine the degradation of EDTA treated with wet tube-type electrostatic precipitators. Dissociation and mineralization of EDTA was recorded. Intermediates like 2-propane, acetone, 3-methoxyisoquinoline-1-carboxaldehyd, 6-methoxymethyle, xanthatin and (1-benzol-1-methylethyl) A, were determined with HPLC analysis.

At pH 3 (2.5) and with 0.98 g/l of H_2O_2

Various intermediates formed from EDTA at pH 3 are 2-propane, acetone, ethyl 9, 9-diformylnona-2, 4, 6, 8-tetrae benzene, 1-ethoxy-2-fluoro-4(1H)-pyrimidinone, 2, 3-dihydro-2-thi, benzene acetic acid, .alpha., crotonitrile, butane nitrile.

At pH3 and with 0.98 g/l of H_2O_2 (plus 1 g/10 l of TiO_2)

Mineralization of EDTA was recorded and formation of intermediates at various process conditions was discussed separately. Various intermediates determined at pH=3 are 2-propane, Acetone, s-tri azolo (1, 5-a) pyridine, 8-methyle-2 benzene, azido- phenyl azide, D-Dihomoestra-1, hexacholoro-benzene, benzene ethamine, 3-choloro-5-phenyle1,2, 4 Tri-azine.

Literature [83] described the degradation mechanism of EDTA from the effluents treated with UV-radiation at different operation conditions. Several authors also discussed the effect of peroxide and pH on EDTA degradation. S. Chitra [84] studied

the combined effect of Ultrasonic process with Fenton and hydrogen peroxide. He observed higher degradation rate of EDTA and formation of acidic intermediates. Literature [85] focused on de-complexing and oxidation of different chalets with electrochemical processes. This pre-treatment process enhances the efficiency of biological processes.

Degradation and mineralization of EDTA through wet tube-type electrostatic precipitation equipped with brush discharge electrodes is comparable with literature [[83]-[85]]. WESP is capable of emitting UV radiation and produces oxidizing reagents. UV radiation and oxidizing reagents directly attack and react with EDTA molecules to disintegrate and cleave complex and hazardous chemicals.

UV-irradiation recorded with the wet electrostatic precipitator equipped with brush type discharge electrodes is shown in **Figure 78**. Peak intensity of UV-irradiation at different applied voltage was in the range of 235 nm to 255 nm.

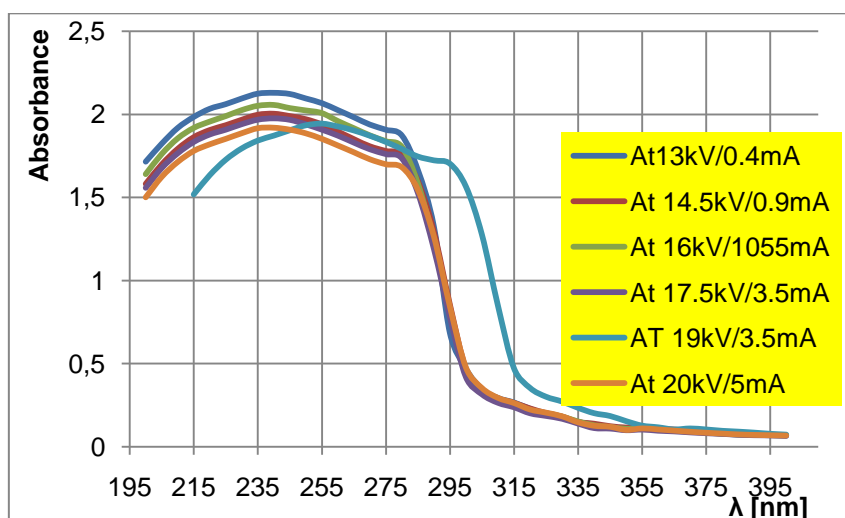


Figure 78: UV-irradiation recorded at various applied voltage with WESP.

Table 21: Various chemicals, concentration and volume of solution used for actinometric experiments

Chemical	C_i [mol/l]	M [g/mol]	V_R [l]	M_i [g]
Potassium iodide (KI)	0.60	166.01	4	398.44
Potassium iodate (KIO ₃)	0.10	214.00	4	85.60
Borax Na ₂ B ₄ O ₇ *10 H ₂ O	0.01	381.37	4	15.26

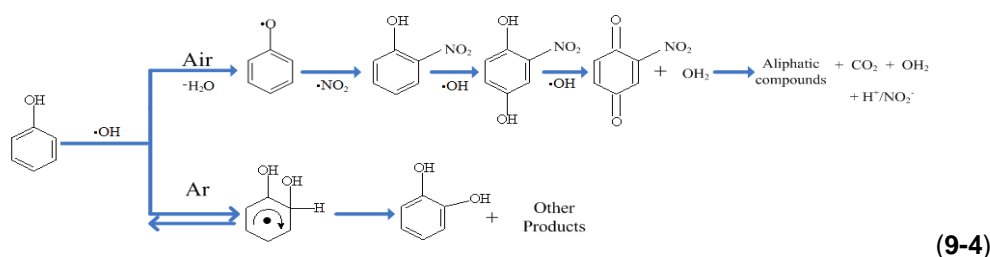
Table 22: UV-radiation recorded at various operations conditions (kV/mA) with brush discharge electrode. Data was recorded with spectrophotometer (UV-160A).

UV-rad. [nm]	kV/mA [13/0.4]	kV/mA [14.5/0.9]	kV/mA [16/1.55]	kV/mA [17.5/2.5]	kV/mA [19/3.5]	kV/mA [20/5]
	Absorbance	Absorbance	Absorbance	absorbance	absorbance	absorbance
400	0.068	0.076	0.070	0.066	0.068	0.067
395	0.070	0.077	0.071	0.069	0.069	0.069
390	0.072	0.079	0.073	0.07	0.072	0.071
385	0.074	0.081	0.075	0.073	0.074	0.074
380	0.080	0.087	0.079	0.078	0.079	0.079
375	0.087	0.093	0.086	0.082	0.086	0.084
370	0.092	0.098	0.092	0.087	0.092	0.09
365	0.098	0.104	0.096	0.093	0.097	0.097
360	0.104	0.110	0.104	0.097	0.105	0.104
355	0.113	0.117	0.111	0.104	0.111	0.11
350	0.113	0.116	0.109	0.100	0.105	0.101
345	0.119	0.124	0.119	0.110	0.118	0.12
340	0.135	0.139	0.13	0.113	0.128	0.126
335	0.149	0.150	0.153	0.140	0.155	0.147
330	0.178	0.182	0.182	0.169	0.186	0.183
325	0.198	0.203	0.202	0.186	0.203	0.205
320	0.229	0.231	0.217	0.202	0.235	0.224
315	0.267	0.264	0.252	0.238	0.273	0.263
310	0.294	0.292	0.281	0.265	0.302	0.294
305	0.347	0.347	0.332	0.316	0.355	0.353
300	0.469	0.468	0.445	0.419	0.473	0.476
295	0.683	0.854	0.802	0.780	0.849	0.842
290	1.324	1.293	1.235	1.190	1.276	1.265
285	1.664	1.597	1.583	1.527	1.566	1.546
280	1.872	1.759	1.804	1.735	1.704	1.682
275	1.907	1.780	1.838	1.761	1.724	1.700
270	1.938	1.808	1.873	1.790	1.747	1.730
265	1.982	1.851	1.916	1.830	1.792	1.772
260	2.025	1.897	1.959	1.872	1.835	1.813
255	2.067	1.94	2.007	1.908	1.872	1.853
250	2.095	1.971	2.023	1.940	1.904	1.886
245	2.122	1.990	2.037	1.967	1.928	1.908
240	2.129	2.004	2.056	1.976	1.945	1.92
235	2.124	1.998	2.051	1.968	1.935	1.917
230	2.095	1.968	2.025	1.941	1.905	1.887
225	2.061	1.935	1.989	1.908	1.873	1.853
220	2.033	1.906	1.956	1.879	1.843	1.82
215	1.984	1.863	1.918	1.834	1.796	1.78
210	1.918	1.793	1.855	1.766	1.728	1.714
205	1.823	1.699	1.761	1.677	1.635	1.624
200	1.715	1.582	1.64	1.558	1.519	1.501

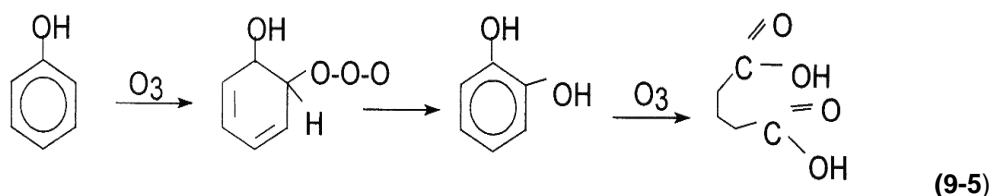
9.6 Phenol degradation and mineralization

Phenol is a poorly degradable and persistent chemical, mostly present in waste effluents. Technologies available are costly and need huge capital investment. Process of phenol degradation was investigated with wet tube-type electrostatic precipitation and mineralization was observed along with minor degradation of phenol.

Hsu-Hui Cheng et al [86] also discussed the degradation pathway of phenol with hydroxyl radicals as shown in reaction equation (9-4) and the effect of wave length on oxidation of pollutants was focused in literature[] shown below.



Literature [88] also described the reaction scheme of phenol with ozone and reaction products may be oxidative aromatics or short chain aliphatic acids, aldehydes and carbon dioxide.



As discussed earlier, wet electrostatic precipitation with brush type discharge electrodes produces ozone and ozone may directly react with phenol molecules, as explained in literature [88] Equation (9-5).

Comparatively a fast decreasing trend of total organic carbon (TOC) was observed in first three operational hours with declining trend as shown in **Figure 79**. Contrary to literature [87] absolute degradation of phenol was not observed but a suitable degradation trend was recorded.

Effect of titanium dioxide (0.05 g/l) on degradation of phenol was also investigated and there was no remarkable change in TOC value for similar operation conditions. Photolysis effect was not recognised at given concentration of TiO_2 . Possibly the concentration of TiO_2 was higher in the phenol water mixture than needed. This investigation shall be repeated in a separate program.

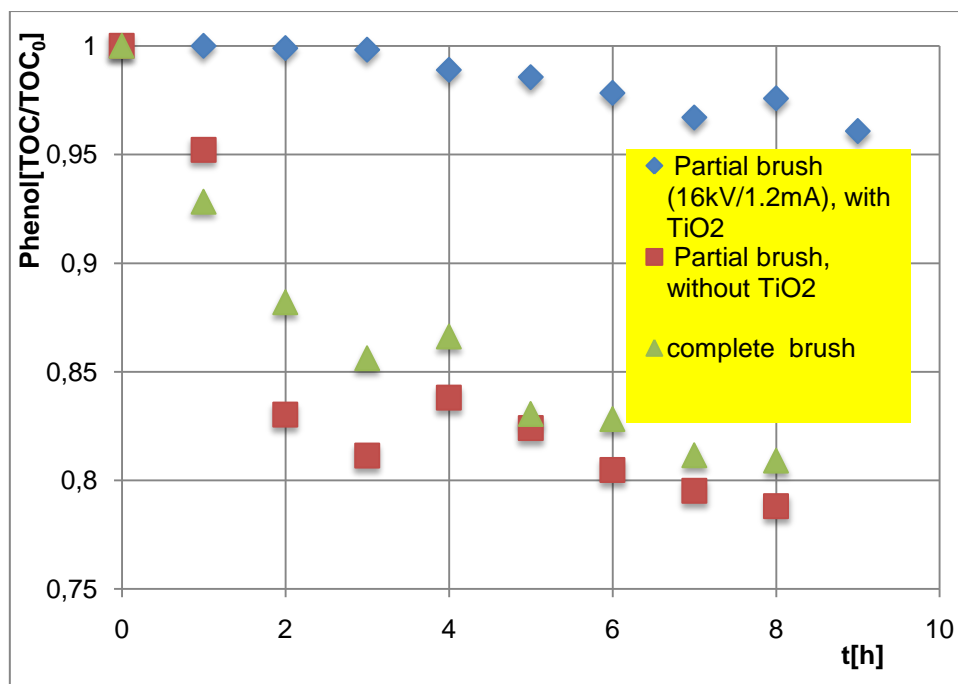


Figure 79: Decrease of the TOC (phenol) in a wet tube-type electrostatic precipitator equipped with partial brush discharge electrode and complete brush type discharge electrodes. The wet electrostatic precipitator was operated at ambient operation conditions.

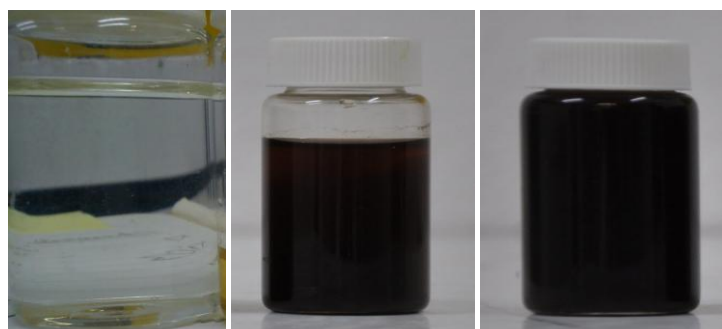


Figure 80: Change of colour of phenol solution from colourless to black-brown during the operation of wet tube electrostatic precipitators.

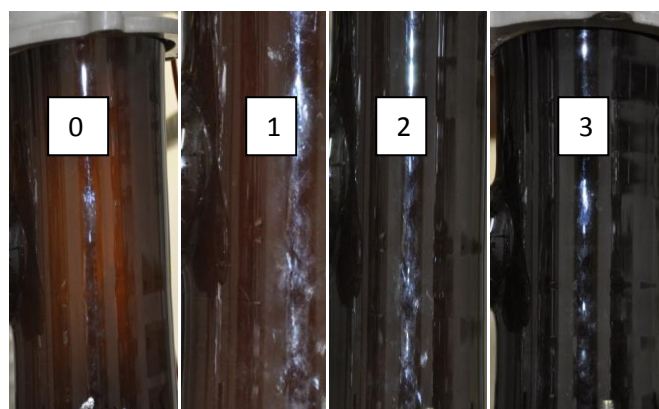


Figure 81: Colour change of industrial waste water containing phenol solution from light brown to black-brown color during treatment in the wet tube type electrostatic precipitator. Image also shows falling film and corona discharge from discharge electrodes. Samples were collected after every 4 h.

9.6.1 Colour observation

4.5g phenol was mixed in 10liter of de-ionised water and used for investigations. Phenol water mixture was colourless at time of start and during the process its colour was changed to light brown and finally dark brown or brown- blackish.

By mixing the titanium dioxide phenol water mixture was white-turbid mixture and during operation of the wet tube electrostatic precipitator the colour of the phenol solution was changed rapidly to brownish to green brownish and finally brown blackish. Change in colour was remarkable as shown in **Figure 80**. Water containing phenol constituents was colourless before treatment and dark brown after treatment with WESP.

High pressure liquid chromatograph (HPLC) was use to analyse the samples and to find the intermediates (reaction products) from phenol degradation during operation of the tubular corona reactor. Phenolic family compound were determined and few unknown compounds were also detected which is matter of further analysis and investigation.

9.6.2 Phenolic industrial waste water treatment through corona discharge

Industrial waste water containing high concentration of phenol was also treated through wet electrostatic precipitation to investigate the power of corona technology and its limitations.

Table 23; Shows degradation of phenol during operation of the wet electrostatic precipitator. Physical and chemical changes are summarized.

Time [h]	Volume [l]	Phenol index [mg/l]	X.phenol index [%]	Phenol index[g/5l]	colour
0	5	1079.0	0.0%	5.3950	Light brown
12	5	343.6	68.2%	1.7180	Blake-brown

The wet electrostatic precipitator was operated with 0.5 m³/h air purge conditions and at 15.5 -16.5 kV applied voltage. The process was operated over a long time. Degradation and mineralization of phenol was observed in terms of phenol index. The phenol index was high at zero time and a decreased index was recorded after 12-14hours of continuous treatment with WESP. The degradation data is shown in

Table 23. Recorded data shows a decrease of phenol index after a specific time at specific corona current.

Investigated and recorded data show a remarkable decrease in phenol contents in waste water. **Table 23** shows the decrease of the phenol index from 1079 to 343.6 which corresponds to a decrease of nearly 68% of phenol contents (5.4 g to 1.7 g). Colour of wastewater was changed from light brown to black or brown black colour, shown in **Figure 81**, and similar colour change was recorded with phenol solution prepared at laboratory.

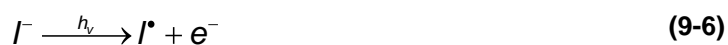
The wet electrostatic precipitator equipped with brush type discharge electrode is capable of disintegrating and mineralizing the phenol family constituents from waste water as described in **Table 23** and **Figure 79**.

9.7 Actinometric measurements

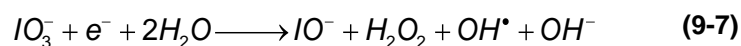
Chemical actinometric conversions are applied for determination of the photon flux of UV/VIS lamps. This tool was used to evaluate the capability of WESP for actinometrical reaction yield (UV-intensity). The UV-impact of corona discharge was determined by converting photo chemically active redox couples with a Rahn actinometer [Literature]. Conversion yield can be calculated or determined by measuring the amount of product formed (mean tri-iodide concentration).

Method; A solution of 0.6M potassium iodide (KI) and 0.1 M potassium iodate (KIO_3) in 0.01 M borax ($\text{Na}_2\text{B}_4\text{O}_7 \cdot 10\text{H}_2\text{O}$) can be used as a chemical actinometer with UV-extinction (absorption) mainly of 254 nm wavelength. The actinometer solution is optically opaque at a wavelength of 290 nm and optically transparent at wavelength of 330 [nm]. By UV irradiation of potassium iodide and potassium iodate, tri-iodide is formed and its concentration shows the quantum yield in the photo reactor. Potassium iodate acts as an electron collector (scavenger) and prevents the back reaction of electrons with free iodine. Borax is used as a buffer and ensures that the pH of the actinometer solution during the photochemical reaction at pH=9.25 remains constant.

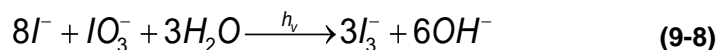
Photochemical excitation of potassium iodide results in the formation of iodine atoms and electrons. Reaction can be explain as



In the presence of potassium iodate, hypo-iodite, hydrogen peroxide, hydroxyl radicals and hydroxide are formed



There are many basic reactions involved for the formation of tri-iodide from potassium iodide and iodate solution. Equation (9-8) represents an overall reaction.



The resulting tri-iodide has maximum absorption at a wavelength of 352 [nm]. By measuring the absorbance at this wavelength, the concentration of tri-iodide can be determined.

Before UV irradiation, the iodide/iodate mixture absorbs any radiation at a wavelength of 290[nm] and no absorption of radiation of a wavelength of $\lambda=330$ [nm]. After photochemical excitation, the mixture has maximum absorption at a wavelength of $\lambda=352$ [nm], which is due to the formation of tri-iodide. The quantum yield of the overall reaction depends on the temperature of the solution, concentration of potassium iodide and the wavelength.

$$\phi = 0.75 \left[+0.02(T - 20.7) \right] + 0.23(C - 0.577) \quad (9-9)$$

At temperature of $T=24.1$ [° C], a potassium iodide concentration of $C_{KI}=0.6$ [mol/l] and wavelength of $\lambda=254$ [nm], the quantum yield is $\Phi=0.805$. The optimum ratio of potassium iodide to potassium iodate is 6:1. Deviation from the actual ratio from the optimum can change the results of quantum yield, as explained by Rahn et al (1997, 2003), [89].

9.7.1 Photon flux

To determine the tri-iodide concentration, the absorbance at a wavelength of $\lambda=352$ [nm] was measured with a photometer. Prior to the photometry, the tri-iodide samples were diluted with the initial solution because the absorbance must be kept in the operation range of the photometer and the Lambert-Beer law with which the tri-iodide concentration is calculated is valid for dilute solutions only.

The molar extinction coefficient of tri-iodide (at 352 nm) is 27600 [$M^{-1} \text{ cm}^{-1}$]. Together with the measured absorbance, the cell thickness $d=1\text{cm}$ and the dilution factor S , the concentration of tri-iodide formed by UV irradiation can be determined by using equation Error! Reference source not found.)

$$c_{I_3} = \frac{A_{352} \cdot S}{\epsilon_{352} \cdot d} \quad (9-10)$$

By multiplying the concentration difference of successive tri-iodide sample ΔC_{I_3} with the reactor volume V_R and then dividing by the quantum yield of the actinometer systems Φ_λ obtained from the equation (9-9). The radiation intensity E can be calculated from Equation (9-11)

$$E = \frac{\Delta C_{I_3} * V_R}{\Phi_\lambda} \quad (9-11)$$

The photon flux (ϕ_P) of irradiation source can be calculated by using Eq. (9-12).

$$\phi_P = \frac{E}{\Delta t} \quad (9-12)$$

By Plank's equation (9-13), the power P_λ of the radiation source can be calculated.

$$P_\lambda = \phi_P \cdot \frac{h \cdot c}{\lambda} \cdot N_A \quad (9-13)$$

9.7.2 Preparation of solution and experimental method

The required concentrations of potassium iodide, potassium iodate and borax were taken as recommended by Rahn et al [89]. The potassium iodide, potassium iodate and borax is dissolved in de-ionized water. Various solution concentrations are summarized in **Table 21**. Volume and concentration of various chemicals used is given in this table.

9.8 Experimental method

An actinometric solution of 3.8 liter was used in a WESP and an appropriate quantity of solution was kept for dilution purpose. After starting the pump and formation of a uniform liquid film, the high voltage generator was started. The system was set at voltage of 18 [kV] which corresponds to a specific corona current of 0.5 mA/0.7 m. After specific exposure times ($t = 0, 30, 60, 90, 120, 150, 180, 210, 240$ [min]) samples were taken (each 5 ml). To obtain real and accurate results, the sample vial and apparatus was covered with aluminum foil to avoid external impact of light on solution. Precautions are also needed during solution preparation and for preserving the samples.

Investigations were conducted to determine the conversion yields of tri-iodide formation with WESP. Change in colour of solution after 30min, 60min and 90min are shown in

Figure 82 and these samples are diluted because the actual colour of solution was dark as shown in **Figure 83**. As darker color or highly concentrated solution was not accurately measured with photometer because measurement is valid for dilute

solution only. Recorded colour change indicates the formation of tri-iodide from actinometric measurement.

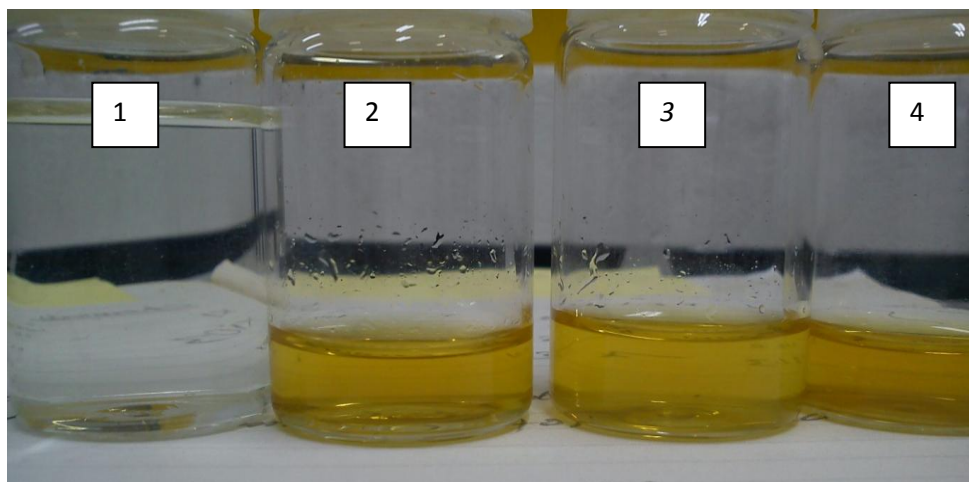


Figure 82: Actinometric solution colour during operation of wet tube electrostatic precipitator Sample 1, 2 and 3 are diluted samples. Sample 1, 2, 3, and 4 corresponds to sampling time at 0min, 30min, 60min and 90 minutes respectively.



Figure 83; colour change of the actinometric solution during operation of wet electrostatic precipitator equipped with brush type discharge electrodes. Colour of solution is increased with time, a physical indication for tri-iodide formation. Equipment was wrapped with aluminium foils.

The wet electrostatic precipitator with brush discharge electrode was operated under air purge condition and at various applied voltage. First batch operation was investigated at 18 kV and the amount of tri-iodide formed is shown in **Figure 84**. It was also recorded that moles of tri-iodide were increased with the increase of operation time (treatment time).

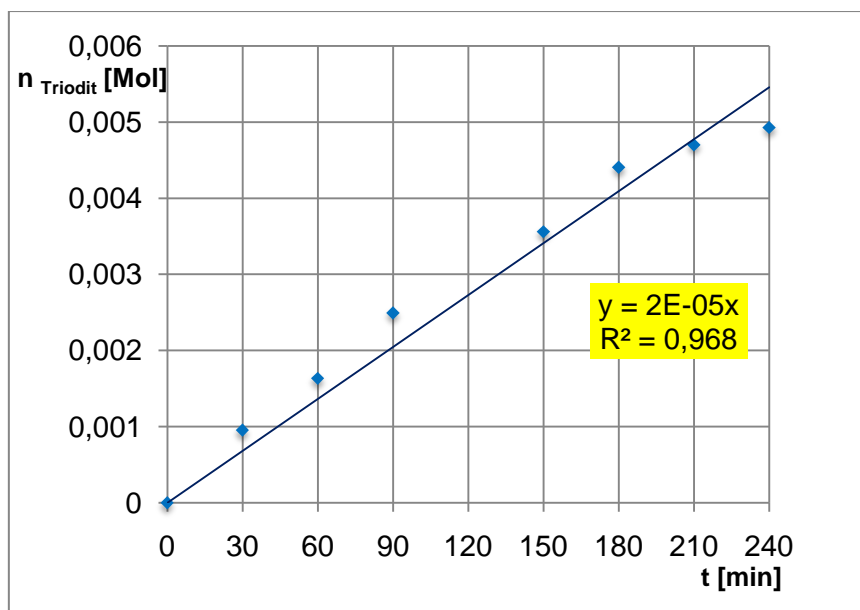


Figure 84: Measurement of the amount of tri-iodide absorption at a wavelength of $\lambda = 352$ [nm] with corona discharge from wet tube type electrostatic precipitator at 18 kV.

Investigations were extended to determine the effect of applied voltage and experiments were conducted at 17-20 kV while the other conditions remained same. Formation of tri-iodide in the wet electrostatic precipitator at enhanced applied voltage is shown in **Figure 85** and formation is a function of applied conditions. A linear increase of tri-iodide with time was recorded and shown below.

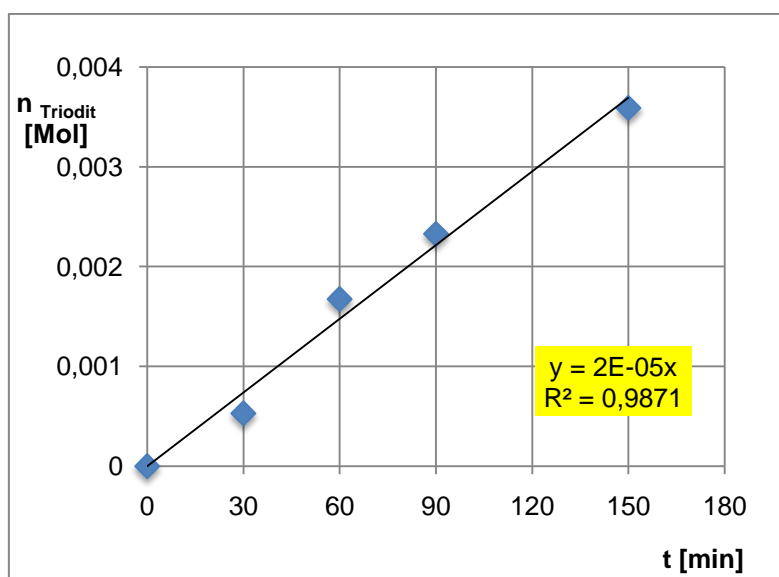


Figure 85: Measurements of the amount of tri-iodide absorption at a wavelength of $\lambda = 352$ [nm] through photometric determination. Conversion was accomplished with the wet tube type electrostatic precipitator equipped with brush type discharge electrodes operated at 17-20 kV.

Recorded data of pH increase during operation of the electrostatic precipitator was demonstrated in **Figure 86**. Increasing trend of pH with increase in reaction time at 17-20 kV applied voltage was observed. After 90min of reaction time pH become constant and further increase of applied voltage (up to 20 kV) again boosts the conversion reaction and slight rise in pH is recorded.

Experimentally recorded data indicate that formation of tri-iodide is also a function of applied voltage (corona current respectively). Formation of tri-iodide was confirmed by analyzing samples with the photometer, measuring the pH change (shown in **Figure 85**) and color change (**Figure 82** and **Figure 83**) of actinometrical solution.

Table 24: Experimentally obtained yield of tri-iodide with WESP operated at 18 kV

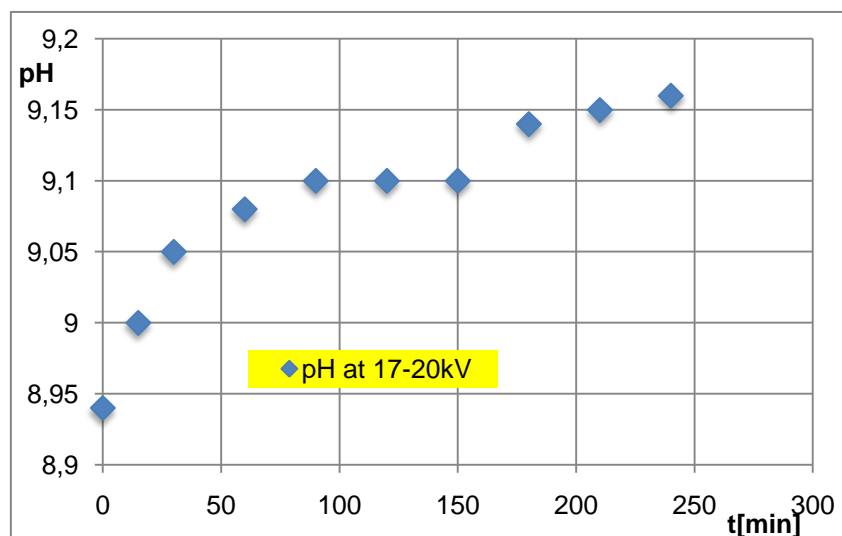
Sample Nr. [-]	Time t [min]	Extinktion A with 352 [nm] [-]	Dilution S [-]	Concentration of Triiodid $c_{I_3^-}$ [mol/l]	Concentration- difference Δc [mol/l]	Volume used V [l]
0	0	0.000	1	0.000E+00	-	3.80
1	30	0.693	10	2.511E-04	2.511E-04	3.80
2	60	0.791	15	4.299E-04	1.788E-04	3.80
3	90	0.905	20	6.558E-04	2.259E-04	3.80
4	120	0.626	20	4.536E-04	-2.022E-04	3.80
5	150	1.034	25	9.366E-04	4.830E-04	3.80
6	180	1.280	25	1.159E-03	2.228E-04	3.80
7	210	1.366	25	1.237E-03	7.790E-05	3.80
8	240	1.432	25	1.297E-03	5.978E-05	3.80

Sample Nr. [-]	Mole $n_{I_3^-}$ [mol]	Temp. T [°C]	Quantum yield Φ [-]	Radiation- intensity E [Einstein]	Photon- flux Φ_p [Einstein/s]	Power P [W]
0	-	24.1	0.805	-	-	
1	9.541E-04	24.1	0.805	1.185E-03	6.583E-07	
2	1.634E-03	24.1	0.805	8.438E-04	4.688E-07	
3	2.492E-03	24.1	0.805	1.066E-03	5.923E-07	
4	1.724E-03	24.1	0.805	-9.54E-04	-5.30E-07	
5	3.559E-03	24.1	0.805	2.279E-03	1.266E-06	
6	4.406E-03	24.1	0.805	1.052E-03	5.842E-07	
7	4.702E-03	24.1	0.805	3.676E-04	2.042E-07	
8	4.929E-03	24.1	0.805	2.821E-04	4.634E-07	
					4.237E-06	2.0

Table 25: Experimentally obtained yield of tri-iodide with WESP operated at 17-20 kV

Sample Nr. [-]	Time t [min]	Extinktion A with 352 [nm] [-]	Dilution S [-]	Concentration of Triiodid $c_{I_3^-}$ [mol/l]	Concentration- difference Δc [mol/l]	Volume used V [l]
0	0	0.000	1	0,00E+00	-	3.25
1	30	0.225	20	1.63E-04	1.63E-04	3.25
2	60	0.711	20	5,15E-04	3.52E-04	3.25
3	90	0.988	20	7,16E-04	2,007E-04	3.25
4	120	0.233	80	1.10E-04	2,2030E-04	3.25
5	150	0.381	80	1,16E-03	1,681E-04	3.25

Sample Nr. [-]	Mole $n_{I_3^-}$ [mol]	Temp. T [°C]	Quantum yield Φ [-]	Radiation- intensity E [Einstein]	Photon- flux Φ_P [Einstein/s]	Power P [W]
0	-	20.	0.743	-	-	
1	5.2E-04	20	0.743	7.128E-03	3.960E-07	
2	1.67E-03	20	0.743	1.540E-04	8.553E-07	
3	2.37E-03	20.5	0.751	8.687E-03	4.826E-07	
4	3.04E-03	21.5	0.766	9.346E-03	5.129E-06	
5	3.59E-03	22	0.774	7.063E-03	3.924E-07	
					3.181E-06	1.5

**Figure 86:** Change in pH recorded during the operation of wet tube type electrostatic precipitator equipped with brush type discharge electrodes. Process was conducted at 17-20 kV(0.35 -1.05 mA).

9.9 Summary

The wet tube type electrostatic precipitator was investigated under air purge and water circulation conditions to evaluate and process constituent degradation and the chemical actinometric activity. The corona discharge process was optimized for specific air and water flow to avoid process instabilities and sparking.

It can be concluded that the wet tube type electrostatic precipitator equipped with brush type discharge electrodes is capable of efficiently attacking organic compounds in water and waste water. It has highly interesting features for detoxification of wastewater. Further the wet tube-type electrostatic precipitator also provides some UV-irradiation intensity.

Acetone:

Complete degradation of acetone was recorded with the wet tube electrostatic precipitator and results are comparable with UV-radiation with a low pressure mercury lamp.

Phenol:

The capability of the tubular corona reactor (WESP) was analyzed for the decomposition of phenolic compounds with and without TiO_2 . Degradation of phenol is accomplished in case of operation without TiO_2 . Change in colour from colourless to brown indicates that WESP is capable of degrading phenol into various intermediates with little loss in TOC.

The photocatalytic effect of 0.05 g/l of TiO_2 was recorded and no significant change was observed regarding phenol degradation. Higher concentration of TiO_2 in phenol solution may retard photochemical interaction.

EDTA:

Degradation and major mineralization of EDTA was recorded. Experimentally investigated and recorded data shows dissociation of EDTA and formation of various intermediates comparatively less hazardous than EDTA. Effect of pH = 3 and pH = 5.5 was recorded and nearly similar decreasing trend of EDTA concentration was recorded shown in *Figure 77*. Reaction intermediates depend upon the conditions applied. Still it was not clear whether mineralization is achieved either by ozone formation or direct impact of high energy photons emitted from discharge surface.

Tri-iodide formation:

The wet tube-type electrostatic precipitator equipped with brush type discharge electrodes is capable of generating UV-irradiation of 254 nm at specific operation conditions.

The UV-irradiation capability of the wet tube type electrostatic precipitator was quantified with a chemical actinometer and is illustrated in *Table 24*. *Figure 78* shows the UV-radiation recorded at various applied voltage.

The wet tube-type electrostatic precipitator is therefore a highly potential technology for multipurpose applications with the major action in particle precipitation as well as wastewater treatment.

10 Summary

Increased interest of the scientific community in conditioning off-gas and decontaminating wastewater from various industrial sources has underlined the importance of wet electrostatic precipitation in the field of pollution control. The wet electrostatic precipitator has potential to eliminate hazardous pollutants from off-gas and wastewater simultaneously.

Design and development

A wet electrostatic precipitator was designed and developed; design was based on state of the art technical recommendations [1-3]. Technical expertise was primarily utilized to overlap the theoretical knowledge with practical experience to enhance the operation capability. A wet electrostatic precipitator with brush type discharge electrode was constructed within design limitation and operation constraints. Brush type discharge electrodes were constructed under various design schemes on the bases of active length of the discharge electrode. Various schemes of brush type discharge electrodes are partial brush, complete brush and 500 mm active length at the bottom of brush type discharge electrode. Brush type discharge electrodes were designed and fabricated with various diameters like 4 mm, 5 mm, 6 mm and 8 mm. Various brush type discharge electrodes were fabricated with different wire diameters like 0.15 mm and 0.1 mm. The brush type discharge electrodes were fixed in a tube collector under specific tension for smooth operation of the electrostatic precipitator and to measure the current/voltage relation. The wet electrostatic precipitator developed and fabricated is shown in *Figure 2* (chapter design and development).

Current/Voltage characteristic

The wet electrostatic precipitator equipped with brush type discharge electrode was used to investigate the current/voltage characteristic at ambient conditions. Various brush type discharge electrodes of 4 mm, 5 mm, 6 mm, and 8 mm brush diameter were investigated to determine the current/voltage behavior at various operation conditions. The effect of wire diameter (0.1 mm, 0.15 mm) on current/voltage behavior was also investigated. The system was operated under batch, air purge and air plus water circulation mode. Investigations were conducted to measure current/voltage relationships and to model the experimentally investigated data to

characterize brush type discharge electrodes. Experimentally investigated current/voltage data shows an increase of corona current with the increase of applied voltage. Increase of corona current at lower applied voltage was linear but at higher applied voltage increase of corona current was much higher and follows a specific power law.

Experimental investigations were conducted with various brush discharge electrodes and effect of operation conditions was recorded. Experimentally recorded data show that a higher corona current was observed with the increase of brush diameter with similar wire diameter (0.15 mm). Effect of brush wire diameter on current/voltage behaviour was significant. A higher corona current was recorded with 0.1 mm wire than of 0.15 mm wire diameter with same brush diameter and under similar operation conditions.

The current/voltage characteristics were also classified under batch, air purge and water circulation modes. The experimentally recorded data shows a higher corona current with air purge mode than batch and water circulation conditions. It was also demonstrated that enhanced air purging from 0.5 m³/h to 3 m³/h has an increasing effect on the corona current.

Modelling

Experimentally investigated current voltage data with various brush type discharge electrodes was compared with calculated data from state of the art empirical correlation. Enhanced corona current was recorded with brush type discharge electrodes and experimental data do not match with theoretically calculated data from semi-empirical correlation [1-3]. To characterize the brush type discharge electrode a new equation was proposed. Good agreement of experimental data with model data was observed and model equation characterizes the brush type electrodes.

$$I = \sqrt{3} * K * U^2 * \frac{\left(\frac{U - U_0}{U_0}\right)^3}{(R - r_b)^2 * \ln\left(\frac{R - r_b}{r_w}\right)}$$

Ozone

Ozone formation at different corona current values and different operation modes (batch, air purge and air plus water) was investigated to determine the mechanism of

ozone formation. Ozone formation was also recorded with various geometry of brush type discharge electrode and experimental data of ozone formation was modelled to determine the specific rate law. Ozone formation is a function of corona current and impact was significant. Low corona current (0.3 mA to 0.5 mA) produces increased ozone under batch and air purge mode. Decreased ozone was recorded with increase in corona current especially above 0.5 mA.

Comparatively enhanced ozone formation was recorded with 0.5 m³/h air purge mode than for batch and air plus water circulation conditions. A decreased amount of ozone was recorded under water circulation. Actually a significant amount of ozone was then absorbed in water which was used to eliminate pollutants from gas.

Ozone formation data for batch, air purge and air plus water circulation mode was used to determine mechanism of ozone formation and ozone depletion. The calculated data from fit equation was used to determine the “rate” equation for ozone formation against specific corona current. Experimental observed data at various operation modes correspond to a typical rate equation for consecutive reaction. The rate equation (intermediate peak) is based on first order consecutive reaction.

$$C_{O_3} = \frac{C_{A_0} \cdot k_1}{k_2 - k_1} \left(e^{-k_1 \cdot (I - I_0)} - e^{-k_2 \cdot (I - I_0)} \right)$$

Application

The wet electrostatic precipitator equipped with brush type discharge electrode was operated with suitable water circulation containing various pollutants like acetone, EDTA and phenol etc.

Acetone degradation with wet electrostatic precipitator was achieved and degradation trend was comparable to UV-irradiation (mercury lamp) technology. Acetone degradation trend in terms of TOC against time was recorded and nearly complete degradation of acetone was recorded. During operation of the wet electrostatic precipitator pH was monitored and change in pH was an indication of acetone degradation.

Various constituents like EDTA, phenol, and iso-propanol are most common water pollutants. Water containing EDTA and phenol was separately treated in the wet electrostatic precipitator to determine the dissociation and degradation rate under

various operation conditions. Dissociation and mineralization of EDTA and phenol was recorded and various intermediate constituents were observed. Formation of intermediates from EDTA indicates the cleaving capability of WESP.

The wet electrostatic precipitator reduced the phenol index and a remarkable amount of phenol was cleaved into intermediates.

The wet electrostatic precipitator equipped with brush type discharge electrode was operated at 10-20 kV to determine the UV- irradiation along with corona discharge. The system was capable of generating UV-irradiation in the range of 235 nm to 255 nm, confirmed with actinometric measurements which validated the 254 nm irradiation source.

The wet electrostatic precipitator equipped with brush type discharge electrode is a multipurpose reactor. The results of this PhD-thesis confirm the effectiveness in off-gas and wastewater treatment. It can even be operated simultaneously. Wet electrostatic precipitation has potential for industrial application as a multipurpose advanced oxidation reactor.

11 List of figures and table

11.1 List of figures

FIGURE 1: DISCHARGING, IONIZING, MIGRATION OF PARTICLE AND FINALLY PRECIPITATION AND REMOVAL FROM DISCHARGE ELECTRODE.....	10
FIGURE 2: EXPERIMENTAL SET UP. COLLECTING ELECTRODE (E): STAINLESS STEEL; TUBE DIAMETER: 66 MM; TUBE LENGTH: 1500 MM; DISCHARGE ELECTRODE (DE): STAINLESS STEEL, BRUSH TYPE, WITH VARIOUS DIAMETERS LIKE 4 MM, 5 MM, 6 MM AND 8 MM WITH 0.1 MM AND 0.15 MM DIAMETERS OF BRUSH WIRES. FIGURE 1 SHOWS THE DIRECTION OF PHASE FLOW AND THE WATER RINSING SYSTEM.	25
FIGURE 3: HIGH VOLTAGE ELECTRICAL CONTROL PANEL AND DC POWER SUPPLY 3A AND 3B RESPECTIVELY USED FOR ENERGIZING THE WET ELECTROSTATIC PRECIPITATOR.....	26
FIGURE 4: SKETCH OF THE HIGH VOLTAGE ELECTRICAL CONTROL PANEL AND DC SUPPLY ON LEFT AND RIGHT SIDE RESPECTIVELY.	27
FIGURE 5: VARIOUS GEOMETRIES OF RIGID DISCHARGE ELECTRODES MENTIONED IN LITERATURE [27].....	28
FIGURE 6: TUNGSTUN WIRE DISCHARGE ELECTRODE OF 0.15 MM DIAMETER ELECTRODE	29
FIGURE 7: SCREW TYPE DISCHARGE ELECTRODE (3 MM).....	29
FIGURE 8: ROD TYPE DISCHARGE ELECTRODE (COPPER COATED)	29
FIGURE 9: ROD TYPE DISCHARGE ELECTRODE (STAINLESS STEEL).	29
FIGURE 10: BRUSH TYPE DISCHARGE ELECTRODE (STAINLESS STEEL 4 MM DIAMETER).....	29
FIGURE 11: BRUSH TYPE DISCHARGE ELECTRODE (STAINLESS STEEL 5 MM DIAMETER).....	29
FIGURE 12: BRUSH TYPE DISCHARGE ELECTRODE (STAINLESS STEEL 6 MM DIAMETER).....	29
FIGURE 13: BRUSH TYPE DISCHARGE ELECTRODE (STAINLESS STEEL 8 MM DIAMETER).....	29
FIGURE 14: TUBE TYPE COUNTER CHARGED ELECTRODE (STAINLESS STEEL 66 MM INTERNAL DIAMETER, LENGTH 1500 MM AND WALL THICKNESS 2 MM) USED FOR INVESTIGATIONS	31
FIGURE 15: SKETCH OF THE ESPs WITH BRUSH DISCHARGE ELECTRODE AND COLLECTING ELECTRODE MADE OF STAINLESS STEEL.....	31
FIGURE 16: SCHEMATIC OF THE ESP WITH BRUSH-TYPE DISCHARGE ELECTRODE AND GLASS TUBE COLLECTING ELECTRODE	32
FIGURE 17: WATER DISTRIBUTER TO FORM A PROPER WATER FILM ON LEFT SIDE (17A) AND WATER COLLECTOR ON RIGHT SIDE (17B) COLLECT THE FALLING WATER AND FLUSH TO THE CIRCULATION TANK. WATER DISTRIBUTER AND COLLECTOR ARE MANUFACTURED WITH HIGH GRADE POLYMER (TEFLON). THIS HIGH-GRADE POLYMER IS ALSO USED AS INSULATOR.....	33
FIGURE 18: FALLING FILM DEVELOPED DURING THE OPERATION WHILE WATER IS CIRCULATED FROM TOP TO BOTTOM.	33
FIGURE 19: SHAPE OF TUBE TYPE ELECTROSTATIC PRECIPITATOR. THE DISCHARGE ELECTRODE IS LOCATED IN THE CENTRE AND THE TUBE FORMS THE COUNTER ELECTRODE.....	36
FIGURE 20: DOMAIN OF EDTA DISSOCIATION SPECIES VS. PH- VALUE; T = 293 K.....	38
FIGURE 21: WET ELECTROSTATIC PRECIPITATOR IN OPERATION FOR AXONOMETRIC MEASUREMENTS; THE EQUIPMENT WAS PROPERLY WRAPPED IN ALUMINIUM FOIL. PROF. DR. M. SIEBENHOFER IS INSPECTING THE OPERATION OF WESP	42
FIGURE 22: PH METER USED FOR MEASUREMENT OF THE PH CHANGES DURING OPERATION	42
FIGURE 23: TOC ANALYZER USED TO MEASURE CONCENTRATION OF ORGANIC CARBON IN TERMS OF TOC IN TREATED SAMPLES.	42
FIGURE 24: SPECTROPHOTOMETER USED FOR MEASUREMENT OF OZONE ABSORBED IN WATER AND IN GAS WITH 24A AND 24B RESPECTIVELY.....	44
FIGURE 25: IMAGE OF UNIFORM CORONA GENERATION WITH BRUSH TYPE DISCHARGE ELECTRODES AT AMBIENT CONDITIONS AND AT 20KV APPLIED VOLTAGE	45
FIGURE 26: DIFFERENT DESIGN OF BRUSH DISCHARGE ELECTRODES. ELECTRODE AT POSITION 1 IS OF 500 MM LENGTH, INSTALLED AT BOTTOM, ELECTRODE AT POSITION 2 IS PARTIAL BRUSH (700 MM) AND ELECTRODE AT POSITION 3 IS COMPLETE BRUSH (1500 MM).....	48
FIGURE 27: COMPARISON OF CURRENT/VOLTAGE CHARACTERISTICS WITH PARTIAL BRUSH TYPE DISCHARGE ELECTRODES WITH ACTIVE LENGTH OF 700 MM WITH 5 MM DIAMETER AND 0.15 MM WIRE DIAMETER.	

List of Figures and Tables

DISCHARGE ELECTRODES AND COUNTER ELECTRODES ARE OF STAINLESS STEEL. INVESTIGATIONS WERE CONDUCTED AT AMBIENT CONDITIONS WITH AND WITHOUT AIR PURGE MODE. 49

FIGURE 28: COMPARISON OF CURRENT/VOLTAGE CHARACTERISTICS WITH PARTIAL BRUSH TYPE DISCHARGE ELECTRODES WITH ACTIVE LENGTH OF 700 MM WITH 5 MM DIAMETER AND 0.15 MM WIRE DIAMETER UNDER BATCH AND LOW AIR PURGE MODES. DISCHARGE ELECTRODES AND COUNTER ELECTRODES ARE OF STAINLESS STEEL. INVESTIGATIONS WERE CONDUCTED AT AMBIENT CONDITIONS 51

FIGURE 29: COMPARISON OF CURRENT/VOLTAGE CHARACTERISTICS WITH PARTIAL BRUSH TYPE DISCHARGE ELECTRODES WITH ACTIVE LENGTH OF 700 MM WITH 5 MM DIAMETER AND 0.15 MM WIRE DIAMETER UNDER BATCH AND ENHANCED AIR PURGE MODE. INVESTIGATIONS WERE CONDUCTED AT AMBIENT CONDITIONS 52

FIGURE 30: COMPARISON OF OZONE GENERATION. MEAN DURATION PER EXPERIMENT WAS 30MINUTES; PARTIAL BRUSH TYPE DISCHARGE ELECTRODE, OF 5 MM DIAMETER WITH 0.075 MM WIRE RADIUS; INVESTIGATION AT AMBIENT CONDITIONS WITHOUT AND WITH VARIOUS AIR FLOW CONDITIONS..... 53

FIGURE 31: COMPARISON OF OZONE GENERATION AND DEGRADATION FOR VARIOUS CORONA CURRENT VALUES WITH PARTIAL BRUSH DISCHARGE ELECTRODES (PBDE) WITH 5 MM DIAMETER AND 0.15 MM WIRE DIAMETER, WITH AND WITH OUT AIR FLOW CONDITIONS. ACTIVE LENGTH OF PBDE WAS 700 MM. 54

FIGURE 32: COMPARISON OF CURRENT/VOLTAGE BEHAVIOR WITH COMPLETE BRUSH TYPE DISCHARGE ELECTRODES (CBDE) OF 5 MM DIAMETER, 0.15 MM WIRE DIAMETERS UNDER BATCH AND VARIOUS AIR PURGE AT AMBIENT CONDITIONS 55

FIGURE 33: COMPARISON OF CURRENT/VOLTAGE BEHAVIOR WITH COMPLETE BRUSH TYPE DISCHARGE ELECTRODES (CBDE) OF 5 MM DIAMETER, 0.15 MM WIRE DIAMETERS UNDER BATCH AND 0.5M³/H, AIR PURGE MODE AT AMBIENT CONDITION 55

FIGURE 34: COMPARISON OF CURRENT/VOLTAGE BEHAVIOR WITH COMPLETE BRUSH TYPE DISCHARGE ELECTRODES (5 MM DIAMETERS, 0.15 MM WIRE DIAMETERS) UNDER BATCH AND 1.2M³/H AND 2M³/H AT AMBIENT CONDITIONS..... 57

FIGURE 35: COMPARISON OF CURRENT/VOLTAGE BEHAVIOR WITH COMPLETE BRUSH TYPE DISCHARGE ELECTRODE (CBDE, 5 MM DIAMETERS, 0.15 MM WIRE DIAMETERS) UNDER BATCH AND 0.5M³/H, 3M³/HR AT AMBIENT CONDITIONS 57

FIGURE 36: COMPARISON OF OZONE FORMATION WITH COMPLETE BRUSH TYPE DISCHARGE ELECTRODE OF 5 MM DIAMETER AND BRUSH WIRE DIAMETER 0.15 MM. INVESTIGATIONS WERE CONDUCTED AT CONSTANT APPLIED VOLTAGE OF 12kV, 13kV AND 14kV WHICH CORRESPONDS TO A CORONA CURRENT OF 0.05mA, 0.1mA AND 0.35mA RESPECTIVELY..... 59

FIGURE 37: COMPARISON OF OZONE GENERATION WITH COMPLETE BRUSH TYPE DISCHARGE ELECTRODES OF 5 MM DIAMETER, AND BRUSHING WIRE DIAMETER 0.15 MM. INVESTIGATIONS WERE CONDUCTED AT VARIOUS CORONA CURRENT VALUES AT BATCH MODE AND VARIOUS AIR PURGE MODES UNDER AMBIENT CONDITIONS 59

FIGURE 38: COMPARISON OF CURRENT/VOLTAGE BEHAVIOR OF PARTIAL AND COMPLETE BRUSH TYPE DISCHARGE ELECTRODES (PBDE) OF 5 MM DIAMETER, WITH BRUSHING WIRE DIAMETER 0.15 MM. INVESTIGATIONS WERE UNDER BATCH MODE AND VARIOUS AIR FLOW MODES AT AMBIENT CONDITIONS TO CHARACTERIZE THE SPECIFIC BRUSH DISCHARGE ELECTRODES. ACTIVE LENGTH IS MENTIONED IN GRAPHS (33A AND 33B CORRESPOND TO 700 MM AND 1500 MM ACTIVE LENGTH) 63

FIGURE 39: COMPARISON OF OZONE GENERATION WITH COMPLETE AND PARTIAL BRUSH TYPE DISCHARGE ELECTRODE OF 5 MM DIAMETER, AND BRUSHING WIRE DIAMETER 0.15 MM. INVESTIGATIONS WERE CONDUCTED AT VARIOUS CORONA CURRENT SETTINGS UNDER BATCH MODE AND VARIOUS AIR FLOW MODES FOR 3 AND 5MIN DURATION FOR EACH SET OF VOLTAGE AT AMBIENT CONDITIONS TO OPTIMIZE OZONE GENERATION 64

FIGURE 40: COMPARISON OF CURRENT-VOLTAGE CHARACTERISTICS WITH AIR AND WATER CIRCULATION WITH PARTIAL BRUSH DISCHARGE ELECTRODES (5 MM DIAMETER, 0.15 MM WIRE DIAMETER)..... 65

FIGURE 41: COMPARISON OF OZONE GENERATION WITH AIR PURGE MODE, WITH AND WITHOUT WATER CIRCULATION..... 66

FIGURE 42: TREND OF THE PERCENT INCREASE IN CORONA CURRENT WITH INCREASE IN ACTIVE LENGTH OF 53% AT VARIOUS AIR PURGE AND BATCH CONDITION. INCREASING TREND WAS DIFFERENT BELOW AND ABOVE 12-13KV. 66

FIGURE 43: VARIOUS SCHEMES OF BRUSH DISCHARGE ELECTRODES WITH DIFFERENT ACTIVE LENGTH. DISCHARGE ELECTRODES 1 (LEFT SIDE: FIVE BRUSH WERE WELDED TOGETHER AT BOTTOM) HAS 500 MM ACTIVE LENGTH, PARTIAL BRUSH DISCHARGE ELECTRODES 2 (AT CENTER) WITH ACTIVE LENGTH 700 MM (100 MM ACTIVE LENGTH AND 100 MM INACTIVE) AND COMPLETE BRUSH TYPE DISCHARGE ELECTRODES 3 WITH ACTIVE LENGTH OF 1500 MM (RIGHT SIDE). 70

FIGURE 44: COMPARISON OF CURRENT/VOLTAGE CHARACTERISTICS OF BRUSH TYPE DISCHARGE ELECTRODES WITH ACTIVE LENGTH OF 500 MM (4 MM, 0.1 MM WIRE DIAMETER) UNDER BATCH, AIR PURGE AND WATER CIRCULATION CONDITIONS. CORONA CURRENT GENERATED WITH ACTIVE LENGTH OF 0.5M WAS CONVERTED INTO MA/M..... 70

FIGURE 45: COMPARISON OF OZONE GENERATION WITH 4 MM BRUSH TYPE DISCHARGE ELECTRODES (0.1 MM WIRE) UNDER BATCH, AIR AND AIR PLUS WATER CONDITIONS WITH GIVEN TEST FACILITY. 72

FIGURE 46: COMPARISON OF CURRENT/VOLTAGE CHARACTERISTICS FOR BRUSH TYPE DISCHARGE ELECTRODES (5 MM, 0.15 MM WIRE) WITH 500 MM ACTIVE LENGTH AT BOTTOM UNDER BATCH, AIR AND AIR PLUS WATER CIRCULATION CONDITIONS..... 72

FIGURE 47: COMPARISON OF OZONE GENERATION WITH BRUSH TYPE DISCHARGE ELECTRODES (5 MM, 0.1 MM WIRE) WITH ACTIVE LENGTH OF 500 MM AT BOTTOM UNDER BATCH, AIR AND WATER FLOW CONDITIONS WITH STAINLESS STEEL SETUP..... 75

FIGURE 48: COMPARISON OF CURRENT/VOLTAGE CHARACTERISTICS OF BRUSH TYPE DISCHARGE ELECTRODES (6 MM, 0.1 MM WIRE) WITH ACTIVE LENGTH OF 500 MM AT BOTTOM UNDER BATCH, AIR AND AIR PLUS WATER CIRCULATION CONDITIONS..... 75

FIGURE 49: COMPARISON OF OZONE GENERATION WITH BRUSH TYPE DISCHARGE ELECTRODES (6 MM, 0.1 MM WIRE) WITH ACTIVE LENGTH OF 500 MM AT BOTTOM UNDER BATCH, AIR AND AIR PLUS WATER CIRCULATION CONDITIONS..... 75

FIGURE 50: COMPARISON OF CURRENT/VOLTAGE CHARACTERISTICS OF BRUSH TYPE DISCHARGE ELECTRODES (6 MM, 0.15 MM WIRE) WITH ACTIVE LENGTH OF 500 MM AT BOTTOM UNDER BATCH, AIR AND AIR PLUS WATER CIRCULATION CONDITIONS..... 77

FIGURE 51: COMPARISON OF OZONE GENERATION WITH DISCHARGE ELECTRODES (6 MM, 0.15 MM WIRE) UNDER BATCH, AIR AND AIR PLUS WATER CIRCULATION CONDITIONS 77

FIGURE 52: COMPARISON OF CURRENT/VOLTAGE CHARACTERISTICS OF BRUSH TYPE DISCHARGE ELECTRODES (8 MM, 0.1 MM WIRE) UNDER BATCH, AIR AND AIR PLUS WATER CIRCULATION CONDITIONS. 78

FIGURE 53: COMPARISON OF OZONE GENERATION WITH BRUSH TYPE DISCHARGE ELECTRODES (8 MM, 0.1 MM WIRE) WITH ACTIVE LENGTH AT BOTTOM (500 MM) UNDER BATCH, AIR AND AIR PLUS WATER CIRCULATION CONDITIONS. 78

FIGURE 54: COMPARISON OF CURRENT/VOLTAGE CHARACTERISTICS OF BRUSH TYPE DISCHARGE ELECTRODES (8 MM, H 0.15 MM WIRE) UNDER BATCH, AIR AND AIR PLUS WATER CONDITIONS..... 80

FIGURE 55: COMPARISON OF OZONE GENERATION WITH 8 MM DISCHARGE ELECTRODES UNDER BATCH, AIR AND AIR PLUS WATER AND SIMILAR APPLIED VOLTAGE CONDITIONS 80

FIGURE 56: COMPARISON OF OZONE GENERATION (SIMULATED DATA) WITH VARIOUS DIAMETERS OF BRUSH TYPE DISCHARGE ELECTRODES (4 MM, 5 MM, 6 MM, AND 8 MM) WITH ACTIVE LENGTH OF 500 MM AT BOTTOM UNDER BATCH MODE AND SIMILAR APPLIED VOLTAGE CONDITIONS. 80

FIGURE 57: COMPARISON OF OZONE GENERATION FOR VARIOUS DIAMETER OF BRUSH TYPE DISCHARGE ELECTRODES WITH WIRE DIAMETERS OF 0.1 MM AND 0.15 MM UNDER AIR PURGE MODE AND VARIOUS APPLIED VOLTAGE (CORONA CURRENT CONDITIONS). THE DISCHARGE ELECTRODE WAS ARRANGED AT THE BOTTOM OF THE ESP ACCORDING TO FIGURE 43. 83

FIGURE 58: CURRENT/VOLTAGE CURVES WITH TUNGSTEN WIRE ($r=0.15$ MM) WITH ACTIVE LENGTH OF 1500 MM AND BRUSH TYPE DISCHARGE ELECTRODES (8 MM, 0.15 MM, $0.5\text{m}^3/\text{h}$ AIR PURGE) WITH ACTIVE LENGTH OF 500 MM. EXPERIMENTAL INVESTIGATIONS WERE CONDUCTED AT AMBIENT OPERATION CONDITIONS. 87

FIGURE 59: CURRENT/VOLTAGE CURVES WITH BRUSH TYPE DISCHARGE ELECTRODES (6 MM, 0.15 MM) WITH ACTIVE LENGTH OF 500 MM AT BOTTOM WITH 0.5M³/H AIR PURGE (DATA WAS CONVERTED INTO MA/M FOR GRAPHICAL REPRESENTATION). EXPERIMENTAL INVESTIGATIONS WERE CONDUCTED AT AMBIENT CONDITIONS. 88

FIGURE 60: CURRENT/VOLTAGE CURVES WITH BRUSH TYPE DISCHARGE ELECTRODES (5 MM, 0.15 MM) WITH ACTIVE LENGTH OF 500 MM AT BOTTOM WITH 0.5M³/H AIR PURGE (DATA WAS CONVERTED INTO MA/M FOR GRAPHICAL REPRESENTATION). EXPERIMENTAL INVESTIGATIONS WERE CONDUCTED AT AMBIENT CONDITIONS. 88

FIGURE 61: CURRENT/VOLTAGE (EXPERIMENTAL AND SIMULATED DATA) CURVES WITH BRUSH TYPE DISCHARGE ELECTRODES (5 MM, 0.15 MM) WITH ACTIVE LENGTH OF 500 MM AT BOTTOM AT BATCH, AIR PURGE AND AIR PLUS WATER CIRCULATION (DATA WAS CONVERTED INTO MA/M FOR GRAPHICAL REPRESENTATION). CURRENT/VOLTAGE CURVES ARE REPRESENTATION OF THE TYPICAL POWER EQUATION 8010. 90

FIGURE 62: CURRENT/VOLTAGE(EXPERIMENTAL AND SIMULATED) CURVES WITH BRUSH TYPE DISCHARGE ELECTRODES (6 MM, 0.15 MM) WITH ACTIVE LENGTH OF 500 MM AT BOTTOM AT BATCH, AIR PURGE AND AIR PLUS WATER CIRCULATION (DATA WAS CONVERTED INTO MA/M FOR GRAPHICAL REPRESENTATION). CURRENT/VOLTAGE CURVE FOLLOW THE TYPICAL POWER EQUATION 8010. 91

FIGURE 63: CURRENT/VOLTAGE(EXPERIMENTAL AND SIMULATED) CURVES WITH BRUSH TYPE DISCHARGE ELECTRODES (4 MM, 0.1 MM) WITH ACTIVE LENGTH OF 500 MM AT BOTTOM AT BATCH, AIR PURGE AND AIR PLUS WATER CIRCULATION (DATA WAS CONVERTED INTO MA/M FOR GRAPHICAL REPRESENTATION). CURRENT/VOLTAGE CURVE FOLLOW THE TYPICAL POWER EQUATION 8010 92

FIGURE 64: CURRENT/VOLTAGE(EXPERIMENTAL AND SIMULATED) CURVES WITH BRUSH TYPE DISCHARGE ELECTRODES (6 MM, 0.1 MM) WITH ACTIVE LENGTH OF 500 MM AT BOTTOM AT BATCH, AIR PURGE AND AIR PLUS WATER CIRCULATION (DATA WAS CONVERTED INTO MA/M FOR GRAPHICAL REPRESENTATION). CURRENT/VOLTAGE CURVE FOLLOW THE TYPICAL POWER EQUATION 8010 93

FIGURE 65: CURRENT/VOLTAGE(EXPERIMENTAL AND SIMULATED) CURVES WITH BRUSH TYPE DISCHARGE ELECTRODES (8 MM, 0.15, 0.1 MM) WITH ACTIVE LENGTH OF 500 MM AT BOTTOM AT BATCH, AIR PURGE AND AIR PLUS WATER CIRCULATION (DATA WAS CONVERTED INTO MA/M FOR GRAPHICAL REPRESENTATION). CURRENT/VOLTAGE CURVE FOLLOW THE TYPICAL POWER EQUATION 8010 94

FIGURE 66: OZONE (EXPERIMENTAL AND SIMULATED) CURVES WITH BRUSH TYPE DISCHARGE ELECTRODES (8 MM, 0.15 MM) WITH ACTIVE LENGTH OF 500 MM AT BOTTOM AT BATCH (DATA WAS CONVERTED INTO MA/M FOR GRAPHICAL REPRESENTATION). 97

FIGURE 67: OZONE (EXPERIMENTAL AND SIMULATED) CURVES WITH BRUSH TYPE DISCHARGE ELECTRODES (8 MM, 0.15 MM) WITH ACTIVE LENGTH OF 500 MM AT BOTTOM AT AIR PURGE CONDITIONS (DATA WAS CONVERTED INTO MA/M FOR GRAPHICAL REPRESENTATION). OZONE DATA ASSESSED WITH TABLE CURVE 2D AND VARIOUS CURVE- FIT SCHEMES ARE DEMONSTRATED..... 98

FIGURE 68: OZONE (EXPERIMENTAL AND SIMULATED) CURVES WITH BRUSH TYPE DISCHARGE ELECTRODES (8 MM, 0.15 MM) WITH ACTIVE LENGTH OF 500 MM AT BOTTOM AT AIR PURGE PLUS WATER CIRCULATION MODE (DATA WAS CONVERTED INTO MA/M FOR GRAPHICAL REPRESENTATION). OZONE DATA ASSESSED WITH TABLE CURVE 2D AND VARIOUS CURVE- FIT SCHEMES ARE DEMONSTRATED. 99

FIGURE 69: OZONE (EXPERIMENTAL AND SIMULATED) CURVES WITH BRUSH TYPE DISCHARGE ELECTRODES (6 MM, 0.15 MM) WITH ACTIVE LENGTH OF 500 MM AT BOTTOM AND AT BATCH MODE (DATA WAS CONVERTED INTO MA/M FOR GRAPHICAL REPRESENTATION). 101

FIGURE 70: OZONE (EXPERIMENTAL AND SIMULATED) CURVES WITH BRUSH TYPE DISCHARGE ELECTRODES (6 MM, 0.15 MM) WITH ACTIVE LENGTH OF 500 MM AT BOTTOM AND AIR PURGE MODE (DATA WAS CONVERTED INTO MA/M FOR GRAPHICAL REPRESENTATION). 102

FIGURE 71: OZONE (EXPERIMENTAL AND SIMULATED) CURVES WITH BRUSH TYPE DISCHARGE ELECTRODES (6 MM, 0.15 MM) WITH ACTIVE LENGTH OF 500 MM AT BOTTOM AND AIR PURGE PLUS WATER CIRCULATIONS MODE (DATA WAS CONVERTED INTO MA/M FOR GRAPHICAL REPRESENTATION)..... 103

FIGURE 72: OZONE (EXPERIMENTAL AND SIMULATED) CURVES WITH BRUSH TYPE DISCHARGE ELECTRODES (5 MM, 0.15 MM) WITH ACTIVE LENGTH OF 500 MM AT BOTTOM UNDER BATCH, AIR PURGE AND AIR PURGE PLUS WATER CIRCULATIONS MODE (DATA WAS CONVERTED INTO MA/M FOR GRAPHICAL

REPRESENTATION). OZONE DATA ASSESSED WITH TABLE CURVE 2D AND VARIOUS CURVE-FIT SCHEMES ARE DEMONSTRATED 106

FIGURE 73: COMPARISON OF EXPERIMENTAL DATA WITH FIT 2D CURVE AND MODEL DATA WITH BRUSH TYPE DISCHARGE ELECTRODE 4 MM (0.1) UNDER BATCH, AIR PURGE AND WATER CIRCULATION MODE. COMPARISON OF EXPERIMENTAL AND MODEL DATA WAS MADE TO DETERMINE THE COEFFICIENT OF DETERMINATION. APPLIED VOLTAGE (kV) IS ON X-AXIS AND mA/M ON Y-AXIS. 110

FIGURE 74: DECREASE OF TOC DURING THE OPERATION OF A WET TUBE TYPE ELECTROSTATIC PRECIPITATOR AND UNDER UV-RADIATION WITH LOW PRESSURE Hg LAMP. WESP WAS EQUIPPED WITH PARTIAL BRUSH TYPE DISCHARGE ELECTRODE AND OPERATED AT AMBIENT CONDITIONS. 118

FIGURE 75: SHOWS THE pH CHANGE OF ACETONE SOLUTION DURING THE OPERATION OF THE WET ELECTROSTATIC PRECIPITATOR EQUIPPED WITH BRUSH-TYPE DISCHARGE ELECTRODE. DEGRADATION IS COMPARED WITH LOW PRESSURE Hg LAMP (RADIATION SOURCE) IRRADIATION. 118

FIGURE 76: TREND OF EDTA DEPLETION IN A WESP EQUIPPED WITH PARTIAL BRUSH DISCHARGE ELECTRODE, OPERATED AT VARIOUS APPLIED VOLTAGE AND AMBIENT OPERATION CONDITIONS. EDTA DEGRADATION WAS MONITORED WITH Fe (II) AND Fe (III) WITH SIMILAR APPLIED VOLTAGE AND OPERATION CONDITIONS. 120

FIGURE 77: EDTA DEGRADATION TRENDS AT VARIOUS pH AND APPLIED VOLTAGE WITH COMPLETE BRUSH TYPE DISCHARGE ELECTRODES AT AMBIENT CONDITIONS. WET ELECTROSTATIC PRECIPITATOR WAS OPERATED AT 16.5kV (1.95mA) AND 13-20kV. pH OF EDTA SOLUTION (pH=3) WAS MAINTAINED BY USING SULPHURIC ACID. 121

FIGURE 78: UV-IRRADIATION RECORDED AT VARIOUS APPLIED VOLTAGE.... **ERROR! BOOKMARK NOT DEFINED.**

FIGURE 79: DECREASE OF THE TOC (PHENOL) IN A WET TUBE-TYPE ELECTROSTATIC PRECIPITATOR EQUIPPED WITH PARTIAL BRUSH DISCHARGE ELECTRODE AND COMPLETE BRUSH TYPE DISCHARGE ELECTRODES. THE WET ELECTROSTATIC PRECIPITATOR WAS OPERATED AT AMBIENT OPERATION CONDITIONS..... 126

FIGURE 80: CHANGE OF COLOUR OF PHENOL SOLUTION FROM COLOURLESS TO BLACK-BROWN DURING THE OPERATION OF WET TUBE ELECTROSTATIC PRECIPITATORS..... 126

FIGURE 81: COLOUR CHANGE OF INDUSTRIAL WASTE WATER CONTAINING PHENOL SOLUTION FROM LIGHT BROWN TO BLACK-BROWN COLOR DURING TREATMENT IN THE WET TUBE TYPE ELECTROSTATIC PRECIPITATOR. IMAGE ALSO SHOWS FALLING FILM AND CORONA DISCHARGE FROM DISCHARGE ELECTRODES. SAMPLES WERE COLLECTED AFTER EVERY 4 HOURS. 126

FIGURE 82: ACTINOMETRIC SOLUTION COLOUR DURING OPERATION OF WET TUBE ELECTROSTATIC PRECIPITATOR SAMPLE 1, 2 AND 3 ARE DILUTED SAMPLES. SAMPLE 1, 2, 3, AND 4 CORRESPONDS TO SAMPLING TIME AT 0MIN, 30MIN, 60MIN AND 90 MINUTES RESPECTIVELY 131

FIGURE 83; COLOUR CHANGE OF THE ACTINOMETRIC SOLUTION DURING OPERATION OF WET ELECTROSTATIC PRECIPITATOR EQUIPPED WITH BRUSH TYPE DISCHARGE ELECTRODES. COLOUR OF SOLUTION IS INCREASED WITH TIME, A PHYSICAL INDICATION FOR TRI-IODIDE FORMATION. EQUIPMENT WAS WRAPPED WITH ALUMINUM FOILS..... 131

FIGURE 84: MEASUREMENT OF THE AMOUNT OF TRI-IODIDE ABSORPTION AT A WAVELENGTH OF $\lambda = 352$ [NM] WITH CORONA DISCHARGE FROM WET TUBE TYPE ELECTROSTATIC PRECIPITATOR AT 18kV. 132

FIGURE 85: MEASUREMENTS OF THE AMOUNT OF TRI-IODIDE ABSORPTION AT A WAVELENGTH OF $\lambda = 352$ [NM] THROUGH PHOTOMETRIC DETERMINATION. CONVERSION WAS ACCOMPLISHED WITH THE WET TUBE TYPE ELECTROSTATIC PRECIPITATOR EQUIPPED WITH BRUSH TYPE DISCHARGE ELECTRODES OPERATED AT 17-20kV. 132

FIGURE 86: CHANGE IN pH RECORDED DURING THE OPERATION OF WET TUBE TYPE ELECTROSTATIC PRECIPITATOR EQUIPPED WITH BRUSH TYPE DISCHARGE ELECTRODES. PROCESS WAS CONDUCTED AT 17-20kV WHICH CORRESPONDS TO 0.35mA -1.05mA.XXXX..... 134

FIGURE 87: COMPARISON OF EXPERIMENTAL CURRENT/VOLTAGE DATA WITH FIT 2D CURVE AND MODEL DATA WITH BRUSH TYPE DISCHARGE ELECTRODE 5 MM (0.15), 6 MM(0.1), 6 MM(0.15), 8 MM(0.15) AND 8 MM(0.1) UNDER BATCH, AIR PURGE AND WATER CIRCULATION MODE. COMPARISON OF EXPERIMENTAL AND MODEL DATA WAS MADE TO DETERMINE THE COEFFICIENT OF DETERMINATION. 159

11.2 List of tables

TABLE 1: METHODS USED FOR WATER TREATMENT AND SPECIFICATION OF PROCESSES	6
TABLE 2: PHOTOCHEMICAL ADVANCED OXIDATION PROCESSES USED AND AVAILABLE IN THE MARKET	7
TABLE 3: ORGANIC AND INORGANIC POLLUTANTS IN AIR	8
TABLE 4: VARIOUS FUNCTIONS OF THE HV POWER SUPPLY AND CONTROL PANEL	27
TABLE 5: TYPE OF DISCHARGE ELECTRODES UNDER INVESTIGATION AND THEIR SPECIFICATION	30
TABLE 6: TOTAL VOLUME AND SURFACE AREA OF COLLECTOR	32
TABLE 7: CHANGE OF TYPE OF WATER FLOW WITH REYNOLDS NUMBER.....	35
TABLE 8: CALCULATION OF CORONA CURRENT	46
TABLE 9: CORONA CURRENT VALUES AT APPLIED VOLTAGE OF 18KV WITH PARTIAL BRUSH TYPE DISCHARGE ELECTRODES UNDER VARIOUS OPERATION CONDITIONS.	52
TABLE 10: EXPERIMENTALLY OBSERVED CORONA CURRENT VALUES WITH PARTIAL AND COMPLETE BRUSH DISCHARGE ELECTRODES UNDER BATCH MOD AND PERCENT INCREASE IN CURRENT	61
TABLE 11: EXPERIMENTALLY OBSERVED CORONA CURRENT VALUES WITH PARTIAL AND COMPLETE BRUSH DISCHARGE ELECTRODES AT 3M ³ /H MODE AND PERCENT INCREASE IN CURRENT	62
TABLE 12: SHOWS EXPERIMENTALLY OBSERVED OZONE PEAKS WITH VARIOUS BRUSH TYPE DISCHARGE ELECTRODES WITH ACTIVE LENGTH OF 500 MM AT BOTTOM AT VARIOUS OPERATION MODES. OZONE GENERATION WAS CALCULATED ON THE BASIS OF 1M ACTIVE LENGTH OF BRUSH TYPE DISCHARGE ELECTRODES.....	82
TABLE 13: SHOWS THE PEAK EXPERIMENTAL CORONA CURRENT (mA) FOR VARIOUS BRUSH DISCHARGE ELECTRODES AT 20KV AT BATCH, AIR, AIR PLUS WATER OPERATION CONDITIONS	83
TABLE 14: SHOWS VARIOUS PARAMETERS GENERATED FROM APPROXIMATING FUNCTIONS FOR BRUSH TYPE DISCHARGE ELECTRODES 5 MM (0.15 MM) INVESTIGATED UNDER VARIOUS OPERATION MODES	90
TABLE 15: SHOWS VARIOUS PARAMETERS GENERATED FROM APPROXIMATING FUNCTIONS FOR BRUSH TYPE DISCHARGE ELECTRODES 6 MM (0.15 MM) INVESTIGATED UNDER VARIOUS OPERATION MODES.....	93
TABLE 16: EMPIRICAL CORRELATIONS AND PROPOSED MODEL	108
TABLE 17: COMPARISON OF EXPERIMENTALLY OBTAINED CURRENT/VOLTAGE DATA, FIT DATA WITH (TABLE CURVE) AND CALCULATED DATA WITH MODEL EQUATION. DATA CORRESPOND TO SPECIFIC BRUSH DISCHARGE ELECTRODES AT SPECIFIC START UP VOLTAGE	109
TABLE 18: SHOWS THE COEFFICIENT OF DETERMINATION OF MODEL AND EXPERIMENTAL DATA AGREEMENT. EFFECT OF APPLIED CONDITIONS ON START UP VOLTAGE IS ALSO ILLUSTRATED.	112
TABLE 19: SHOWS VARIOUS FIT RATE EQUATION DETERMINED WITH TABLE CURVE 2D PROGRAM FOR OZONE GENERATION. VARIOUS PARAMETERS FOR RATE EQUATION ARE ALSO DEMONSTRATED.	115
TABLE 20: RATE EQUATIONS DETERMINED WITH TABLE CURVE 2D PROGRAM FOR OZONE GENERATION. VARIOUS PARAMETERS FOR RATE EQUATION ARE ALSO DEMONSTRATED.	115
TABLE 21: UV-RADIATION RECORDED AT VARIOUS OPERATIONS CONDITIONS (KV/MA) WITH BRUSH DISCHARGE ELECTRODE. DATA WAS RECORDED WITH SPECTROPHOTOMETER (UV-160A).	124
TABLE 22; SHOWS DEGRADATION OF PHENOL DURING OPERATION OF THE WET ELECTROSTATIC PRECIPITATOR. PHYSICAL AND CHEMICAL CHANGES ARE SUMMARIZED.....	127
TABLE 23: VARIOUS CHEMICALS, CONCENTRATION AND VOLUME OF SOLUTION USED FOR ACTINOMETRIC EXPERIMENTS.....	123
TABLE 24: EXPERIMENTALLY OBTAINED YIELD OF TRI-IODIDE WITH WESP OPERATED AT 18KV.....	133
TABLE 25: EXPERIMENTALLY OBTAINED YIELD OF TRI-IODIDE WITH WESP OPERATED AT 17-20 K.....	134
TABLE 26: SHOWS THE EXPERIMENTALLY OBTAINED CURRENT/VOLTAGE DATA, FIT DATA WITH (TABLE CURVE) AND CALCULATED DATA WITH MODEL EQUATION. DATA CORRESPOND TO SPECIFIC BRUSH DISCHARGE ELECTRODES (4 MM, 0.1 MM) AT SPECIFIC START UP VOLTAGE	160
TABLE 27: SHOWS THE EXPERIMENTALLY OBTAINED CURRENT/VOLTAGE DATA, FIT DATA WITH (TABLE CURVE) AND CALCULATED DATA WITH MODEL EQUATION. DATA CORRESPOND TO SPECIFIC BRUSH DISCHARGE ELECTRODES (5 MM, 0.15 MM) AT SPECIFIC START UP VOLTAGE	161
TABLE 28: SHOWS THE EXPERIMENTALLY OBTAINED CURRENT/VOLTAGE DATA, FIT DATA WITH (TABLE CURVE) AND CALCULATED DATA WITH MODEL EQUATION. DATA CORRESPOND TO SPECIFIC BRUSH DISCHARGE ELECTRODES (MM, 0.1 MM) AT SPECIFIC START UP VOLTAGE	162

TABLE 29: SHOWS THE EXPERIMENTALLY OBTAINED CURRENT/VOLTAGE DATA, FIT DATA WITH (TABLE CURVE) AND CALCULATED DATA WITH MODEL EQUATION. DATA CORRESPOND TO SPECIFIC BRUSH DISCHARGE ELECTRODES (8 MM, 0.15 MM) AT SPECIFIC START UP VOLTAGE 163

TABLE 30: SHOWS THE EXPERIMENTALLY OBTAINED CURRENT/VOLTAGE DATA, FIT DATA WITH (TABLE CURVE) AND CALCULATED DATA WITH MODEL EQUATION. DATA CORRESPOND TO SPECIFIC BRUSH DISCHARGE ELECTRODES (8 MM, 0.15 MM) AT SPECIFIC START UP VOLTAGE 164

TABLE 31: SHOWS THE EXPERIMENTALLY OBTAINED CURRENT/VOLTAGE DATA, FIT DATA WITH (TABLE CURVE) AND CALCULATED DATA WITH MODEL EQUATION. DATA CORRESPOND TO SPECIFIC BRUSH DISCHARGE ELECTRODES (8 MM, 0.1 MM) AT SPECIFIC START UP VOLTAGE 165

TABLE 32: SHOWS THE EXPERIMENTALLY OBTAINED OZONE FORMATION DATA, FIT DATA WITH (TABLE CURVE) WITH BEST FIT RATE EQUATION. DATA CORRESPOND TO SPECIFIC BRUSH DISCHARGE ELECTRODES (8 MM, 0.1 MM) AT SPECIFIC START UP VOLTAGE..... 166

TABLE 33: SHOWS THE EXPERIMENTALLY OBTAINED OZONE FORMATION DATA, FIT DATA WITH (TABLE CURVE) WITH BEST FIT RATE EQUATION. DATA CORRESPOND TO SPECIFIC BRUSH DISCHARGE ELECTRODES (4 MM, 0.1 MM) AT SPECIFIC START UP VOLTAGE..... 166

TABLE 34: SHOWS THE EXPERIMENTALLY OBTAINED OZONE FORMATION DATA, FIT DATA WITH (TABLE CURVE) WITH BEST FIT RATE EQUATION. DATA CORRESPOND TO SPECIFIC BRUSH DISCHARGE ELECTRODES (4 MM, 0.1 MM) AT SPECIFIC START UP VOLTAGE..... 167

TABLE 35: REPRESENT THE REACTION DETAILS OF FIRST ORDER INTER MEDIATE (8069), 8071 AND 8010 AS WELL..... 167

12 Literature

- [1] M. Siebenhofer, OFF-GAS PURIFICATION, 9th EDITION, 2007.
- [2] K. R. Parker, *Applied Electrostatic Precipitation*, Chapman and Hall, London, U.K., 1997.
- [3] Perry Hand book of chemical engineering.
- [4] H. Seeger¹. The history of German waste water treatment. *European Water Management*, 2(5), 1999.
- [5] Thomas Oppenlander, Photochemical purification of water and air, page 5-6, 2002.
- [6] K. Tanaka, et al. Photocatalytic water treatment on immobilized TiO₂ combined with ozonation. *Journal of Photochemistry and Photobiology A: Chemistry*, 101(1):85–87, November 1996.
- [7] Keping Yan, Electrostatic precipitation, 2008.
- [8] J. S. Chang, P. A. Lawless and T. Yamamoto. Corona discharge processes. *Plasma Science, IEEE Transactions on*, 19(6):1152–1166, 1991.
- [9] Nakano, M., Mizuno, A., Abdel-Salam, and M. Corona-induced pressures, potentials, fields and currents in electrostatic precipitator configurations. *Journal of Physics D: Applied Physics*, 40(7):1919–1926, April 2007.
- [10] Jen-Shih Chang. Recent development of plasma pollution control technology: a critical review. *Science and Technology of Advanced Materials*, 2(3-4):571–576, 2001
- [11] Nakano, M., Mizuno, A., Abdel-Salam, and M. Corona-induced pressures, potentials, fields and currents in electrostatic precipitator configurations. *Journal of Physics D: Applied Physics*, 40[7]:1919–1926, April 2007.
- [12] M.abdel-Salam¹ and A. Gabr². Characteristics of corona and silent discharges as influenced by geometry of the discharge reactor. *JOURNAL OF PHYSICS D: APPLIED PHYSICS* J. Phys. D: Appl. Phys. 36, 252-260. 2003
- [13] Nicole and And. Technical note: Performance of a personal electrostatic precipitator particle sampler. *Aerosol Science and Technology* 36: 162-165, 2002
- [14] A Yehia et al, On the characteristics of the corona discharge in a wire-duct reactor, *J. Phys. D: Appl. Phys.* 33, 2807–2814, 2000.
- [15] M. Takayama, K. Ebihara, H. Stryczewska, T. Ikegami, Y. Gyoutoku, K. Kubo, and M. Tachibana. Ozone generation by dielectric barrier discharge for soil sterilization. *Thin Solid Films*, 506-507:396–399, May 2006.

- [16] Chang. Effects of some geometric parameters on the electrostatic precipitator efficiency at different operation indexes. *Aerosol science and technology*, 33:228–238, 2000.
- [17] Abdel-Sattar S, The international J. for computer and Math in Electrical and Electronics 10. 27-43 [1991]
- [18] [14] J.S. Chang, A.J. Kelly, and J.M. Crowley [Eds], *Handbook of Electrostatic Processes*, New York, Dekker, 1995.
- [19] Ilie Suarasana, et al, Experimental characterization of multi-point corona discharge devices for direct ozonization, of liquids, *Journal of Electrostatics* 54 [2002] 207–214
- [20] M. Glor and K. Schwenzfeuer. Direct ignition tests with brush discharges. *Journal of Electrostatics*, 63(6-10):463–468, June 2005.
- [21] Z. Tamus, I. Kiss, N. Szedenik, and M. Keindl. Effective method for measuring the energy of propagating brush discharges. *Journal of Electrostatics*, January 2009
- [22] L. Ungera, et al, Unipolar field charging of particles by electrical discharge: effect of particle shape, *Aerosol Science* 35 ,965–979, 2004.
- [23] Sheng-Hsiu Huang and Chih-Chieh Chen. Loading characteristics of a miniature wire-plate electrostatic precipitator. *Aerosol Science and Technology*, 37(2):109–121, 2003.
- [24] Yosuke Kuroda et al, Effect of electrode shape on discharge current and performance with barrier discharge type electrostatic precipitators, *Journal of Electrostatics* 57, 407–415, 2003
- [25] D. Brocilo, J. Podlinski, J. S. Chang, J. Mizeraczyk, and R. D. Findlay. Electrode geometry effects on the collection efficiency of submicron and ultra-fine dust particles in spike-plate electrostatic precipitators. *J. Phys.: Conf. Ser.*, 142[1]: 2008.
- [26] M. Talaie. A new method to evaluate the voltage–current characteristics applicable for a single-stage electrostatic precipitator. *Journal of Electrostatics*, 53[3]:221–233, 2001
- [27] Gustl Mischkulnig. Enhanced corona discharge using innovative rigid discharge electrodes (RDE). *ICESP 2004*.
- [28] Abdel-Salam.y, a mizunoz and k shimizuz. Ozone generation as influenced by gas flow in corona reactors *J. Phys. D: Appl. Phys.*, 30:864–870, 1997

- [29] Yehia, A, Abdel-Salam M and Mizuno A , on assessment of ozone generation in dc coronas *J. Phys. D: Appl. Phys.* 33 831–5, 2000
- [30] M. Abdel-Salam et al. Ozone generation as influenced by gas flow in corona reactors. *J. Phys. D: Appl. Phys.*, 30:864–870, 1997.
- [31] K. Yanallah, et al. Ozone generation by negative corona discharge: the effect of joule heating. 41(19):195206+, 2008.
- [32] U. Kogelschatz et al, Ozone generation from oxygen and air: Discharge physics and reaction mechanism. *Ozone science and engineering*, 367-378, 1998
- [33] K. Hensel et al, Capillary microplasmas for ozone generation. *Eur. Phys. J. Appl. Phys.* Volume 47, Number 2, August 2009
- [34] Seiji Kanazawa et al, Simultaneous Measurements of Wire Electrode Surface Contamination and Corona Discharge Characteristics in an Air-Cleaning Electrostatic Precipitator, *TRANSACTIONS ON INDUSTRY APPLICATIONS*,. 33, 219, JANUARY-FEBRUARY 1997
- [35] Seiji Kanazavra et al, Contamination of the Discharging Electrode in an Air-Cleaning Electrostatic Precipitator, *industry Applications Society Annual Meeting* , 1870-1874, , 1993.
- [36] Andrew S. Viner, Ozone Generation in dc-Energized Electrostatic Precipitators, *IEEE TRANSACTIONS ON INDUSTRY APPLICATIONS*, VOL. 28, NO. 3, MAY/JUNE 1992.
- [37] Y. Nomoto, T. Ohkubo, S. Kanazawa, and T. Adachi. Improvement of ozone yield by a silent-surface hybrid discharge ozonizer. *Industry Applications, IEEE Transactions on*, 31[6]:1458–1462, 1995.
- [38] T. Ohkubol et al, The effect of corona wire heating on the ozone generation in an air cleaning electrostatic precipitator
- [39] Zhi. Fang, et al, Experimental study on discharge characteristics and ozone generation of Dielectric barrier discharge in a cylinder–cylinder reactor and a wire–cylinder reactor, *Journal of Electrostatics* 66 [2008] 421–426
- [40] Jae-Duk Moon, A wire-to-wire type nonthermal plasma reactor with ferroelectric pellet barrier, *Journal of Electrostatics* 64 [2006] 699–705
- [41] Jae-Duk Moon. Effective corona discharge and ozone generation from a wire-plate discharge system with a slit dielectric barrier. *Journal of Electrostatics*, 65:660666+, 2007.

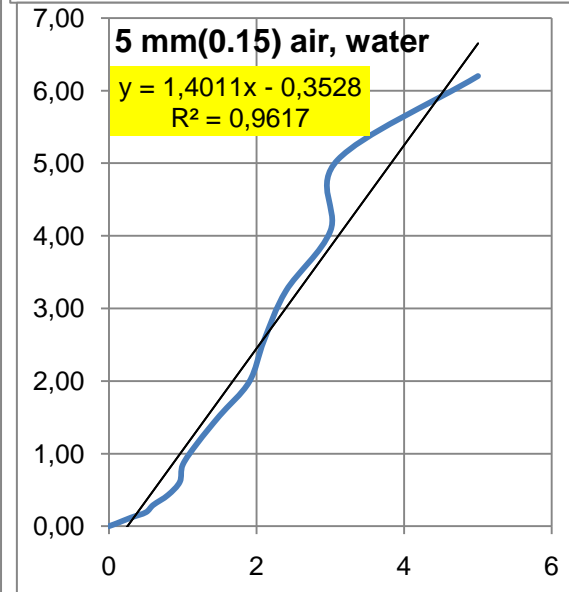
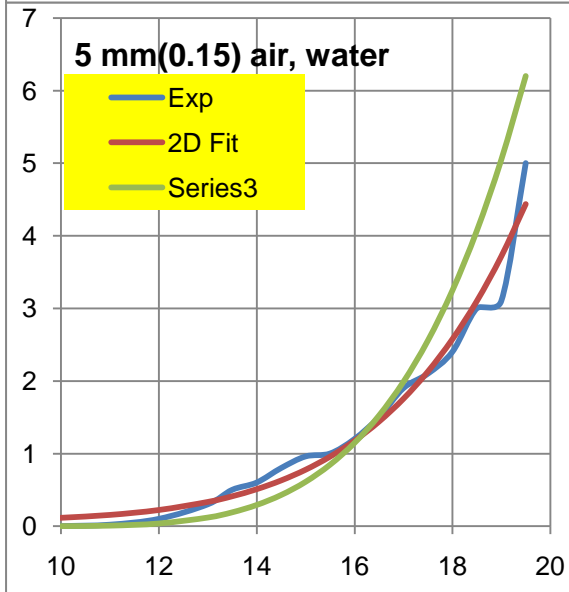
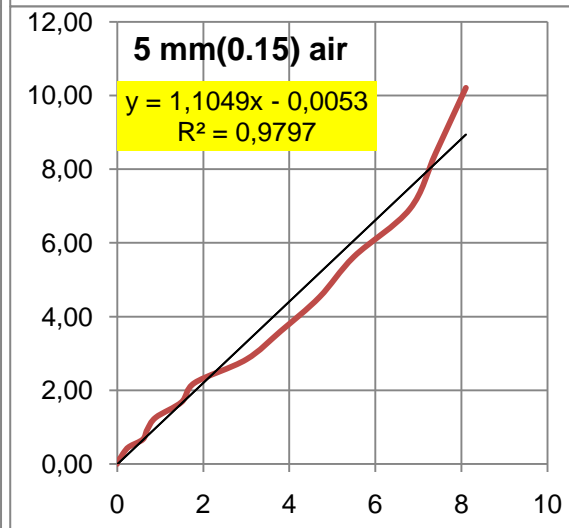
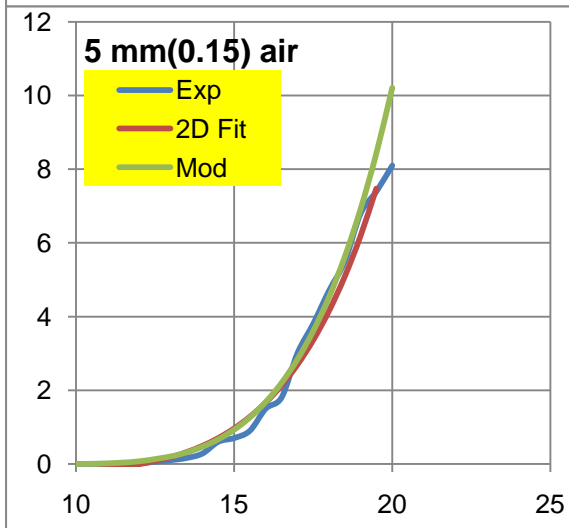
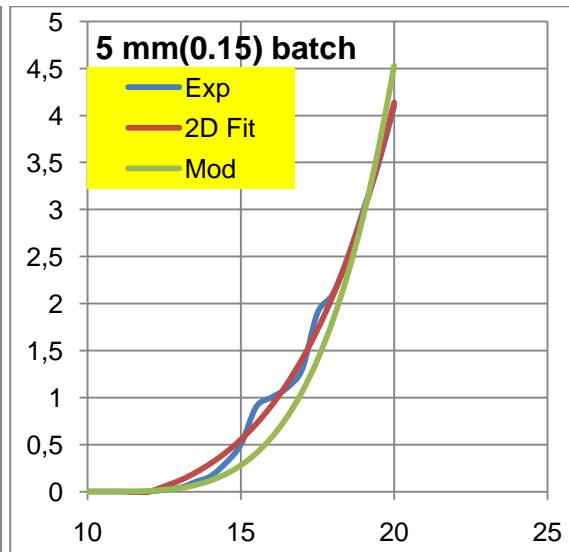
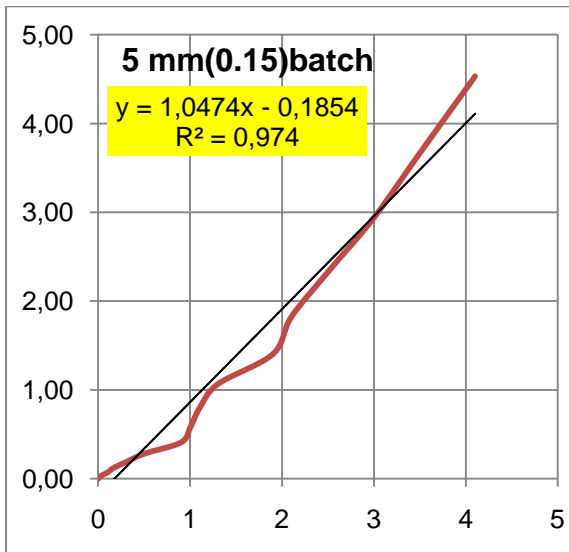
- [42] Jae-Duk Moon and Sang-Taek Geum. Discharge and ozone generation characteristics of a ferroelectric-ball/mica-sheet barrier. *Industry Applications, IEEE Transactions on*, 34[6]:1206–1211, 1998.
- [43] Jae-Duk Moon. Effective corona discharge.
- [44] I Jenei, et al. Development of ozone generator by modification of the field distribution, *Journal of Physics: Conference Series* 142 [2008]
- [45] S. Park, J. Moon, S. Lee, and S. Shin. Effective ozone generation utilizing a meshed-plate electrode in a dielectric-barrier discharge type ozone generator. *Journal of Electrostatics*, 64[5]:275–282, May 2006
- [46] Jody. Ozone production in electrostatic air cleaner with contaminated electrode by IEEE TRANSACTION ON INDUSTRY APPLICATION, 30[2]:370–376, 1994
- [47] K. HENSELM and MORVOVA, the Conversion of NO, in a Corona Discharge Electrode with Variation of material, *Contrib. Plasma Phys.* 36 , 51-61, 1996
- [48] Z. Xie et al, The effect of residential time on the reduction of CO₂ from combustion flue gases by corona torch reactor.
- [49] YI Chengwu, et al, Study on the Removal of SO₂ from Simulated Flue Gas Using Dry Calcium-Spray with DBD Plasma, *Plasma Science and Technology*, Vol.10, No.1, Feb. 2008
- [50] Yan Wu*, Jie Li, Ninghui Wang, Guofeng Li, Industrial experiments on desulfurization of flue gases by pulsed corona induced plasma chemical Process, *Journal of Electrostatics* 57 [2003] 233–241
- [51] Robert Noyes, *Handbook of Pollution Control Processes* [1991, 198- 200,],
- [52] Moo Been Chang. Removal of so₂ from gas streams using a dielectric barrier discharge and combined plasma photolysis. *J. Appl. Phys.* 69 [8], :4409+, 1991
- [53] T. Ohkubo et al, NO_x Removal by a Pipe with Nozzle-Plate Electrode Corona Discharge System. *IEEE TRANSACTIONS ON INDUSTRY APPLICATIONS*, VOL. 30, NO. 4, JULY / AUGUST 1994.
- [54] Y. Nomoto, T. Ohkubo, S. Kanazawa, and T. Adachi. Improvement of ozone yield by a silent-surface hybrid discharge ozonizer. *Industry Applications, IEEE Transactions on*, 31[6]:1458–1462, 1995.
- [55] Hyun Ha Kima et al, Performance evaluation of discharge plasma process for gaseous pollutant removal, *Journal of Electrostatics* 55 [2002] 25–41

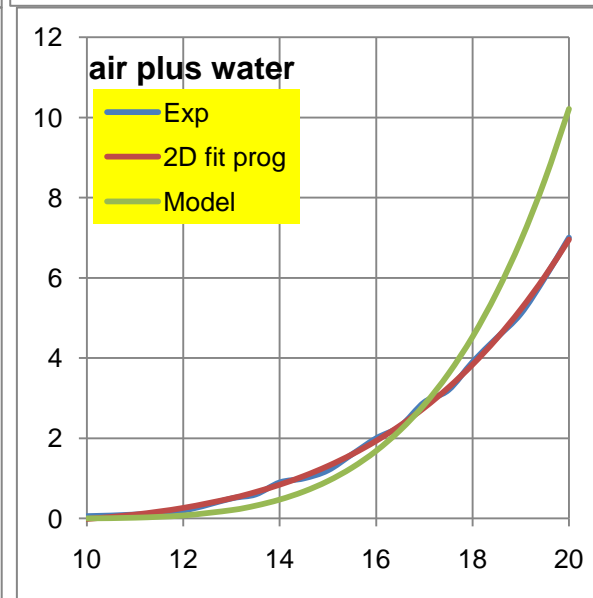
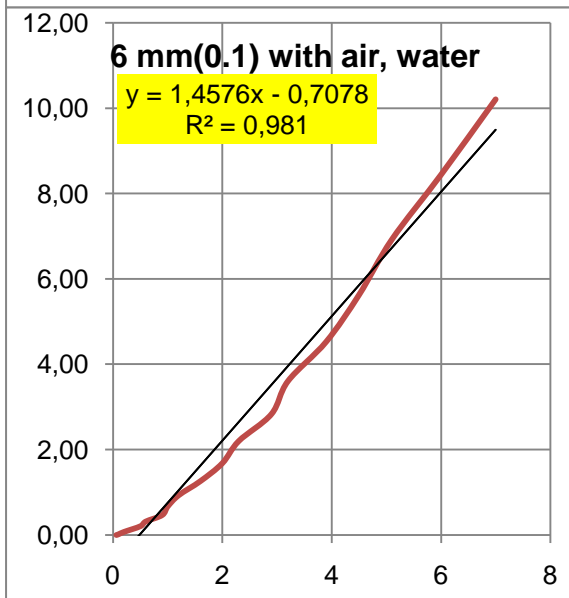
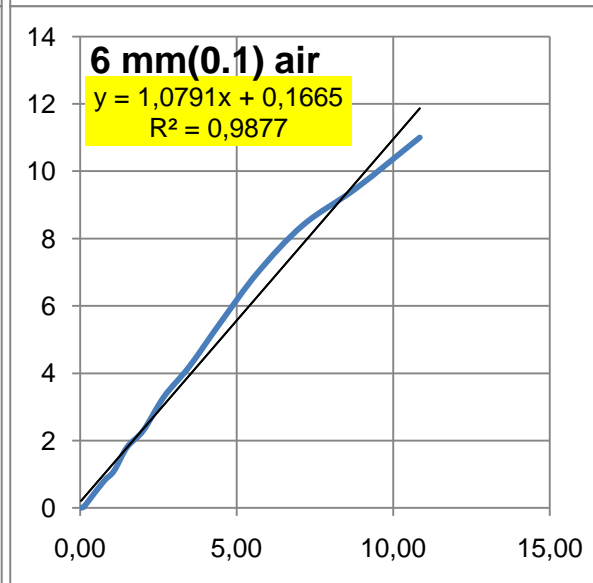
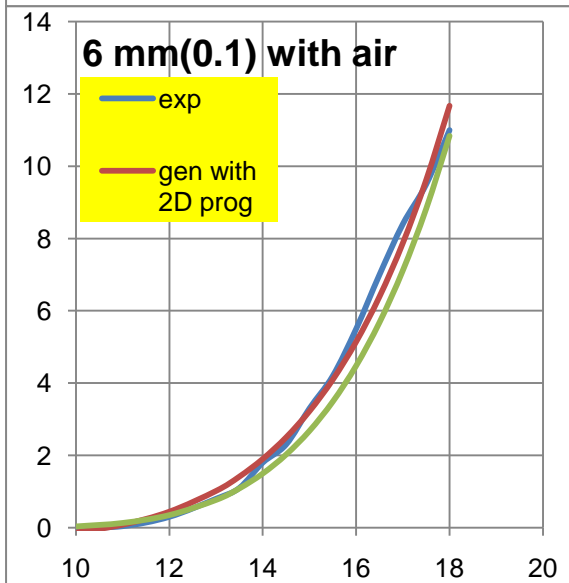
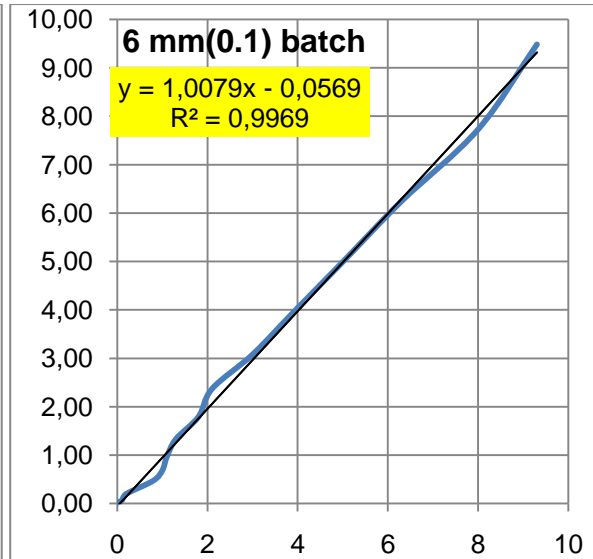
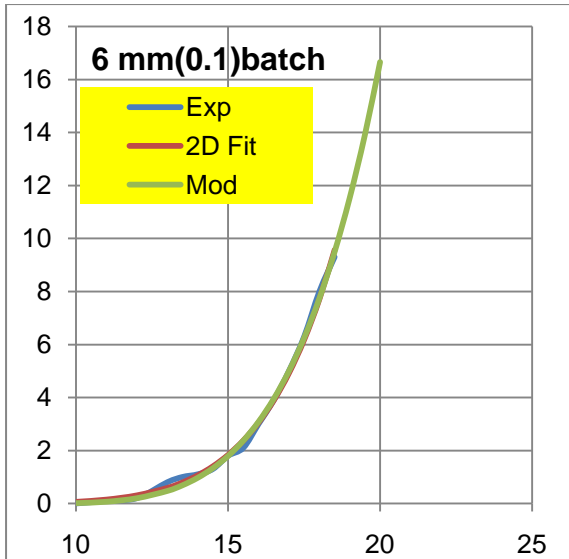
- [56] Jae-Woo Chung et al , Study on Reduction of Energy Consumption in Pulsed Corona Discharge Process for NO_x Removal, *Plasma Chemistry and Plasma Processing*, Vol. 20, No. 4, 2000
- [57] Y Mok  Modeling of pulsed corona discharge process for the removal of nitric oxide and sulphur dioxide ,*Chemical Engineering Journal*, Vol. 85, No. 1. [15 January 2002], pp. 87-97.
- [58] Y. Mok. Flue gas treatment using pulsed corona discharge generated by magnetic pulse compression modulator. *Journal of Electrostatics*, 53[3]:195–208, September 2001.
- [59] S. Masuda and H. Nakao. Control of NO_x/SO_x by positive and negative pulsed corona discharges. *Industry Applications, IEEE Transactions on*, 26[2]:374–383, 1990.
- [60] Moo B. Chang. Removal of so₂ from gas streams using a dielectric barrier discharge and combined plasma photolysis. *J. Appl. Phys.* 69 [8], 15 April 1991, 69[8]:4409+, April 1991.
- [61] Y. Kuroda et al, Effect of electrode shape on discharge current and performance with barrier discharge type electrostatic precipitators, *Journal of Electrostatics* 57, 407–415, 2003.
- [62] Anatol Jaworek et al. *Journal of Electrostatic* 65: 133-155. 2007
- [63] A Yehia et al On the characteristics of the corona discharge in a wire-duct reactor, *J. Phys. D: Appl. Phys.* 33, 2807–2814, 2000.
- [64] Claus Reihle , Mass flux and effective migration velocity in electrostatic precipitators, *Powder technology* 86 , 95-102 , 1996.
- [65] L. Ungera, et al, Unipolar field charging of particles by electrical discharge: effect of particle shape, *Aerosol Science* 35 ,965–979, 2004.
- [66] Akinori Zukeran et al, Collection Efficiency of Ultrafine Particles by an Electrostatic Precipitator under DC and Pulse Operating modes, *IEEE Industry Applications Society Annual Meeting New Orleans, Louisiana, October 5 - 9, 1997*
- [67] J. H. Park et al, Lab-scale test of a ventilation system including a dielectric Barrier discharger and UV-photo catalyst filters for simultaneous removal of gaseous and particulate contaminants, *Indoor Air* 2008; 18: 44–50, *Journal compilation _ Blackwell Munksgaard* 2007
- [68] Y. Kuroda et al, Effect of electrode shape on discharge current and performance with barrier discharge type electrostatic precipitators, *Journal of Electrostatics* 57, 407–415, 2003.

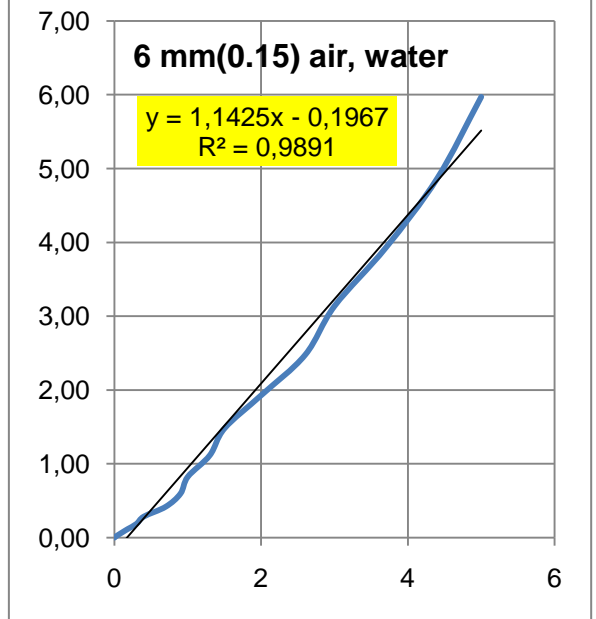
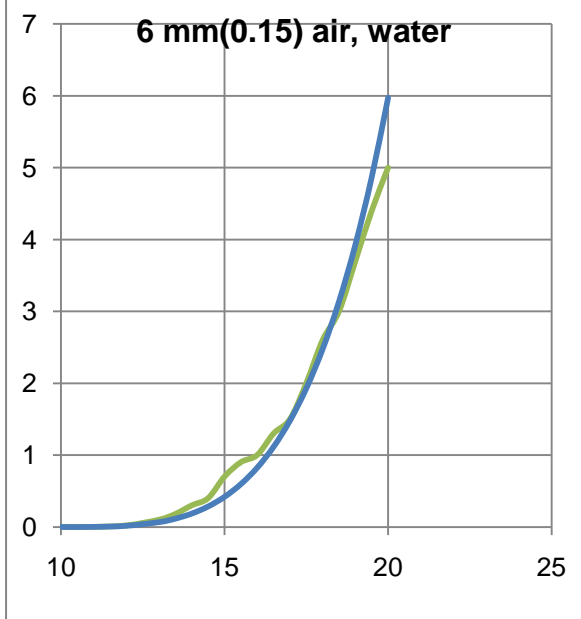
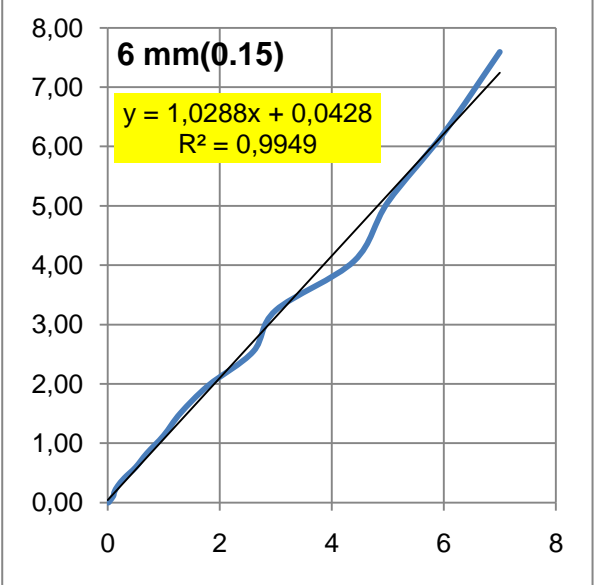
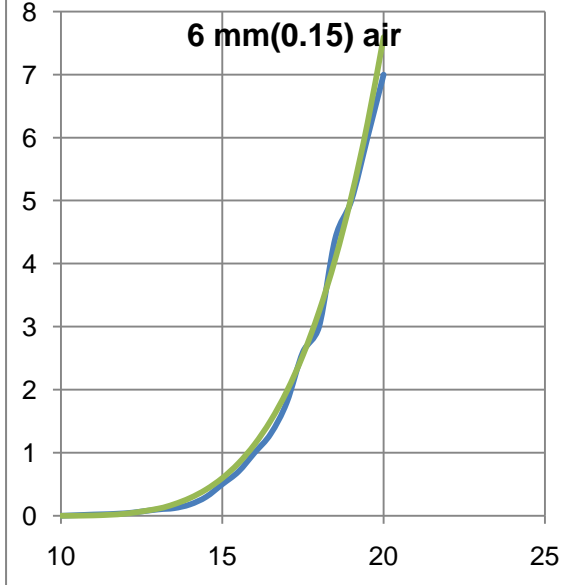
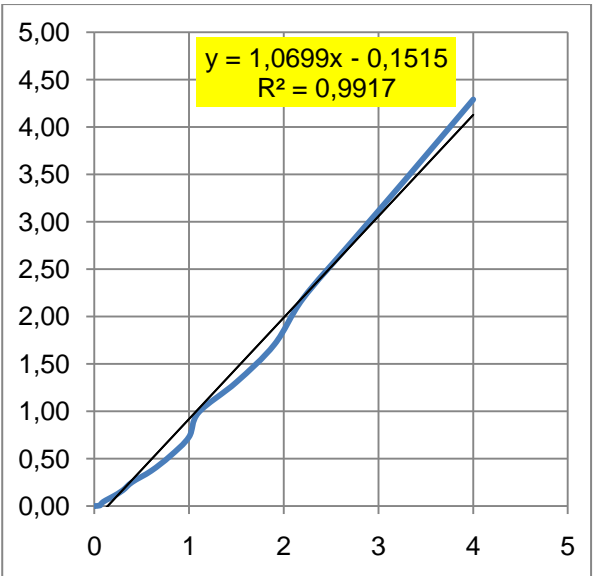
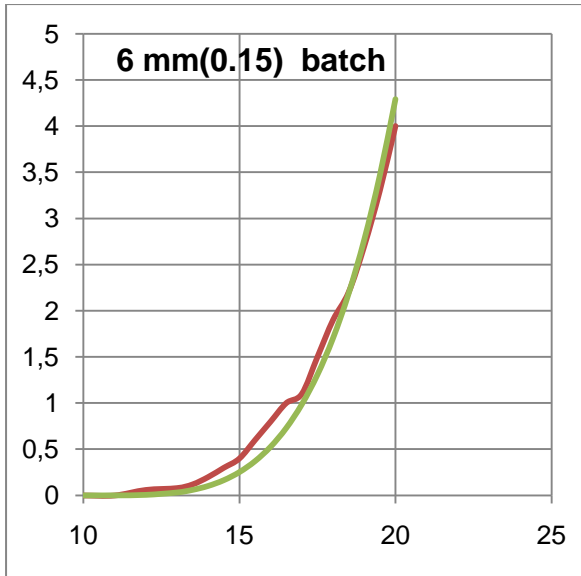
- [69] D. Brocilo, J. Podlinski, J. S. Chang, J. Mizeraczyk, and R. D. Findlay. Electrode geometry effects on the collection efficiency of submicron and ultra-fine dust particles in spike-plate electrostatic precipitators. *J. Phys.: Conf. Ser.*, 142[1]:012032+, 2008.
- [70] Kimio Yamada, An empirical formula for negative corona discharge current in point-grid electrode geometry, *JOURNAL OF APPLIED PHYSICS VOLUME 96, NUMBER 5 1 SEPTEMBER 2004* ,
- [71] Chang. Effects of some geometric parameters on the electrostatic precipitator efficiency at different operation indexes. *Aerosol science and technology*, 33:228–238, 2000.
- [72] Mayank Sahni and Bruce R. Locke, Quantification of Hydroxyl Radicals Produced in Aqueous Phase Pulsed Electrical Discharge Reactors, *Ind. Eng. Chem. Res.* 2006, 45, 5819-5825.
- [73] M. Christofi, et al. Electric discharge in water as a source of UV radiation, ozone and hydrogen peroxide, *J. Phys. D: Appl. Phys.* 34 [2001] 993–999
- [74] Cheng rong. Dielectric barrier discharge using corona-modified silicone rubber. *EPL*, 84 [2008] 25002, [October, 2008].
- [75] Y. Nomoto, T. Ohkubo, S. Kanazawa, and T. Adachi. Improvement of ozone yield by a silent-surface hybrid discharge ozonizer. *Industry Applications, IEEE Transactions on*, 31[6]:1458–1462, 1995.
- [76] Yinghui Han, Feasibility Analysis of Simultaneous DeSO₂/DeNO_x Using Plasma and Combined Photo catalysis, 2008
- [77] Jerome Taranto, et al combining cold plasma and TiO₂ photo catalysis to purify gaseous effluents: A preliminary study using methanol-contaminated air. *Industrial & Engineering Chemistry Research*, 46(23):7611–7614, November 2007
- [78] Liu W. LIN Youwen. Multi-pollutants Simultaneous Removals from flue gas, *11th international conference on Electrostatic precipitators*, page 12-18, 2008.
- [79] Avinash Chandra. Enhancement of collection efficiency of electrostatic precipitator: Indian experiments, *11th international conference on Electrostatic precipitators*, page 12-18, 2008.
- [80] Liu W. LIN Youwen. Development of Chinese electrostatic precipitator technology, *11th international conference on Electrostatic precipitators*, page 3-11, 2008.
- [81] D. Vione, C. Minero, V. Maurino, M. Carlotti, T. Picatotto, and E. Pelizzetti. Degradation of phenol and benzoic acid in the presence of a tio-based

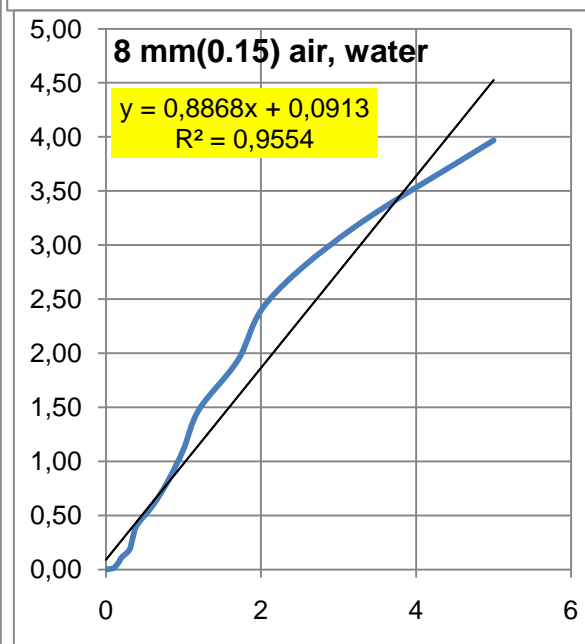
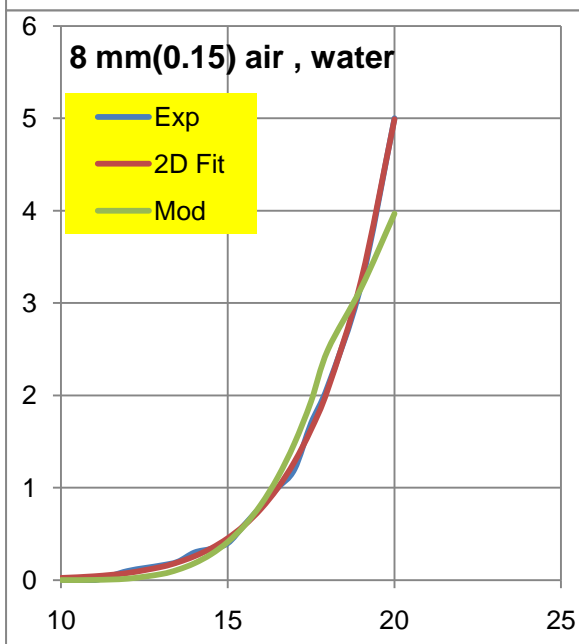
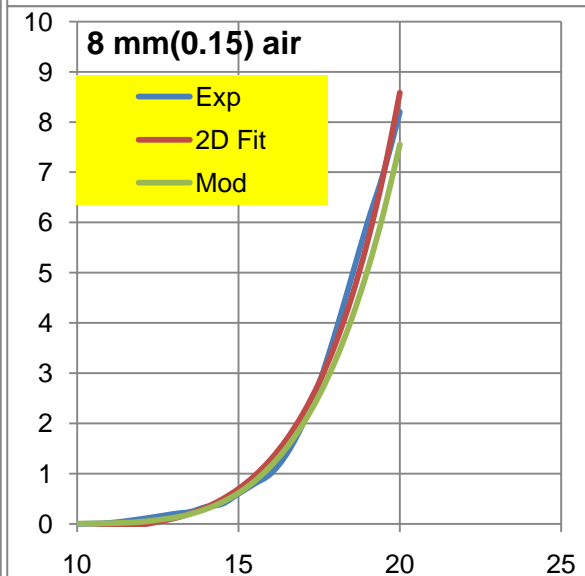
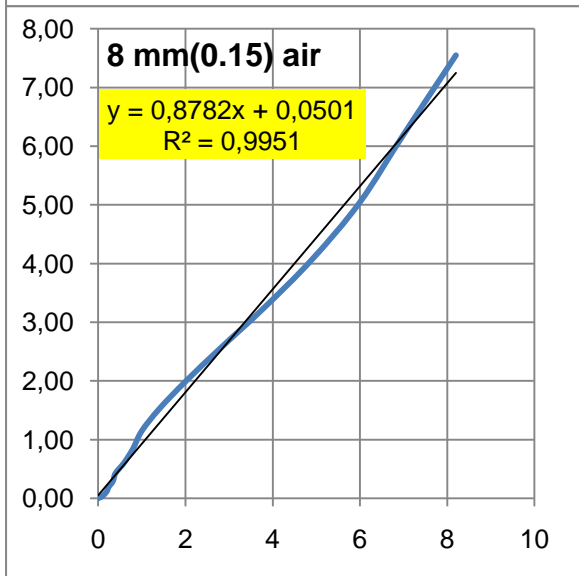
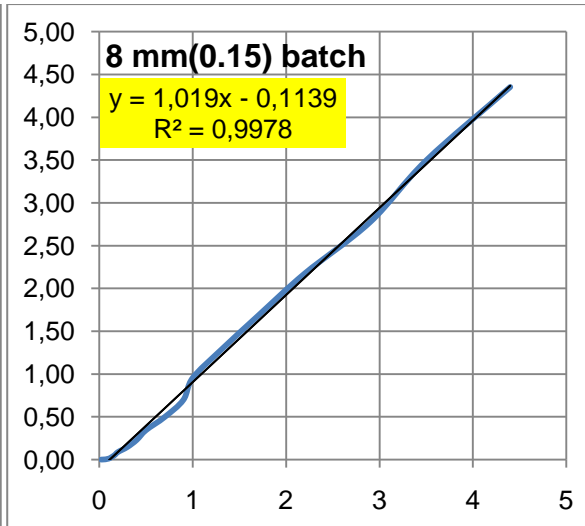
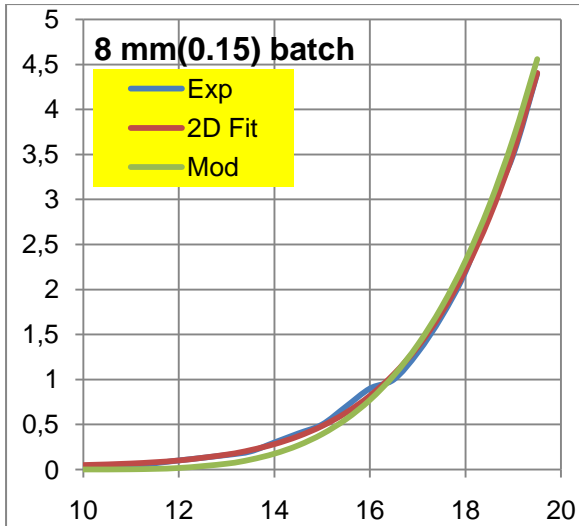
- heterogeneous photocatalyst. *Applied Catalysis B: Environmental*, 58(1-2):79–88, June 2005.
- [82] Taek-Soo Kim, Removal of organic impurities in an aqueous solution using UV-irradiation produced from high and low pressure hg lamps. *Industrial & Engineering Chemistry Research*, 46(14):4799–4810, July 2007.
- [83] Carolina Baeza1. Degradation of edta in a total chlorine free cellulose pulp bleaching effluent by uv/H₂O₂ treatment. *Journal of the Chilean Chemical Society versión On-line ISSN 0717-9707*, 1(52), 2007.
- [84] S. Chitra. Ultrasonic treatment of liquid waste containing EDTA. *Journal of Cleaner Production*, 12(4):429–435, May 2004.
- [85] Geert Lissens, Electrochemical decomplexing and oxidation of organic (chelating) additives in effluents from surface treatment and metal finishing. *Journal of Chemical Technology & Biotechnology*, 78(10):1054–1060, 2003.
- [86] Hsu-Hui Cheng, , Shiatsu-Shing Chen, Yung-Chih Chen, Wei Luen Tseng, and Min-Pei Ling5. Liquid-phase non-thermal plasma technology for degradation of two high strength phenols in aqueous solution.
- [87] W Chu, C. Y. Kwan, K. H. Chan, and C. W. Wu. Comprehensive study of the wavelength effect on oxidation processes of 2-chloroaniline. *Industrial & Engineering Chemistry Research*, 45(11):3769–3775, May 2006.
- [88] Guy Bablon, William D. Bellamy, et al . Ozone in water treatment, Application and engineering. *Fundamental aspect*, page 47-48, 1991.
- [89] Rahn, R. O. 1997. Potassium iodide as a chemical actinometer of 254 nm radiation: use of iodate as an electron scavenger. *Photochem. Photobiol* 66:450–455
- [90] Hoislbauer (2009), Dissertation for PhD from TVTUT TU Graz.
- [91] Peter So mmersacher (2010) , DIPLOMARBEIT from TVTUT TU graz.
- [92] Gangl-thesis 2006, Dissertation for PhD from TVTUT Graz.
- [93] Zelenka-thesis 2006, Dissertation for PhD from TVTUT Graz.

13 Appendix









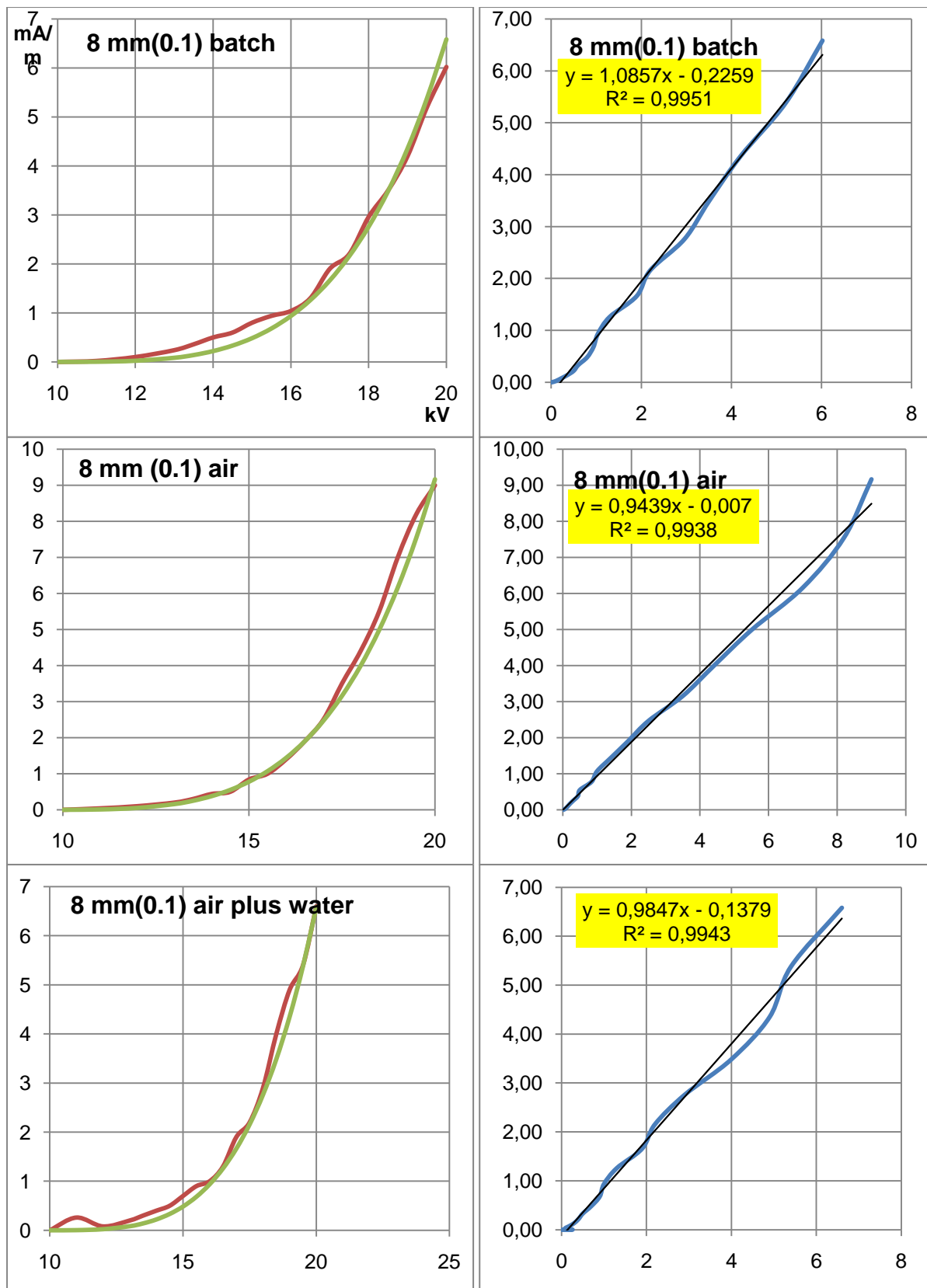


Figure 87: Comparison of experimental current/voltage data with fit 2D curve and model data with brush type discharge electrode 5 mm (0.15), 6 mm(0.1), 6 mm(0.15), 8 mm(0.15) and 8 mm(0.1) under batch, air purge and water circulation mode. Comparison of experimental and model data was made to determine the coefficient of determination.

Table 26: Shows the experimentally obtained current/voltage data, fit data with (table curve) and calculated data with model equation. Data correspond to specific brush discharge electrodes (4 mm, 0.1 mm) at specific start up voltage

kV	4mm (0.1) batch [Spec. I mA/m]			4mm (0.1) plus air [Spec. I mA/m]			4mm (0.1) +air. + water [Spec. I mA/m]		
	Exp.	Fit. 2D	Model	Exp.	Fit. 2D	Model	Exp.	Fit. 2D	Model
10	0	0.11	0.00	0.04	0.02	0.00	0.06	-0.01	0.00
11	0.02	0.15	0.00	0.06	0.09	0.03	0.1	0.09	0.01
12	0.1	0.2	0.03	0.2	0.21	0.10	0.2	0.25	0.04
13	0.3	0.3	0.10	0.4	0.42	0.26	0.5	0.49	0.13
13.5	0.5	0.4	0.16	0.6	0.57	0.39	0.6	0.65	0.21
14	0.6	0.5	0.25	0.96	0.76	0.57	0.9	0.83	0.31
14.5	0.8	0.6	0.37	1	1.00	0.80	1	1.05	0.46
15	0.96	0.7	0.54	1.2	1.30	1.10	1.2	1.30	0.65
15.5	1	0.9	0.75	1.7	1.66	1.48	1.6	1.59	0.89
16	1.2	1.2	1.02	2.1	2.12	1.96	2	1.93	1.20
16.5	1.5	1.4	1.36	2.6	2.67	2.55	2.3	2.31	1.59
17	1.9	1.7	1.79	3.2	3.34	3.27	2.9	2.75	2.06
17.5	2.1	2.1	2.30	4.2	4.15	4.14	3.2	3.26	2.64
18	2.4	2.5	2.93	5.1	5.13	5.18	3.9	3.83	3.34
18.5	3	3.1	3.69	6.2	6.29	6.41	4.5	4.48	4.18
19	3.5	3.7	4.59	8	7.68	7.86	5.1	5.21	5.17
19.5	5	4.4	5.65	9.5	9.32	9.56	6	6.03	6.34
20	6	5.5	6.5	11	11.25	11.53	7	6.95	7.70
Coefficient of determination (R^2)			0.9841	0.9977			0.98		
Start up Voltage (U_0)			9.65	8.8			9.1		

Table 27: Shows the experimentally obtained current/voltage data, fit data with (table curve) and calculated data with model equation. Data correspond to specific brush discharge electrodes (5 mm, 0.15 mm) at specific start up voltage

kV	5mm (0.15) batch [Spec. I mA/m]			5mm (0.15) air [Spec. I mA/m]			5mm (0.15) air. Water [Spec. I mA/m]		
	Exp.	Fit. 2D	Model	Exp.	Fit.2D	Model	Exp.	Fit. 2D	Model
10	0	-0.13	0.00	0	-0.18	0.00	0	0.12	0.00
11	0	-0.081	0.00	0	-0.12	0.02	0.02	0.15	0.01
12	0	-0.002	0.01	0.02	-0.00	0.07	0.1	0.22	0.04
13	0.04	0.117	0.04	0.1	0.188	0.19	0.3	0.33	0.12
13.5	0.1	0.198	0.07	0.16	0.325	0.30	0.5	0.41	0.20
14	0.16	0.296	0.12	0.28	0.495	0.44	0.6	0.51	0.30
14.5	0.3	0.413	0.19	0.6	0.712	0.63	0.8	0.63	0.44
15	0.5	0.553	0.28	0.7	0.96	0.88	0.96	0.77	0.63
15.5	0.9	0.718	0.41	0.9	1.28	1.20	1	0.96	0.87
16	1	0.914	0.58	1.5	1.66	1.61	1.2	1.17	1.18
16.5	1.1	1.143	0.79	1.8	2.13	2.11	1.5	1.44	1.57
17	1.3	1.41	1.06	3	2.69	2.72	1.9	1.75	2.05
17.5	1.9	1.72	1.40	3.8	3.355	3.47	2.1	2.13	2.63
18	2.1	2.08	1.82	4.7	4.15	4.37	2.4	2.57	3.34
18.5	2.5	2.496	2.33	5.5	5.08	5.43	3	3.1	4.19
19	3	2.97	2.94	6.8	6.18	6.69	3.1	3.71	5.20
19.5	3.5	3.51	3.67	7.4	7.47	8.17	5	4.43	6.39
20	4.1	4.137	4.53	8.1	8.97	9.90			
Coefficient of determination (R^2)			0.974	0.9797			0.9617		
Start up Voltage (U_0)			10.4	9			9.5		

Table 28: Shows the experimentally obtained current/voltage data, fit data with (table curve) and calculated data with model equation. Data correspond to specific brush discharge electrodes (mm, 0.1 mm) at specific start up voltage

kV	6mm (0.1) batch [Spec. I mA/m]			6mm (0.1) air [Spec. I mA/m]			6mm (0.1) air. water [Spec. I mA/m]		
	Exp.	Fit. 2D	Model	Exp.	Fit. 2D	Model	Exp.	Fit. 2D	Model
10	0	0.06	0.01	0	-0.134	0.04	0.06	-0.01	0.00
11	0.1	0.14	0.07	0.04	0.08	0.13	0.1	0.09	0.02
12	0.2	0.30	0.20	0.3	0.44	0.35	0.2	0.25	0.07
13	0.8	0.58	0.47	0.8	1.016	0.77	0.5	0.49	0.21
13.5	1	0.79	0.69	1.1	1.41	1.09	0.6	0.65	0.32
14	1.1	1.06	0.97	1.8	1.90	1.50	0.9	0.83	0.47
14.5	1.3	1.40	1.33	2.3	2.49	2.02	1	1.05	0.67
15	1.8	1.83	1.79	3.3	3.22	2.68	1.2	1.30	0.93
15.5	2.1	2.37	2.37	4.2	4.09	3.49	1.6	1.59	1.27
16	3	3.05	3.08	5.5	5.14	4.48	2	1.93	1.68
16.5	3.9	3.89	3.95	7	6.39	5.68	2.3	2.31	2.20
17	5	4.92	4.99	8.4	7.87	7.12	2.9	2.75	2.84
17.5	6.3	6.18	6.25	9.5	9.61	8.83	3.2	3.26	3.61
18	8	7.71	7.73	11	11.6	10.84	3.9	3.83	4.53
18.5	9.3	9.56	9.48				4.5	4.48	5.63
19							5.1	5.21	6.92
19.5							6	6.03	8.44
20							7	6.95	10.2
Coefficient of determination (R^2)			0.9969	0.9984			0.9801		
Start up Voltage [U_0]			8.2	7.8			9.0		

Table 29: Shows the experimentally obtained current/voltage data, fit data with (table curve) and calculated data with model equation. Data correspond to specific brush discharge electrodes (mm, 0.15 mm) at specific start up voltage

kV	6mm (0.15) batch [Spec. I mA/m]			6mm (0.15) air [Spec. I mA/m]			6mm (0.15) air. water [Spec. I mA/m]		
	Exp.	Fit. 2D	Model	Exp.	Fit. 2D	Model	Exp.	Fit. 2D	Model
10	0	-0.04	0.00	0	-0.15	0.00	0	0.01	0.00
11	0	-0.03	0.00	0.02	-0.11	0.01	0	0.01	0.00
12	0.06	0.03	0.01	0.04	-0.05	0.03	0.02	0.02	0.02
13	0.08	0.1	0.03	0.1	0.07	0.11	0.1	0.03	0.07
13.5	0.12	0.1	0.06	0.12	0.16	0.18	0.18	0.12	0.12
14	0.2	0.2	0.10	0.18	0.27	0.28	0.3	0.2	0.19
14.5	0.3	0.3	0.16	0.3	0.41	0.42	0.4	0.3	0.29
15	0.4	0.4	0.25	0.5	0.59	0.60	0.7	0.43	0.42
15.5	0.6	0.57	0.37	0.7	0.83	0.83	0.9	0.59	0.60
16	0.8	0.74	0.53	1	1.12	1.13	1	0.79	0.83
16.5	1	0.94	0.73	1.3	1.47	1.51	1.3	1.04	1.12
17	1.1	1.18	0.99	1.8	1.91	1.98	1.5	1.3	1.48
17.5	1.5	1.47	1.31	2.6	2.41	2.55	2	1.6	1.93
18	1.9	1.82	1.70	3	3.09	3.24	2.6	2.1	2.48
18.5	2.2	2.42	2.19	4.4	3.87	4.07	3	2.5	3.14
19	2.7	2.7	2.77	5	4.82	5.06	3.7	3.04	3.93
19.5	3.3	3.3	3.47	6	5.95	6.22	4.4	4.3	4.87
20	4	3.98	4.29	7	7.30	7.59	5	5.08	5.97
Coefficient of determination (R^2)			0.9917	0.9949			0.9891		
Start up Voltage [U_0]			10.55	9.6			10.0		

Table 30: Shows the experimentally obtained current/voltage data, fit data with (table curve) and calculated data with model equation. Data correspond to specific brush discharge electrodes (8 mm, 0.15 mm) at specific start up voltage

kV	8mm (0.15) batch			8mm (0.15) air [Spec. I mA/m]			8mm (0.15) air. water [Spec. I mA/m]		
	Exp.	Fit.2D	Model	Exp.	Fit.2D	Model	Exp.	Fit.2D	Model
10	0.02	0.05	0,00	0	-0.13	0.00	0	0.02	0.00
11	0.04	0.067	0,00	0.02	-0.09	0.01	0	0.04	0.01
12	0.1	0.102	0,01	0.1	-0.01	0.04	0.1	0.07	0.04
13	0.16	0.166	0,05	0.2	0.109	0.13	0.16	0.14	0.12
13.5	0.2	0.216	0,09	0.24	0.2	0.21	0.2	0.19	0.19
14	0.3	0.28	0,15	0.34	0.33	0.32	0.3	0.25	0.29
14.5	0.4	0.37	0,23	0.4	0.49	0.47	0.34	0.34	0.43
15	0.5	0.48	0,34	0.6	0.69	0.67	0.4	0.45	0.61
15.5	0.7	0.63	0,50	0.8	0.95	0.92	0.6	0.59	0.85
16	0.9	0.82	0,70	1	1.28	1.24	0.8	0.77	1.15
16.5	1	1.06	0,95	1.4	1.69	1.64	1	0.99	1.52
17	1.3	1.36	1,28	2	2.19	2.14	1.2	1.2	1.99
17.5	1.7	1.74	1,68	2.8	2.82	2.74	1.7	1.6	2.56
18	2.2	2.2	2,17	3.8	3.57	3.47	2.1	2.06	3.24
18.5	2.9	2.8	2,77	4.9	4.52	4.34	3.2	3.245	4.07
19	3.5	3.52	3,49	6	5.62	5.38	5	4.99	5.05
19.5	4.4	4.4	4,35	7	6.96	6.59	5.5	5.48	5.57
20				8.2	8.584	8.02			
Coefficient of determination (R^2)			0.9979	0.995			0.94		
Start up voltage U_0			10.3	9.4			9.5		

Table 31: Shows the experimentally obtained current/voltage data, fit data with (table curve) and calculated data with model equation. Data correspond to specific brush discharge electrodes (8 mm, 0.1 mm) at specific start up voltage

kV	8mm (0.1) batch			8mm (0.1) air [Spec. I mA/m]			8mm (0.1) air. water [Spec. I mA/m]		
	Exp.	Fit.2D	Model	Exp.	Fit.2D	Model	Exp.	Fit. 2D	Model
10	0	0.03	0.00	0	-0.04	0.00	0	0.01	0.00
11	0.02	0.05	0.00	0.04	0.002	0.01	0	0.04	0.00
12	0.1	0.12	0.02	0.1	0.02	0.05	0.1	0.11	0.02
13	0.24	0.23	0.07	0.2	0.83	0.16	0.16	0.14	0.08
13.5	0.36	0.32	0.12	0.3	0.23	0.25	0.2	0.19	0.14
14	0.5	0.42	0.19	0.44	0.34	0.38	0.3	0.29	0.22
14.5	0.6	0.5	0.29	0.5	0.48	0.55	0.34	0.34	0.33
15	0.8	0.7	0.42	0.84	0.89	0.78	0.4	0.45	0.48
15.5	0.94	0.92	0.60	1	1.18	1.07	0.6	0.59	0.68
16	1.04	1.76	0.83	1.4	1.56	1.44	0.8	0.77	0.94
16.5	1.3	1.48	1.12	1.9	2.02	1.90	1	0.99	1.26
17	1.9	1.84	1.49	2.5	2.58	2.47	1.2	1.28	1.66
17.5	2.2	2.29	1.94	3.5	3.28	3.16	1.7	1.63	2.16
18	2.96	2.82	2.50	4.4	4.14	3.99	2.1	2.06	2.76
18.5	3.5	3.82	3.16	5.5	5.18	4.98	3.2	3.24	3.49
19	4.2	4.20	3.96	7	6.44	6.16	5	4.52	4.35
19.5	5.2	5.08	4.90	8.2	7.96	7.55	5.3	5.54	5.38
20	6.02	6.13	6.20	9	9.778	9.16	6.03	6.77	6.58
Coefficient of determination (R^2)			0.9979	0.9938			0.9943		
Start up voltage U_0			10	9.3			9.85		

Table 32: Shows the experimentally obtained ozone formation data, fit data with (table curve) with best fit rate equation. Data correspond to specific brush discharge electrodes (8 mm, 0.1 mm) at specific start up voltage

8mm(0.1).Batch (8071)			8mm(0.1).air (8069)			8mm.air+water (8069)		
mA/m	O ₃ [ppm] Expt	Fit. Data	mA/m	O ₃ [ppm] Expt	Fit. Data	I [mA/m]	O ₃ [ppm] Expt	Fit. Data
0	0	0.19	0	11.07	-28.1	0	0	3.11
0.02	0.4	0.19	0.04	132.5	188.4	0.26	0.26	3.11
0.1	367.26	366.6	0.1	457.8	474.0	0.08	0.4	3.11
0.24	1063.1	1046.	0.2	910.5	859.7	0.2	14.8	10.5
0.36	1225.7	1285.	0.3	1204.5	1153.9	0.3	84.1	41.2
0.5	1410.2	1335.	0.44	1374.6	1448.5	0.4	96.5	110.9
0.6	1238.1	1283.	0.5	1495.6	1542.1	0.5	155.5	171.5
0.8	1120.1	1082.	0.84	1815.6	1828.3	0.7	233.8	268.8
0.94	911.6	918.3	1	1973	1871	0.9	347.8	339.4
1.04	802.6	804.1	1.4	1891.4	1856	1	358.4	366.4
1.3	505.6	546.3	1.9	1639.2	1731	1.3	471.2	420.3
1.9	243.3	199.1	2.5	1595.7	1543	1.9	461.9	444.7
2.2	100.3	119.1	3.5	1183	1235	2.2	393.7	431.7
2.96	49.3	39.2	4.4	909.0	986.8	2.9	314.9	371.5
3.5	24.19	24.8	5.5	810.4	719	4	301.4	258.
4.2	21.66	18.8	7	484.7	411	4.9	163.8	179.9
5.2	11.72	17.4	8.2	145.6	204	5.4	97.4	145
6.02	10.3	17.3	9	74.6	83	6.6	40.3	84

Table 33: Shows the experimentally obtained ozone formation data, fit data with (table curve) with best fit rate equation. Data correspond to specific brush discharge electrodes (4 mm, 0.1 mm) at specific start up voltage

4mm(0.1).Batch (8069)			4mm(0.1).air (8069)			4mm.air+water (8069)		
mA/m	O ₃ [ppm] Expt	Fit. Data	mA/m	O ₃ [ppm] Expt	Fit. Data	I [mA/m]	O ₃ [ppm] Expt	Fit. Data
0,02	0	35.6	0,04	51,6	102.0	0,06	0,4	102.0
0,06	1,1	35.6	0,06	243,6	186.5	0,1	12,3	186.5
0,2	561,1	544.6	0,2	673,6	672.4	0,2	57,01	672.4
0,5	1474,2	1585.8	0,4	1099,3	1116.2	0,5	135,2	1116.
0,7	1737,4	1702.0	0,6	1353,8	1359.2	0,6	183,7	1359.
0,8	1802,2	1687.9	0,96	1541,4	1503.2	0,9	267,6	1503.
0,96	1726,4	1615.3	1	1541,5	1504.6	1	323,0	1504.
1,04	1518,3	1565.8	1,2	1420,7	1485.1	1,2	393,2	1485.
1,2	1374,8	1454.9	1,7	1318,2	1329.2	1,6	396,8	1329.
1,4	1293,4	1310.5	2,1	1112,4	1169.4	2	388	1169.
1,8	1066,8	1043.5	2,6	1112,7	976.5	2,3	428,2	976.5
2	847,4	927.9	3,2	743,6	777.1	2,9	248,1	777.1
2,3	714	777.3	4,2	478,2	528.0	3,2	248,4	528.0
2,8	569,4	579.6	5,1	352,2	374.4	3,9	247,5	374.4
3,4	484,4	410.3	6,2	295	249.1	4,5	192,6	249.1
4	345,8	293.6	8	144,0	134.0	5,1	165,2	134.0
4,9	264,6	183.0	9,5	77,6	85.5	6	100,2	85.5
5,5	109,2	137.1	11	52,5	59.3	7	13,5	59.3

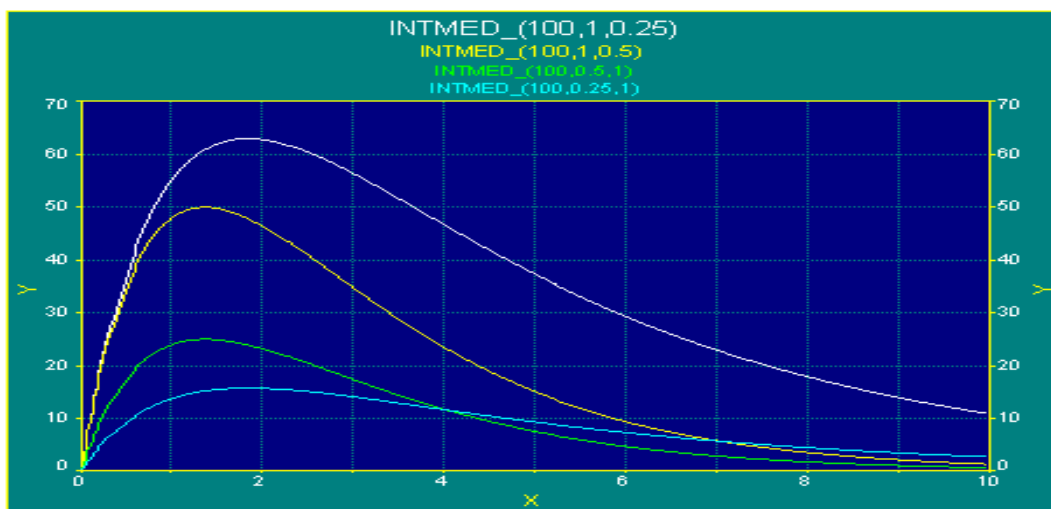
Table 34: Shows the experimentally obtained ozone formation data, fit data with (table curve) with best fit rate equation. Data correspond to specific brush discharge electrodes (4 mm, 0.1 mm) at specific start up voltage

5mm(0.15) Batch			5mm(0.15) air			5mm(0.15) air. water		
mA/m	Expt	Simu	mA/m	Expt	Simu	mA/m	Expt	Simu
0	0.0	2.19	0	0.0	22.9	0	0.0	36.42
0	0.4	2.19	0	2.5	22.9	0.02	1.1	36.42
0	0.4	2.19	0.02	243.0	211.5	0.1	48.8	36.42
0.04	1.2	2.19	0.1	830.7	790.1	0.3	154.0	36.42
0.1	1.4	2.19	0.16	1080.9	1080.7	0.5	191.2	171.7
0.16	1.3	2.19	0.28	1391.3	1419.2	0.6	226.7	243.4
0.3	712.0	710.8	0.6	1423.9	1573.1	0.8	303.1	320.5
0.5	1700.9	1711.9	0.7	1634.7	1532.6	0.96	332.0	339.4
0.9	1496.5	1288.9	0.9	1542.1	1415.5	1	352.0	340.2
1	1105.8	1161.0	1.5	1077.0	1039.6	1.2	249.3	328.2
1.1	894.7	1044.1	1.8	675.1	883.1	1.5	319.9	283.4
1.3	717.6	842.8	3	507.6	457.5	1.9	247.3	213.7
1.9	599.9	442.5	3.8	369.3	294.8	2.1	165.4	182.3
2.1	379.7	357.1	4.7	207.0	179.6	2.4	116.4	142.8
2.5	257.5	232.8	5.5	100.4	115.5	3	83.6	89.5
3	99.9	136.7	6.8	40.0	56.1	3.1	57.9	83.5
3.5	60.0	80.6	7.4	9.9	40.09	5	9.6	40.3
4.1	37.0	43.3	8					

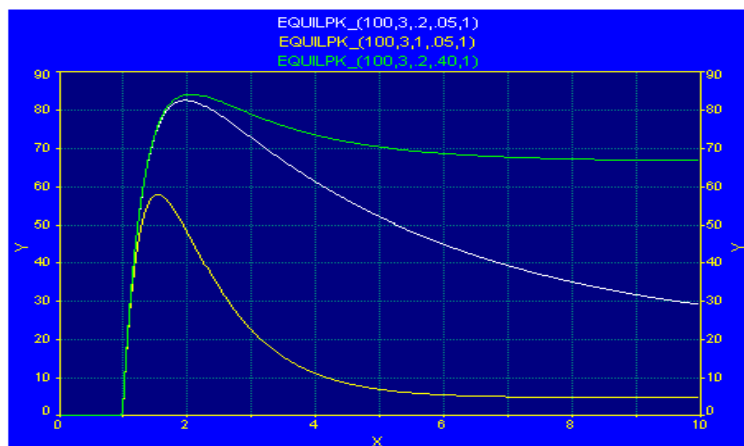
Table 35: Reference M Represent the Reaction details of First order intermediate

(8069), 8071 and 8010 as well.

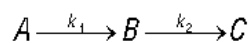
First Order Intermediate



Equilibrium Peak



First Order Intermediate



Concentration of B

Initial concentration of A: a
 Rate constants k_1 and k_2 : b and c

$$y = \frac{ab(\exp(-bx) - \exp(-cx))}{c - b}$$

Non-Intercept form is Eqs. **8128**, **8130**, intercept form is Eqs. **8129**, **8131**.
 Eqs. **8128**, **8129** fit case where $b > c$, Eqs. **8130**, **8131** fit case where $b < c$.

Amplitude
 Max Conc of B

$$\frac{a - b}{c - b} \left[\exp\left(\frac{b \ln b - b \ln c}{c - b}\right) - \exp\left(\frac{c \ln b - c \ln c}{c - b}\right) \right]$$

X at Max:

$$\frac{(\ln c - \ln b)}{(c - b)}$$

Area

$$\frac{a}{c}$$

Constraints

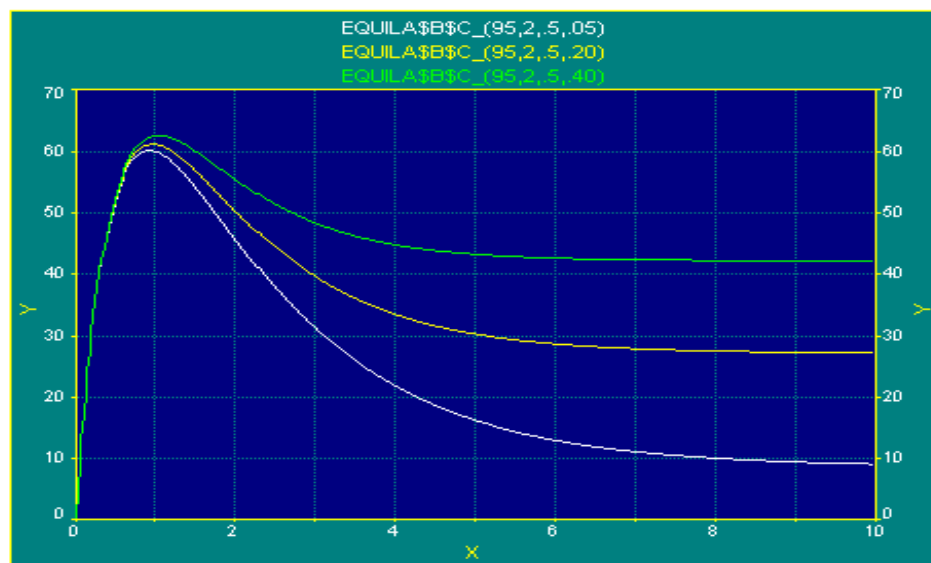
$$x > 0, b > 0, c > 0, b \neq c$$

Built-in Function

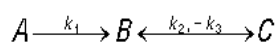
$$\text{INTMED}_-(a, b, c)$$

Both steps are first order. These equations are identical to the Intermediate [Peak Eqns. 8068 and 8069](#) in the peak group except that here the reaction begins at time $x=0$.

First Order Intermediate with Equilibrium



First Order Intermediate with Equilibrium



Concentration of B

Initial concentration of A: a

Rate constants k_1 , k_2 , and k_3 ; b , c and d

$$y = a \left[1 - \exp(-bx) - \frac{c}{c+d} \left(1 + \frac{b \exp(-(c+d)x) - (c+d) \exp(-bx)}{c+d-b} \right) \right]$$

Non-Intercept form is Eqs. **8132**, **8134**, intercept form is Eqs. **8133**, **8135**.

Eqs. **8132**, **8133** fit case where $b > c$, Eqs. **8134**, **8135** fit case where $b < c$.

$$\text{X at Max } x_e = \frac{\ln(bc(-c-d)) - \ln(b(c+d)(d-b))}{c+d-b}$$

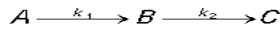
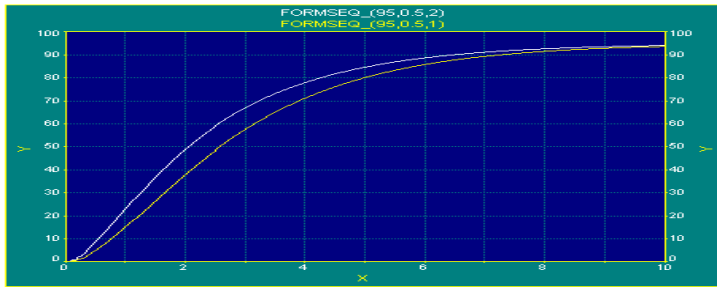
$$\text{Amplitude Max Conc of B } a \left[1 - \exp(-bx_e) - \frac{c}{c+d} \left(1 + \frac{b \exp(-(c+d)x_e) - (c+d) \exp(-bx_e)}{c+d-b} \right) \right]$$

$$\text{Equilibrium Conc } a \left(1 - \frac{c}{c+d} \right)$$

Constraints $x > 0, b > 0, c > 0, d > 0, (c+d) \neq b$

Built-in Function EQUILA\$B\$C_(a,b,c,d)

First Order Sequential Formation



Concentration of C

Maximum concentration: a
 First Order Rate Constants: k_1 is b , k_2 is c

$$y = a \left(1 + \frac{b \exp(-cx) - c \exp(-bx)}{c - b} \right)$$

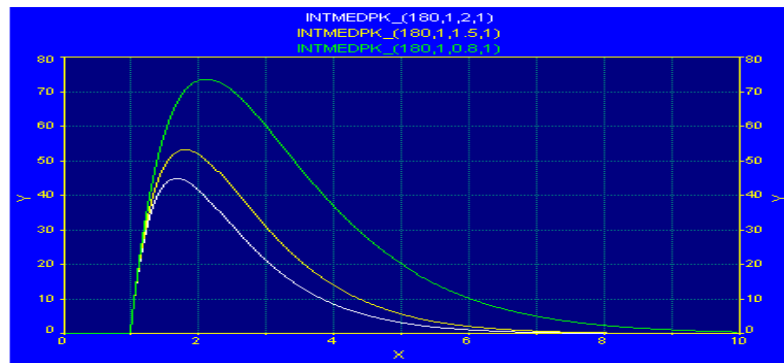
Non-Intercept form is Eq. 8136, intercept form is Eq. 8137

X50 Analytic Solution Unknown

Constraints $x > 0, b > 0, c > 0, b \neq c$

Built-In Function FORMSEQ_(a, b, c)

Intermediate Peak



Note that b is the smaller of k_1 and k_2 , and c is the larger (b and c are interchangeable). Note also that the [Cascade](#) function within the [transition equations](#) is this same sequential formation with an additional term that computes the start of the reaction.

General Non-Linear Equations

Power	8156 $y = ax^b$	
	8010 $y = a + bx^c$	
Single Exponential	8157 $y = a \exp(-x/b)$	
	8002 $y = a + b \exp(-x/c)$	
Two Exponential	8016 $y = a \exp(-x/b) + c \exp(-x/d)$	
Straight Line	8160 $y = a + bx$	Minimize $\sum (y_i - \hat{y}_i)^2$
	8161 $y = a + bx$	Minimize $\sum y_i - \hat{y}_i $
	8162 $y = a + bx$	Minimize $\sum \ln(1 + y_i - \hat{y}_i ^2)$
	8163 $y = a + bx$	Minimize $\sum \ln(\sqrt{1 + y_i - \hat{y}_i ^2})$